MODELING ICE LOADS USING PASSIVE ICE METER OBERVATIONS IN QUEBEC

by

Kamal El-Fashny

Department of Civil Engineering
and Applied Mechanics

McGill University
Montréal, Québec, Canada

August 2002

A thesis submitted to the Faculty of Graduate Studies and Research in partial fulfilment of the requirements for the degree of Doctor of Philosophy

National Library of Canada
Bibliothèque nationale du Canada

Acquisitions and Bibliographic Services
Acquisisitons et services bibliographiques

395 Wellington Street
Ottawa ON K1A 0N4
Canada

395, rue Wellington
Ottawa ON K1A 0N4
Canada

Your file Votre référence
ISBN: 0-612-88460-0
Our file Notre référence
ISBN: 0-612-88460-0

ABSTRACT

Climatic loads (wind speed and ice accumulation) are the main factors that govern the planning and design of telecommunication towers and electric transmission lines. Whilst wind loads are covered comprehensively in the literature and in design standards, ice loads and rules for combination of wind speed on ice-covered-structures are still in development. The main difficulty in achieving a design that meets a target reliability level as specified in design codes is the uncertainty in the temporal and spatial variation of ice accretion. Due to the lack of sufficient direct field measurements, empirical models are usually utilized in combination with meteorological data to estimate the intensity of ice accumulation at specific locations.

A unique database of direct measurements on ice accumulation is available in Quebec. More than 20 years of observations from a network of 180 Passive Ice Meters (PIM) are available throughout the province. The objective of this study is to analyze this data set in order to improve existing regional design criteria and for better understanding of the atmospheric icing phenomena in Quebec. The research is limited to the study of glaze ice, which occurs in conjunction with freezing precipitation.

Firstly, several extreme-value statistical models are investigated to determine the best one or ones for describing the intensity of glaze ice accumulation. In order to increase the sample size, an event-based model, in which every icing event is counted as an independent event, is adopted. Twelve probability distribution functions are examined. The distributions are compared on the basis of the overall fit to the data and the sampling characteristics of the right tail of the distributions. No single distribution fits the data perfectly at all stations. However, the three-parameter distributions, and in particular, the Pearson type III, Generalized Pareto, Generalized Normal, and Generalized Extreme-Value distributions are the best on average. The commonly used Gumbel distribution is consistently outperformed by the three-parameter distributions.

Secondly, a reliability-based procedure is proposed for the analysis of the combined wind and ice loads and in particular for associated pressure on overhead transmission lines. Advantages of the procedure are that: (1) all sources of uncertainty for the analysis can be considered, (2) the most likely combination for the random variables for a specific return period can be identified, (3) specific combinations for every type of structure and mode of failure can be derived, and (4) the procedure is consistent with the methodology used in modern design codes.

Finally, a procedure for the spatial interpolation of design criteria is investigated. Spatial interpolations of the design ice thickness for a 50-years return period is performed using Kriging. Interpolations based on this model were evaluated through cross validation and were found to result in inaccurate predictions. Better results were obtained by first fitting a regional non-parametric trend surface to the data. Interpolations based on Kriging of the trend surface are very well correlated to the spatial variation in severity of the storms that have been reported historically. However, the local residuals remain significantly large and show almost no spatial correlation.

Résumé

Les charges climatiques (vent et verglas), sont les facteurs principaux qui gouvernent la conception des pylônes de télécommunication et des pylônes des lignes de transmission électriques. Les charges du vent ont déjà fait l'objet de plusieurs études dans la littérature et sont bien décrites dans les normes de conception. Par contraste, les charges de verglas et les règles de combinaison pour les charges de vent et de verglas sont encore en développement. La difficulté principale dans l'obtention du niveau de fiabilité spécifié dans les normes de conception est l'incertitude sur la variabilité temporelle et spatiale de l'accumulation de verglas. Les mesures directes des charges sont peu nombreuses et sont généralement utilisées en combinaison avec les dossiers météorologiques pour estimer l'intensité du verglas à un endroit spécifique.

Une base de données unique sur l'accumulation du verglas est disponible au Québec. Plus de 20 années d'observations ont été recueillies sur le réseau de glacimètres d'Hydro-Québec à plus de 180 stations distribuées à travers la province. L'objectif de cette étude est d'analyser ces données afin d'améliorer les critères de conception au Québec et pour une meilleure compréhension du phénomène de verglas atmosphériques. L'étude est limitée au verglas associé à la précipitation verglaçant.

La première partie de l'étude porte sur l'analyse de plusieurs modèles statistiques pour décrire l'accumulation du verglas à chacune des stations. Pour augmenter la taille de l'échantillon, un modèle basé sur chaque épisode de verglas est adopté. Douze fonctions de distribution en probabilité sont examinées. Les distributions sont comparées sur la base de statistiques et mesurent le degré d'accord avec les données et les caractéristiques d'échantillonnages de la queue des distributions.

Dans la deuxième partie, une procédure basée sur l'analyse de la fiabilité est proposée pour l'analyse des charges combinées de vent et de verglas et en particulier, pour la pression associée sur les conducteurs électriques aériens. Les avantages de la procédure sont que : 1. toutes les sources d'incertitude pour l'analyse peuvent être considérées, 2. le

combinaison le plus probable des variables pour une période du retour spécifique peut être identifiée, 3. les combinaisons spécifiques pour chaque type de structure et mode de rupture peut être dérivée, et 4. le procédure est conforme avec les procédures modernes d'élaboration des normes.

Et finalement, une procédure pour l'interpolation spatiale à des sites où il n'y a pas de station de mesure est développée. Les interpolations spatiales des paramètres de la distribution de la probabilité d'accumulation de verglas et de l'accumulation du verglas pour une période du retour donnée est effectuée par Kriging. La validation de la procédure est validée par "cross-validation."

ACKNOWLEDGEMENTS

First and foremost, the author would like to express his deepest gratitude to Professor Luc E. Chouinard, the supervisor of this research project for his invaluable advice and support. The completion of this work would not be possible without his continuous and unconditional encouragement, patience, and guidance for many years. It is of my great pleasure and honour to work with him, to learn from him, and to have him as a good friend. I am also indebted to him for providing financial supports.

The author would like to express his sincere thanks to Professor Van T. V. Nguyen, the co-supervisor of this research for his expert guidance in the statistical analysis aspects and for his invaluable support and sincere encouragement throughout this study.

Financial support from Les Fonds pour la Formation de Chercheurs et l'Aide à la Recherche (FCAR) is gratefully acknowledged. The financial support provided by Hydro-Quebec is greatly appreciated. The author would like to express his gratitude to Mr. J. Laflamme and Mr. G. Périard from Hydro-Quebec for providing the PIM data and for their advices and collaborations throughout the study.

The understanding and support of my colleagues and superiors at SNC-Lavalin are greatly appreciated.

The author would like to take the opportunity to express his profound gratitude to his uncle, Dr. S. Samaan, Consulting Engineer, and Professor Emeritus, Department of Civil Engineering, Cairo University for being the mentor, the example as an engineer, a scholar, and above all a noble person.

Last but certainly not the least, the author would like to thank his wife, Wafaa Gerges, and his daughters, Sarah and Manar for their constant support, encouragement, patience and love.

Table of Contents

List of Figures

List of Tables

Chapter 1. Introduction

1.1. Ice on structures

Atmospheric icing of structures constitutes a major problem for designers of electrical and telecommunication towers. This natural phenomenon is especially important in the northern countries of Europe, Asia, and North America where many failures causing interruption of electric or communication services have been reported (details are given in section 2.1). Furthermore, an increasing reliance on electric and telecommunication networks dictates a higher degree of reliability for each component of the networks. Antenna-supporting structures, for instances, as a part of a telecommunication network are traditionally considered perfectly reliable. However, recent studies of tower failures have shown that this is not always the case. Mulherin reported 140 failures of telecommunication towers in the United States between 1959 and 1996 (Mulherin, 1996). In Canada, a study of tower failures (Magued et al 1989) showed that a yearly rate of tower failures, due to wind or ice overloading, is estimated at 0.055%, which is five times higher than the reliability level in the Canadian Design Codes (CSA-S37). The same can be said for overhead transmission lines where a devastating interruption of service due to the 1998 ice storm in Montreal metropolitan area exceeded all expectations relative to the level of damage that could be caused by ice storms.

Current Canadian Design Codes (e.g. CAN/CSA-S37 Antenna, Towers, and Antenna-Supporting Structures) specify values of ice loads based on a simplified regionalisation of ice accretion estimated at meteorological stations using an empirical formulation that is a function of meteorological data (Chaîné and Skeates, 1974). However, meteorological stations usually located at airports are distant from each other, and do not provide direct measurements of ice accretion. Ice storms are generally meteorological phenomena that are very localized and may go undetected by surrounding meteorological stations (note that the ice storm of 1998 is exceptional in scale and location). Consequently, the environmental loads specified in the standards, such as CSA-S37, are based on indirect estimates of ice accretion using other meteorological parameters. Moreover, some of the parameters of the ice accretion models, e.g. liquid water content and droplet size, are also not directly measurable.

In addition, reliability classes and wind-on-ice factors specified by the CSA-S37 code are over simplified. Bruneau et al (1989) concluded that "*... there is still a significant number of deficiencies in current knowledge, preventing better control of the reliability of guyed towers. The probability characteristics of glazing ice remain mostly unknown.... Increased knowledge about these environmental conditions would greatly enhance the reliability of the S37 standard as a whole.... The development will require a review of the statistical parameters applicable to the behaviour of this class of structure as a system.*" For wind-on-ice loads, Wahba et al (1993) show that the ratio of wind speed during ice storms to the maximum annual wind speed vary between 0.3 to 0.9 depending on the location of the meteorological station. Wahba et al. demonstrate that the factor of 0.71 specified by S37 is adequate for 85% of the stations, but Makkonen (1995), in a discussion of the previously mentioned paper, regards this ratio to be too low compared to those used in other parts of the world. Nevertheless, the specification of a single factor for all locations in Canada may be an oversimplification that results in a large variability in the reliability of towers across the country.

Direct measurements of ice accretion, on a spatial grid fine enough to detect local events, would be the most effective way to qualify and quantify the effects of ice storms, however, this type of measurements have not been available historically.
Due to a lack of data on atmospheric icing at specific locations, many empirical models have been proposed to derive estimates of atmospheric icing from data usually collected at meteorological stations on precipitation, temperature, and

wind speed. Many ice accretion models are available in the literature. Yip and Mitten (1991) and McComber et al. (1995) reviewed many of those models. The models are either physical, experimental, or numerical-simulation models.

1.2. PIM program

Specific data sets on ice accumulation are very rare. One of the most comprehensive to date has been compiled by Hydro-Québec. In 1974, Hydro-Québec initiated a pioneering project to deploy a simple measuring instrument over most of the territory covered by its transmission system. Approximately 180 Passive Ice Meters (PIM) have been deployed across the province of Québec (Fig. 1.1). The instrument, the Passive Ice Meter (PIM), consists of standardized cylindrical and flat surfaces acting as ice collectors from different directions. Measurements are collected during icing storms and consist of: the type of ice and the total accumulation on each collector, the ambient air temperature, the wind speed and direction, and the start and end of the precipitation. More than twenty years of recorded observations are available from the PIM program. This data set is unique in its kind given the large number of stations and their spatial coverage. The measurement program was specially designed for ice accretion on conductors and structures, and in consequence, is more relevant and comprehensive than data derived empirically from airport weather stations which is the basis for current ice hazard zonation maps in the CSA standards.

1.3. Type of ice accumulation

There are three types of ice accretion on structures: glaze ice, rime ice, and wet snow. Meteorological variables that determine the type of icing event are air temperature, wind speed, size of the supercooled water droplets, and atmospheric water-content. Table 1.1 summarizes the different physical characteristics of each type. While all these types of ice accretions are recorded by the PIM, the program was originally intended for icing due to freezing rain and freezing drizzle (Felin 1988), and this fact is reflected in the location of the PIM stations. Glaze ice, formed mainly due to freezing rain, is the most severe type of icing in terms of its density, its spatial extent and its adhesion to objects. Consequently, this study is limited to the analysis of data related to glaze ice accumulation due to freezing rain.

Table 1.1: Physical characteristics of each type of atmospheric ice

Characteristic	Soft Rime	Hard Rime	Glaze	Wet Snow
Density	< 600 kg/m^3	From 600 to 900 kg/m^3	900 kg/m^3	From 200 to 800 kg/m^3
Adhesion	Slight	Strong	Very strong	Variable
Internal Structure	Granular, many air pockets	Compact, with alternating clear and opaque layers	Compact, with occasional air bubbles	Compact wet snow
Appearance	Whitish crusty snow forming needles	Hard ice, white and opaque	Icicles and smooth transparent ice	Opaque, white and crusty

Glaze ice is associated with frontal systems between cold (polar) and warm (tropical) air masses. When a warm air mass overruns an underlying colder air mass, a temperature inversion may occur within the bottom portion (1 or 2 km above ground) of the atmosphere (Figure 1.2). Snowflakes formed at high altitude, above the inversion, melt as they fall through the warmer layer. Water droplets then fall through the layer of cold air and become supercooled (i.e. water droplets remain liquid for temperatures below the freezing point). The supercooled droplets freeze and accumulate on any object encountered near or at the ground surface (Battan 1984 and Felin 1976). This situation usually does not last more than several hours and is restricted to a sweeping but narrow band associated with the warm front (again, the January 1998 ice storm was exceptional with respect to its duration where three episodes of freezing precipitation were involved). Glaze ice is usually translucent, homogeneous, hard, highly adhesive, and very dense.

1.4. Scope

The overall objective of this study is to contribute toward improving the regional design criteria for telecommunication and electric transmission towers under atmospheric icing hazards. Of particular importance for the estimation of hazards is the reduction of the uncertainty related to environmental loads (wind and ice). Environmental loads over an iced structure are a function of the frequency and severity of atmospheric icing storms and of the associated wind speed. The characterization of icing storms in the province of Québec can be improved by using the PIM network data.

The main objective of this study is to formulate and estimate an event-based model for the joint distribution of the thickness of glaze ice and wind speed in different regions of Québec. This objective will be achieved in two phases. The first phase is to find the best site-specific statistical model for the severity of icing storms. In order to increase the sample size, an event-based model, in which every icing event is counted as an independent event, is adopted. The selection criteria for the statistical model is based on the goodness-of-fit of the proposed probability distribution functions and the sampling characteristics of their extrapolated right tail.

The second phase of the study is to develop procedures for spatial interpolation of the model to locations where there are presently no measuring stations. The latter requires the estimation of the recurrence rate of icing storms, their spatial extent, and the identification of site-specific features that increase the ice storm hazards. The spatial interpolation of the quantiles of the distributions shows the need for more sophisticated schemes that incorporate, in addition to the correlation between neighbouring stations or those with similar characteristics, other meteorological and topographic parameters.

Wind-on-ice loads have been treated separately and with particular emphasis on icing of overhead power transmission lines. Wind data is analysed to derive distributions for the maximum wind speed during ice storms and during the entire year. Reliability procedures have also been proposed for analyzing the effect of load combinations on a structure. The resulting design forces are compared to the forces derived from the simple combination rules of IEC 826.

1.5. Limitations

This study aims to contribute to the understanding of the load effect of atmospheric icing on exposed structures through the analysis of the PIM data. However, such a goal cannot be completely achieved in a single study. The scope has to be limited for obvious reasons; such as availability and reliability of data, time frame, learning progress, and multidisciplinary complexity of the subject.

Glaze ice caused by freezing precipitation is the only type of icing considered here. The study is limited also to the PIM data from Hydro-Québec; icing at other locations could have different characteristics. The maximum value of atmospheric ice accumulation on the four cylinders of the PIM is used in the analyses, and directional effects have been ignored. Statistical characteristics of the data are the main theme of this research; consequently, empirical models of ice accretion based on meteorological data are outside the scope of this study. Wind-on-ice analysis is limited to its application to conductors. Finally, the spatial analysis of icing distributions was based solely on the relative distance matrices.

Given the time frame of the study, ice data used in the analysis is based on data sets provided by Hydro-Québec and includes observations up to 1994/95-winter season. The wind-on-ice analysis, however, includes observations up to 1999/00-winter season. Ice thickness is defined as the total ice thickness measured on the PIM, except in Chapter 5, where ice thickness is converted to equivalent radial ice thickness based on Hydro-Québec empirical formula.

1.6. Organization of the thesis

Chapter 2 contains a brief review of the state-of-the-art on atmospheric icing of structures. It includes a description of the 1998 ice storm and its devastating effect. Ice accretion models as well as ice measurement programs are briefly reviewed. Ice and wind-on-ice loads specified in national and international standards are summarized.

Chapter 3 describes the Passive Ice Meter program of Hydro-Québec and the database of ice measurements in Québec. Data filtering and analyses, and definition of ice events are presented. The preparation of the database and the procedure used for the identification of separate ice storms are described.

Chapter 4 presents analyses on extreme distributions for ice accumulation data in Québec. Twelve probability distribution functions are examined and compared based on the overall fit and the behaviour of the right tail of the distribution. Parameter estimates are obtained using L-moment and Maximum Likelihood. The characteristics of the right tail are examined using a bootstrap resampling technique.

In Chapter 5, the combined loads from wind and ice accumulation on conductors are modeled using a reliability-based approach. A data set is derived by merging ice data from the PIM network and meteorological data from Environment Canada. The method is used to define load combinations of wind and ice at several stations in Québec. The results are compared with the simple combination rules that are prepared in existing design codes.

Chapter 6 presents a method for the spatial interpolation of design ice loads at locations where there is no measuring stations. An ad-hoc method based on Kriging is proposed. The procedure includes the separation of the large-scale component that represent a regional trend and the small-scale component that represent a site effect.

Finally, Chapter 7 presents the main contributions of this research as well as recommendations for future research works.

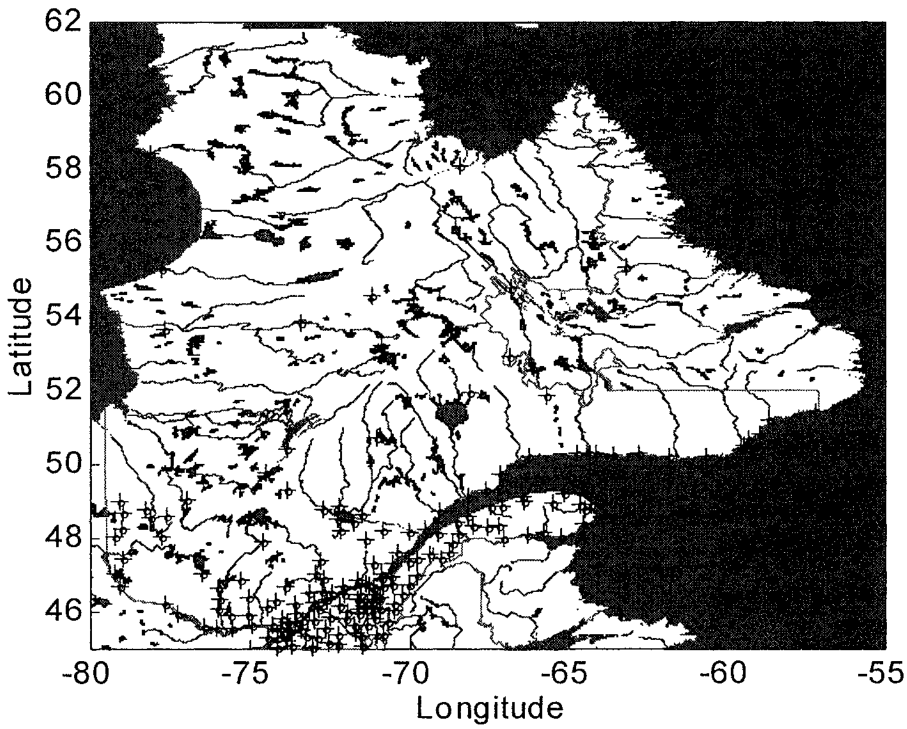

Figure 1.1: Deployment of the PIM network

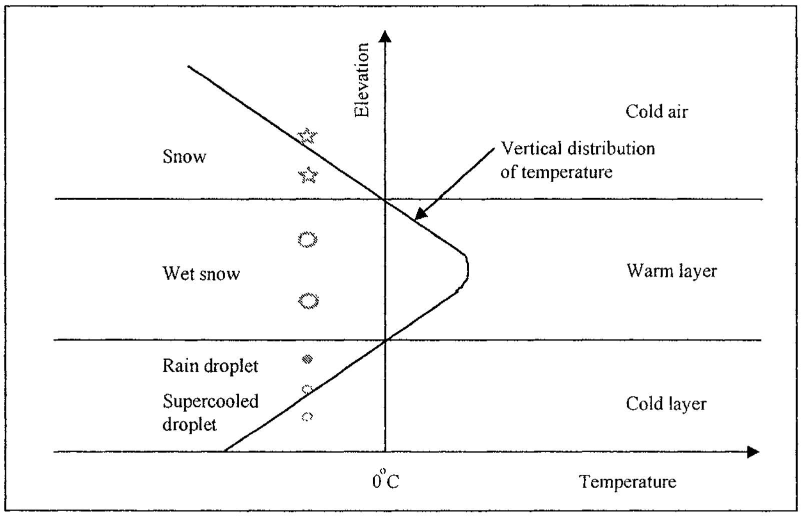

Figure 1.2: Description of freezing rain formation

Chapter 2. Literature Review

2.1. Structural failures due to icing

The study of atmospheric icing of structures has a relatively short history; most of the relevant research has been performed from the seventies to present. Nevertheless, earlier studies, dated back to the beginning of the century, were done by railway companies that collected statistics on the failure of railway communication wood poles (Jones 1998). Interest in ice loads was renewed after several recent structural failures of electrical and telecommunication facilities. Many of these facilities are deployed in rural areas; however, more attention is usually given to storms and failures occurring in highly populated areas. In Québec, major ice storms causing failure of Hydro-Québec transmission towers were reported in 1956, 1969, and 1973 (Felin 1976). Chaîné reported a major ice storm that was encountered in the Montreal area in March 1972 that caused considerable damage to public utilities (Chaîné 1973). Sixty thousand people were without electricity, and 900 wooden poles collapsed under the combined effect of two inches (50 mm) of ice accretion and wind of 40-50 mph (65-80 km/h). Hall (1996) reports damage to electrical facilities from three severe ice storms in Manitoba between 1977 and 1991.

Similar events in the United States have been reported by Mulherin (Mulherin 1996) relative to the failure of more than 140 telecommunication towers from 1959 to 1996 during ice storms. Blackout and tree damage associated with atmospheric icing are more frequent and only major events are usually reported. Jones and Mulhein (1998) compiled information relative to many major US ice storms and report that damage to transmission lines can often extend over hundreds of miles. Similar damage to electrical and telecommunication structures were reported in different countries all over the northern hemisphere (IWAIS' 82, 84, 86, 88, 90, 93, 96, 98, 00 and 02).

2.1.1. January 1998 Ice Storm

In January 1998, a major ice storm struck southeastern Canada and the northeastern United States. The severity of the storm in terms of total accumulation, duration, and extents of affected area were exceptional. Moreover, the trajectory of the storm went through one of the most highly populated areas in Canada rendering it the worst natural disaster ever to hit Canada in recent history. The storm came as three waves of freezing rain between January 5^{th} and January 10^{th} with a total precipitation (mostly freezing rain) reaching 100 mm in Montreal (Figure 2.1). The total number of hours of freezing precipitation exceeded 80 hours in Montreal (Environment Canada, 1998), which is almost double the total annual average (Figure 2.2). The area affected by the storm in Canada extended from eastern Ontario to parts of New Brunswick and Nova Scotia, passing through western Québec and the Eastern Townships (a distance of over 1000 km). In the U.S.A, the states of New York, Vermont, New Hampshire, and Maine were affected by the storm (FEMA 1998). The extent of the storm is shown on Figure 2.3. Among affected areas, southwestern Québec was by far the hardest hit, the heaviest ice accumulation being recorded in the Montréal and Montérégie areas. Hydro-Québec's interpretation of the intensity of the storm expressed in terms of maximum radial ice thickness on a conductor is shown on Figure 2.4. The storm moved in an easterly direction causing extensive damage in its path and major disturbances and interruptions of all types.

The destructive effects of this storm on nature and the built environment resulted on damages estimated in the hundreds of millions of dollars. The damage in eastern Ontario and southern Québec was so severe that major rebuilding of the electrical grid had to be undertaken. Over one million households in Québec were without power for periods extending from a few days to a few weeks. Millions of trees, thousands of kilometres of power lines and telephone cables, several major transmission towers and thousands of wooden utility poles were damaged or destroyed (Environment Canada, 1998).

The cost to restore and upgrade the electricity distribution and transmission network has been estimated at almost one billion dollars while the total cost to society may have exceeded three times that amount (Hydro-Québec 1998). The number of damaged lines and structures as reported by Hydro-Québec are shown in Table 2.1.

Table 2.1: Number of damaged lines due to the 1998 ice storm in Québec (Hydro-Québec 1998)

Voltage Class KV	Number of Damaged Lines	Number of Collapsed Structures
1. Transmission		
735 kV	10	150
315 kV	12	60
230 kV	13	300
120 kV	67	1100
49 kV	14	1500
Total	116	3110
2. Distribution		
25 kV	350	16000

The extent and location of the damage in Montreal and surrounding regions are shown on Figure 2.5. Photos of some collapsed towers are shown in Figure 2.6; and photos of measured ice accumulations on a conductor and a wire of a collapsed line, on a road sign and on a PIM are shown in Figure 2.7. At the peak of the storm a total of some 9 million kW of electric load was lost.

Line failure analyses were performed by Hydro-Québec for individual transmission and distribution lines (Hydro-Québec 1998). The result of the analyses showed that older steel towers failed since they were designed for much lower ice load (older steel tower lines are defined as those built prior to 1974 and designed in accordance with the CSA standard prevailing at the time, mostly CSA C22, Overhead Lines). The older towers were generally designed for an ice load equivalent to approximately 35mm of radial ice thickness. During the January 1998 storm, old lines in the affected areas suffered extensive damage.

New lines, on the other hand, generally performed better. New steel towers are defined as those built after 1974, the year when, following the 1969 and 1973 major line failures, Hydro-Québec decided to review its design criteria for transmission lines for the entire province. In particular, the ice-carrying capacity of transmission lines was raised from 35 to 45 mm of radial ice and steps were taken to achieve a better overall design including provisions for anti-cascade towers.

All distribution poles were designed to CSA standards and jointly used by power and telecommunication utilities. Failure analysis demonstrates that wood poles failed as expected since the applied loads exceeded by far their design capacity.

In rural areas, farming operations were disrupted extensively since electricity is essential for dairy operations and restoration of power was slow. Many Québec maple syrup producers, who account for 70% of the world supply, were financially ruined with much of their sugar bush permanently destroyed (Environment Canada 1998).

On the U.S. side, none of the highly populated urban areas were affected; however, the storm damaged over 7 million hectares of rural and urban forests throughout the northern states and power outages extended up to 23 days (FEMA 1998). Few transmission towers collapsed and most outages were caused by the collapse of distribution lines due to trees leaning or falling (Jones and Mulherin 1998). Jones and Mulherin (1998) also report the collapse of 18 telecommunication towers.

2.2. Icing models based on meteorological data

Due to the lack of direct measurements of ice deposits on cables or structural members during ice storms, most of the research on atmospheric icing was directed on analytical, empirical, or numerical models of ice accretion as a function of meteorological data. Several models exist in the literature, for example, Chaîné and Skeated (1974), McComber et al. (1982), Goodwin et al. (1983), Makkonen (1989), Draganoiu et al. (1996) and Jones (1998).

Generally, ice accretion models can be grouped into empirical, semi-empirical, and physical (numerical) models. The basic ice accretion formula can be expressed as (Makkonen 1984):

$$\text{Rate of ice accretion} = E \,.V \,.W \,.n \qquad \text{(mass/area/time)} \tag{2.1}$$

where E is the collection efficiency, defined as the ratio between the mass of the droplets that hit the object to the total mass of all droplets in the flow; V is the wind velocity; W is the air liquid water content (mass/volume); and n is the freezing fraction, defined as the ratio between the water droplets that remain on the object to the total droplets that hit the object. Wind velocity is the only parameter directly available from meteorological records. The other parameters, E, W, and n, are obtained theoretically or experimentally. The experimental approach relates these parameters to available meteorological data, such as total precipitation and air temperature. The theoretical approach is based on solving heat balance equations at the ice-covered surface, and on fluid dynamics models for the path of particles around the object. Meteorological data is used in combination with the models to simulate ice accretion. In general, these models have not been validated with a large number of measured icing events and are dependent on the availability of meteorological data.

In Canada, the most popular model is the one developed by Chaîné and Skeates (1974). Chaîné's model is based on a formulation originally developed by McKay and Thompson (1969). The model describes the formation of an elliptical ice deposit as a function of the horizontal accretion and wind speed. The shape of the deposit is empirically converted to an equivalent radial ice thickness using a calibration from experiments by Stallabrass and Hearty (1967).

Yip and Mitten (1991) compared predictions from nine icing models with ice observations during ice storms and with results of laboratory experiments. They concluded that Chaîné's model was the best for predicting freezing rain, and that Makkonen's model was the best for predicting in-cloud icing and the second best for predicting freezing rain. Makkonen (1996) evaluated ten models for the prediction of freezing precipitation and investigated deficiencies of the earlier empirical models. He concluded that all models are either poor or fair for predicting extreme events. Makkonen suggested using numerical methods in case of freezing precipitation icing.

The advantage of using empirical models is the availability of meteorological data from standard weather stations over relatively long period of time. However, weather stations are usually located in populated areas, mostly in airports, and relatively far from each other. Since freezing rain usually affects small regions, many storms can go undetected by any weather station.

The accuracy of each model is measured by its ability to predict the amount, type and shape of ice accretion under specified weather conditions. However, finding these input data in a similar accuracy and on particular sites not close to weather stations cannot be guaranteed, and interpolating between different sites may also misleading. Other shortcomings of these models are that they cannot predict the residency period of ice deposit on an object, and do not include small-scale variation such as topography. And finally these models, in general, do not follow a probabilistic approach in order to account for the uncertainty of the data.

2.3. Ice measurement data

The HQ ice measurement program is by far the most extensive of its kind in terms of coverage in time and space. Chapter 3 deals in detail with the PIM program and database. Besides the PIM program, HQ also introduced the icing rate meter (IRM or the Givromètre) that has been tested on Mt. Blair test site (McComber et al., 1996) and deployed in 23 measurement stations since 1993 (Laflamme, 1996). The IRM provides real-time ice monitoring and icing rate growth and transfer these data to central computer. The instrument and the program are under continuous improvements.

In other parts of Canada, there is no ice data bases collection of a similar size as the Québec one. In Ontario, measurements from four sites on instrumented transmission towers started in 1975 (Krishnasamy, 1982). The towers were equipped with load cells, strain gauges and rotating transducers. This combination is able to measure vertical, longitudinal and transversal components of conductor loads. The data acquisition system consists of microprocessors and digital data recorder.

In Newfoundland, in the seventies, a dozen of test towers had been deployed in the northern part of the island and in the southern part of Labrador (Butt, 1986). The Passive Ice Meter of Hydro-Québec was used for these test sites. The data collection was not frequent (monthly) and the towers were not instrumented. Most of ice accretions were of the in-cloud icing type, in which the technique of freezing-rain icing measurement is not effective.

In other countries, the measurements are mainly for one or a small number of test sites and for limited number of seasons. The main purpose in most cases is collecting information about a purposed site for new facility or planning a transmission line route. The collected information is mainly used to validate empirical ice models or to better understand the characteristics of icing in a particular region. Ice measurement programs targeting at building regional maps of ice loads are almost non-existent.

In the U.S.A., there had been no systematic ice data collection program since 1937 (Seppa, 1996). Seppa suggested using a tension monitoring system, already installed by electrical utilities to measure thermal rating, to measure ice loads on lines. Seppa stated that the utilities are not interested in supporting this program. The Rosemount Ice Detector, originally developed for icing on aircraft, has been tested for ice accretion measurement (Tattelman, 1982). An example of individual site measurements in the U.S.A. is the Tyee Lake instrumented tower in Alaska where load cells and inclinometers were installed on the test tower (Peabody, 1996). Standard weather measurements were also made at the site. Another example is the measurements on instrumented cables at CRREL Laboratory on Mt. Washington (Govoni and McKley, 1982). The measurements took place during the years of 1977-1981. The test line was instrumented by single-axial and tri-axial load cells. The purpose of the experiment was to establish drag coefficients for wind on different ice accretion types. Mt. Washington is at high altitude and the main type of ice formation is in-cloud icing.

Similar test sites have been instrumented in different countries. For example, in Norway, a measurement program was started in the late seventies; Fikke et al. (Fikke et al. 1982) mentioned 11 test stations owned by the state power system. The test stations were located along the routes of proposed power lines and consisted of test spans and tubes with different configurations. The test spans were equipped with dynamometers, while the tubes were inspected manually. The inspections were either daily or weekly. Since this measurement program was performed for routing the lines and for estimating maximum ice loads at specific sites, most of the stations were located in high altitude where in-cloud icing is more likely to occur.

Measurements of ice accretion were made at few locations in Finland during the seventies (Makkonen and Ahti, 1982). The objective was to study the rime ice formation and its relation to meteorological parameters. In former USSR, each weather station is equipped with passive ice collectors consisting of two 5 mm diameter conductors located 2 meters above ground and oriented North-South and East-West respectively (Nikiforov, 1982; Golikova et al., 1982).

Other means of collecting historical information about ice storms have also been attempted. For example, dendrochronology, where damage to vegetation is measured by ring growth patterns, can be an indicator of past severe ice storms (Felin and Rivest, 1982; Mallory and Leavengood, 1982). Other means include descriptive information from weather-concerned agencies such as NOAA and NCDC in U.S.A., aviation agencies, or power utilities (Shan et al., 1998).

2.4. Ice load based on measurement

The conventional procedure for developing regional design criteria for icing of structures using measurements has three steps: (1) obtain samples of annual maximum ice thickness at each site in the region, (2) estimate the design ice thickness for a given return period by fitting the Gumbel distribution to the sample data at each site, and (3) derive contour lines of design ice thickness by qualitatively smoothing the estimates. The shortcomings of this procedure are: (1) there are several stations where there is very little data for fitting a distribution; (2) there is no comprehensive study which demonstrates that the Gumbel distribution is adequate for representing icing data; and (3) the spatial variation in design ice thickness is usually erratic due to the small sample size at each station.

One procedure to address the latter issue is to pool data from neighbouring stations to increase the sample size. Laflamme (1993) suggests that pooling of data from three neighbouring stations (triad) improves the fit of the Gumbel distribution to the sample of maximum yearly observations. The main difficulty with pooling is the identification of a group of homogenous stations with similar climatological and topographical characteristics. Alternatively, an event-based model can be used to increase the sample size at each station by including all major icing observations.

2.5. Probability distribution functions for ice loads

Justification for the choice of the best distribution function for ice loads on structures is not well defined in the literature. Two-parameter distributions are popular choices, and particularly the Gumbel distribution. Chaîné and Skeates (1974) analysed the synthetic (using Chaîné model) ice data as well as wind speed during ice storms using the Gumbel distribution to calculate design values for different return periods. Laflamme also utilized the Gumbel distribution to analyse the ice thickness data collected from the PIM network (Laflamme, 1995). The Gumbel distribution is also used in design standards such as IEC 826. Pezard (1993) compared Gumbel, Weibull, Gamma, and a two-step distributions to fit wet snow and in-cloud ice loads on a 15 mm conductor in France and recommended the Gamma and the two-step distributions while excluding the Gumbel distribution. Eliasson and Thorstiens (1993) analysed 10-year ice data from test spans in Iceland and compared the Gumbel, Extreme type II and III, Weibull and LogNormal distributions. They concluded that Gumbel is a reasonable choice and superior to the LogNormal distribution. Fahleson (1995) compared also the same distributions for data collected at a telecommunication tower test site in Sweden. Due to limited data, it was not possible to identify a best-fit distribution, but the Gumbel distribution was chosen for its simplicity. In brief, there is no previous comprehensive study that provides guidance for selecting a distribution function for ice measurements.

2.6. Icing hazard maps

Icing hazard maps based on an analysis of direct observations on ice accumulation are almost not existent in the literature due to the lack of sufficient data both in duration and in spatial coverage. Ice measurement programs have been established in many countries, but most are at a few specific sites or cover a short period of time. The development of severity maps for ice accumulation and associated wind loads in current Canadian design codes (e.g. CSA S37-94) is based mostly on experience. This is exemplified by the wide differences in ice severity maps for different codes and the treatment of the effects of special topographical and climatological features.

2.7. Combined wind and ice loads

There are several options to estimate the probability distribution function of the associated wind speed during an icing event. The most direct approach is to use observations of wind speed during an icing event when available. For example, Fehleson (1995) performed a comprehensive analysis of ice and wind loads on an instrumented telecommunication guyed-tower using observations over a period of six years.

Observations are available for the PIM stations; however, the observed wind does not correspond to the maximum wind during the whole icing event but to the wind speed observed by the inspector at the time of the ice measurements. The wind data available at weather (meteorological) stations can be used to derive synthetic samples of concurrent wind speed (Chaîné and Skeates 1974, study VI). This data is readily available at weather stations over a relatively long period of time (about 40 years). However, these stations are sparsely distributed in space, and are usually not located in regions that may be critical for the telecommunication or electrical distribution systems. The probability distribution function of the maximum wind speed for given residency periods can be derived from the distribution of maximum annual wind speed (Criswell 1986 and Mozer 1989). This estimate is quite sensitive to the residency period, which is usually not well defined due to lack of data and has to be assumed for several sites.

Section 7 of IEC826 deals with combination of wind and ice. The stochastic characteristic of the loads is recognized, and in particular wind speed, ice thickness and the form of accumulation (i.e. the drag factor). The philosophy of the standard is to identify the combinations of these variables with the same probability of exceedance. Each load combination includes one variable with weak probability and the other variables with strong probability. Definition of weak and strong probabilities for different reliability levels is shown in Table 2.2. The correlation between the variables is recognized in theory but neglected in the application of the standard.

Table 2.2: Definition of weak and strong probabilities in the IEC 826

<table>
<tr><th></th><th>Reliability level</th><th>Return period (years)</th><th>Probability of exceedance for the load</th></tr>
<tr><td rowspan="3">Weak probability. For the maximum for one of the variables</td><td>1</td><td>50</td><td>65%</td></tr>
<tr><td>2</td><td>100</td><td>30%</td></tr>
<tr><td>3</td><td>500</td><td>10%</td></tr>
<tr><td rowspan="3">Strong probability. For the maximum value for one of the variables.</td><td>1</td><td rowspan="3">3</td><td rowspan="3">100%</td></tr>
<tr><td>2</td></tr>
<tr><td>3</td></tr>
</table>

The wind associated with ice is the average wind during a period of 10 minutes at 10 m elevation above the ground during an ice storm. The wind with high probability is estimated using the Gumbel distribution for the return period mentioned above from the maximum annual wind. If the observations during the ice storms are not available, the winds associated with ice is estimated in two ways:

1) By identifying the yearly maximum wind observed during freezing precipitation and during the following period while the air temperature is under the freezing point (the suggested maximal period is 72 hours),

2) By using the reference wind as prescribed in the clause 5.5.2 of the standard with a reduction factor based on experience and analyses of local meteorological conditions.

$$\begin{aligned} V_{RL} &= (0.60 \ to \ 0.85) \cdot V_R \\ V_{RH} &= (0.40 \ to \ 0.50) \cdot V_R \end{aligned} \tag{2.2A,B}$$

where V_{RL} and V_{RH} are the associated wind speed with low and high probabilities respectively, and V_R is the reference wind speed, the determination of the reference wind is obtained from the meteorological stations or by interpolating from geostrophysical winds. The determination of the reference wind is a function of the reliability level required for the structure. The reference wind is estimated using the following equation for the Gumbel distribution,

$$V = \overline{V} - \frac{C_2 \sigma}{C_1} - \frac{\sigma}{C_1}[\ln(-\ln(1-\frac{1}{T}))] \tag{2.3}$$

where $\overline{V}$ is the observed mean value, σ is the standard deviation, T is the return period, and constants C_1 and C_2 are function of the size of the sample. For the case where the number of observations approaches infinity, the expression is simplified to,

$$V = \overline{V} - 0.45\sigma - \frac{\sigma\sqrt{6}}{\pi}[\ln(-\ln(1-\frac{1}{T}))] \tag{2.4}$$

2.8 Ice loads in the design codes

Most building codes and design standards for northern countries have provisions concerning the effect of ice accumulation on ice-sensitive structures such as lattice structures, guyed masts, overhead lines and cable systems. The provisions of the codes address this problem either directly by specifying regional ice maps with minimum design ice loads for each region, or indirectly by providing guidelines and referring to local environmental historical data to determine the severity of ice accumulation for a particular site. In general, ice loads specified in the codes are in the form of equivalent radial ice thickness uniformly covering all surfaces of the exposed elements. The density of ice varies depending on the type of ice. However, for design purpose the density of glaze ice of 900 kg/m^3 is generally used.

NBCC 1995

The National Building Code of Canada (NBCC) does not provide explicit values for ice loads on structures; instead, they are included in snow loads provisions (NBCC 1995, clause 4.1.7. Live loads due to snow, ice and rain). The snow loads provisions are intended mainly for building roofs rather than lattice open structures. The structural commentaries of the code (NBCC, Structural Commentaries 1995, commentary H Snow Loads) refer to the models used in the CSA-S37 code, and the Ontario Highway Bridge Design code (recently integrated into CSA-S6, Bridge Design Code) for ice accretion on exposed vertical and horizontal surfaces and cables. Commentary B, Wind Loads, states that wind forces should be calculated for ice-covered surfaces if the strongest winds and ice accumulation occur simultaneously. The values of wind and ice loads to be combined are not specified and designers are referred to local authorities, if available.

CSA-S37-94 (Antennas, Towers, and Antenna-Supporting Structures)

Ice load is considered as a major factor in the design of telecommunication structures. Firstly, as a main contributor to the total gravity loads on the structure and secondly, as a contributor for higher horizontal force from the wind as a result of the increase in the exposed surface area of structural members as well as due to changes in surface conditions. S37 specifies minimum design ice thickness based on an ice map of Canada. The country is divided into four regional classes of ice severity varying from 10mm to 50mm nominal ice thickness. Most of southern eastern Québec is situated in the class II region (25mm); and most of western Québec starting from Québec City and including the townships and lower Saint-Lawrence is situated in the class III region (40mm). The wind pressure on ice-covered members is specified as 50% of that used for bare elements. This loading condition is equivalent to approximately 70% of the design wind speed. The ice map is based on information from weather stations, usually located at airports or near populated area. S37 recommends supplementing the ice map with local icing data for locations far from existing meteorological stations, for sites near water bodies, and for those located at high elevations.

CSA-C22.3-97 (Overhead Systems, Part III-Outside wiring)

Similar to S37, C22.3 specifies a severity map of Canada for minimum climatic loading for design of cables and their supports and attachments. Three regional loading conditions (ice and wind combinations) are recognized: heavy, medium A and medium B. The heavy and medium A conditions were adopted from earlier CSA standards, while medium B condition was added to the 1976 edition of the standard. The radial ice thickness on wire for vertical load calculations is 12.7 mm for heavy and medium B conditions and is 6.35mm for medium A condition. Ice density is considered 913 kg/m^3. The code specifies also the transversal pressures due to wind corresponding to the three loading conditions on ice-covered wires. The horizontal wind loadings are 385 N/m^2 for heavy and medium A conditions and 285 N/m^2 for medium B condition. The code recommends using the ice map only as a guide that must be supplemented with experience of local weather condition.

CSA-S6-00 (Canadian Highway Bridge Design Code)

CSA-S6-00 requires that ice loads be considered on all exposed surfaces of bridges and road elements. A national ice map similar to that of S37 is provided for the design ice thickness. Four zones are defined throughout the country with ice thickness varying from 10mm to 66mm. There are noticeable differences between the S37 and the S6 maps. It should be noted that the ice map of S37 represents the equivalent radial ice thickness, and that is not the case for S6 ice map. It is obvious that atmospheric ice loads (sea ice is excluded) does not represent a major load case for bridge structural components and does not lead to structural failure. On the other hand, ice load is critical for other road elements such as sign panels. The accumulation on such elements is superficial (on one side) rather than radial. The specified unit weight of ice is 9.8 kN/m^3, which is the highest among all design standards.

ASCE 7-98 (Minimum Design Loads for Buildings and Other Structures)

The ASCE 7-98 requires that atmospheric ice loads be considered in the design. These ice loads include ice accretion due to freezing rain and drizzle, snow, and in-cloud icing. The ice accretion is assumed to be a uniform radial deposit around the exposed surfaces of all structural members. The ice thickness should be based on the analysis of historical data, if available, or from the analysis of meteorological data. ASCE 7-98 commentaries provide two ice maps for the contiguous U.S as a guide for selecting design ice loads for ice-sensitive structures. These maps are applicable only for freezing rain icing. The first map was derived from the available physical ice models applied to historical weather data from 230 weather stations. The map does not provide information for the southern and western regions of the U.S. The map provides ice thickness and concurrent wind speed for a 50-years return period. The second map is a freezing rain map for the Pacific Northwest based on ice map developed by Meteorological

Research Inc. (MRI). The MRI map does not provide concurrent wind speed. Again, structures located in more exposed areas such as valleys or mountains should be evaluated individually. The region located directly south of the border with Québec corresponds to ice thickness of one inch (~25mm) and concurrent wind speed of 40 mph (~65km/h). Compared to the S37 map, this region is located partially in class II (25mm) and in class III (40mm).

TIA/EIA-222 (Structural Standards for Steel Antenna Towers and Antenna Supporting Structures)

The ANSI/TIA/EIA-222-F-1996 does not provide an ice map or recommended values for ice thickness. However, the standard requires that ice loads be considered if the structure is located where ice accumulation is expected. Wind pressure should be assumed acting on the ice covered structural members and appurtenances. No specific recommendation is given for wind speed during icing.

CEI / IEC 826 and IEC 60826

The technical report of the International Electrotechnical Commission CEI / IEC 826 " Loading and Strength of Overhead Transmission Lines" will be replaced in 2003 by IEC model standard 60826 "Design Criteria for Overhead Transmission Lines".

IEC 826 provides a standard method to determine the climatic loads for a particular site. The ice load should be estimated using a statistical approach and using historical ice observations at sites along the corridor of the proposed overhead line. Ice measurements should be made on a 30mm conductor located 10m above ground. The reference design load (x) is a function of the reliability level of the line, the mean value and the standard deviation of ice observations, number of years of observations, conductor diameter and height above ground. The estimation of the mean value and standard deviation depends on the type and number of years of observations. If more than 10 years (20 years is recommended) of yearly maximum ice value is available, the design ice load for a given return period can be estimated using the Gumbel probability distribution function

$$x = \bar{x} - \frac{c_2 \sigma}{c_1} + \frac{\sigma}{c_1}\left[-\ln\left(-\ln\left(1 - \frac{1}{T}\right)\right)\right] \tag{2.5}$$

where x is the design value, $\bar{x}$ is the mean value, σ is the standard deviation, T is the return period in years, and C_1 and C_2 are constants that depend on the sample size (number of years of observation).

The mean value is the calculated mean value of the yearly maximum values, and the standard deviation is calculated or estimated as a percentage of the mean value. When only the maximum value of ice during a certain number of years is available, the mean value is estimated as 0.45 of the maximum value, and the standard deviation as 0.5 of the mean value. When there is no direct measurement available, the yearly maximum ice loads is calculated using meteorological data. Combined wind and ice loads on IEC826 are already dealt with in section 2.7.

ISO – TC98/SC3/WG6 (Atmospheric Icing on Structures)

The ISO standard expresses the design ice thickness at a given site by introducing the Ice Risk Level (IRL) terminology. The IRL is used to define ice severity levels to a region or to characterize a particular site. IRL is defined as a 50-year return period ice accretion on a 30mm diameter cylinder rotating around its axis and placed 10m above ground perpendicular to the wind direction. Five categories of IRL are specified for glaze ice, G1 to G5, with corresponding radial ice thickness from 10 to 50 mm respectively. The sixth category G6 is reserved for extreme ice accretions with no specified value for the ice thickness. Similarly, nine categories of IRL are specified for rime ice, R1 to R9, with corresponding ice masses from 0.5 to 50 kg/m respectively. The tenth category R10 is also reserved for extreme accretions. Combined wind and ice loads is treated by considering two load scenarios similar to IEC; the first scenario is low intensity wind combined with high intensity ice; and the second scenario is high intensity wind combined with low intensity ice. The high intensity wind is the 50-year wind pressure reduced by a factor depending on the IRL value, and the low intensity wind is further reduced by a factor that has been not specified. The high intensity ice is the 50-year ice thickness, and the low intensity ice is 30% of the 50-year ice thickness.

Hydro-Québec design criteria

The Hydro-Québec transmission system is a high voltage network covering long distances, parts of which lie in areas prone to heavy icing. Because of this characteristic, ice-related design criteria over the past twenty five years has been more stringent than the Canadian Standard Association Standards and are adjusted upwards periodically when damage due to ice storms occurred or when more data became available.

2.9 Other research works related to icing of structures

Specification of design ice loads is not the only approach for increasing reliability of structures relative to atmospheric icing hazard. Other areas of research are oriented towards the prevention of ice accretion or deicing. Prevention can be achieved by breaking or weakening the ice adhesion using coating compounds applied onto the conductors or the antennas. Deicing can be achieved mechanically by vibration or electrically by heating. Other structural problems related to the presence of ice on structures and conductors are galloping of conductors, ice shedding, flashover and guy wire vibration. However, these topics are outside the scope of the present study.

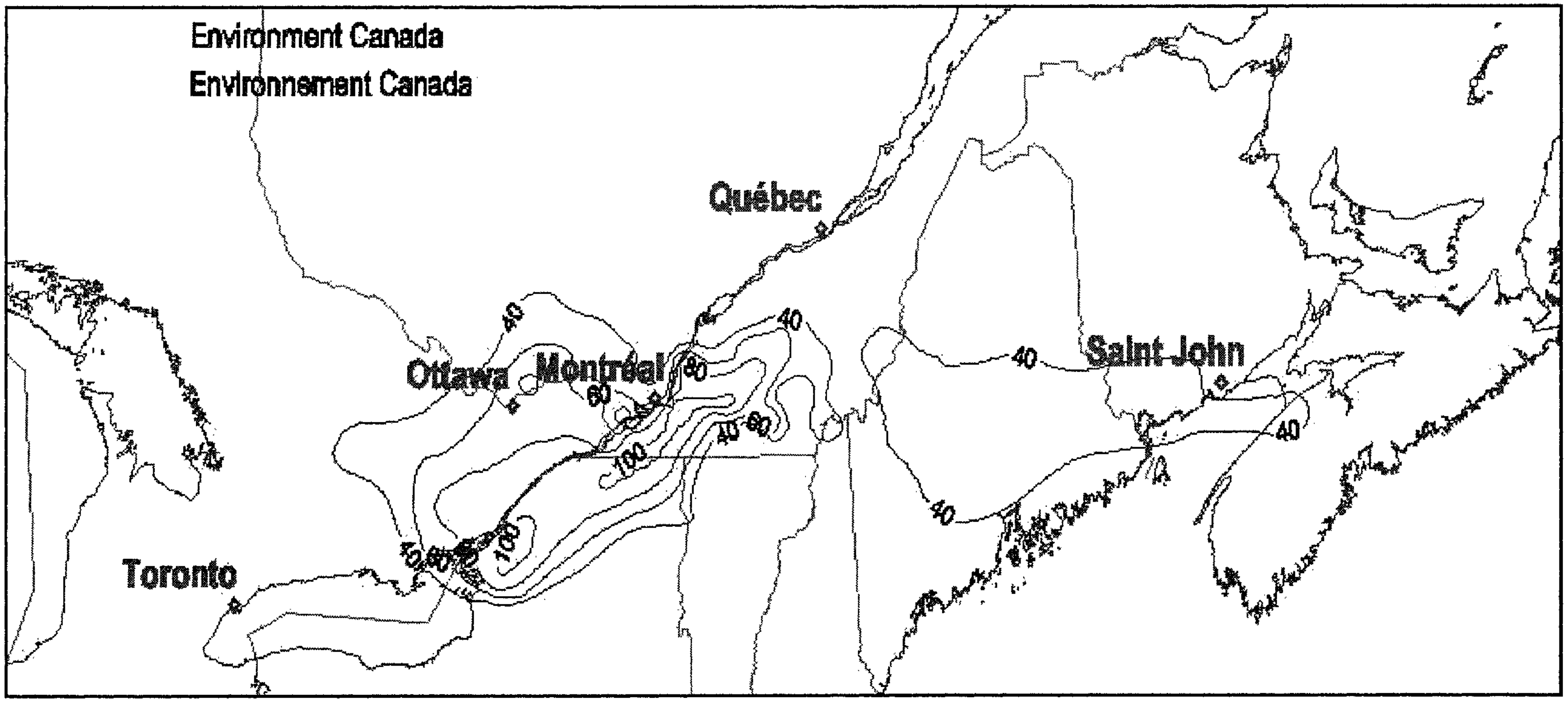

Figure 2.1: Total freezing rain accumulations in mm due to January 1998 ice storm

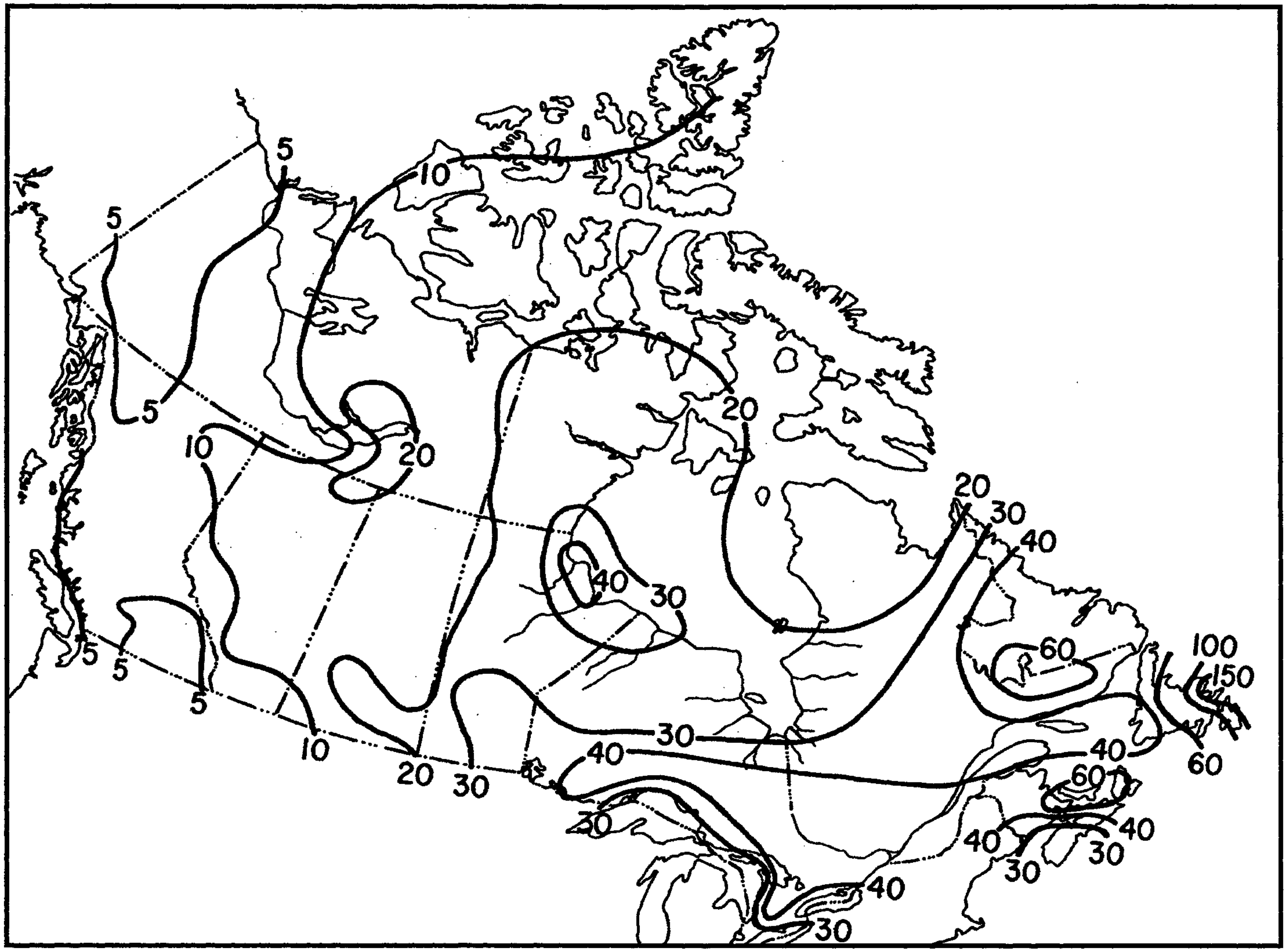

Figure 2.2: Mean annual number of hours with freezing precipitation (Boyed 1968)

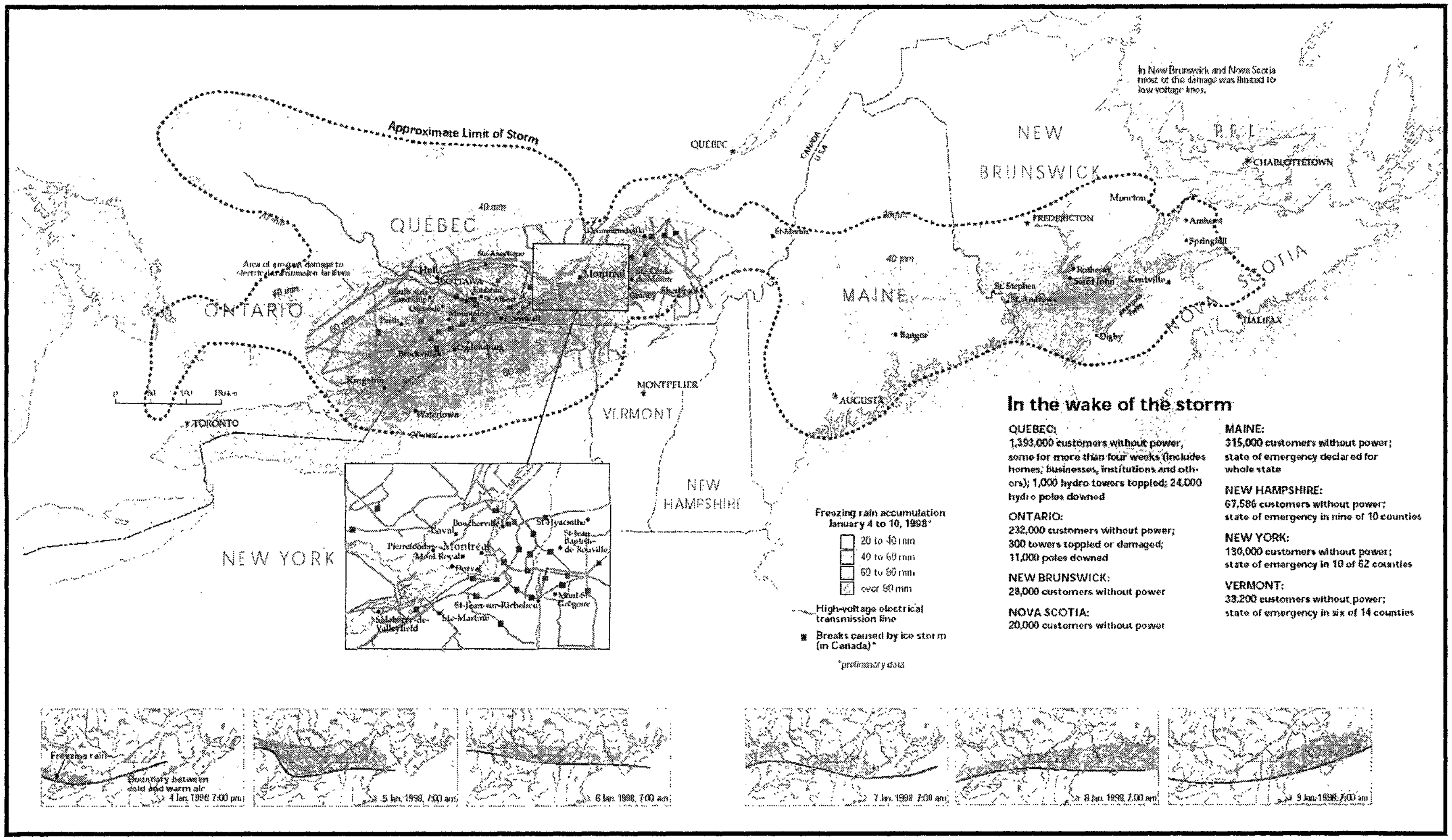

Figure 2.3: Extent of storm of January 1998 (Hydro-Québec 1998)

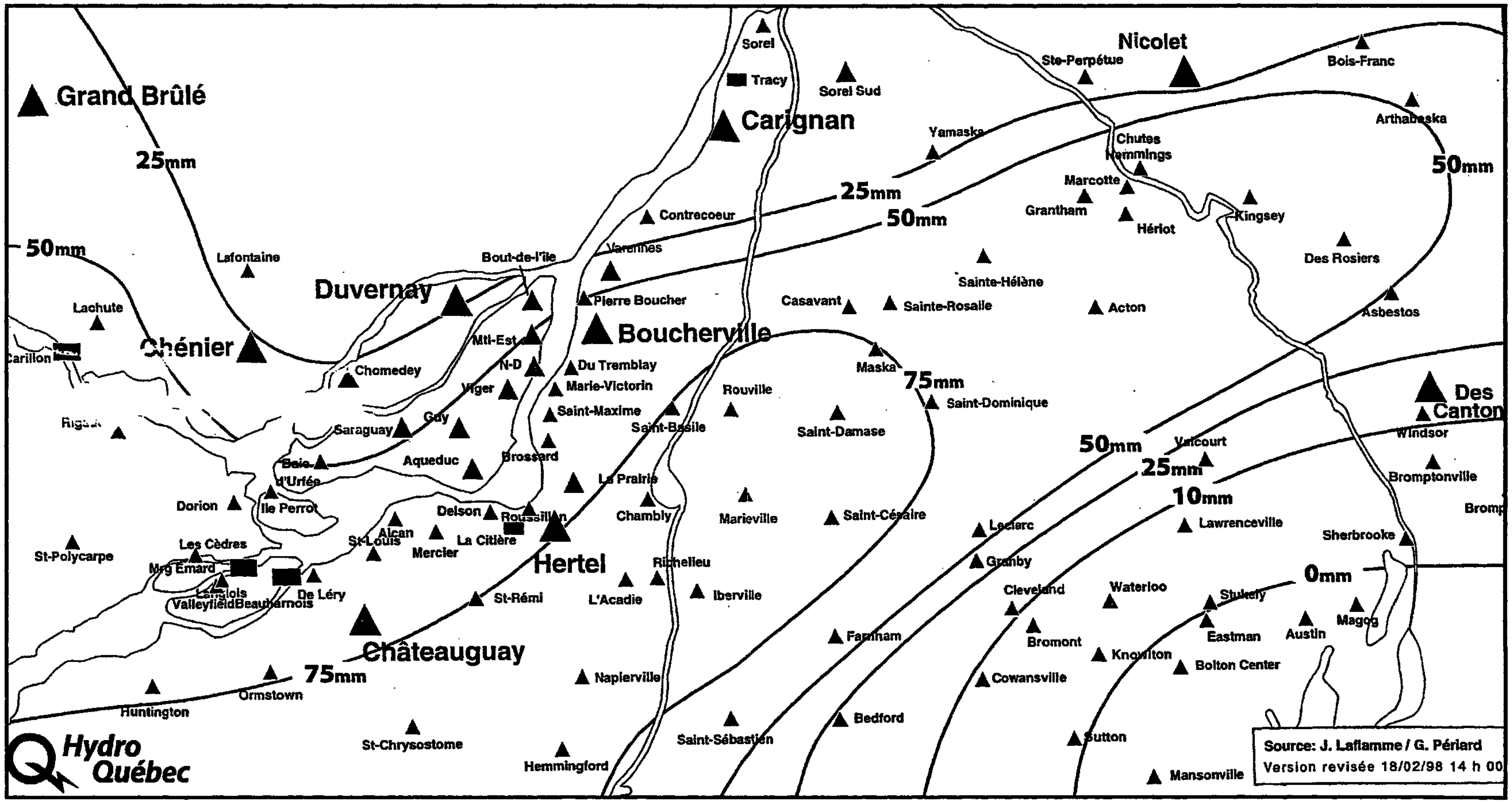

Figure 2.4: Maximum radial ice thickness on a conductor (January 9, 1998 at 6:00pm) in mm

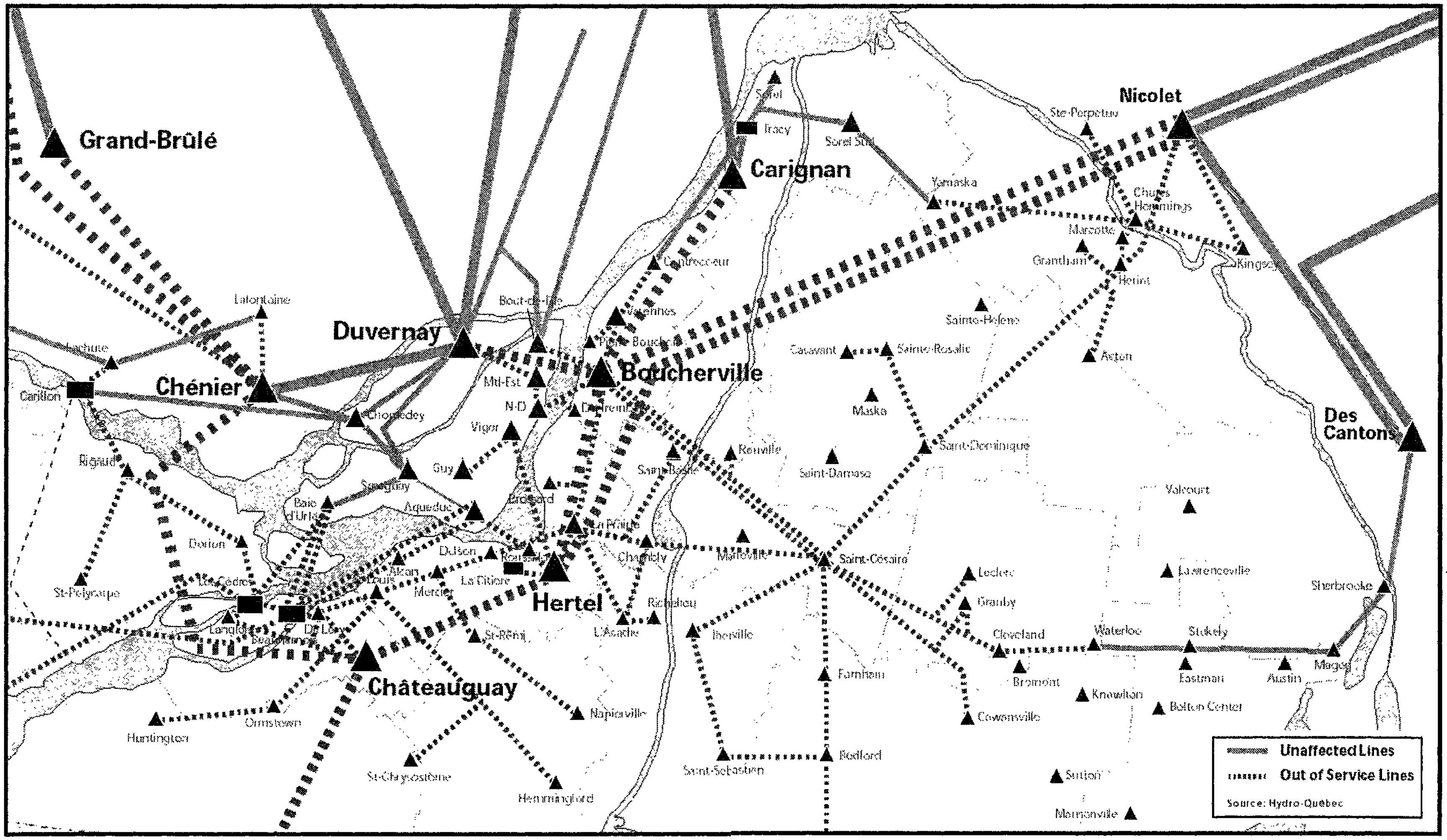

Figure 2.5: Extent of transmission lines damage due to January 1998 ice storm

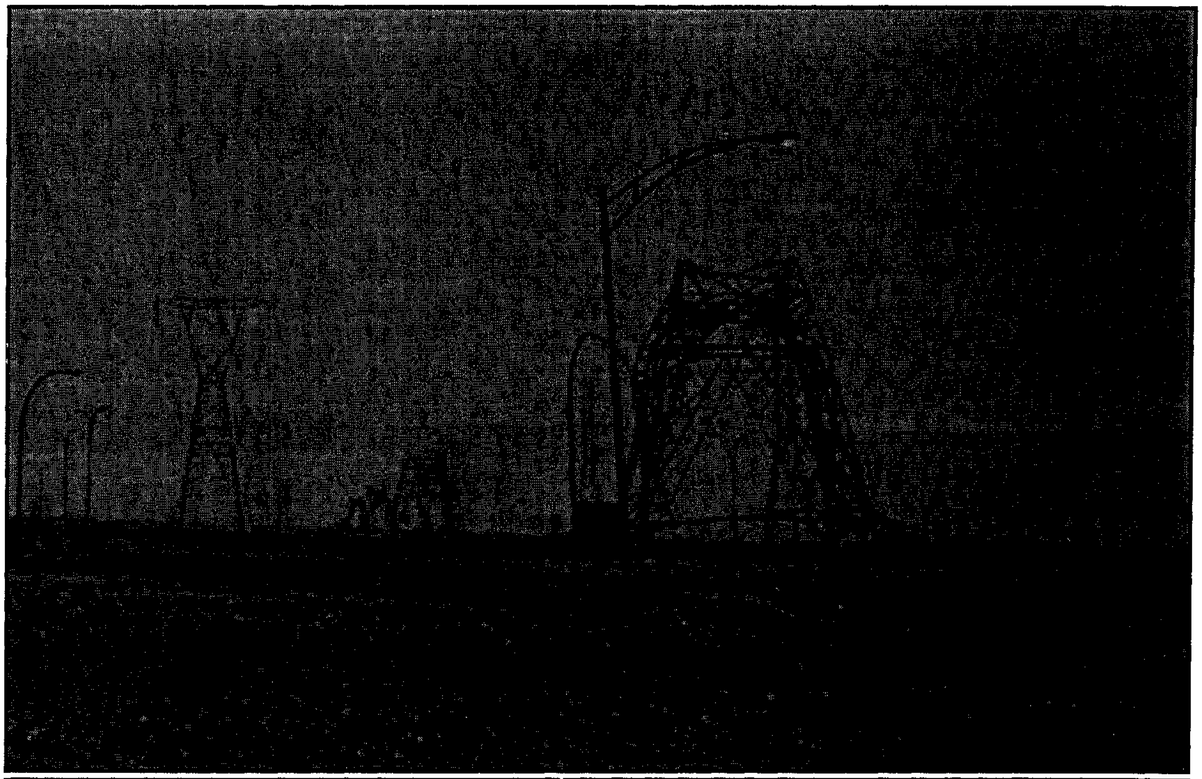

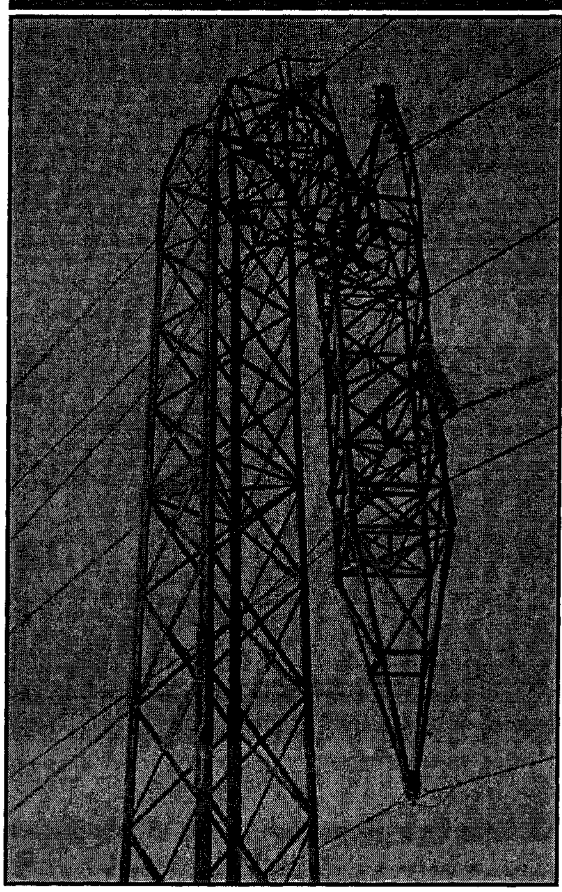

Figure 2.6: Collapse of transmission towers due to January 1998 ice storm (photos by ElFashny)

Figure 2.7: Ice thickness on a conductor and a wire for a collapsed line, on a vertical surface and on a PIM after January 1998 ice storm (Photos by G. Périard)

Chapter 3. Description of the PIM data base

3.1. Hydro-Québec's transmission and distribution network

Hydro-Québec's generating facilities include 49 hydroelectric plants and 29 thermal plants with a total installed capacity of 31,400 MW. More than 93% of this power is produced from hydraulic sources most of which are located up to one thousand kilometers from the load centers. Currently under construction, the Sainte-Marguerite-3 generating station located approximately 800 km north of Montreal with a capacity of 880 MW. In addition to its own generating capacity, Hydro-Québec also has access to most of the power generated at the Churchill Falls hydroelectric plant with a capacity of 5,400 MW.

TransÉnergie, Hydro-Québec's transmission division, is responsible for the high voltage network extending over 32,000 km. Five 735 kV lines carry power from Churchill Falls and the Manic-Outardes complex while six other lines of the same voltage carry power from the La Grande complex. In addition, a 450 kV direct current line runs from James Bay to southern Québec and down to the Boston area. There is also a 765-kV line between Châteauguay, near Montréal, and the Massena substation in New York State. The main arteries of the power system end at the Montréal metropolitan 735 kV loop. The transmission and sub-transmission system includes over five hundred substations to supply the distribution system and major industrial loads. Hydro-Québec's distribution system includes more than 3,000 lines with a total length of approximately 100,000 km. Over 90% of the distribution system is overhead. The Hydro-Québec generation centers and transmission networks are presented on Figure 3.1 (HQ 1998). Hydro-Québec owns and operates its own telecommunication network to provide remote control and protection for lines and equipment of its power grid. The total number of telecommunication towers owned by Hydro-Québec was 187 according to the1991 data (Martoni et al., 1991).

3.2. PIM measurement program

The Passive Ice Meter (PIM) measurement program was initiated in 1974. The purpose of the program was to build a database on icing due to freezing rain and freezing drizzle precipitations on a standardized collector. The program was activated in response to the need to build long-distance overhead lines to transport electricity from major hydropower plants located in the northern part of the province to the populated areas mostly in the southern part of the province. These lines transverse unpopulated regions where information on climatic conditions was limited. Furthermore, failures of lines due to ice storms drew attention to the need for a better understanding of the phenomena and for better estimates of the severity and recurrence of ice loads on structures. The program was conducted in collaboration with the Atmospheric Environment Service of Canada and the Québec Ministry of the Environment, since the instruments were initially deployed in existing climatological and meteorological stations.

3.3. Description of the PIM

The passive ice meter consists of a metal box and two groups of standardized cylinders (Figure 3.2). The dimensions of the box are approximately 125 x 250 x 250 mm and it is placed on a pole at an elevation of 1.5 m. The diameters of the two groups of cylinders are 10 and 25 mm. The PIM was designed to measure ice deposits on the horizontal surface on top of the box, on four vertical faces of the box, and on the two groups of the four cylinders. The vertical faces and the cylinders are oriented toward the North, South, East and West. The intent of this configuration is to simulate different components of transmission lines. Special interest, however, is given to the first set of cylinders (25mm in diameter) that simulates the electrical conductors for overhead lines. Ice accumulation on the conductors is a major contribution to the force imposed on the towers. The other set of cylinders (10mm in diameter) simulates the ground wires, where excessive ice accumulation can cause short circuit. The flat surfaces simulate structural and other components of the towers.

3.4. Observation and recording of ice events

Data is collected between October 15 and May 15 for stations south of 50° in latitude, and between September 15 and June 15 for stations north of 50° in latitude. All forms of frozen deposits that adhere to surfaces and cannot be blown off or brushed off by hand are recorded. Observations are obtained twice a day at climatological stations and more frequent at synoptic stations (at airport weather stations, ice data is collected every 3 hours during freezing events and every 12 hours otherwise). Observations are recorded during and after the storm up until there is no more deposit on any surface.

Ice measurements are recorded on two forms: the data sheet and the monthly summary. Data sheets report ice thickness on different surfaces and directions, type of deposits, precipitation, temperature, and wind speed and direction. Sketches of the shape of the deposit and comments about unusual events are also included on the data sheet. On the monthly summary form, overall deposit information is recorded daily as: 1) nothing, 2) trace, 3) measure, 4) persistence and 5) exceptional ice. For each "measure" entry, one data sheet is filled. If after two days of measurements, the deposit has not changed, the observer records "persistence" for the rest of the days of deposit presence without any further ice thickness measurements.

Three different measuring instruments are used, a dial caliper for the total diameter of the iced cylinder, an outside caliper to measure deposits on the sides of the box, and a graduated pick to measure the ice deposit on the horizontal surface. The measurements of the thickness of deposits on the cylinder and the sides always include the diameter of the cylinder and the thickness of the side plate respectively. All measurements are for the maximum ice thickness along each surface (Figure 3.3).

Observations collected during icing storms are: (1) the type of ice deposit, (2) the total accumulation on each collector, (3) the type and amount of precipitation, (4) the ambient air temperature, (5) the wind speed and direction, and (6) the start and end of the precipitation. The deposits are categorized as rime ice, glaze ice, glaze ice with icicles, and other frozen deposits (refers mostly to wet snow). The precipitation is either snow or rain or both, and the amount of precipitation is the total water depth in millimeters. Ambient air temperature is measured to the tenth of a degree Celsius. Wind speed and direction are measured instrumentally at synoptic station and manually at other stations. Wind speed is measured in kilometers per hour and wind direction in degrees clockwise from the north. The start and end of precipitation are also recorded in days and hours.

3.5. Temporal and spatial coverage

The Passive-Ice-Meter (PIM) program was initiated with 35 stations in 1974. In the following years new stations were added, some were closed, replaced or transferred to other sites. At the time the data was initially received (1994/95 winter season), a total of 249 PIMs had been installed, but records for 31 of these had been removed from the database due to unreliable data. From a remaining total of 218 stations, 148 were still active and 70 were closed (Figure 3.4). Among the permanently closed stations, 32 stations are listed separately in the database, while data for 38 stations were transferred to currently active neighbor stations.

In total, observations for 180 stations are available in the database covering periods varying from 1 to 21 years. Figure 3.5 shows the number of stations and the corresponding observation periods. As of the winter of 1994/95, there were 25 stations with 21 years of continuous operation; 66 stations with observations during 20 years or more; and 138 stations with at least 10 years of observations.

In 1995, meteorologists at Hydro-Québec have validated the database for accuracy and reliability. For the 180 stations, 3 stations were completely eliminated and part of the data was eliminated for other 30 stations.

The PIM program was developed mainly for obtaining design criteria for transmission lines. Consequently, the spatial density of the PIMs conforms more or less to the location of the transmission network. As a result most of the instruments are located within the St.-Lawrence Valley, Lac St.-Jean, and the southeastern part of the province. The PIMs in the North of the province are very sparsely distributed. Detailed information about each station includes an identification number, name, longitude, latitude, and elevation is shown in Appendix A.

3.6. Description and classification of the database

All data was original provided in 1995 by the Service études et normalisation of Hydro-Québec. Three groups of files were provided: 1) the station information file, 2) the icing events files, and 3) the persistence and trace files.

The stations information file lists the identification number, name, longitude, latitude, elevation, declination, type, affiliation, region, and state of each station. There are three types of stations: Climatologic, Synoptic and Other. There are five affiliations : Environment-Québec, Environment-Canada, Ministère du Transport, Hydro-Québec(SEBJ), and others. The state of a station is: Active or Closed (Table 3.1). Finally, the stations are grouped into 10 different administrative regions (Table 3.2).

The icing events files comprise separate files for each region, and contain information relative to each recorded icing event. This information includes: the date and time of the observation and precipitation, temperature, wind, and ice deposit measurements. Table 3.3 shows an example of the recorded data with the name and the measurement units for each field. The icing events files contain 13,000 records of icing events with a possible field of 37 descriptors for each event.

Table 3.1: State, type and affiliation of PIM stations as of 1995

Qualification	Category	Number of stations
State	Active	148
	Closed	70
Type	Climatologic	174
	Synoptic	39
	Other	5
Affiliation	Environment-Québec	172
	Environment-Canada	25
	Ministère du Transport	16
	Hydro-Québec(SEBJ)	2
	Others	3

Table 3.2: Number of stations by regions

Region name	Region number	Number of Stations
Laurentides	50	24
La Grande	70	21
Maisonneuve	11	7
Manicouagan	13	21
Matapédia	80	26
Mauricie	60	14
Montmorency	40	37
Richelieu	30	15
Sagueney	90	13
Others	99	2
Total after transferring		180

The persistence and trace files comprise separate files for each region. The fields include the date and time of the observation and a logical variable "P" or "T" for persistence or trace respectively. Persistence is defined as a deposit on the ice meter for more than two consecutive days without any changes. A trace is a deposit less than one millimeter thick. Ice events are recorded either in the events or persistence/ trace files but not in both.

3.7. Data filtering

The stations that had been grouped and those with non-continuous operation were excluded. The observations are grouped per winter season starting on September 15 and ending on June 15 of the following year. The opening and closing dates of each station are provided in separate file. Any icing events reported outside these dates were removed from the data set.

The data was filtered to remove outliers or erroneous data, such as glaze icing with thickness over 100mm. Missing data appears as "9s" in the database and are not considered except if data is only partially missing (e.g. if the accretion records exists in some directions and missing in the others).

Appendix B shows the number of events for each station and each winter season. The shaded areas represent gaps in the operation of the station as a result of: the opening or closing dates of the station; unreliable information during a certain period; transferring of the data between neighboring stations; or closing of a station for a certain period. Zeros represent a season without any icing event.

The data set is stored in a multi-dimensional array where rows represent time, columns represent the station number, and the third dimension represents the different types of observations. Next, the data was carefully examined to identify missing or mislabeled records, irregular sampling time intervals, bias in observations due to rounding of measurements, and misclassification of the type of accretion (rime, glaze, or wet snow).

3.8. Data analysis

Three statistical processes are required for the estimation of the ice hazard function: 1) the temporal variation in the severity of storms, and 2) the spatial variation of the recurrence (arrival) rate of icing storms, and 3) the residency period of ice on the structural members. For present purpose, the only ice types considered are glaze ice and glaze ice with icicles. Furthermore, only the maximum accretion on the four 25 mm cylinders is considered.

In order to increase the sample size, an event-based model, in which every icing event is counted as an independent event, is adopted in this study. In this case, the maximum observed value for each storm is considered instead of only the yearly maximum observation. The first step in the analysis is to identify icing events both at individual stations and from a regional perspective.

For site-specific analysis, observations of ice accretion on consecutive days at the same site are considered as a single event, and only the maximum of these observations is used in the analysis. Figure 3.6 shows the average and the maximum number of icing events per year for each station.

The number of events in each season varies considerably from year to year and from station to station; from no event up to 18 events. The average yearly number of events for all stations varies from 0.7 in 1993/94 to 3.7 in 1982/83. It should be noticed that the number of events does not account for the severity of the icing.

The maximum yearly events from each station provide a sample of 21 observations at the most. However, the large number of years with no events further reduces the sample size. For example, Lac-Berry has 20 years of observations but only 8 years with non-zero observations. Pooling of adjacent stations can overcome this problem by increasing the sample size. Event-based model is another alternative, which has been used here. In this case every icing event is counted as an independent event.

The second factor is the residency period of the ice on the structure. The longer the residence period the more likely the exposure of the iced structure to high wind speeds. Consecutive days of ice observations are considered as a single event; and the number of consecutive days is counted towards the residency period for this event. The days identified as persistence in the trace/persistence files are added to the residency period. Most of the events have duration of only one day, and the maximum persistence periods are 37 and 36 days at Duchesnay and Val-D'or-A respectively. The maximum average persistence is 3.3 days per event at St-Jean-de-Cherbourg station (Figure 3.7).

3.9. Definition of icing events

Different types of event-based models can be derived from the data set depending whether the analysis is site specific or regional. In both cases, events are assumed to be independent. The variables of an event-based model are the yearly number of storms, the severity of the storms defined as the maximum ice accumulation, and the persistence of the storm defined as the period of time until complete melting or shedding of the accumulated ice. The first two variables are used to estimate the ice hazard function, while the last variable is used to estimate the wind on ice hazard function. The icing hazard function is defined as the exceedance rate (expected number of events per year) with ice accumulations larger than the specified thickness (t),

The initial and most important step in the formulation of an event-based model is the definition of the events. The complete sequence of an ice storm consists of: (1) the start of freezing precipitation, (2) ice accumulation, (3) the end of precipitation, (4) a period of residency of ice accumulation on objects, and (5) melting or shedding of the ice. The PIM records are obtained at intervals of 3 to

12 hours and often do not document the complete sequence of each storm. However, data (e.g. temperature, precipitation) from meteorological stations and from neighboring stations can be used to characterize each event.

Empirical rules for the identification of individual storms were next derived from prior knowledge on storm characteristics and by using engineering judgment. For this purpose, episodes are defined as continuous periods of time over which glaze ice is accumulating, while events are defined as continuous periods of time over which glaze ice is present on the PIM (or PIM network) and may consist of several episodes.

For example, previously published data indicate that the maximum storm duration of freezing rain is 26 hours (Environment Canada, 1984). In consequence, records within the same 24 hours period are a priori considered as part of a single episode. After 24 hours of the start of an episode, any new accretion is considered as a new one. Otherwise, any existing ice is attributed to the persistence of the ice accretion from the earlier episode. In the case of very severe storms, both in terms of ice accumulation and spatial extent, a new episode of ice accumulation may occur before the disappearance of ice from the previous one. If only glaze is present during the duration of the episodes, the maximum ice thickness measured on the 25mm cylinder for the duration of the event is included in the sample.

This procedure is first performed for all individual stations for the estimation of site-specific icing hazard functions without considering neighboring stations. Second, icing events at each station are defined on a regional basis for the purpose of estimating regional variations of the icing hazard function and to account for simultaneous occurrences of glaze ice at neighboring stations. The procedure for the identification of atmospheric icing events at a regional level is based on the analysis of the total regional ice accumulation as a function of time. For this application, only the southern portion of the province that is well covered by the PIM network is analyzed.

First, a Voronoi tessellation is generated using the points defining the location of the stations (Figure 3.8). The Voronoi tessellation separates the region into polygons such that points within each polygon are closest to the station at the center of the polygon. The polygons can be obtained by connecting the midpoints of the segments of a Delaunay triangulation that originate from a given station.

The Delaunay triangulation is defined by a set of triangles with stations as vertices such that no station is contained in any triangle (Figure 3.9). The Voronoi tessellation is used to calculate the tributary area associated with each station. Adjoining polygons are also used to identify the set of neighboring polygons to estimate the spatial extent of each icing event. The intensity of a storm on a regional scale is measured by the total volume of ice accumulation over the region as a function of time. In first approximation, the total volume is estimated by assuming that the ice accumulation within each polygon is constant and equal to the accumulation at the associated station,

$$h\,(\underline{x}) = h_i \tag{3.1}$$

where $\underline{x}$ are the spatial coordinates of a location that is contained in the polygon *i*. The total volume of ice over the region as a function of time is estimated as,

$$T_I(t) = \sum_i h_i(t).A_i \tag{3.2}$$

where A_i is the area of the polygon i. Similarly, the total area affected by an ice storm as a function of time is estimated as,

$$A(t) = \sum_i A_i \tag{3.3}$$

where the summation is only over polygons for which h_i is non-zero. Using both of the above quantities, the normalized ice thickness as a function of time is defined as,

$$H_N(t) = \frac{T_I(t)}{A(t)} \tag{3.4}$$

The function $T_I(t)$ is useful for displaying the relative severity of ice storms as a function of time, for analyzing the relative proportion of storms of different intensity, and for detecting any pattern in their recurrence rate. The function A(t) is useful for measuring the spatial extent of the region affected by each storm regardless of the actual amount of ice in each storm. Finally, the function $H_N(t)$ is useful for measuring the relative severity of the storms in terms of the average accumulated ice.

Individual icing events can be identified and classified for further analysis by analyzing the variation of all of the above three quantities as a function of time. The beginning of a storm event corresponds to a sudden increase of all three quantities. This increase can last several days as several storms which are part of the same atmospheric system passes over the region. The icing event is considered as a single event even if several storms are involved as long as the total amount of ice ($T_I(t)$) is non zero. All three quantities typically attain a maximum value and then start decreasing with melting or ice shedding over the affected region.

Figure 3.10 shows the variation of the total amount of ice for the 21 years of record over the region. Figure 3.11 shows in detail the evolution of the total accumulated ice, total number of affected stations, and average ice accumulation in December 1990. Based on the analysis of these functions three major regional icing events and three localized icing events can be identified. Figure 3.12 shows the details of the sites affected by the storms from December 13 to December 25.

Stations with measurable accumulations are marked with a circle and the shaded polygons delimit the region affected by the storms. The shading of the polygons goes from light to dark in the chronological sequence of episodes. In this case, the sequence of episodes indicates that ice accumulation occurred over overlapping regions that increase in size as a function of time. From a design point of view, the series of episodes are considered as a single event since ice accumulation is continuously present in the affected regions.

Table 3.3: Example of recorded data with the name and the measurement units for each field.

1	2	3	4	5	6	7	8	9	10	11	12	13	14	15	16	17	18	19	20	21	22	23	24	25	26	27	28	29	30	31	32	33	34	35	36	37
											Start/End of storm				Type flag						Ice deposite in mm															
Station Number	Station Name	Year	Month	Day	Hour	Rain in mm	Snow in mm	Temp. in 1/10 C	Wind Direction	Wind Speed km/h	Day/Start	Hour/Start	Day/End	Hour/End	Rime	Ice	Icicle	other	Quality Flags		Above	Diameter of icicle	Number of Icicles	Other Types	North Wire	North Cylinder	North Surface	East Wire	East Cylinder	East Surface	South Wire	South Cylinder	South Surface	West Wire	West Cylinder	West Surface
7025250	Montreal--A	80	11	8	7	20	14	-14	0	13	7	18			0	0	0	1			22				0	0	89	0	0	0	0	0	0	0	0	0
7025250	Montreal--A	80	11	8	19	0	4	9999	999	99			8	14	0	0	0	1			0				0	0	82	0	0	0	0	0	0	0	0	0
7025250	Montreal--A	80	11	9	7	0	0	-25	6	8					0	0	0	1			0				0	0	20	0	0	0	0	0	0	0	0	0
7025250	Montreal--A	80	11	9	9	T	6	-24	80	19	9	8	99	99	0	1	0	1			6				11	26	23	11	26	5	11	26	0	11	26	0
7025250	Montreal--A	80	11	10	10	0	T	2	260	30	10	9			0	0	0	1			0				0	0	0	0	0	0	0	0	0	0	0	4
7025250	Montreal--A	80	11	10	13	0	4	-16	260	26					0	0	0	1			0				0	0	0	0	0	0	0	0	0	0	0	32
7025250	Montreal--A	80	11	10	16	0	8	-14	270	12					0	0	0	1			0				0	0	0	0	0	0	0	0	0	0	0	8
7025250	Montreal--A	80	11	10	19	0	10	-16	270	11					0	0	0	1			0				0	0	0	0	0	0	0	0	0	0	0	6
7025250	Montreal--A	80	11	14	8	T	50	1	260	6	13	21	14	7	0	0	0	1			48				20	51	T	17	44	0	23	50	0	19	41	11
7025250	Montreal--A	80	11	25	17	9999	999	2	330	13	25	15			0	0	0	1			2				13	28	12	0	0	0	0	0	0	11	28	8
7025250	Montreal--A	80	11	25	20	0	30	-13	290	17					0	0	0	1			2				11	30	25	12	28	0	12	32	0	11	28	11
7025250	Montreal--A	80	11	25	23	0	30	-25	280	20					0	0	0	1			2				11	30	25	11	28	0	12	31	0	11	28	9
7025250	Montreal--A	80	11	26	7	0	7	-80	240	13			26	1	0	0	0	1			T				0	0	16	0	0	0	0	0	0	0	0	8
7025250	Montreal--A	80	11	26	19	0	37	-53	250	11					0	0	0	1			0				0	0	6	0	0	0	0	0	0	0	0	0
7025250	Montreal--A	80	11	27	2	0	0	-81	00C	0					1	0	0	1			T				T	T	6	T	T	T	T	T	T	T	T	T
7025250	Montreal--A	80	11	27	7	0	0	-84	10	2					1	0	0	1			2				12	27	8	12	27	T	T	T	T	T	T	T
7025250	Montreal--A	80	11	28	7	T	0	-28	50	8	28	3			0	1	0	0			1				T	26	5	T	27	6	11	26	4	11	26	4
7025250	Montreal--A	80	11	28	10	51	0	-15	60	19					0	1	1	0			5				15	31	8	15	30	8	16	31	0	14	30	0
7025250	Montreal--A	80	11	28	13	103	0	5	70	7			99	99	0	1	1	0			6				20	32	9	20	34	9	22	35	0	19	32	0
7025250	Montreal--A	80	12	3	5	22	8	-28	240	33	3	2			0	0	0	1			0				0	0	0	0	0	0	0	0	5	T	T	5
7025250	Montreal--A	80	12	3	17	0	104	-85	280	37			3	14	0	0	0	1			0				0	0	0	0	0	0	0	0	5	0	0	5
7025250	Montreal--A	80	12	7	23	2	0	-19	20	9	7	20			0	1	0	0			2				11	26	5	11	26	5	T	T	0	T	T	0
7025250	Montreal--A	80	12	8	2	T	0	-18	350	4			8	1	0	1	0	0			T				T	26	T	T	26	T	T	26	0	T	T	0
7025250	Montreal--A	80	12	8	7	T	0	-22	40	2	8	6			0	1	0	0			T				T	26	6	T	26	T	T	26	0	T	T	0
7025250	Montreal--A	80	12	8	10	T	0	-8	1	18			8	12	0	1	0	0			1				11	26	4	T	26	0	T	26	0	T	26	0
7025250	Montreal--A	80	12	13	14	T	6	-74	270	19	13	0	13	2	0	1	0	0			0				0	0	5	0	0	0	0	0	0	0	0	0
7025250	Montreal--A	80	12	24	9	2	T	-4	220	11	24	6			0	1	0	0			T				T	T	0	T	T	0	11	26	5	T	26	5
7025250	Montreal--A	80	12	24	21	0	40	-185	330	13					0	1	0	1			4				T	T	T	T	T	T	T	T	T	T	T	T
7025250	Montreal--A	80	12	25	9	T	48	-310	280	26			25	0	0	1	0	1			3				T	T	0	T	T	0	T	T	T	T	T	T

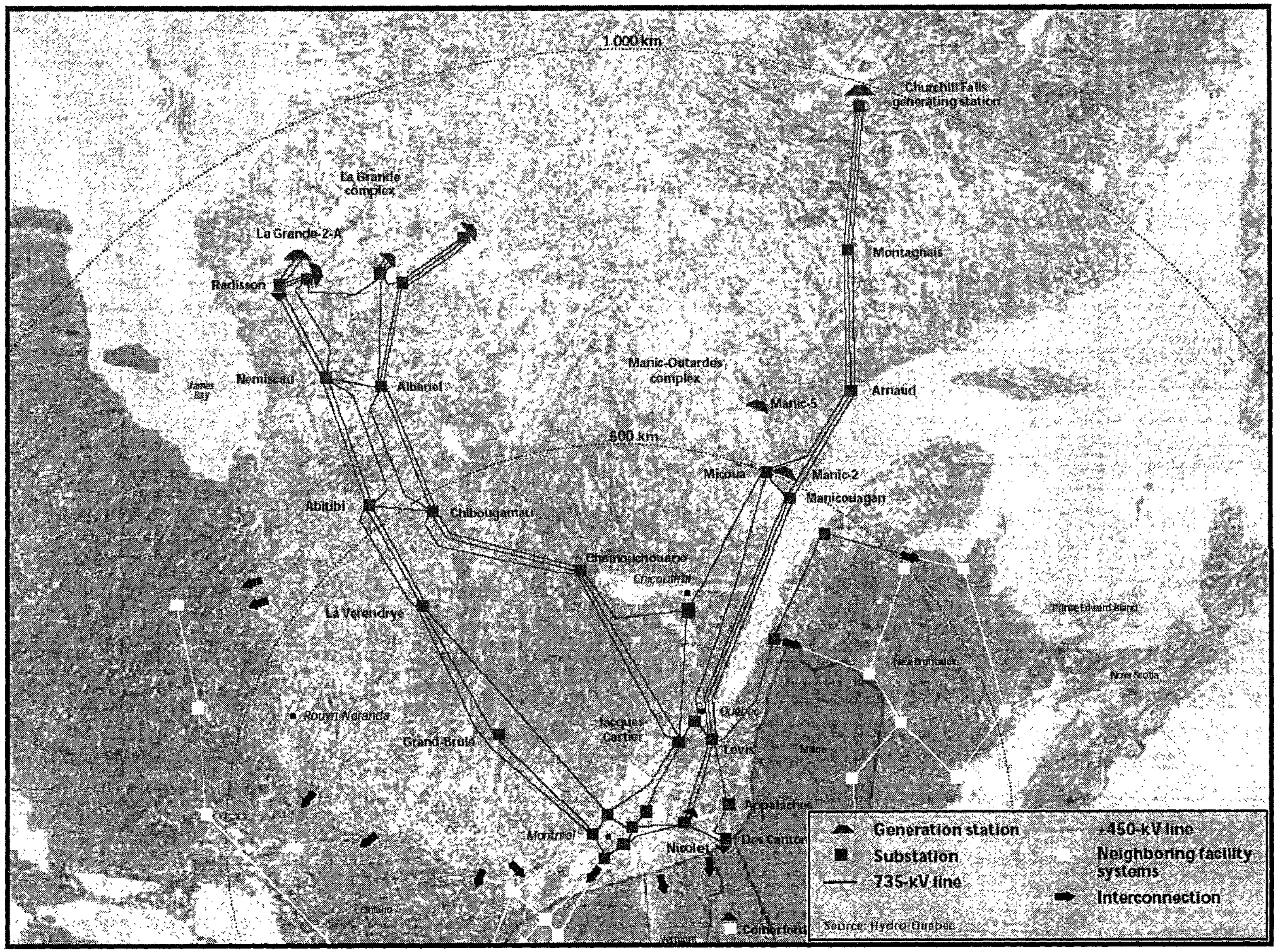

Figure 3-1: Hydro-Quebec Transmission System (Hydro-Quebec 1998)

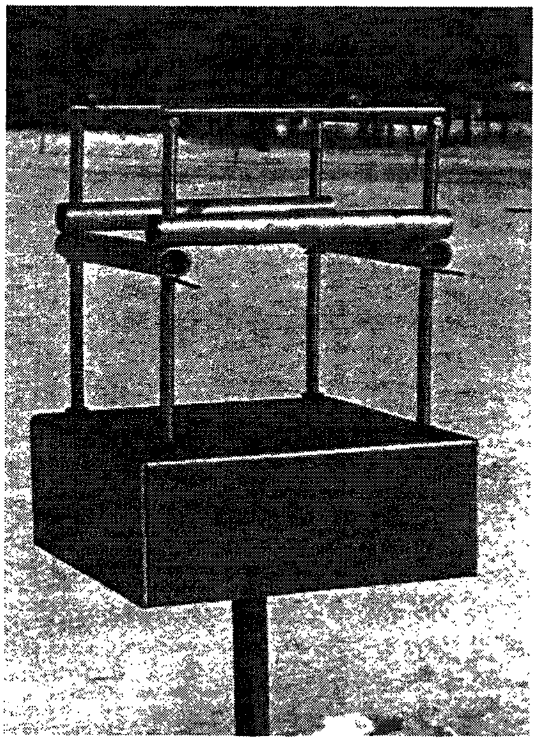

Figure 3.2: The Passive Ice Meter

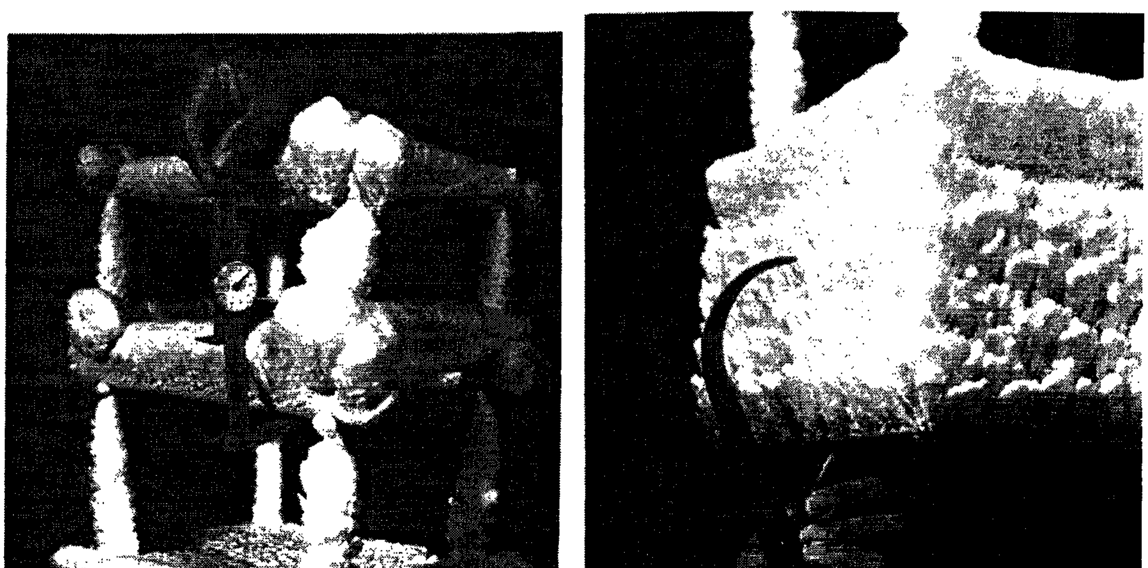

Figure 3.3: Measurement of ice around the cylinder and on the side of the box

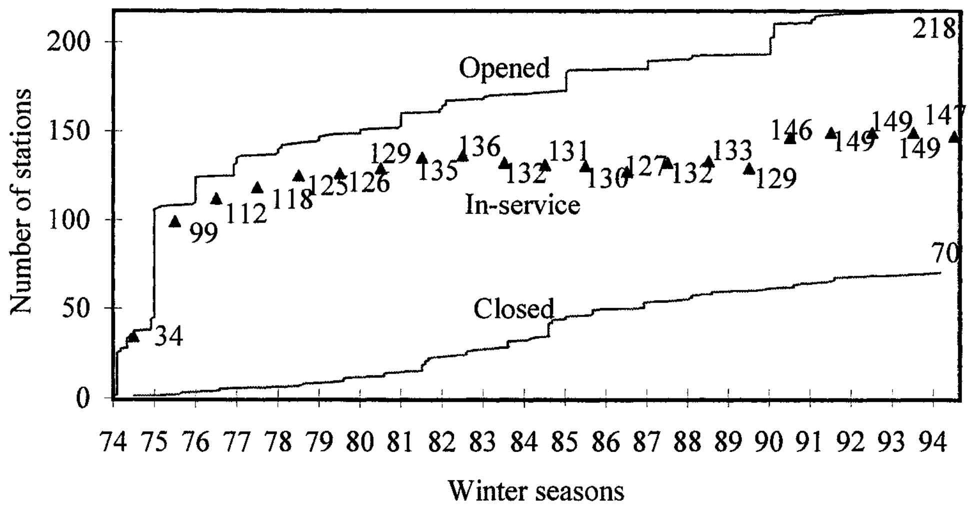

Figure 3.4: Cumulative number of PIM stations during each winter season

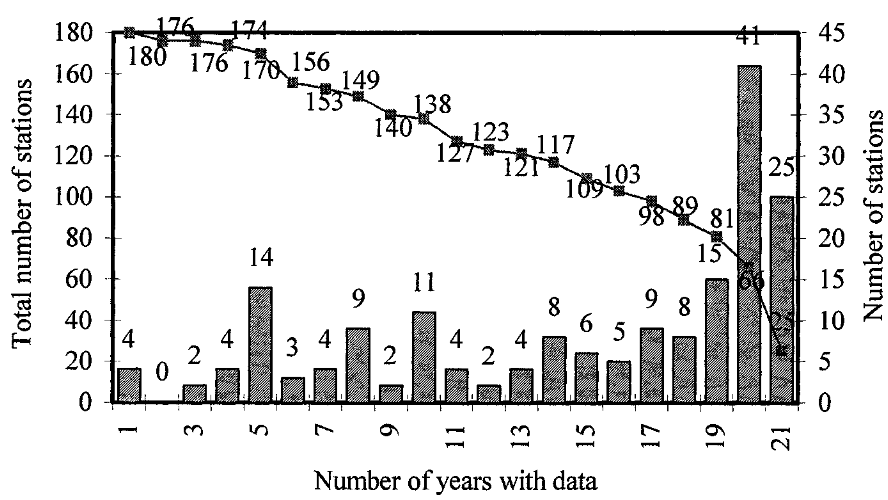

Figure 3.5: Number of stations versus increasing observation periods

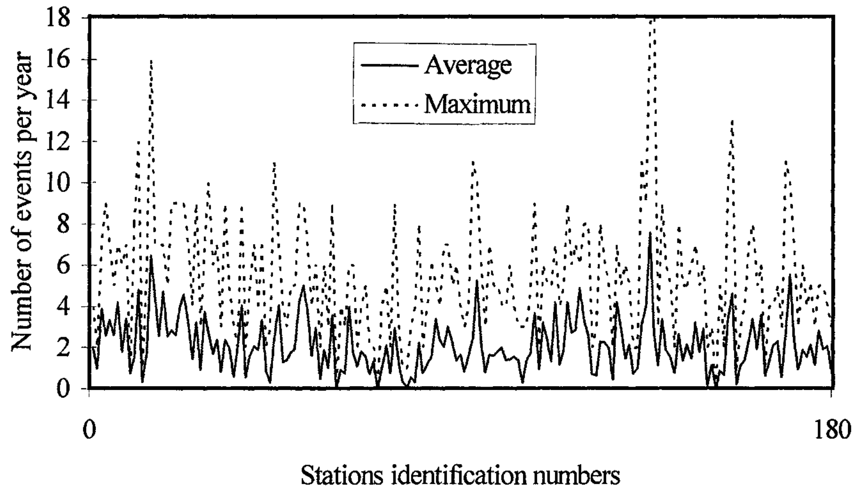

Figure 3.6: Average and maximum number of icing events per year for each station

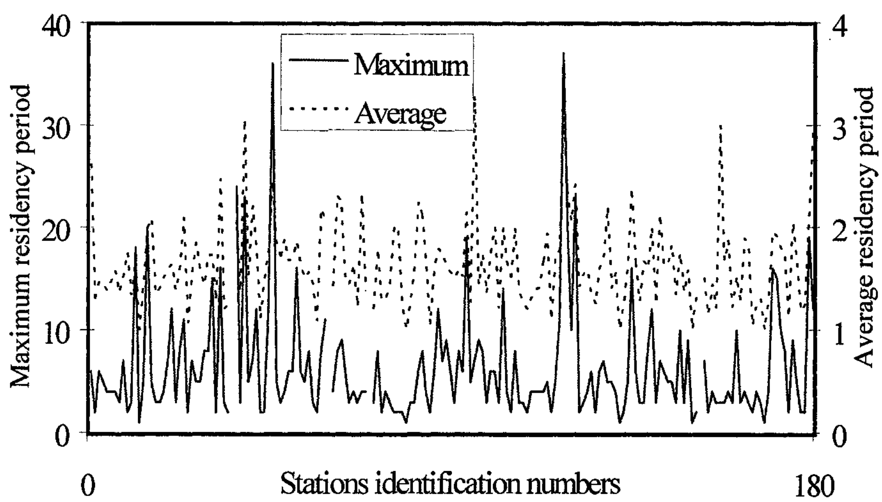

Figure 3.7: Maximum and average residency periods in days for each station

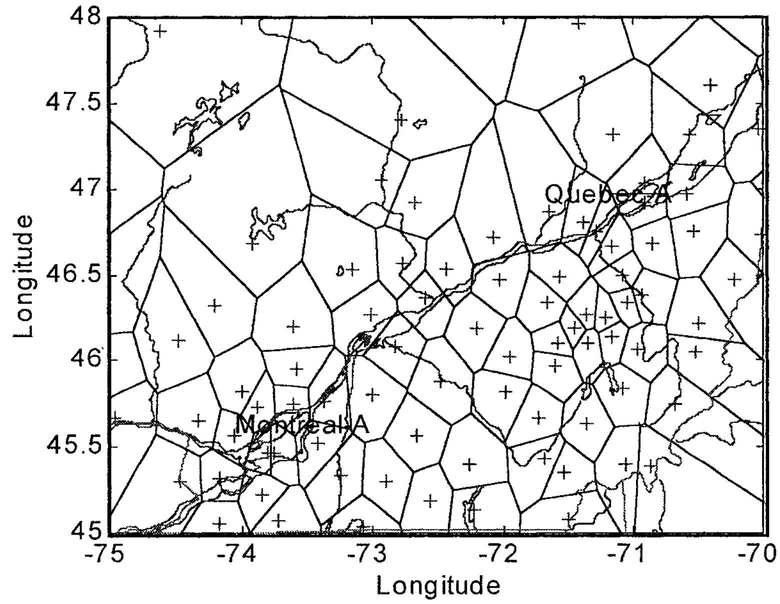

Figure 3.8: Voronoi tessellation for stations on Southern Quebec

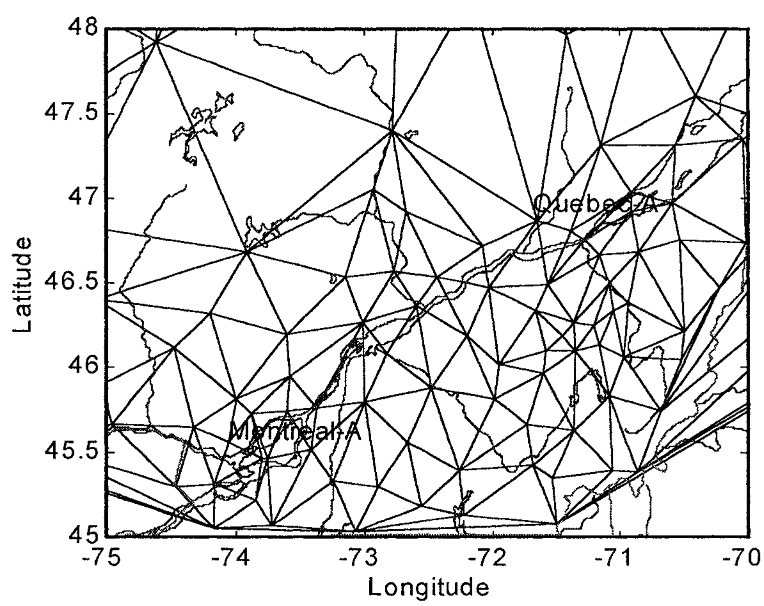

Figure 3.9: Delaunay triangulation for stations on Southern Quebec

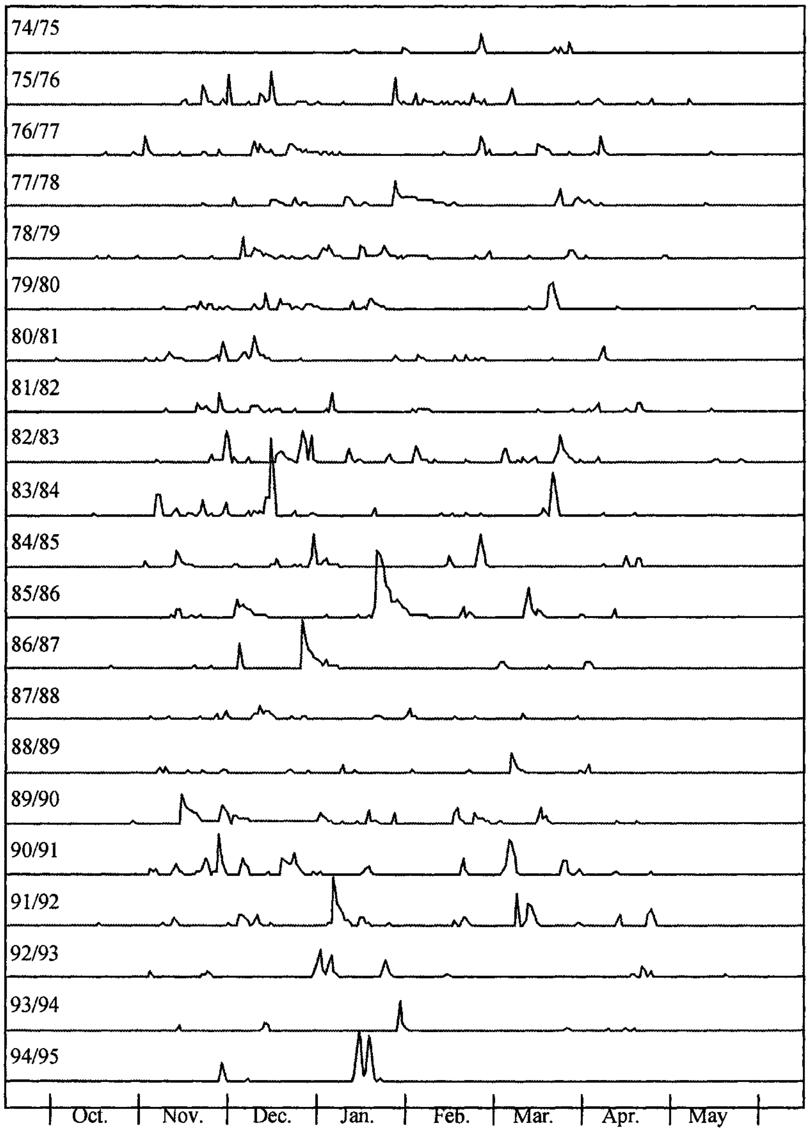

Figure 3.10: Cumulative complete records for the 21 seasons (from Sept. 15, to June 15)

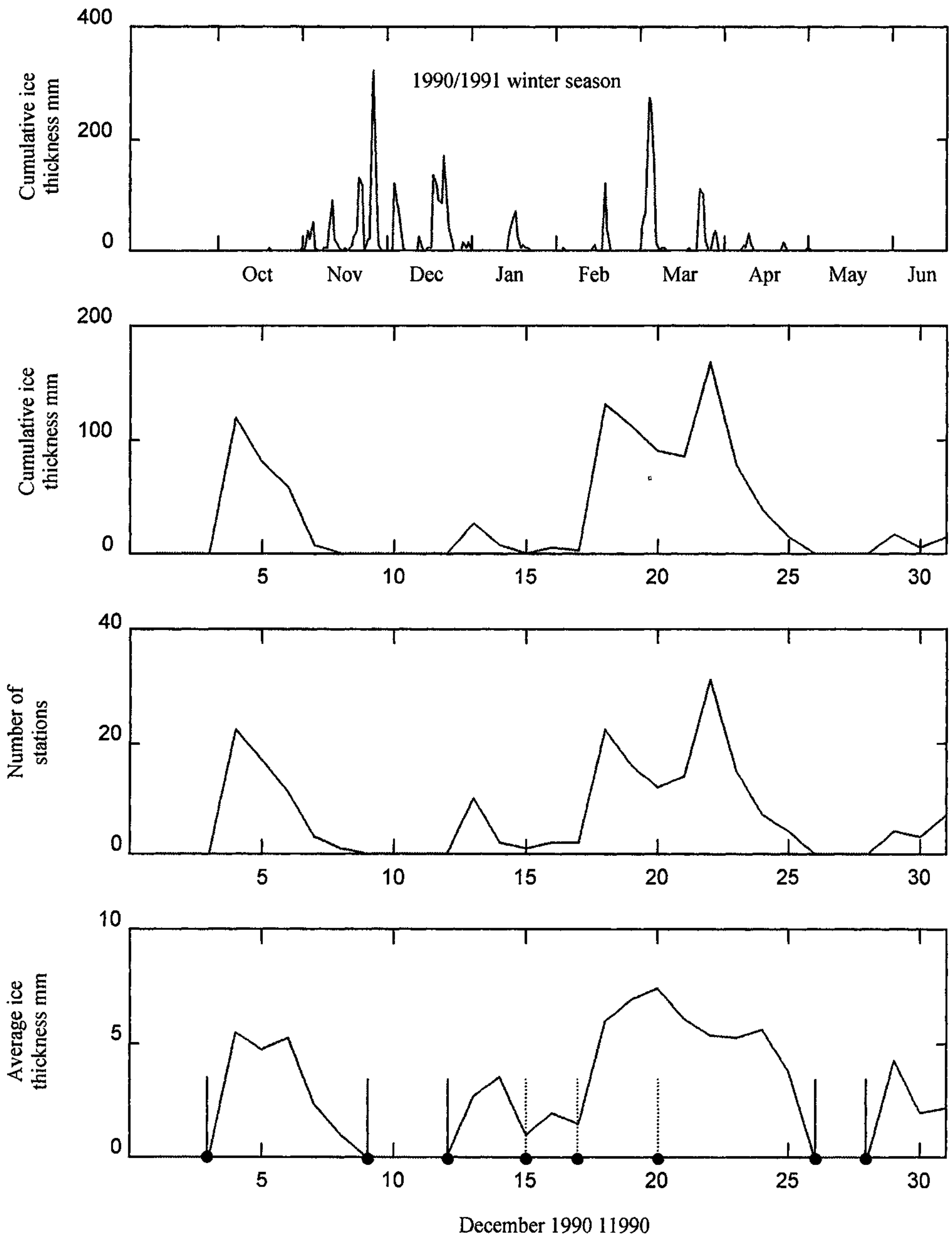

Figure 3.11: Summary of ice accumulation records for December 1990

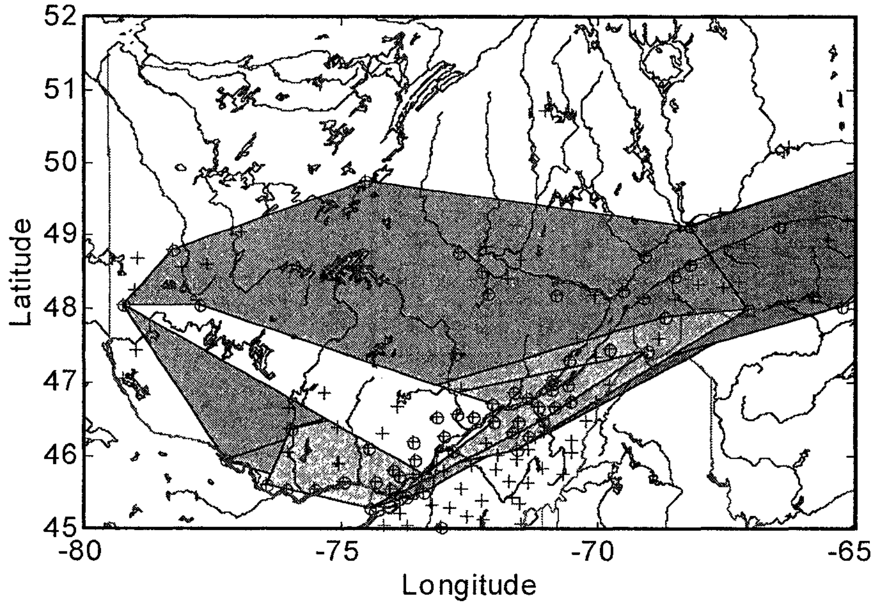

Figure 3.12: Stations affected by storms in December 1990

Chapter 4: Ice-Thickness Probability Distribution Function

4.1. Introduction

Statistical approach to the analysis of ice accumulation data is desirable because of the numerous sources of variability in the physical processes that give rise to observed events. Statistical methods acknowledge the existence of variability and enable its effects to be quantified. The selection of a probability distribution function is very important for the estimation of the severity of icing events with long return periods, typical of those used in designing electric transmission or telecommunications networks.

In general, there are very few direct observations of icing events from which to form a statistically significant sample. Accordingly, there have been virtually no comparative studies on the selection of probability distribution functions for the severity (measured as the total ice accumulation) of ice storms. Traditionally, in the few existing studies, the Gumbel distribution has been used to model the yearly maximum ice accumulation on structures (Laflamme, 1995; Eliasson and Thorsteins, 1993; Fahelson, 1995).

In this chapter, distributions found to be useful in the analysis of extreme environmental events, such as precipitation and floods (Wilks, 1993 and Anderson, 1995), are applied to freezing rain data and compared in order to evaluate their fitness to represent the parent distribution of the given sample (the available data set).

Twelve probability distribution functions are considered for the severity of glaze ice storm data. The distribution parameters are estimated either by the method of L-moments or the method of Maximum Likelihood. The distributions are compared on the basis of the overall fit to the data and the sampling characteristics of the right tail of the distributions.

For the purposes of this analysis, an event at a given station is defined as an uninterrupted period of time with continuous ice observations. The length of the period of observation and the total number of events vary considerably from station to station. Therefore, a subset of 45 stations with at least 20 years of observations and 20 icing events was selected (Figure 4.1). Preliminary data analysis indicated that the data set containing a large number of icing events with small ice accumulations that have only a marginal effect on the reliability of either telecommunications or electric networks, and that negatively influence the goodness-of-fit of the upper tail of the probability distribution functions where the values of more interest exists. In consequence, only icing events above a given threshold are considered in the following analysis.

4.2. Probability distributions

Given a random variable Q, the probability distribution function specifies how frequently the possible values of Q occur. The cumulative distribution function define the probability that a given value of Q is at most equal to x,

$$\mathrm{F(x)} = \mathrm{Pr[Q \leq x]} = \mathrm{p} \tag{4.1}$$

Its inverse function $F^{-1}(p)$ expresses the magnitude of an event in terms of its nonexceedance probability p. If F(x) is differentiable, its derivative f(x) is the probability density function of x,

$$f(x) = \frac{d}{dx} F(x) \tag{4.2}$$

The expectation of the random variable x is defined as,

$$E(X) = \int_{-\infty}^{\infty} x dF(x) = \int_{-\infty}^{\infty} x f(x) dx \tag{4.3}$$

The dispersion of the random variable x can be measured by the variance of x,

$$\mathrm{Var}(x) = E[\{x - E(x)\}^2] \tag{4.4}$$

The event with a return period T is an event that has a probability l/T of being exceeded. For events with a very high return period, the probability of the event with a return period T can be estimated from,

$$F(Q_T) = 1 - 1/T; \tag{4.5}$$

For events with a low probability of occurrence, the corresponding relation is,

$$F(Q_T) = 1/T \tag{4.6}$$

The main goal of the statistical analysis is to obtain a useful estimate of the quantile Q_T for a return period of scientific relevance, the design life of a structure in our case. If data is available at the site of interest, then the observations are a sample of the realization of Q. In many environmental applications the sample size is rarely sufficient to enable quantiles to be estimated reliably. It is generally held that a quantile of return period T can be reliably estimated from a data record of length n only if $T \leq n$. However, in many engineering applications based on annual data this condition is rarely satisfied.

4.2.1. Moments

The characteristics of a probability distribution can be summarized with the help of the moments of the distribution. The first moment is the mean value,

$$\mu = E(x) \tag{4.7}$$

and the higher moments are,

$$\mu_r = E(x - \mu)^r, r = 2,3, \ldots\ldots \tag{4.8}$$

For example, the dispersion of the distribution about its mean value is measured by the variance or second moment,

$$Var(x) = \sigma^2 = [E(x - \mu)^2] \tag{4.9}$$

where σ is the standard deviation. The coefficient of variation (CV), $C_v = \sigma/ \mu$, expresses the dispersion of a distribution as a proportion of the mean. Dimensionless higher moments $\mu_r / \mu_2^{r/2}$ are also used, particularly the skewness,

$$\gamma = \mu_3 / \mu_2^{3/2} \tag{4.10}$$

and the kurtosis,

$$\kappa = \mu_4/\mu_2^2 \tag{4.11}$$

Analogous quantities can be computed from a sample of observations $x_1, x_2, \ldots, x_n$. The sample mean,

$$\bar{x} = n^{-1}\sum_{i=1}^{n} x_i \tag{4.12}$$

is the natural estimator of μ. The higher sample moments,

$$m_r = n^{-1}\sum_{i=1}^{n} (x_i - \bar{x})^r \tag{4.13}$$

are reasonable estimators of the μ_r, but are not unbiased. Unbiased estimators are often used. Unbiased estimators of σ^2, μ_3 and the fourth cumulant $\kappa_4 = \mu_4 - 3\mu_2^2$ are obtained respectively by,

$$s^2 = (n-1)^{-1}\sum_{i=1}^{n}(x_i - \bar{x})^2 \tag{4.14}$$

$$\tilde{m}_3 = \frac{n^2}{(n-1)(n-2)} m_3 \tag{4.15}$$

$$\tilde{k}_4 = \frac{n^2}{(n-2)(n-3)}\left[\left(\frac{n+1}{n-1}\right)m_4 - 3m_2^2\right] \tag{4.16}$$

The sample standard deviation, s = $\sqrt{s^2}$, is an estimator of σ but is not unbiased. The sample estimators of CV, skewness and kurtosis are, respectively,

$$\hat{C}_V = s/x, \qquad g = m_3/s^3, \qquad k = k_4/s^4 + 3. \tag{4.17}$$

Moment estimators have some undesirable properties. The estimators g and k can be severely biased and can have algebraic bounds that depend on the sample size; for a sample of size n the bounds are,

$$|g| \leq n^{1/2} \quad \text{and} \quad k \leq n+3. \tag{4.18}$$

Thus, if a distribution is sufficiently skewed, it may be impossible for this skewness to be reflected in a sample of fixed size. Inferences based on sample moments of skew distributions are therefore likely to be very unreliable. A more satisfactory set of measures of distributional shape is obtained from L-moments, described in the next section (Hosking and Wallis, 1996).

4.2.2. L-moments

L-moments are an alternative system of describing the shapes of probability distributions. Historically, they arose as modifications of the "probability weighted moments". Probability weighted moments of a random variable x with cumulative distribution function F (x.) are defined as,

$$M_{p,r,s} = E\,[x^P\{F(x)\}^r\{1 - F(x)\}^S]\,. \tag{4.19}$$

Particularly useful special cases are the probability weighted moments $\alpha_r = M_{1,0,r}$ and $\beta_r = M_{1,r,0}$. For a distribution that has a quantile function x(u), Equation (4.19) gives,

$$\alpha_r = \int_0^1 x(u)(1-u)^r\,du, \qquad \beta_r = \int_0^1 x(u)u^r\,du\,. \tag{4.20}$$

These equations may be contrasted with the definition of the ordinary moments, which may be written as,

$$E(X^r) = \int_0^1 \{x(u)\}^r\,du\,. \tag{4.21}$$

Conventional moments involve successively higher powers of the quantile function x(u), whereas probability weighted moments involve successively higher powers of u or 1-u and may be regarded as integrals of x(u) weighted by the polynomials u^r or $(1-u)^r$.

In terms of probability weighted moments, L-moments are given by,

$$\lambda_{r+1} = (-1)^r \sum_{k=0}^{r} P^*_{r,k}\alpha_k = \sum_{k=0}^{r} P^*_{r,k}\beta_k\,. \tag{4.22}$$

where $P^*_{r,k}$ is a shifted Legendre polynomial,

$$P^*_{r,k} = (-1)^{r-k}\binom{r}{k}\binom{r+k}{k} = \frac{(-1)^{r-k}(r+k)!}{(k!)^2(r-k)!} \tag{4.23}$$

4.3. Selection of candidate distributions

The distribution selected as the best for a given data set need not be the distribution that gives the closest approximation to the observed data. Even when a distribution can be found that gives a close fit to the observed data, there is no guarantee that future values will match those of the past, particularly when the data arise from a physical process that can give rise to occasional outlying values far removed from the bulk of the data. It is preferable to use a robust approach based on a distribution that will yield reasonably accurate quantile estimates whose accuracy is not seriously degraded when the true physical process deviates from the model's assumptions. There may also be a particular range of return periods for which quantile estimates are required.

There are many families of distributions that might be candidates for being fitted to the data set. Their suitability as candidates can be evaluated by considering their ability to reproduce features of the data that are of particular importance in modeling. The following properties of a distribution may be of importance in any given application.

- Upper bound of the distribution
- Upper tail of the distribution
- Shape of the body of the distribution
- Lower tail of the distribution
- Lower bound of the distribution
- Exact zero values

In analyses of extreme events, quantile estimates in one tail of the distribution will be of particular interest. In such a case, it does not matter if a distribution that can take negative values is fitted to data that can only be positive.

Many physical quantities can be thought of as having an upper bound. The bound may not be known exactly, but some numerical values are so unlikely as to be physically impossible. Imposing the requirement that the distribution have a physically realistic upper bound may compromise the accuracy of quantile estimates at the return periods that are of real interest. Over the range of return periods of interest in a particular study, the true distribution function is likely to be better approximated by an unbounded distribution than by any bounded distribution.

When it appears that the true distribution has an upper bound that is closely approached by the observed data, then it is advisable to fit a distribution that is capable of modeling bounded data. For example, the generalized extreme-value distribution has an upper bound when its shape parameter k is greater than zero. When this distribution is fitted to data, a tendency for the data to lie close to an upper bound will be reflected in an estimated k value greater than zero.

Similar considerations apply to the lower bound of the distribution as to the upper bound. Unlike the upper bound, however, the lower bound may often be known; usually it will be known to be zero. If quantiles of interest are close to zero, it may be worthwhile to require the lower bound of the distribution to be zero. Several distributions, such as the Wakeby, Generalized Pareto, and Pearson type III, retain a convenient form when this requirement is imposed. In some cases, the knowledge that the lower bound is zero is not useful, and better results will be obtained by fitting a distribution that has a lower bound greater than zero or even a distribution that has no lower bound.

In many applications, estimation of the upper tail of the frequency distribution is of particular interest, yet the amount of data is not sufficient to determine the shape of the upper tail with any accuracy. The tail weight, the behavior of the probability density function f(x) as x increases, is important because it determines the rate at which quantiles increase as the return period is extrapolated beyond the range of the data. Tail weights of some common distributions are given in Table 4.1. When there is no reason to assume that only one kind of tail weight is appropriate, it is advisable to use a set of candidate distributions that cover a range of different tail weights. The goodness-of-fit statistics provide means of deciding which distributions, and hence which tail weights, are consistent with a data set.

Table 4.1: Upper-tail weights of some common distribution

(Hosking and Wallis (1996)

Form of f(x) for large x	Distributions
x^{-A}	Generalized extreme-value, generalized Pareto, and generalized logistic distributions with parameter $k < 0$.
$x^{-A \log x}$	Lognormal distribution with positive skewness.
$\exp(-x^A)$, $0 < A < 1$	Weibull distribution with parameter < 1.
$x^A e^{-Bx}$	Pearson type III distribution with positive skewness.
$\exp(-x)$	Exponential, Gumbel.
$\exp(-x^A)$, $A > 1$	Weibull distribution with parameter $\lambda > 1$.
Finite upper bound	Generalized extreme-value, generalized Pareto, and generalized logistic distributions with parameter $k > 0$; lognormal and Pearson type III distributions with negative skewness.

Note: Tail weights are ordered from heaviest to lightest. A and B denote arbitrary positive constants.

Similar considerations apply to the lower tail of the distribution as to the upper tail. However, if interest focuses on the upper tail of the distribution, the form of the lower tail is irrelevant.

Sometimes there are theoretical reasons why a particular family of distributions is appropriate for a given type of data. For example, it has been known that data on extreme events such as annual maximum stream flows or precipitation may be well fitted by extreme-value distributions. For annual maximum, the extreme-value approximation is valid when in each year there are a large number of storm events whose peaks are independent and identically distributed. In practice, the assumptions underlying the extreme-value approximation may not be satisfied. For annual maximum data, the number of storm events in a year is rarely large enough to justify the extreme-value approximation; and the storm event magnitudes, rather than being identically distributed, tend to vary with the seasons of the year. Though an extreme-value distribution may be a candidate for describing the data, it should not be used without comparing its goodness-of-fit with that of other distributions.

Some thought should be given also to the number of unknown parameters in the candidate distributions. Distributions with only two parameters yield accurate quantile estimates when the true distribution resembles the fitted distribution, but estimates of tail quantiles can be severely biased if the shape of the tail of the true frequency distribution is not well approximated by the fitted distribution. The use of a distribution with more parameters, when these parameters can be estimated accurately, yields less biased estimates of quantiles in the tails of the distribution. For most applications, distributions with three to five parameters are appropriate.

4.4. Parameter estimation

4.4.1. Parameter estimation using L-moments

Similar to parameter estimation using the method of moments, estimates are obtained with the method of L-moments by equating the sample L-moments to the corresponding population quantities. The L-moments for many standard distributions are available in the literature.

For order statistics, where the data are arranged in ascending order, L-moments can be defined as the expected values of the linear combination of the elements of an ordered sample. The L-moments of a probability distribution are defined by,

$$\lambda_r = r^{-1}\sum_{j=0}^{r-1}(-1)^j\binom{r-1}{j}E(X_{r-j:r}) \tag{4.24}$$

where $X_{r:n}$ is the r^{th} smallest observation from a sample of size n. The expectation of an order statistics can be written as,

$$E(X_{r:n}) = \frac{n!}{(r-1)!(n-r)!}\int_0^1 x(u)u^{r-1}(1-u)^{n-r}\,du \tag{4.25}$$

Estimation of L-moments from a finite sample of size n arranged in ascending order, can be similarly expressed as,

$$l_{r+1} = \sum_{k=1}^{r} P^*_{r,k} b_k; \qquad r = 0,1,\ldots\ldots,n-1 \tag{4.26}$$

where $P^*_{r,k}$ is defined before, and b_k is the estimator of the probability weighted moment β_k,

$$b_k = n^{-1}\sum_{j=k+1}^{n}\frac{(j-1)(j-2)\cdots(j-k)}{(n-1)(n-2)\cdots(n-k)}x_{j:n} \tag{4.27}$$

Hosking and Wallis (1996) found that the method of L-moments is often more efficient (unbiased and has the least variance of almost all other estimators) than maximum likelihood for small and moderate samples.

4.4.2. Parameter estimation using Maximum Likelihood

For a probability density faction f(x; a, b, ..), where a, b, … are the parameters of the distribution, the likelihood function,

$$L = \prod f(x_i; \alpha, \beta, \cdots); i = 1, \cdots n \tag{4.28}$$

is the probability of obtaining a sample of x_i; i=1,...n from the parent distribution of the random variable x. The maximum likelihood method is to estimate the parameters a, b, ... through maximization of L. The likelihood function is partially differentiated with respect to each parameter and equated to zero to form m equations and m unknowns, where m is the number of the parameters to be estimated.

Maximum likelihood estimators are asymptotically unbiased (E(â) = a as n→ ∞), sufficient (uses all information in the sample), consistent (| â - a | → 0 as n→ ∞), and efficient if adjusted for bias. On the other hand, the method of maximum likelihood requires a considerable amount of numerical computations.

4.5. Goodness-of-fit

Quantile-Quantile (Q-Q) plots are used for qualitatively examining and comparing the goodness-of-fit of the distributions. Q-Q plots describe the relationship between the observations ordered in increasing order and the corresponding predicted values from the fitted distribution. Given the i^{th} largest observation, the estimate of its corresponding cumulative probability is obtained from a plotting position formula. The formula used here is Cunnane plotting position (Cunnane 1978),

$$P_{i,n} = \frac{i - 0.4}{n + 0.2} \tag{4.29}$$

where n is the total number of observations. The corresponding predicted value is obtained as the inverse of the fitted cumulative probability distribution function evaluated at the plotting position,

$$x = F^{-1}(P_{i,n}) \tag{4.30}$$

A perfect fit corresponds to the case where the correlation coefficient between the observed and predicted values is equal to one. A qualitative comparison of the goodness-of-fit for different distributions is based on a visual comparison of the degree of deviation between observed and fitted values. In this study, the Mean Root Square Error (RMSE), the Relative Mean Root Square Error (RRMSE), the Maximum Absolute Error (MAE), and the Correlation Coefficient (CC) are used as quantitative measures of comparison,

$$RMSE = \left[\frac{\sum_{i=1}^{n}(x_i - y_i)^2}{(n-m)}\right]^{\frac{1}{2}} \quad (4.31)$$

$$RRMSE = \left[\frac{\sum_{i=1}^{n}\left(\frac{x_i - y_i}{x_i}\right)^2}{(n-m)}\right]^{\frac{1}{2}} \quad (4.32)$$

$$CC = \frac{\sum_{i=1}^{n}(x_i - \bar{x})(y_i - \bar{y})}{\left[\sum_{i=1}^{n}(x_i - \bar{x})^2 \sum_{i=1}^{n}(y_i - \bar{y})^2\right]^{\frac{1}{2}}} \quad (4.33)$$

$$MAE = \max|x_i - y_i| \quad (4.34)$$

where x_i , i=1,...,n, are the observations, y_i , i=1,...,n, are the predicted values using the probability distribution, n is the number of observations, and m is the number of the estimated distribution parameters. Other goodness-of-fit measures such as the Chi-Square and Kolmogorov-Smirnov statistics are not used here since they are not very informative on the goodness-of-fit of the upper tail of the distribution, which is the main concern in this application.

4.6. The bootstrap procedure

The bootstrap is a computer-based method for assigning measures of accuracy to statistical estimates (Efron and Tibshirani 1993). Given a sample set, $x = (x_1, \ldots, x_n)$, the statistic, say s(x), can be estimated. To obtain an approximate sampling distribution, *B* (where *B* is around 1000 or higher) bootstrap samples are generated. A bootstrap sample is defined as $x^* = (x_1^*, \ldots, x_n^*)$, with a corresponding statistic $\theta(x^*)$.

A bootstrap sample x^* is obtained by randomly sampling n times, with replacement, from the original data points $x_1, \ldots, x_n$. Bootstrap replicates $\theta(x^{*1}), \ldots, \theta(x^{*B})$ are obtained by calculating the value of the statistic $\theta(x)$ for each bootstrap sample. Resampling from the original data is referred to as a nonparametric bootstrap. Parametric bootstrap samples are drawn from a parametric model instead of the data. Estimation of the standard error is the simplest and most known application of the bootstrap technique. It is considered as a generalized measure of the standard deviation.

The bootstrap technique is used here to examine the suitability of each distribution for extrapolating beyond the largest observed datum. Therefore, the interest is mainly in the characteristics of the right tail for each model. A large number of bootstrap samples is drawn with replacement from data at each station. Each of the candidate distributions is fitted to each of the bootstrap samples. The values from the fitted distributions corresponding to the empirical cumulative probabilities of the largest observations in the data sets are then computed. The statistics of the extrapolated tail values are then compared to the corresponding sample values. The best distribution has extrapolated tail values that are closest to the actual tail value with least spread around.

4.7. Analysis of ice data

The icing hazard function is defined as the exceedance rate (expected number of events per year) with ice accumulations larger than the specified thickness (t),

$$\lambda(t) = \lambda_o \cdot (1 - F(t)) \tag{4.35}$$

where F(t) is the cumulative probability distribution function of t, and λ_o is the recurrence rate of icing storms. The hazard function can be estimated using a sample of the annual maximum events (λ_o is equal to 1 by definition) or a sample of all the events larger than a given threshold (event-based method). A variant of the latter, which is used in this application, is obtained by using a sample consisting of the largest N observations from the ordered sample of events over a period of N years (annual maximum exceedance).

Many of the icing events at each site correspond to very small ice accretions (e.g. less than 5 mm) and are not significant for the extreme-value analysis. Consequently, a lower limit was selected to eliminate most of the small observations. This selection is not trivial since a low threshold (1 or 2 mm) does not improve the fit of the extreme value probability distribution functions while a high threshold (5 mm) severely reduces the sample size for a large proportion of the stations. The alternative is to consider only the N largest observations from the ordered sample (annual exceedance series). Table 4.2 shows the number of remaining stations for each option. For example, there are 66 stations with at least 20 years of observations but only three have observations during each of these 20 years. Also, there are respectively 112, 68, and 38 stations with at least 10, 15, and 20 icing events with accumulations of 5 mm or higher. The last row and column indicates that 45 stations have at least 20 years of observations and at least 20 icing events during that period. This last subset of 45 stations is used to compare ice hazard functions derived from annual-maximum and event-based models. Data for maximum ice thickness per event for this subset is given in Appendix C. The station numbers correspond to the numbers used in Appendix B.

Twelve probability distribution functions commonly used for the analysis of extreme precipitation and floods data are investigated for glaze ice data for the subset of the 45 stations. The distributions belong to five different families of distributions (Normal, Exponential, Gamma, Kappa, and Pareto) and range in complexity from two-parameter to five-parameter distributions.

Table 4.2: Number of stations included under different limitations

Minimum number of data points, n		10	15	20
		Number of stations		
Yearly	n data points	102	47	3
	n years	138	109	66
Events	>=1 mm	141	125	101
	>= 2 mm	136	120	95
	>= 3 mm	130	106	74
	>= 4 mm	121	89	54
	>= 5 mm	112	68	38
	>= 6 mm	81	40	22
>= 20 events & >= 20 years				45

Table 4.3: Probability distribution functions

Distribution name	Symbol	Parameters	Estimator
Gamma	GAM	$\alpha\ \beta$	L-Moment
Pearson type III	PE3	$\xi\ \alpha\ k$	L-Moment
Log Pearson type III	LP3	$\xi\ \alpha\ k$	L-Moment
Gumbel	GUM	$\xi\ \alpha$	L-Moment
Generalized extreme-value	GEV	$\xi\ \alpha\ k$	L-Moment
Lognormal	LNO	$\mu\sigma\gamma$	L-Moment
Kappa	KAP	$\xi\ \alpha\ k\ h$	L-Moment
Generalized Pareto	GPA	$\xi\ \alpha\ k$	L-Moment
Generalized Normal	GNO	$\xi\ \alpha\ k$	L-Moment
Beta-K	BEK	$\alpha\beta\theta$	Maximum Likelihood
Beta-P	BEP	$\alpha\beta\theta$	Maximum Likelihood
Wakeby	WAK	$\xi\ \alpha\ \beta\ \gamma\ \delta$	L-Moment

The parameters of the distributions are estimated using the L-moments method ((Hosking and Wallis 1997) in all cases except for the parameters of the Beta-P and the Beta-K distributions which are estimated using maximum likelihood (Wilks 1993). Table 4.3 shows the twelve distributions, the symbols used for each, the number of parameters and the method used for parameter estimates. Appendix D is a detailed description of the distributions and their parameter estimations.

The goodness-of-fit is based on a comparison of the empirical and estimated fractiles of the observations at each station. The measures of discrepancy are the root mean square error (RMSE), the relative root mean square error (RRMSE), the maximum absolute error (MAE), and the correlation coefficient (CC).

4.8. Discussion of results

Q-Q plots were obtained for each of the 45 stations and for each of the 12 probability distribution functions considered (Appendix E). As an example, Figure 4.4 shows the plots for the New-Richmond station. A visual comparison of the Q-Q plots fails to identify a uniformly superior distribution throughout the range of ice accumulation. However, the GNO, GEV, GPA, PE3, and WAK distributions fit the data best on average and have similar Q-Q plots. The LP3 distribution provides a good fit for stations with isolated extreme events; however, in most other cases, the distribution overestimates the frequency of extreme events. Similar remarks can be applied to the LNO and BEP distributions. None of the distributions could adequately describe the data for stations with exceptional ice accumulations. The BEK distribution offers a good fit but does not outperform other 3-parameter distributions. The KAP and WAK distributions did not outperform other distributions despite their large number of parameters. Finally, The GAM and GUM distributions perform well in cases where there are no isolated extreme observations, but underestimate the upper tail otherwise.

The relative goodness-of-fit of the distributions is also evaluated by comparing statistics for the RMSE, RRMSE, MAE, and CC as previously defined for the 45 PIM stations. Figure 4.3 shows modified box and whisker plots for each of these quantities, where whiskers correspond to the minimum and the maximum values, the dimensions of the box to the 10th and 90th fractiles respectively, the median appears as a dashed line, and the mean as a solid square. Goodness-of-fit is best for distributions which minimize the error measures and which exhibit the least amount of variability.

The RMSE shows that the PE3, GPA, and KAP distributions offer the best fit on average, and that the goodness-of-fit to the PE3 distribution is most consistent across the stations with a RMSE less than 4mm for 90% of the stations. Note that the GEV distribution has a better fit than the GUM distribution and that the LP3 distribution is not among the best distributions. The RMSE tends to emphasize the presence of large deviations from the fitted distribution. The RRMSE shows that the KAP, GPA, and PE3 distributions offer the best fit on average, while the fit to the GAM and GUM distributions is noticeably worse on average. The RRMSE tends to emphasize the presence of large relative errors.

The MAE shows that the GNO, GPA, KAP, and PE3 distributions are best on average. The MAE measures the goodness-of-fit and gives equal weight to all the deviations between observed and predicted values. Finally, the CC shows that GNO, GPA, KAP and PE3 are the best distributions on average, while the GAM, GUM , BEK, and BEP distributions are worse on average. Note that CC is not a very powerful statistic since the coefficient of correlation is over 0.95 in 90% of the cases, and is not very sensitive to the presence of a few large deviations.

Based on the above criteria, each distribution was assigned a qualitative rank from 1 to 12 for each distribution and for each station. Figure 4.2 shows the frequency of occurrence of each rank for the GEV, GNO, GPA, GUM and PE3 distributions and indicates that the PE3 and GPA distributions are generally ranked the best. The GEV distribution ranks mostly between the fifth and the tenth places, and the GUM distribution clearly ranks below the other four distributions.

Combining all the previous results, the PE3 distribution offers the best fit among the 3-parameter distributions. The GEV, GNO, and GPA distributions are also very good choices except for a relatively high MAE. The GAM and GUM distributions do not fit the data as well as other distributions except in terms of the RMSE. The KAP distribution has an excellent fit but relatively high MAE. The LNO distribution is always inferior to the GNO distribution. The LP3 distribution is not suitable except for a few stations. The WAK distribution shows inferior results despite its 5 parameters. The BEP distribution is worst among the 3-parameter distributions, while the BEK distribution is comparable to other 3-parameter distributions.

To summarize, the 2-parameter distributions show less adaptability and rank low with most stations. There is not a single distribution that fits perfectly the data for all stations, but on average some distributions outperform others. All distributions fit adequately the data for approximately half of the stations (RMSE < 3 mm, RRMSE < 20%, MAE < 6 mm, and CC > 90%).

4.9. Annual versus event-by-event sampling

Figure 4.5 shows the comparison between the annual and event-based models for the four goodness-of-fit measures. The event-based model generally provides a better fit for the distributions considered in the analysis. The relationship between the third and fourth L-moment ratios (τ_3 and τ_4) can also provide an indication of the best probability distribution function for a given data set (Hosking and Wallis, 1997). The relationship between the τ_3 and τ_4 ratios is one dimensional for 2-parameter distributions, two dimensional for 3-parameter distributions and multi dimensional for distributions with more than three parameters.

Figure 4.6 shows the relationship between the τ_3 and τ_4 ratios for the 45 stations for the annual-maximum and event-based models. The four curves in the figure represent the relation between τ_3 and τ_4 for some selected 3-parameter distributions (the Generalized Extreme Value (GEV), Generalized Normal (GNO), Pearson type 3 (PE3), and Generalized Pareto (GPA) distributions). The Normal and Gumbel distributions are also shown as points. The OLB curve stands for overall lower bound. The average trend for the event-based samples seems to coincide with the Generalized Pareto distribution. The trend for the annual-maximum model is not as clear and no distribution, from the three-parameter distributions, appears to be favored over the others.

4.10. Characteristics of the right tail

In the previous sections, the goodness-of-fit of various distributions was examined for the distribution of glaze ice accumulations at several stations. The characteristics of the upper tail of the distributions are also important for developing design criteria for long return periods. In this section, the same distributions (except GAM, KAP, and LNO) are compared on the basis of the sampling characteristics, bias and uncertainty, of their upper tail. The best distributions are those that minimize both bias and uncertainty.

The sampling characteristics of the distributions are investigated by bootstrap. For each station, 1000 bootstrap samples of 20 observations each were randomly generated from the original data set. The analysis was performed for the same 45 stations previously selected. Predicted values for the four largest observations at each station are obtained from the inverse of the cumulative distribution function evaluated at the Cunnane plotting position. The bootstrap results are summarized using modified box plots that show the mean, the mean ± one standard deviation, the maximum, and the minimum values (Appendix F). Figure 4.7 shows an example of the modified box plots. The best distributions are those where the observations are within one standard deviation of the mean value, and where the variance on the estimates is minimal. The original observations for the four largest ice accumulations are also shown in the figures. For all distributions, except GUM, the largest observed value is within one standard deviation from the mean. The GEV, GNO, GPA, and PE3 distributions exhibit similar upper tail characteristics and are the best overall. The WAK distribution shows similar behaviour, and the BEK, BEP, and LP3 distributions exhibit the most variability.

4.11. Summary

Twelve probability distributions are examined for the intensity of glaze ice storms in Québec at 45 measurement stations. The distributions are compared on the basis of the goodness-of-fit and the sampling characteristics of the upper tail of the distributions. No single distribution fits the data perfectly at all stations. However, the PE3, GPA, GNO, and GEV distributions are best on average. The PE3 and GPA distributions rank first based on several measures of goodness-of-fit followed by the GNO and GEV distributions. The commonly used Gumbel distribution is consistently outperformed by the three-parameter distributions mentioned above, and is included as a special case of the GEV distribution. Finally, the BEP and BEK distributions show mixed results while the LP3 distribution appears adequate in only few cases but mostly overestimates the largest observations.

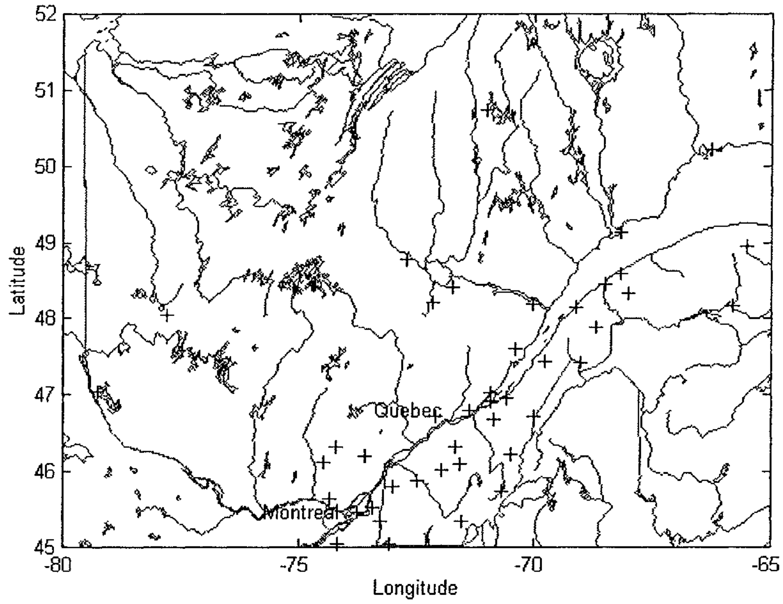

Figure 4.1: Locations of the selected PIM stations

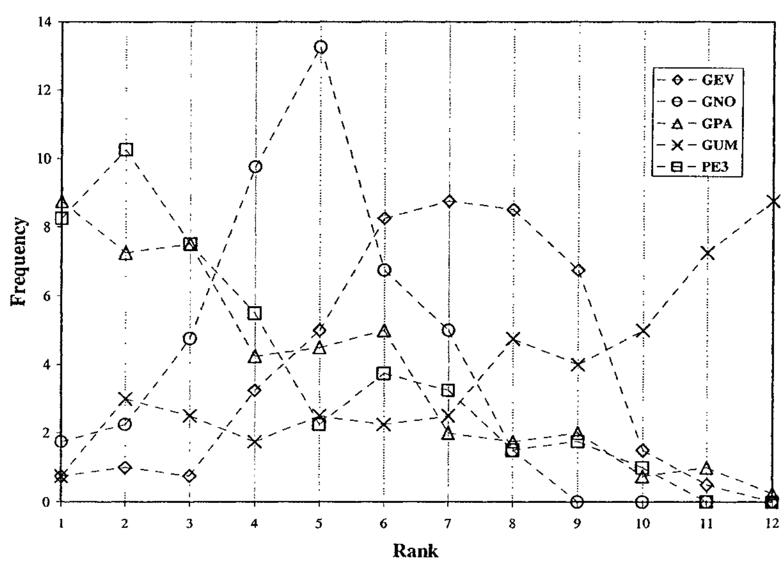

Figure 4.2: Distribution of ranks based on RMSE, RRMSE, MAE, and CC criteria

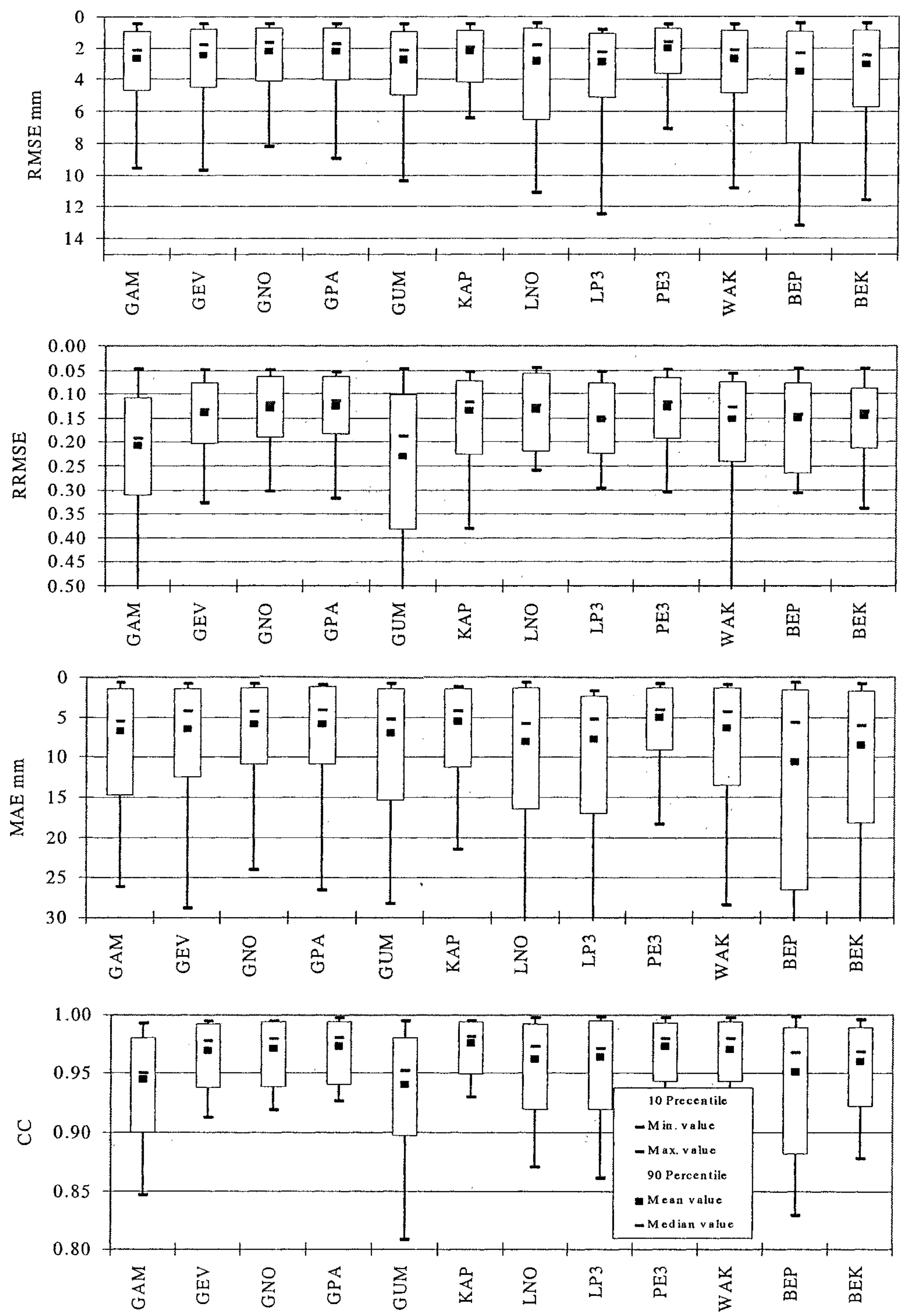

Figure 4.3: Box plots of RMSE, RRMSE, MAE, and CC

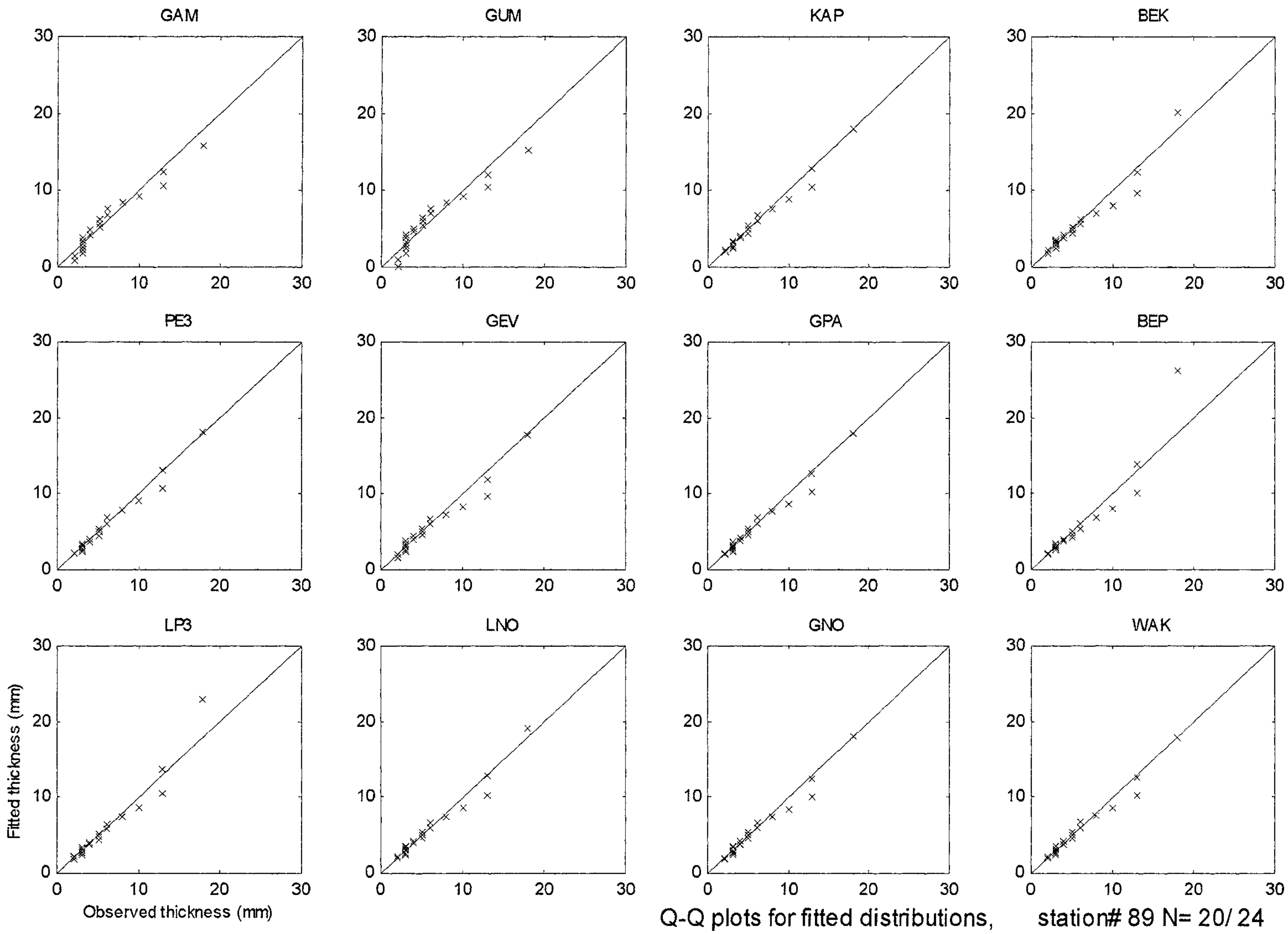

Figure 4.4: Example of Q-Q plot, station #89 "New Richmond"

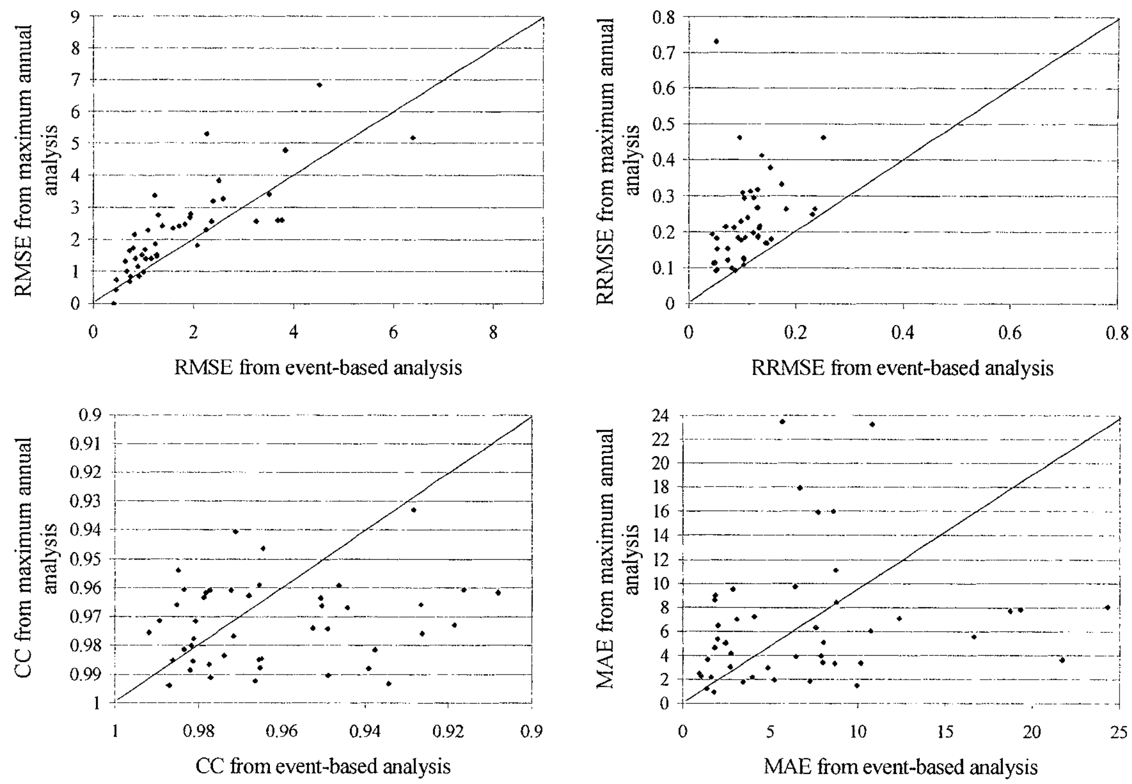

Figure 4.5: Comparison of the annual-maximum and event-based models

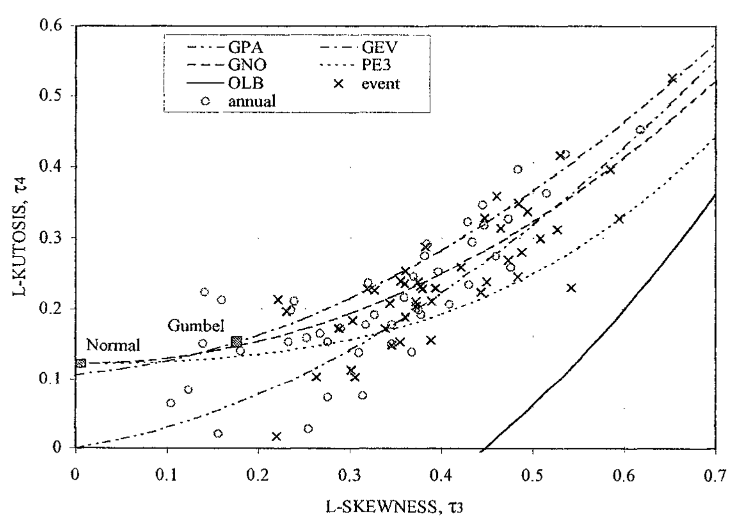

Figure 4.6: Theoretical L-moments relations for different distributions vs. empirical L-moment relations for the annual-maximum and event-based models

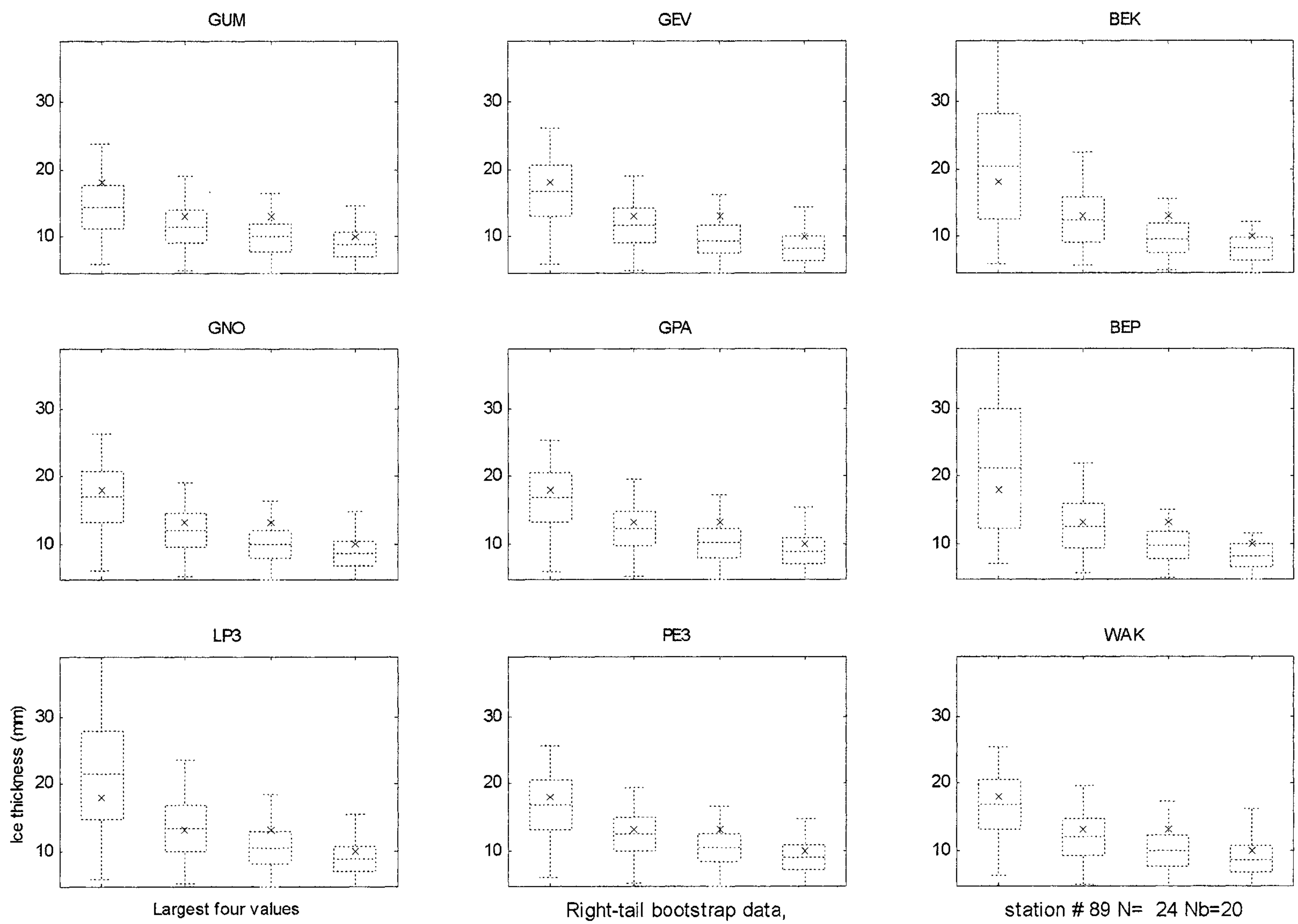

Figure 4.7: Example of box plot of bootstrap data, station number 89 'New-Richmond'

Chapter 5: The Analysis of Combined Wind and Ice Loads

5.1. Introduction

The combination of wind and ice loads is critical for the design of electric transmission lines and telecommunication networks given the increase in the exposed area of an iced structure or conductor to the wind. Winds concurrent with ice accumulation are generally weak; however, the likelihood of strong winds increases with the length of persistence of ice on the structure.

The analysis of the combination of wind and ice loads depends on the type and quantity of information available at a given site. Ideally, every site should be equipped with a meteorological instrumentation for the simultaneous measurement of wind speed, ice accumulation, temperature; and with sensors for the direct measurement of vertical, longitudinal and transversal forces. More and more sites are equipped in such a manner; however, the number of stations and the quantity of data is quite small. Current standards generally specify loads in terms of specific combinations of wind speed and ice accumulation (IEC 826, ASCE 1991, 1998, Chaos and Lee 1992).

Concurrent ice accumulation and wind speed at a given site can be modeled on a combined stochastic process. On the other hand, modeling the joint probability distribution function for the combined loads, or their effects on the structure, can be appropriate for design purposes, since the main objective is the estimation of the most severe event during the service life of the structure.

In general, there is little data available at a given site for the evaluation of the parameters of the joint distribution. In practice, designers have often used the distribution for the yearly maximum wind adjusted for a return period corresponding to the yearly duration of ice episodes (Davenport 1986, IEC 826).

In this chapter, a reliability-based procedure is proposed for the analysis of combined wind and ice loads, and in particular, for the associated pressure on overhead electric conductors. Advantages of these method are that: (1) all sources of uncertainty for the analysis can be considered, (2) the most likely combination for the random variables for a specific return period can be identified, (3) the specific combinations for every type of structure and mode of failure can be derived, and (4) the procedure is consistent with the current practice of codification according to the LRFD or Limit States Design.

5.2. Modeling combined climatic loads

5.2.1. Stochastic process approach

Concurrent ice accumulation and wind speed at a given site forms a complex stochastic process which can be idealized as discrete stochastic processes such as Poisson or Ferry-Borges-Castanheta (FBC) processes (Ferry-Borges-Castanheta 1971). FBC processes can be visualized as rectangular pulses in time with equal duration; for each duration the random variable X has a new value independent of other realizations of the process. The maximum intensity during a period of time T has a distribution,

$$F_{\max}(x) = [F_x(x)]^n \tag{5.1}$$

where $F_X(x)$ is the distribution function of the random variable X, and n is the number of pulses during the period T (a deterministic value). The mixed FBC process accounts for durations with zero value (no event). For a non-zero event, a positive random value S, whose cumulative distribution function is $F_S(x)$, occurs with probability ρ, and stays constant until the next event and returns to zero. Events with zero intensity occur with probability 1-ρ. The maximum intensity during a period of time T has a distribution,

$$F_{\max}(x) = [1 - \rho(1 - F_s(x))]^n \tag{5.2a}$$

which can be approximated as,

$$F_{\max}(x) = 1 - n\rho(1 - F_s(x)) \tag{5.2b}$$

The events in a FBC process occur at fixed intervals in contrast with a Poisson process that has variable durations between events. The FBC process is suitable for the proposed event-based ice model due to the nature of the observations that are taken at equal intervals.

Wind, on the other hand, intrinsically is a continuous stochastic process in time. Thus, it is more appropriate to be idealized by a discrete process with variable time intervals, such as a Poisson process. For a Poisson process, the distribution function of the time between two events is exponential,

$$F_t\ (t)=1-\exp(-\nu t), \tag{5.3}$$

where ν is the mean arrival rate (intensity of the process). Given that the duration of extreme wind events is relatively short, it is reasonable to use a filtered Poisson process for the occurrence of the events. Filtered Poisson process can be simplified with the assumption that the duration is very short relative to the arrival rate and consequently, the probability that two pulses overlap is negligible. The maximum intensity during a period of time T can be approximated by,

$$F_{\max}(x) = e^{-\nu T(1-F_s(x))} \tag{5.4}$$

The combined process of wind and ice can be represented by two separate processes in time; where events of strong wind are represented by short impulses arriving according to a filtered Poisson process, and the ice storm events are represented by a FBC process with fixed intervals (Fahleson 1995).

5.2.2. Joint probability distribution function approach

Several simplified methods for combined wind and ice loads have introduced in national as well as international design codes. The choice of the combination method is very important for the specification of combined load scenarios for design.

These methods can fall into one of the following two general categories:

1) Methods based on the joint distribution of environmental variables.
2) Methods based on the effect of the combined variables.

The IEC 826 standard approach for combined wind and ice loading follow the first category. The principle is based of the calculation of the probability of exceedance or the recurrence rate of a certain combination for the climatic variables given the joint distribution of the variables,

$$G_{\underline{X}}(\underline{x}) = 1 - F_{\underline{X}}(\underline{x}) = P\left[\bigcap_{i=1}^{n} X_i > x_i\right] = \frac{1}{T_R} \tag{5.5}$$

where $\underline{x}$ = wind speed and equivalent radial ice thickness. IEC 826 considers two scenarios, one of weak winds with heavy ice, and the other of strong winds with light ice. The heavy ice scenario combines an ice thickness smaller than the ice thickness specified for the scenario of ice alone, while the light ice scenario combines wind speeds smaller than the maximum annual wind speed.

In the case where the joint distribution of wind and ice is defined for the maximum ice thickness, Equation 5.5 is modified to account for the annual average number of ice storms (E[N]),

$$G_{\underline{X}}(\underline{x}) = 1 - F_{\underline{X}}(\underline{x}) = P\left[\bigcap_{i=1}^{n} X_i > x_i\right] = \frac{1}{E[N] \cdot T_R} \tag{5.6}$$

Some hypotheses are needed for the estimation of the joint distribution of wind and ice during the icing event. Figure 5.1 illustrates the evolution of the temperature, ice accumulation, and wind speed for Montréal during the January 1998 ice storm. As expected, the maximum values of wind and ice do not occur concurrently. Given that ice measurements are taken twice a day, a linear variation is assumed between observations. A more precise estimate of the evolution of the accumulation could be obtained using the correlation between the accumulation and the precipitation; however, this is not considered in this study.

On the other hand, it is not practical to model the evolution of ice thickness and wind speed during storms since each time-series are highly correlated in time, and no clear pattern of ice storm evaluation could be formed from examination of data at several stations. Figure 5.2 shows the evolution of wind, ice, and the horizontal force applied on a conductor of 20mm diameter (Equation 5.8), where the drag coefficient is considered constant and equal to 1.0. A conservative approach based on the combination of the maximum values of wind speed and ice accumulation for each storm is usually acceptable. In the present example, the maximum ice thickness is 36.4mm and the maximum wind speed is 33 km/h for a calculated maximum force of 5 N/m compared to a "maximum observed" force of 4.3 N/m. It is interesting, in this example, to notice that the period of fast accumulation of ice coincides with a significant increase in wind speed.

An example of the second type of specification is the approach used in ASCE 7. In this case, the design criteria is formulated relative to the design ice thickness, defined as the equivalent radial ice thickness for a given return period. The associated wind speed is calculated for a horizontal force equal to the maximum horizontal force expected for a given return period. The time series of meteorological observations at a given site is used in order to calculate a sample for the maximum horizontal force applied to the conductor per ice storm. The drag in the calculation of the horizontal force is generally set equal to one. The wind speed, temperature and precipitation data is obtained directly from the meteorological stations, whilst ice observations are calculated using theoretical or empirical accumulation models. The maximum horizontal force for each event is used to form the sample of maximum horizontal force per event. The advantage of this procedure is that it avoids the combination of extreme values for both wind speed and ice accumulation. On the other hand, the procedure neglects the uncertainty in Equation 5.8 and in the drag factor. The new generation of measuring instruments for Hydro-Québec's network (IRM) allows establishing a less conservative design criteria by combining the observations of the force simultaneously with the observation of the wind and accumulated ice. However many years of observations will be needed to construct a sufficiently large sample for statistical analysis.

The joint distribution of wind speed and ice accumulation depends on meteorological conditions during ice accumulation and during persistence of ice on structures. In general, the probability of severe winds increases with the length of this period given the possibility of the arrival of a new meteorological front. The joint distribution of wind speed and ice accumulation can be expressed by the product of the marginal distributions of the ice accumulation and the conditional distribution of wind speed during an ice storm,

$$f_{V,H}(v,h) = f_{V|H=h}(v) \cdot f_H(h) \tag{5.7}$$

Note that the conditional distribution of wind speed given an ice storm $f_{V/H=h}$ may be independent of the actual amount of ice accumulation and vice-versa. This appears to be the case for several sites where data was available on ice accumulations and wind speed during icing storms in the province of Québec.

The joint distribution can be used to analyze several aspects of the network performance of the network. For example, the distribution can be used to estimate the maximum loads on components of supporting structures and to specify combinations of loads for different recurrence periods. The horizontal force applied on a conductor can be estimated with the following expression,

$$F = \tfrac{1}{2}\rho \cdot V^2 \cdot (D + 2 \cdot h) \cdot C_d + \varepsilon \tag{5.8}$$

where ρ is the air density, V is the wind speed (perpendicular to the axis of a conductor or the structure), D is the diameter of the conductor, h is the equivalent radial ice thickness, C_d is the drag coefficient, and ε represents the uncertainty on the model (generally a variable Normally distributed with a zero mean value and a standard deviation σ_ε). The drag coefficient is often considered constant (1.0 for conductors); while actually this coefficient is very variable and depends on the shape of the accumulation. The shape of the accumulation, on the other hand, depends on the wind speed, the temperature at the time of the accumulation, and the conductor flexibility in torsion.

The cumulative distribution for the horizontal load can be derived from the joint distribution of wind and ice with the following expression,

$$1 - F_F(f) = P[F > f] = \iiint_{v,h,c_d} P[F > f \mid h, v, c_d] \cdot f_{H,V}(v,h) \cdot f_{C_d}(c_d \mid v,h)\; dh\; dv\; dc_d \tag{5.9}$$

where the uncertainty on the drag coefficient has been included in the form of a conditional distribution of wind and ice. For design purposes, a load can be selected from the cumulative distribution for a given return period. The combination of wind and ice that contribute the most to the design load can be determined from Equation 5.9. The most likely combination of wind and ice for a given force level is used for the specification of design loads according to the

LRFD format (Load and Resistance Factored Design) (CSA, 1981; Chao and Lee 1992; Ellingwood and Tekie 1999).

Figure 5.3 shows the joint complementary cumulative distribution of wind and ice for different return periods. The contour line for a probability of exceedance equals to 0.02 corresponds to all possible combinations for wind and ice that are exceeded in a 50 years recurrence period. The second family of curves represents the calculated horizontal loads with the equation 5.8 while assuming a conductor with a diameter of 20 mms, a drag coefficient of 1.0 and the perpendicular wind to the axis of the conductor. The contour line for the 50 years return period can be used to select various combinations of wind and ice for design. A similar analysis can be done for the vertical load and combined loads (horizontal and vertical).

For a given return period, an infinite number of wind-ice combinations can be identified. Among these combinations, only one produces the maximal horizontal load. Cases of light ice and heavy ice mentioned in the standards IEC 826 do not correspond to the horizontal maximal load.

Note that distributions described above correspond to the maximal values of wind and ice observed at any time during an ice storm and that they are not generally concurrent. An alternative approach would be to model the time series of wind and ice for every episode. The cumulative distribution of wind loads can be calculated by deriving the time series of loads from a historic or synthetic data sample. Keeping the maximum values for every episode, an extreme type distribution can then be fitted to the sample. A disadvantage of this procedure is that uncertainties on the model of loads as well as on the drag coefficient are excluded from the analysis. Finally, another alternative is to use measured maximal loads from sites equipped with force sensors. The estimated values following this last alternative are not biased, however, the uncertainty on these values is typically very high given the small number of observations in the sample.

5.3. Reliability based procedure

A better procedure to determine the optimal combination for wind and ice for a type of structure and given data is to use a reliability-based procedure (Chao and Lee 1992, Winterstein and al. 1993). The cumulative distribution of maximum horizontal loads during ice storms can be estimated as follows,

$$F_F(f) = 1 - \iiint_{\Omega_{\underline{X}}} f_{\underline{X}}(\underline{x})\, d\underline{x} = 1 - \iiint_{\Omega_{\underline{X}}} f_{C_d}(c_d) \cdot f_V(v) \cdot f_H(h)\, d_{c_d}\, dv\, dh \tag{5.10}$$

where $\Omega_{\underline{X}}$ is a region in the sample space of random variables $\underline{x}\{C_d, V, H\}$ where the force F exceeds f. A number of random variables can be considered throughout this analysis. Figure 5.4 illustrate the concept described by equation 5.10 for the case where wind and ice are the only random variables. The first group of contour lines represents the contours of the joint distribution of wind and ice, while the second group of curves corresponds to the applied horizontal load on a 20- mm-diameter conductor. The shaded area on the figure corresponds to a region $\Omega_{\underline{X}}$ in the space of random variables $\underline{x}$ where F > 14 N/m and its probability content is equal to P[F > 14 N/m]. The point on the contour line that is tangent to the line defined by F = 14 N/m corresponds to the most likely combination of wind and ice for this level of load. In the vocabulary of reliability, this point is the design point and is used to specify the design random variable combination. The First-Order Reliability Method (FORM) can be used to find the design point numerically. In FORM, a random vector is transformed into an equivalent standardized multivariable Normal vector. The design point can then be obtained by searching the minimum distance β from the origin to the nearest point on the $\Omega_{\underline{X}}$ space. Finally, the probability content can be approximated by,

$$P_F(f) = \Phi(-\beta) \tag{5.11}$$

where Φ is the standard cumulative Normal distribution function; and β is the reliability index.

5.4. Examples of the analysis for selected sites

The proposed method is applied to several stations in Québec where wind and ice data is readily available. The results are compared with the combination rules for the maximum force based on the IEC826 concept and are also compared with the simplified rules of the draft IEC 60826.

The data set for wind speed during ice storms is obtained from the Environment Canada hourly wind database. The data is considered to be accurate; however, it is possible that some observations could have been affected by icing of the anemometer, especially for events with very large accumulations. The data sets for ice using the event-based selection concept have been described in Chapter 4. However, an update for the selected sites has been incorporated in this chapter where more years of observations have been included. It should be noted that the conversion formula suggested by Hydro-Québec (Radial ice thickness = 0.7 * (maximum measured thickness of iced cylinder – 25mm cylinder diameter) have been included in this chapter as well.

The joint distribution for wind and ice is estimated for twelve sites in Québec. To simplify the analyses, wind and ice are considered independent. This seems to be a reasonable assumption for the investigated sites. The uncertainty on the drag coefficient and the uncertainty on the model are not considered. The data points have been selected using the peak-over-threshold concept where episodes with ice accumulation of 4mm or more are considered. However, for comparison with IEC 60826 values, the maximum yearly data for wind and ice is used instead of the event-based ones in order to evaluate the results of the simplified rules. The number of events is then set to one per year and corrections have been made to account for the difference between the number of years of observations and the number of storms. Tables 5.1 and 5.2 show the maximum yearly ice thickness and maximum yearly wind speed during an ice storm respectively.

The approach described in IEC 826 comprises two scenarios having the same return period: (1) a heavy ice scenario combined with light winds (i.e. low probability ice with high probability wind) and (2) a light ice scenario combined with severe winds (i.e. low probability wind with high probability ice). A disadvantage of this procedure as illustrated in the Figure 5.3 is that these two scenarios do not include the combination of wind and ice that produces the maximum horizontal load. For both scenarios, the proposed IEC 60826 standard suggests using the value corresponding to a given return period for the variable with low probability combined with the mean value for the variable with high probability.

Forces on a 30mm-conductor for the stations analyzed are determined based on the combination that produces the maximum force for a specific return period. Design points for each station are also obtained using a FORM algorithm and assuming Gumbel distributions for both wind and ice; and by assuming a Gumbel distribution for wind speed and a General Pareto distribution for ice.

Forces obtained with the reliability-based procedure are always higher than the ones obtained from the combination of wind speed and ice accumulation corresponding to the same return period. The difference in the horizontal forces for the Montréal and St-Hubert stations are 30% and 40% respectively when Gumbel distribution are used for both wind and ice. When the General Pareto distribution is used for ice, the estimated horizontal forces are even higher. The choice of the distribution has an important influence in the extrapolation of ice accumulations for long return periods. However, this has been investigated in

Chapter 4 and will not be discussed further here. Note that the uncertainty on these values is very high and a regional adjustment of the design values is necessary. The results showed that the simplified rules of the IEC 60826 are mostly conservative and suitable for design purpose in most cases.

5.5. Wind speed distribution during ice

As discussed previously, design rules are based on the combination of wind speed and ice accumulation with specific return period. This can be done when data sets can be obtained for wind speed during ice storms. However, in many cases, such data sets are not available and designers must rely on simple rules based on data sets for annual maximum wind. The most common rule is to assume that the distribution for the annual maximum wind speed can be used to derive the wind speed that would apply during an ice storm. The underlying assumption is that the form of the distribution is valid for the entire year and that the distribution is scaled down to account for the length of time that ice is present on a structure relative to the entire year (Davenport, 1986; and IEC 826). A comparison of the distributions of maximum wind speeds and wind direction during the whole year and during ice storms at several sites in Québec indicates that this assumption is not accurate and that the distribution of maximum wind speeds during ice storms cannot be derived by a simple scaling of the distribution of annual maximum wind speed. Ice storms appear to be associated with recurrent and well-defined meteorological systems that are characterized by winds that have distinct distributions both in intensity and direction.

The sites of Monteral, Québec, Sept-Îles, Baie Comeau and St-Hubert are located in or near the St-Laurent River valley while the site of Sherbrooke is inland. All sites are located in southern Québec within the region most affected by ice storms. In general, the direction of annual maximum wind is fairly uniformly distributed at most sites. This is specially the case for the sites of Sept-Îles and Baie Comeau on the north shore of the St-Laurent River. Other sites can exhibit some directional preference in the direction of annual maximum winds (southwest for Montréal, southwest or northeast for Québec, west for Sherbrooke). During ice storms, the directions of the maximum winds show significant differences at all sites relative to the distributions for the annual maximum winds indicating that the meteorological systems associated with ice storms are quite different than those that generate the maximum annual winds. For the sites near the St-Laurent River, maximum winds tend to be aligned with the general orientation of the river, especially for Montréal, St-Hubert, Québec, Sept-Îles, and Baie Comeau. For the site of Sherbrooke, results are more difficult to interpret; however, two distinct meteorological systems with westerly and northeast winds dominate (Figure 5.5).

In the absence of specific information at a site, IEC 60826 suggests a reduction factor between 60 and 85% of the maximum yearly winds for a given return period when combined with the average of the yearly extreme ice accumulation. Another suggested loading scenario is to combine the yearly maximum ice accumulation for a given return period with the average of the extreme wind during ice storms. If the distribution for the latter is not known, IEC 60826 suggests a value between 40 and 50% of the reference wind (annual maximum wind with the same return period).

Extreme value distributions type I (Gumbel) were obtained from the data sets at each of the 6 stations previously mentioned. The data sets consist of the sample of annual maximum wind speeds and of the maximum yearly wind speed during ice storms.

Figure 5.6 shows the distributions obtained for the maximum annual wind speeds and the maximum annual wind speed during an ice storm. Also shown is the ratio of the wind pressure for the two wind speeds as a function of the return period. For some sites the distributions are quite similar, while for others the distribution of wind speeds during ice storms is much less severe. Figure 5.7 shows the ratio of maximum wind speeds during ice storms and during the whole year for different return periods at the six sites. The IEC 60826 recommended upper ratio is exceeded for the sites of St-Hubert and Québec City, while a lower ratio is obtained for the site of Sherbrooke. For Baie Comeau, Montréal, and Sept-Îles, the ratios are in the upper range of the recommended values. This finding is consistent with the comments of Makonnen (1995) about a minimum ratio of 0.80 that in use in Russia; and with the recommended ratio higher than 0.60 by Krishnasamy and Kulendran (1998) for sites in Ontario. In the province of Québec, the sites that are the most exposed to glaze ice hazards are located in the southern part of the province and within the St-Laurent River valley. This is also the region where winds are the most intense, especially for sites around the Gulf of St-Laurent.

Figure 5.8 shows the ratio of the average maximum annual wind speed during ice storms to the reference wind (V_R) as a function of the return period for the six sites. The figure shows that the IEC 826 recommended ratios, 0.4 to 0.5 of the reference wind, are conservative for almost all sites and return periods considered for design. The maximum yearly wind speeds for the stations in southern Québec (the first four stations) are quite similar, while the wind speeds are markedly more intense for the stations in the Gulf of St-Laurent. The trend is slightly different for the maximum yearly wind speed during ice storms. The winds are less severe for the site in the mountainous area (Sherbrooke), while the wind speeds are similar for all the other stations located along the St-Laurent River, with a tendency for increasing values from the south to the north.

5.6. Summary

The combination of wind and ice accumulation is a major concern for the design and operation of electric distribution and transmission networks. Current design criteria is generally based on the specification of design wind speed as a fraction of the maximum annual wind speed in combination with the maximum annual ice accumulation for a specified return period. In other cases, two equally likely scenarios are considered consisting of a heavy ice scenario combined with light winds, and a light ice scenario combined with strong winds.

Reliability procedure has been proposed for analyzing the effect of load combinations on a structure. The resulting design forces are compared to the forces derived from the simple combination rules of IEC 826, and the proposed IEC 60826. Advantages of reliability procedures are that the uncertainty on all the random variables describing the performance of the structure can be included in the analysis and that the most likely performance-specific combination of environmental variables can be identified.

Wind data are also analysed to derive distributions for the maximum wind speeds during ice storms and during the entire year. These distributions are then compared at selected return periods to validate the simple rules proposed in IEC 60826.

Table 5.1: Maximum yearly ice thickness in mm

	Montreal	St-Hubert	Quebec	Sherbrooke	Sept iles	Val d'or	Roberval	Baiecomeau	Gaspe	Maniwaki	Montjoli	Natashquan
1975	20.3	3.5	7		3.5	3.5		7			4.9	24.5
1976	8.4	26.6	9.1		10.5	1.4		3.5		0.7	5.6	14
1977	5.6	8.4	7	3.5	3.5	1.4		2.1	0.7	3.5		4.9
1978	14.7	3.5	9.1			4.2		4.9	10.5		0.7	
1979	11.9	9.1	11.2		3.5	4.9		8.4	0.7		8.4	7.7
1980	7	2.1	7.7		9.1	3.5		2.1	2.8	4.9	2.8	35
1981	2.1	2.1	2.8	3.5	8.4	1.4			0.7	2.1	2.8	2.8
1982	15.4	11.9	17.5	2.8	5.6	2.8	0.7	9.1	4.2	4.2	4.2	8.4
1983	18.2	30.1	32.2	4.2	7	11.2	5.6	9.8	6.3	4.9	12.6	
1984	11.2	11.9	11.2	3.5	15.4	14	11.9	10.5	8.4	3.5	7.7	11.9
1985	10.5	9.8	5.6	3.5	7	5.6	9.8	3.5	7	4.2	3.5	
1986	9.1	12.6	18.2	4.9	1.4	5.6	8.4	12.6	11.9	3.5	12.6	7
1987	0.7	2.8	10.5	1.4	7.7	2.1		1.4	2.1	2.8		
1988	2.8		10.5		6.3	4.9		0.7		4.2	10.5	
1989	9.8	9.8	10.5	3.5		17.5			2.1	2.1		1.4
1990	9.8	7	8.4	2.8	16.1	9.1	10.5	9.1	9.1	5.6	3.5	12.6
1991	7.7	23.8	13.3	8.4	14.7	4.2	0.7	2.1	2.8	2.1	1.4	7
1992	7	11.2	16.1	8.4	8.4	5.6	5.6	14.7	2.1	4.2	25.2	7.7
1993	9.8	11.2	5.6	7	14	3.5	4.9	10.5	5.6		5.6	4.9
1994	4.9	4.9	14	2.1		1.4	7.7	2.8				5.6
1995	9.8	7.7	13.3		6.3	6.3	3.5	7	4.2	4.9	8.4	7.7
1996	3.5	4.2	4.9		5.6			1.4		2.8		2.8
1997	3.5	4.9	4.9		4.2			2.1		4.2		
1998	36.4	64.4			5.6			9.1	0.7	14.7	5.6	3.5
1999	2.1	2.1			9.1			7	2.8	2.1	4.2	9.1
2000												

No ice data   No wind data   Ice thickness < 4mm

Table 5.2: Maximum yearly wind during icing in km/h

	Montreal	St-Hubert	Quebec	Sherbrooke	Sept iles	Val d'or	Roberval	Baiecomeau	Gaspe	Maniwaki	Montjoli	Natashquan
1975	34				26	34		50				
1976	45				40	19		27				
1977	37		56	19	13	56		50	37			
1978	56	44	65			41		80	33		44	
1979	69	74	48		15	30		35	7		46	
1980	24	41	70		56	46		59	30		43	
1981	26	28	37	19	46	26			24		30	
1982	35	48	43	33	56	31	30	44	28		48	
1983	37	39	52	30	67	35	30	41	37		44	
1984	37	41	46	22	56	30	33	50	20		44	
1985	44	59	46	41	70	41	46	44	28		43	
1986	33	30	46	30	35	37	39	33	19		46	63
1987	28	31	59	30	33	31		28	31			
1988	26		37		41	28		31			22	
1989	37	37	52	22		46			24			24
1990	46	35	41	33	52	39	28	44	19		30	30
1991	44	39	52	28	46	26	26	26	37		33	35
1992	46	50	46	31	57	44	31	37	30		35	41
1993	30	30	33	30	39	24	9	52	22		33	26
1994	31	37	26	19		24	13	30				43
1995	28	44	52		33	31	22	30	30		37	26
1996	37	63	28		37			35				26
1997	52	57	52		46			20				
1998	33	33			41			26	28		65	37
1999	31	28			69			20	26		48	65
2000												

No ice data

No wind data

Ice thickness < 4mm

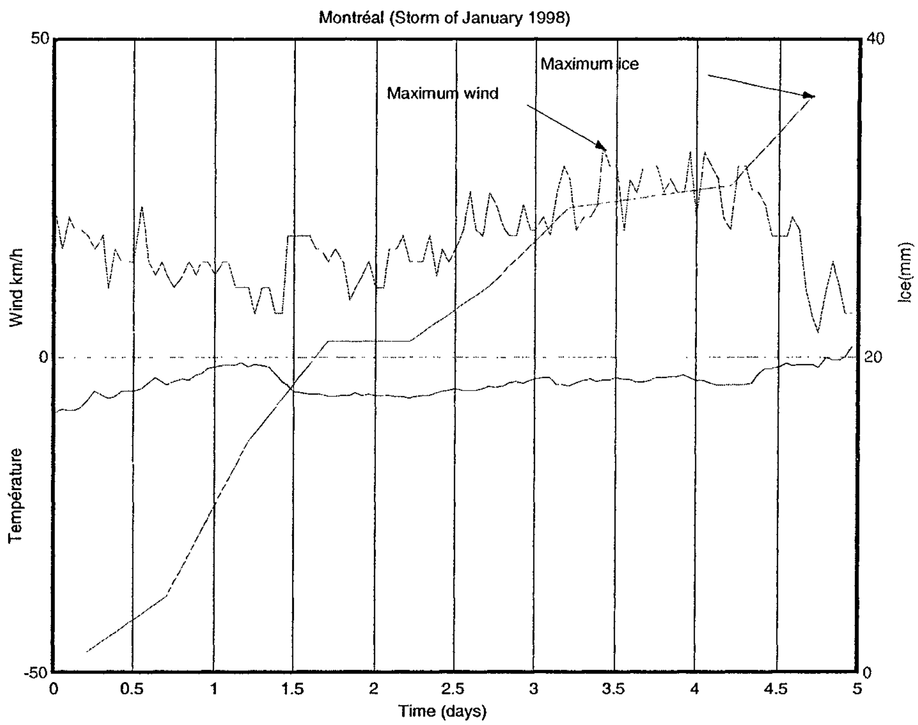

Figure 5.1: Wind , Temperature and Ice during January 1998 ice-storm (Montreal)

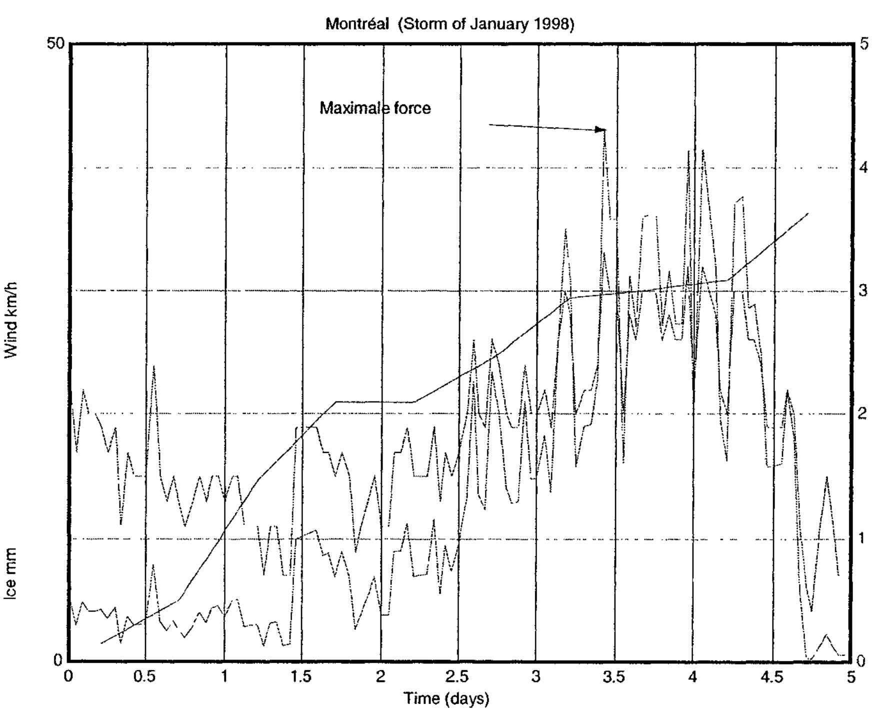

Figure 5.2: Wind, ice and horizontal force on a 20mm conductor during January 1998 storm (Montreal)

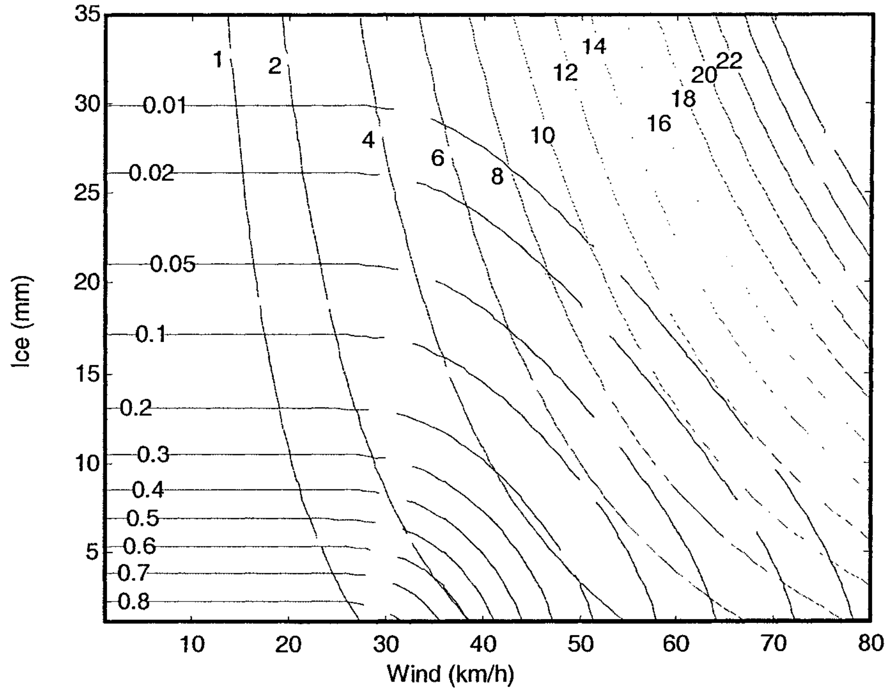

Figure 5.3: Probability of exceedence of wind, ice, and horizontal force on a 20 mm conductor.

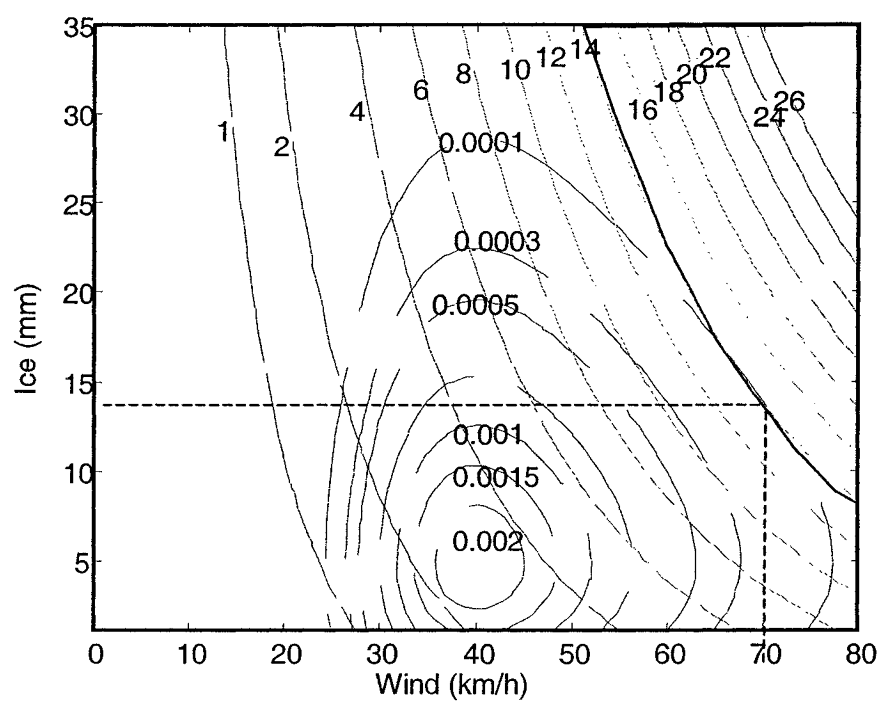

Figure 5.4: Joint probability function of wind and ice, and the horizontal force on a 20 mm conductor.

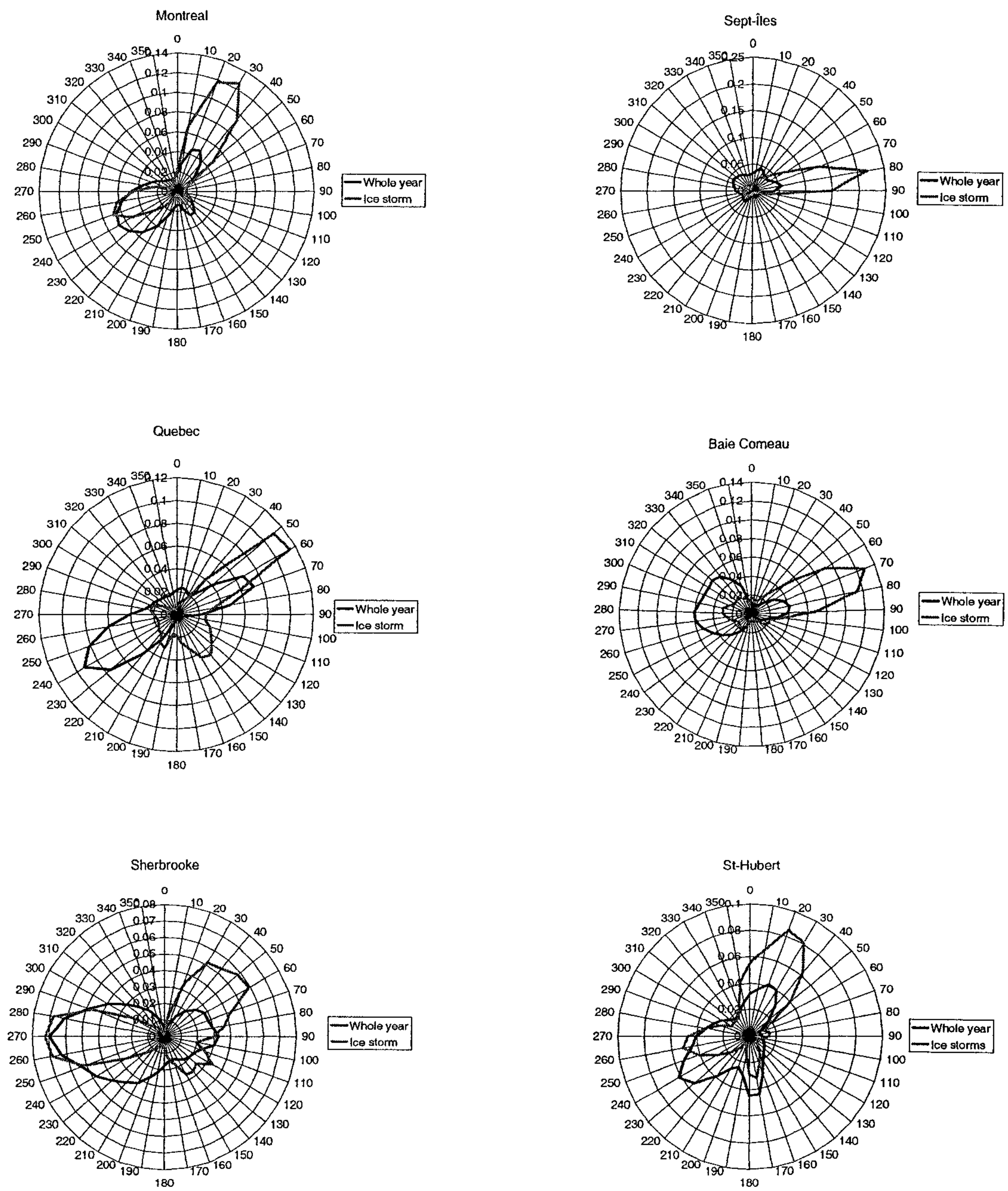

Figure 5.5: Wind rose for maximum winds during the whole year and during ice storms.

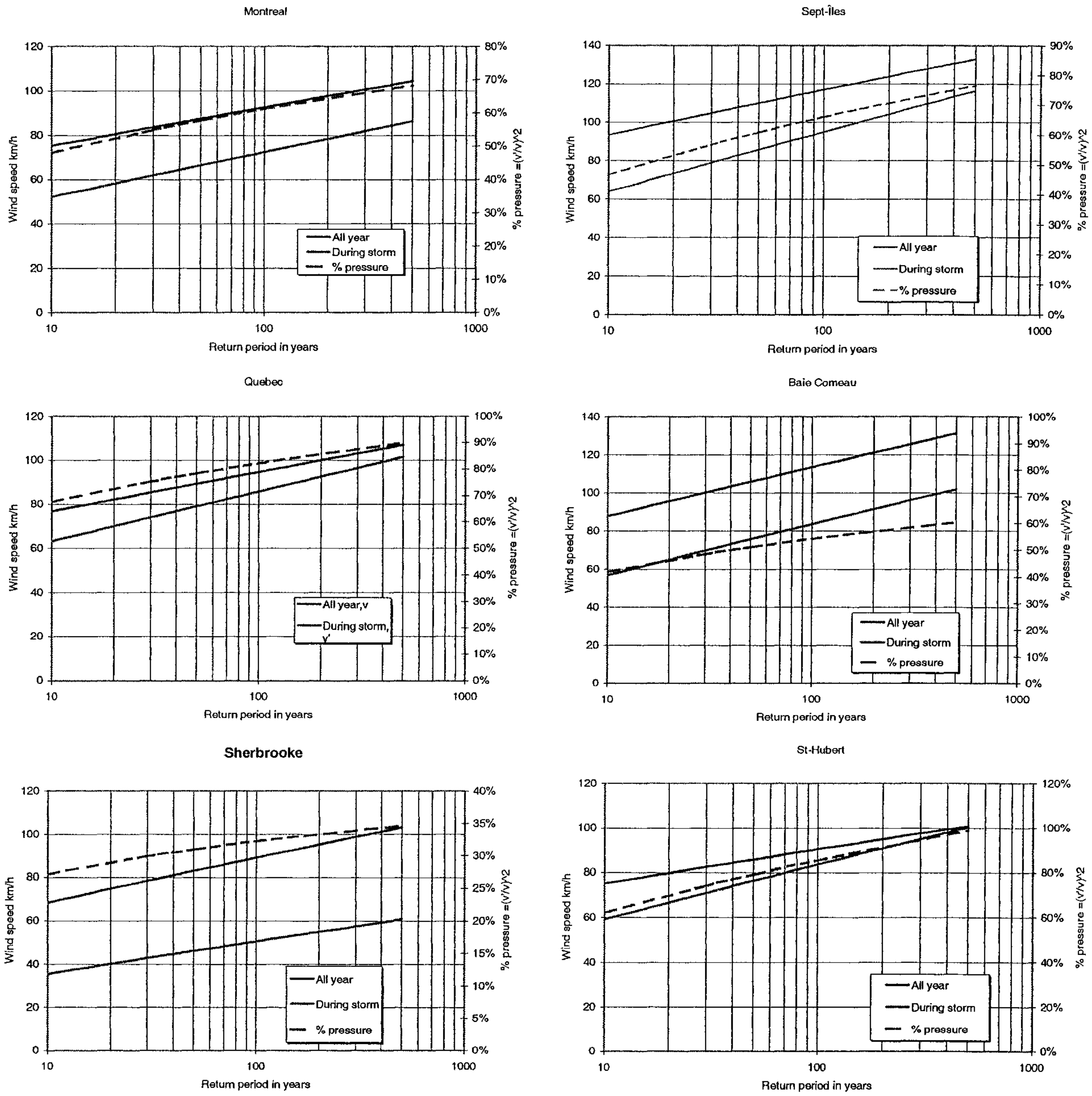

Figure 5.6: Return period of ice storm maximum winds and of extreme.

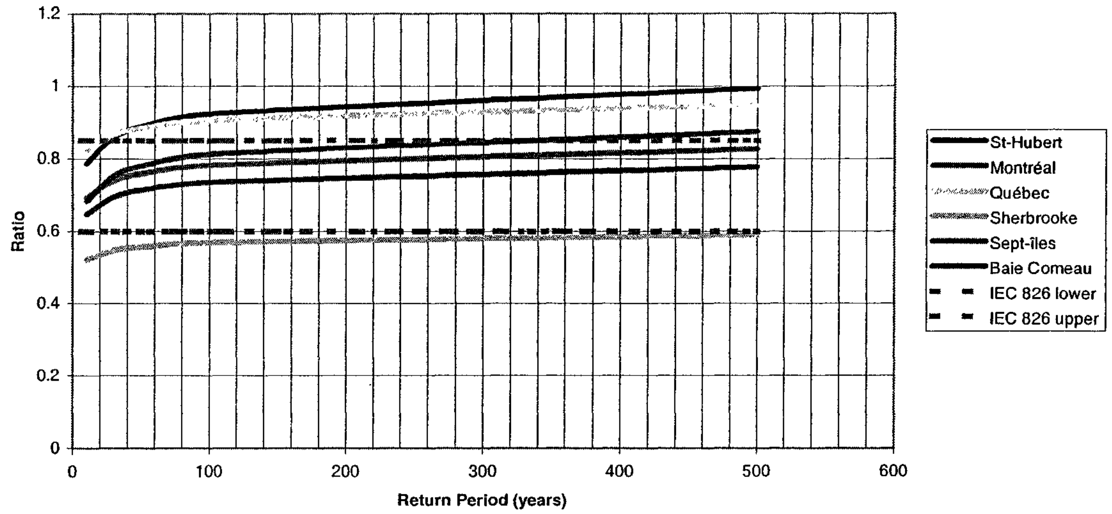

Figure 5.7: Ratio of the maximum yearly wind speed during ice storms to the maximum yearly wind speed as a function of the return period.

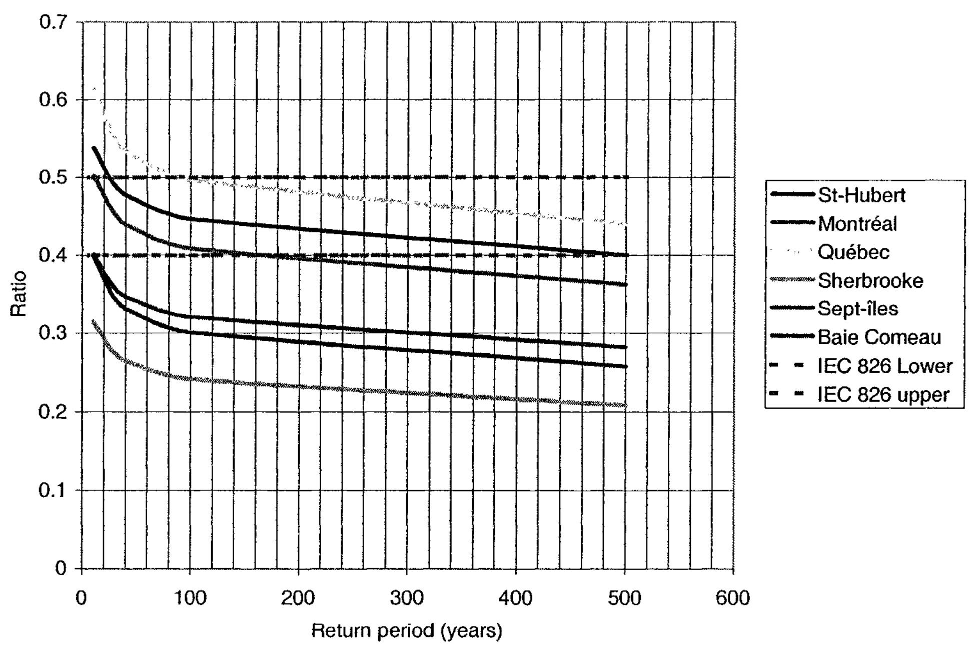

Figure 5.8: Ratio of the expected maximum yearly wind speed during ice storms to the maximum yearly wind speed as a function of the retunr period.

Chapter 6: Spatial Analysis of Icing Events

6.1. Introduction

Statistical analyses of ice accumulation from the network of Passive Ice Meters (Chapter 4) can be used to estimate the design ice thickness at each station for different return periods. Estimates of design criteria for locations where there is no PIM require interpolation of model parameters for both the intensity of the ice accumulation and the recurrence rate of ice storm.

Interpolated estimates of design criteria are important since new constructions are most likely not located in proximity to measurement stations. In addition, highly vulnerable facilities such as electric transmission lines require estimates of the atmospheric icing hazard function everywhere along its length since this type of facility is a weakest-link system. Currently, there is no formal or analytical procedure for deriving a map of icing hazards. Makkonon and Ahti (1995) found that the thickness of rime ice on structures is correlated to the local terrain elevation. Laflamme (1995) uses pooling of data between three neighbouring stations to define the sample of annual maximum glaze ice accumulations and reports a significant improvement in the goodness-of-fit for the probability distribution function of ice accumulation. A regional map of ice hazards is traditionally obtained by a qualitative fit, through the estimates of design ice thickness for a given return period, that incorporates knowledge on local topographical and climatological features, and for convenience predefined geo-political regions.

In this chapter, spatial interpolation methods based on Kriging are investigated for the estimation of design values from an irregularly spaced network of measurement stations. Such methods are commonly used for the analysis of spatial data in the fields of mining, geography, and atmospheric science (Isaaks and Srivastava, 1989; Bailey and Gatrell, 1995). In all cases, only spatial proximity is being considered as a criterion for interpolation. Interpolations based on additional information such as characteristics of individual storms, topographical and climatological features are beyond the scope of this study.

Spatial interpolations are performed on the parameters of the Generalized Extreme Value distribution (GEV) and on the design glaze ice thickness for different return periods. Only interpolation results for the 50-years return period are presented here for a region delimited by the Montréal-Québec corridor. Cross-validation is used to evaluate the relative performance of the interpolation procedures.

6.2. Methodology

6.2.1. Spatial interpolation methods

Formally, the problem of spatio-temporal prediction is to estimate a quantity $Z(s;t)$ at a site with location (s), from data $\{Z(s_{1,i};t_i),\ldots,Z(s_{n,i};t_i):i=1,\ldots,n\}$ at n surrounding locations. This data set is an incomplete realization of the stochastic random process,

$$Z(s;t):\ s\in D(t);\ t\in T \tag{6.1}$$

where $t_1 < t_2 < \ldots < t_n < t$, and $(s_1, s_2,\ldots,s_n)$ are the locations of the n sites with data, and D(t) is a time dependent region that contains the n locations (Cressie, 1993).

For the determination of static or equivalent static design structural loads, the main concern is to estimate the maximum value of $Z(s,t)$ that can be upcrossed during a given period of time as opposed to the complete time history of the process. This allows separating the spatial and temporal components of the process. In this application the process is assumed to be stationary in time and only the spatial component is investigated. The spatial component can be expressed as a random process,

$$Z(s): s \in D \tag{6.2}$$

For spatially continuous data, interpolation can be performed using geometrical (e.g. tessellation), algebraic (e.g. inverse distance), or statistical (e.g. Kriging) methods. Most of these methods are based on a linear weighted combination of observations,

$$\tilde{z}(s) = \sum_{i=1}^{n} w_i z(s_i) \tag{6.3}$$

where w_i is the weight of the observation at station s_i, n is the number of known data points, and $\tilde{z}(s)$ is the interpolated value. The weights w_i are usually normalized and sum to one and are a function of the proximity between pairs of points as defined by geometry, distance, or other attributes (e.g. elevation). Although many of these methods have been investigated, only Kriging procedures are discussed in detail in the present study.

6.2.2. Interpolation by Kriging

Kriging is a weighted averaging procedure where the weights are selected in order to obtain the Best Linear Unbiased Estimator (BLUE). The two main steps in Kriging are: 1) the analysis of the spatial structure of the data, and 2) the optimal interpolation of the variable at unsampled locations. The first step consists in estimating and fitting a covariance function C(d), or a semi-variogram γ(d) to the data. These are respectively defined as,

$$C(d(s_i,s_j)) = \mathrm{cov}(Z(s_i), Z(s_j)|d(s_i,s_j)) \tag{6.4}$$

and

$$\gamma(d(s_i,s_j)) = 1/2\ [\mathrm{var}(Z(s_i),-Z(s_j))|\ d(s_i,s_j)] \tag{6.5}$$

where $d(s_i,s_j)$ is the distance between stations i and j. A parametric model is then fitted to the sample covariogram or variogram that provides a continuous description of the spatial correlation structure (Figure 6.1). The most widely used parametric models are the linear, spherical, exponential and Gaussian models (Bailey and Gatrell, 1995). The fitting of the model is usually done by the method of Least Squares or Maximum Likelihood.

The second step is the interpolation of the variable at sites without data. Kriging provides the minimum variance linear unbiased estimator for a given covariance function. Several variants of Kriging are available depending on the assumptions used for the estimation of the first order variation (mean or trend). In ordinary Kriging, it is assumed that the mean μ is constant but unknown,

$$Z(s) = \mu + \delta(s) \tag{6.6}$$

where $\delta(s_i)$ is the residual process. The estimator of Z(s) at an unsampled location s is,

$$\hat{Z}(s) = \sum_{i=1}^{n} \lambda_i Z(s_i), \tag{6.7}$$

and the weights λ are calculated from,

$$\lambda' = \left[\gamma + \mathbf{1} \frac{(1 - \mathbf{1}'\Gamma^{-1}\gamma)}{\mathbf{1}'\Gamma^{-1}\mathbf{1}} \right]' \Gamma^{-1} \tag{6.8}$$

or

$$\lambda' = \left[c + \mathbf{1} \frac{(1 - \mathbf{1}'\Sigma^{-1}c)}{\mathbf{1}'\Sigma^{-1}\mathbf{1}} \right]' \Sigma^{-1} \tag{6.9}$$

where $\gamma = [\gamma(s_1 - s), \ldots, \gamma(s_n - s)]'$, $\Gamma = [\gamma(s_i - s_j), i=1,\ldots,n, j=1,\ldots,n]$, $c = [c(s_1, s), \ldots, c(s_n, s)]'$, $\Sigma = [c(s_i, s_j), i=1,\ldots,n, j=1,\ldots,n]$, and **1** is the vector of ones.

The elements of γ and c are respectively calculated from the variogram and covariogram functions. These predictors minimize the mean squared error $E[(Z(s)- \lambda'Z)^2]$ among all linear predicators $\lambda'Z$ that satisfy the unbiasedness condition,

$$\sum_{i=1}^{n} \lambda_i = 1 \tag{6.10}$$

6.2.3. Ad Hoc interpolation procedure

Kriging requires that the first order variation of the process (mean or trend) over the region be identified. In simple Kriging, the mean is removed from the data and Kriging is applied to the residuals. In ordinary and universal Kriging, the mean or trend is assumed a priori, usually in the form of a polynomial or other function, but does not have to be removed from the data. It is also a common practice to perform Kriging in a local neighbourhood to reduce computing time.

In the case on hand, there is no previous indication for the choice of trend function and in addition computing time is not a problem. Consequently, in this application, a procedure based on spatial averaging of observations at neighbouring stations is used for estimating the regional trend. This practice is usually recommended when there is no priori justification for a parametric trend. The process can be viewed as a means of separating regional and small-scale components of the process (site effect).

First, natural neighbours to each station are identified from the Delaunay triangulation for all existing stations. The Delaunay triangulation, as mentioned before in Chapter 3, corresponds to a set of triangles with stations as vertices such that there are no stations within the circumcircle around each triangle (Figure 6.2).

Second, the average of the observations at the vertices of each triangle is computed and assigned to the mid-point of each triangle. The residuals are obtained at the original stations as the difference between the observations and the mean, which is locally estimated by taking the average of the process over all connecting triangles. The interpolations of the regional trend and of the local effect are performed using Kriging with two different correlation structures.

6.3. Results and discussion

The most significant results from the evaluation of the interpolation procedures are summarized next. The interpolation procedures were tested on the parameters of the GEV distribution and on the estimates of the design ice accumulation for a 50 years return period, but only the results for the latter case are discussed in detail.

Cross validation, which consists in eliminating each station one at a time and to make a prediction of the model parameters, was used to evaluate the accuracy of the Kriging procedure. Cross validation showed that ordinary Kriging by itself is not an appropriate interpolating method for glaze ice hazards due to the erratic nature of the spatial fluctuations in the hazard function.

The sample variogram does not show strong spatial dependencies at any scale for the design ice thickness for a 50-year return period. Two options were investigated for fitting the variogram. In the first case, it was assumed that only a short-range dependency is present in the data. In the second, the assumption of short-range dependency was relaxed and replaced by a large nugget effect (Figure 6.3). In both cases, cross-validated statistics on the performance of the interpolators indicated that the mean value dominates the estimates while the residuals are poorly distributed.

Improvement in interpolations is achieved by replacing the global mean by a regional non-parametric trend surface. The procedure used to estimate the regional trend surface has been described above in section 6.2. This procedure provides a robust estimator of the regional trend and residuals that are most likely associated with local effects. The sample variogram for the regional trend is shown in Figure 6.4 along with the variograms for the original data and for the residuals. As expected, the spatial correlation for the regional trend is less erratic and the variation of the residuals is reduced although no spatial dependency is apparent. The exponential form of the variogram with a small nugget effect is used for the region mean (Figure 6.5). The variogram selected for the residuals corresponds to a short range and a nugget effect. Note that the spatial dependency of the residuals can not be completely characterized using current data since the distances between stations may exceed the range over which the residuals exhibit some spatial dependency.

Figure 6.6 shows the original values for the ice thickness with a 50-year return period over the region segmented by Voronoi polygons and Delaunay triangles using the coordinates of the PIM stations. The figure also shows the interpolated surface obtained by: (1) Kriging of the original data, (2) Kriging of the regional trend, and (3) Kriging of the residual process.

Figure 6.7 shows examples of spatial interpolations using three different methods (triangulation, inverse-distance, and Kriging) for the thickness of glaze ice with a 50-years return period for the Montréal-Québec corridor using the Generalized-Extreme-Value distribution. Cross-validation was used to evaluate predictive ability of the various interpolation procedures and all were found to give poor results due to large fluctuations in the estimates of the parameters from station to station. Note that these interpolations are solely based on the distance between stations and do not account for correlation of icing storms with climatological and topographical features. The correlation structure for the glaze ice data based on distance was found to be poor.

Interesting features of the interpolated surface for the regional trend are the regions where icing hazards are more severe on average. These are located in the Richelieu valley and the Lower St-Lawrence valley near and north of Québec City and have been identified historically as high hazard regions for atmospheric icing (Laflamme and Periard, 1998). Conversely, mountainous regions in the Eastern Townships and the Laurentians appear as regions of lower atmospheric icing hazards on average. These features can be explained by variations in the regional climate and topography. However, the analysis of the residual process (after removing the interpolated trend surface from the original data) shows no spatial dependency within the range of the inter-station distances, which indicates that significant local variations remain unexplained.

More studies are required to determine if these fluctuations can be explained by incorporating additional variables in the model (e.g. through co-Kriging), such as local terrain elevation, slope, and slope orientation, or by dividing the observations into different populations based on the spatial extent and severity of the storm.

6.4. Summary

Spatial interpolation procedures based on Kriging were investigated for the purpose of developing regional maps of atmospheric icing hazards in the province of Québec. The data analyzed consisted of up to 20 years of observations at about 40 measurement stations in the Montréal-Québec City corridor. Kriging was applied to the expected glaze ice thickness for a 50-year return period. The variogram for this data showed very little spatial dependency and a large nugget effect. Interpolations based on this model were evaluated through cross validation and were found to result in inaccurate predictions. Better results were obtained by first fitting a regional non-parametric trend surface to the data. Interpolations based on Kriging of the trend surface are very well correlated to the spatial variation in severity of the storms that have been reported historically. However, the local residuals remain significant and show almost no spatial correlation. Other procedures are recommended for further investigation in order to improve the spatial variation of atmospheric hazards. These include analyses for different storm populations, and co-Kriging with local topographical and climatological features.

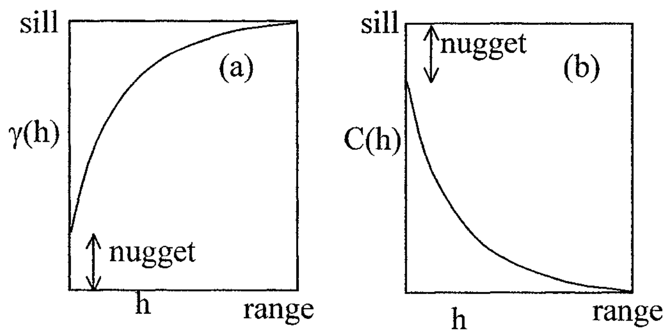

Figure 6.1: Spatial correlation structure (a) variogram (b) covariogram

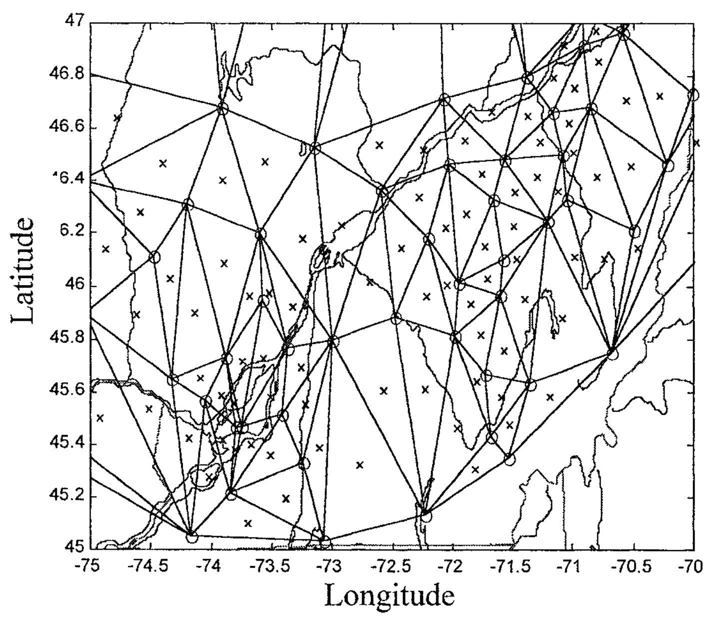

Figure 6.2: Local mean using Delaunay triangulation

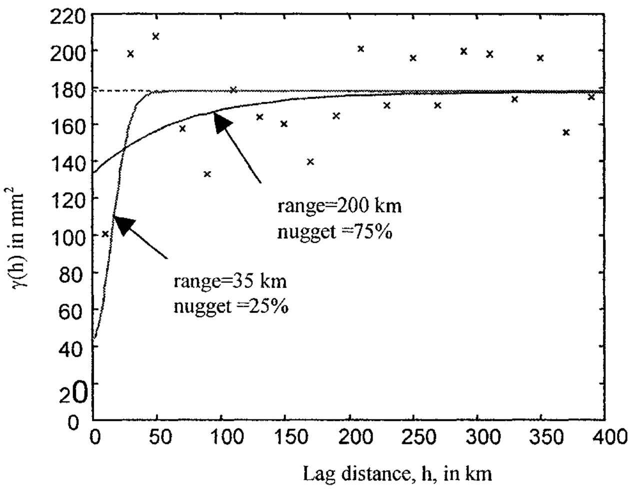

Figure 6.3: Models of the variogram for original data

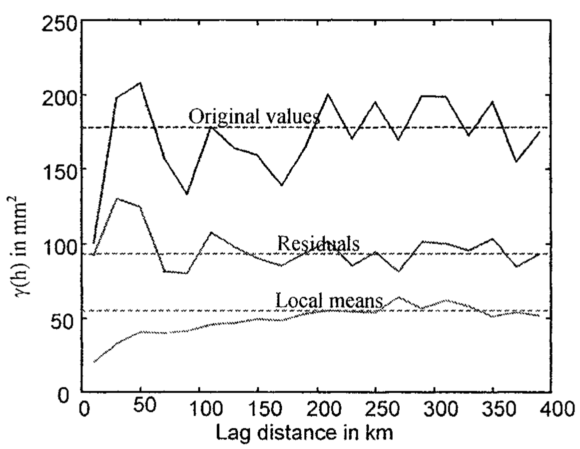

Figure 6.4: Sample Variograms of original data, local mean and residuals

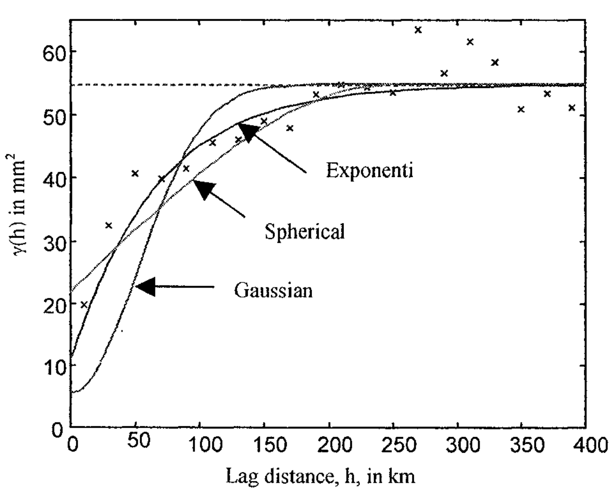

Figure 6.5: Models of varigram for local means using Exponential, Spherical and Gaussian models

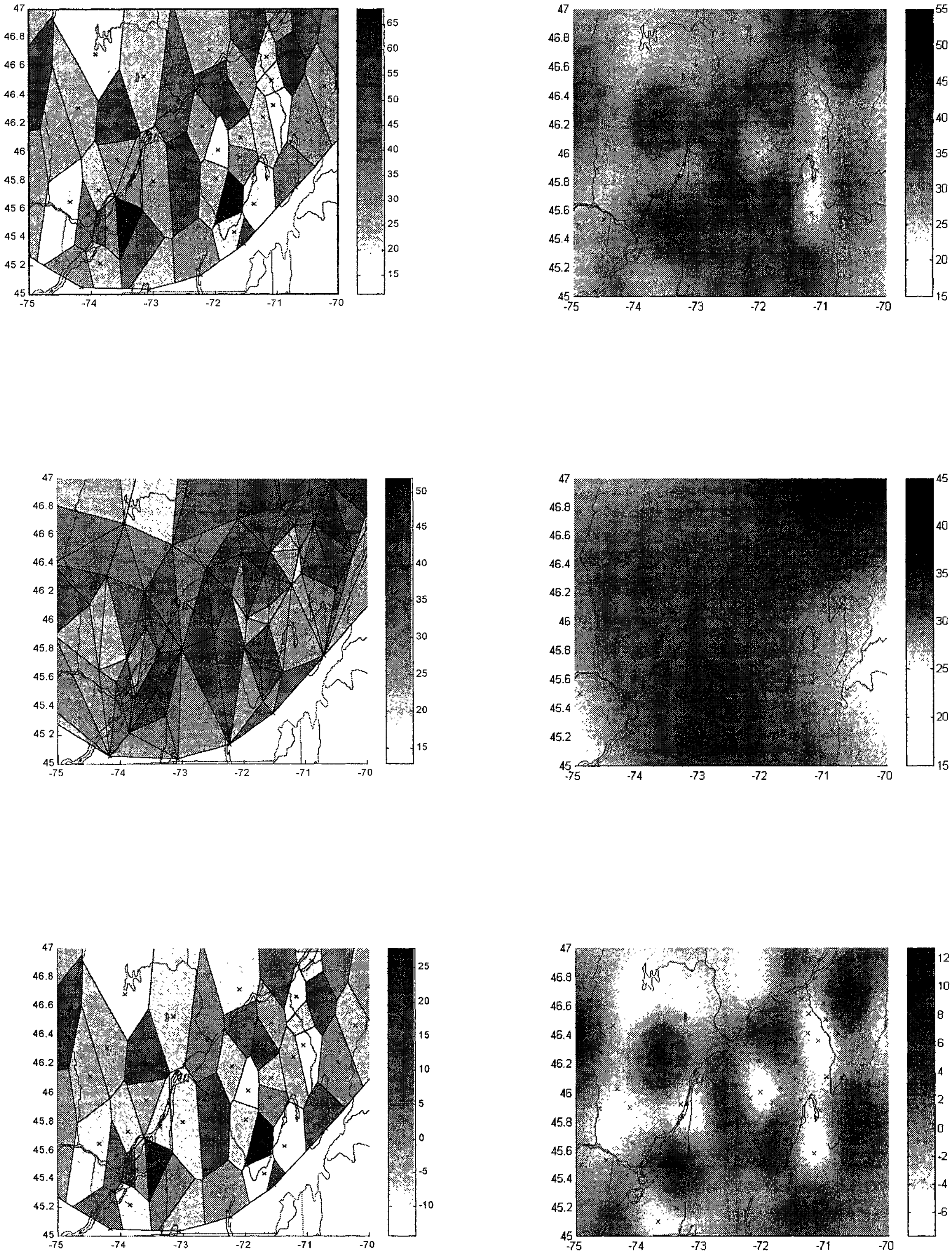

Figure 6.6: Regionalized and interpolated 50-year return period ice thickness (a) Original data and ordinary kriging, (b) Regional means and trend surface, (c) Residuals

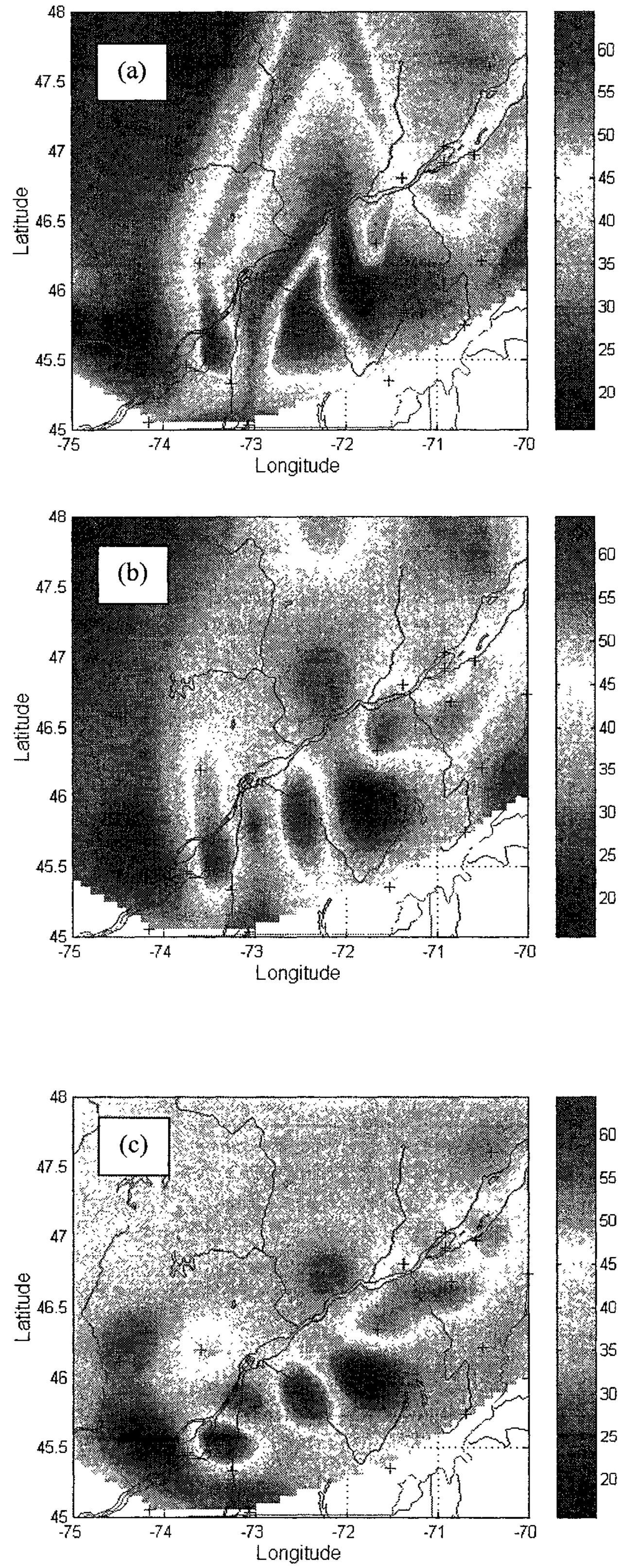

Figure 6.7:Spatial distribution of 50-years return period ice thickness in mm; (a) using triangulation, (b) using inverse distance, and (c) using kriging

Chapter 7 Conclusions and Recommendations

7.1 Conclusions

The PIM network represents a unique data set for the analysis of atmospheric icing hazards in Québec. The data set is used to perform statistical analyses to estimate the recurrence rate and the severity of ice storms across Québec. An event-based model is used to form the sample at each station. Events are defined either at each station or over a region by identifying periods of uninterrupted ice accretion. A comparison between annual-maximum and event-based models shows that the latter provides better results.

Twelve probability distributions are examined for representing the intensity of ice storms in Québec at 45 measurement stations. The distributions are compared on the basis of goodness-of-fit statistics and sampling characteristics of the upper tail of the distributions. No single distribution fits the data perfectly at all stations. However, the Pearson type III, Generalized Pareto, Generalized Normal, and Generalized Extreme-Value distributions are the best on average. The Pearson type III and Generalized Pareto distributions rank first based on several measures of goodness-of-fit followed by the Generalized Normal and Generalized Extreme-Value distributions. The commonly-used Gumbel distribution is consistently outperformed by the three-parameter distributions. Finally, the Beta-P and Beta-K distributions show very mixed results while the Log Pearson type III distribution appears adequate in only few cases but mostly overestimates the largest observations.

Reliability procedures have also been proposed for analyzing the effect of load combinations due to wind and ice on a structure. The resulting design forces are compared to the forces derived from the simple combination rules of IEC 826, and the proposed IEC 60826. Advantages of the reliability procedures are that the uncertainty on all the random variables describing the performance of the structure can be included in the analysis, and that the most likely combination of variables at failure can be determined for different types of structures and different failure modes. Wind data is also analysed to derive distributions for the maximum wind speed during ice storms and during the entire year. These distributions are then compared at selected return periods to validate the simple rules proposed in IEC 60826, relating yearly maximum wind and maximum wind during ice storms.

Spatial interpolation procedures based on Kriging were investigated for the purpose of developing regional maps of atmospheric icing hazards in the province of Québec. The data analyzed consisted of up to 20 years of observations at about 40 measurement stations in Southern Québec. Kriging was applied to the design ice thickness for a 50-year return period. The variogram for this data showed very little spatial dependency and a large nugget effect. Interpolations based on this model were evaluated through cross validation and were found to result in inaccurate predictions. Better results were obtained by first fitting a regional non-parametric trend surface to the data. Interpolations based on kriging of the trend surface are very well correlated to the spatial variation in severity of the storms that have been reported historically. However, the local residuals remain significantly large and show almost no spatial correlation.

7.2 Originality

This study is the first attempt to utilize state-of-the-art statistical tools to study the PIM ice storm data. The analysis and comparison of twelve distributions for modeling ice accumulation is the most comprehensive analysis of its type relative to ice storm data. Previously, the Gumbel distribution has been used but without any justification or comparison with other distributions.

In addition, a reliability-based procedure has been used to analyze the combined loads due to wind and ice accumulation during ice storms. A unique data set has been compiled by combining data sets from Hydro-Québec and from

Environment Canada at meteorological stations in Québec. This analysis has been useful in estimating appropriate load combinations for different return periods and different locations in Québec; and has highlighted problems with combination rules specified in IEC 826.

Finally, the spatial interpolation using Kriging, a geostatistical tool, has been used for the first time to estimate the spatial variation of ice storm design criteria across Québec.

7.3 Recommendations for future work

7.3.1 Analysis of ice storm data

The PIM is a simple and effective device for ice accumulation measurements. The reliance on observers for data collection has its advantages and disadvantages. An experienced and enthusiastic observer records carefully major events and identify accurately the type and shape of the deposit. On the other hand, missing the peak of a major event, or wrongly identifying the ice type, can be misleading. The PIM database has to be used only after a comprehensive review and verification of the data. These can be achieved in several ways:

1) By studying events on a regional basis rather than on a site-specific basis. The author tried this approach and found that many events have spatial extent, while others are single site events. Even for the former ones, not all neighbouring sites have a record. These phenomena could be due to short duration of the events, topographic effects, or simply inconsistency in the observations. This approach can be useful for events with a dense array of PIM sites; however, for remote sites, no additional information can be added.

2) By comparison with other available meteorological data such as temperature and precipitation records. Temperature records can be used to verify the persistence period and precipitation can be used to verify the ice accumulation.

3) By employing an empirical model for prediction of ice accretion and comparing the results with the PIM records. The empirical models usually need more meteorological data than what is available from regular meteorological records. Some assumptions have to be made based on experimental studies for a specific climatological region. Sites located far from meteorological stations will need more assumptions and extrapolations.

New generation of ice measurement instruments, automated ice meter "Givromètre" and load cells, has been recently deployed at many sites in Québec. The new data, when available, will be useful to verify and complement the available PIM data.

Another approach is to utilize an empirical ice model together with the PIM data to develop regional ice load criteria. The PIM network is very dense around the Saint-Lawrence valley but very sparse in the remote areas of the province. To provide an ice map for the whole province, an empirical model based on available meteorological data has to be validated using PIM observations. A reliability approach similar to these of Chapter 5 can be employed to consider the uncertainty of the parameters involved in the model in order to estimate ice load for a given return period.

The procedures that are developed from the analysis of the PIM data set should be used with other data sets, such as those generated from meteorological data for defining ice levels in ASCE 7. The objective would be to validate the approach that was used in Québec and to compare results with other approaches.

An aspect of ice storms that has not been investigated in detail in past studies is the occurrence of extreme ice storms such as the one of 1998. This type of ice storm is unique both in terms of its intensity and spatial extent. Typically, data points from such storms appear as outliers when compared to other data at a single station. This type of event may have to be treated as if it belongs to a separate population. An interesting avenue would be to develop a separate data set of extreme ice storms for Eastern North America and to analyze the recurrence rate, the spatial extent and the severity of such storms.

Another issue that should be examined is the spatial extent and intensity of ice storms. This issue could have an important impact in determining ice storm hazards for transmission lines.

Finally, it would be interesting to compare the design criteria derived using the procedures presented in this thesis with those based on superstations (Jones, 1998) and triads (Laflamme, 1993). In the former case, the design criteria may be underestimated while in the second case design values are more appropriate as a regional estimate of icing hazards.

7.3.2. Analysis of combined wind and ice loads

Wind-on-ice analysis in this study was limited to its application to conductors of overhead lines; applications on other types and shapes of structures need to be studied.

The PIM data includes ice accumulation records on four perpendicular cylinders and surfaces. The accumulation on each of these cylinders and surfaces can be correlated with the corresponding maximum wind speed during freezing precipitations and during the residency period of the ice deposit.

The relation between the PIM ice measurement and equivalent radial ice thickness on a conductor or a surface needs to be further investigated. Ice accumulation on structural members other than cylindrical shapes needs also more investigations.

And finally, a study of the predominant wind direction during icing can also be useful in planning the orientation of overhead lines.

7.3.3. Spatial analysis of ice storms

The spatial analysis of ice storms performed in the study was successful in identifying the regions where ice storms are the most severe. In particular, the analysis showed that the St-Lawrence River valley and the Richelieu River valley are both regions that can be severely affected by ice storms.

Spatial interpolation of the quantiles of the distributions shows the need for more sophisticated schemes that incorporate climatological and topographic information. Procedures that include analyses for different storm populations, and co-Kriging with local topographical features are suggested. The effect of the topography on the accumulation needs to be also studied further. It has been noticed that some adjacent sites have completely different record for the same events. Topography could be one of the governing factors in terms of altitude, slope, and direction of slope relative to the predominant wind during ice storms.

A detailed analysis of wind data during ice storms has also highlighted the fact that storm patterns that affect various sites have very specific characteristics as a function of location. For example, for sites in the St-Lawrence River valley, prevalent winds are well aligned with the general orientation of the coastline or valleys. More work should be done to clearly establish a link between topographical and climatological patterns, and the frequency and severity of ice storms.

Bibliography:

Anderson, F.G. (1995). "A Comparison of Some Well Known Probability Distributions for Describing Annual Maximum Precipitation in Quebec." Master Project Report, Department of Civil Engineering and Applied Mechanics, McGill University, Montreal.

ASCE (1998). "Minimum Design Loads for Buildings and Other Structures." ASCE 7-98, American Society of Civil Engineers, Reston, Virginia.

Battan L.J. (1984). "Fundamentals of Meteorology." Chapter 7, Prentice Hall.

Benjamin, J.R. and Cornell, C.A. (1970). "Probability, Statistics, and Decision for Civil Engineers.", McGraw-Hill.

Boyd, D.W. (1970). "Icing of Wires in Canada." Technical Report No. 317 of the Division of Building Research, National Research Council of Canada, Ottawa.

Boyd, D.W., and Williams G.P. (1968). "Atmospheric Icing of Structures." Technical Report No. 275 of the Division of Building Research, National Research Council of Canada, Ottawa.

Bruneau, M., Magued, M., and Dryburgh, R. (1989). "Recommended Guidelines for Upgrading Existing Towers." Canadian Journal of Civil Engineering, 16, 733-742.

Butt, D. (1986). " Ice Observations in Newfoundland and Labrador." 3rd International Workshop on Atmospheric Icing of Structures IWAIS'86, Vancouver, 287-292.

Chaîné, P.M. (1974). "In-cloud Icing." Industrial Meteorology - Study V, Environment Canada, Toronto.

Chaîné, P.M. (1973a). "Glaze and its misery: The ice storm of 22-23 March 1972 North of Montreal." Weatherwise, June 1993.

Chaîné, P.M. (1973b). "The Variability of Glaze Ice in Quebec." Industrial Meteorology - Study I, Environment Canada, Toronto.

Chaîné, P.M., and Castonguay, G. (1974). "New Approach to Radial Ice Thickness Concept Applied to Bundle-Like Conductors." Industrial Meteorology - Study IV, Environment Canada, Toronto.

Chaîné, P.M., and Skeates, P. (1974a). "Ice Accretion Handbook, Freezing Precipitation." Industrial Meteorology - Study VI, Environment Canada, Toronto.

Chaîné, P.M., and Skeates, P. (1974b). "Wind and Ice Loading, Criteria Selection." Industrial Meteorology - Study III, Environment Canada, Toronto.

Chouinard L., ElFashny, K., and Sabourin, G. (2002). "Analysis of Combined Wind and Ice Loads in Quebec for the Design of Electric Transmission Lines." IWAIS'02, Brno, Czech Repablic.

Chouinard L., ElFashny, K., Nguyen, V., and Laflamme, J. (1998). "Modeling of Icing Events Based on Passive Ice Meter Observations in Quebec." Atmospheric Research, Elsevier Science, 46 (1-2), 169-179.

Christakos, George (1992). "Random Field Models in Earth Sciences." Academic Press.

Cressie, Noel A. C. (1993). "Statistics for Spatial Data." Wiley Series in Probability and Mathematical Statistics.

Criswell, M. E. (1986). " The Combined Ice Plus Wind Loading on Transmission Line Structures." IWAIS'86, Vancouver, 461-468.

CSA (2000). "Canadian Highway Bridge Design Code." CAN/CSA-S6-00, Canadian Standard Association, Rexdale, Ontario.

CSA (1994). "Antennas, Towers, and Antenna-Supporting Structures." S37-94, Canadian Standard Association, Rexdale, Ontario.

CSA (1987). "Canadian Electrical Code, Part III-Outside Wiring." CAN/CSA-C22.3 No. 1-M87 (Reaffirmed 1997), Canadian Standard Association, Rexdale, Ontario.

CSA (1981). "Guidelines for the Development of Limit States Design." Special Publication S408-1981, Canadian Standard Association, Rexdale, Ontario.

Cunnane, C. (1978) "Unbiased Plotting Position – A Review", Journal of Hydrology, 37 (3), 205-222.

Davenport, A.G. (1984). "Combined Loading of Ice and Wind on Guyed Towers." IWAIS'84, Trondheim, Norway, 169-172.

Ditlevsen, O., Olesen, R., and Mohr, G. (1987). "Solution of a Class of Load Combination Problems by Directional Simulation." Structural Safety, Elsevier, 4, 95-109.

Draganoiu, G., Lamarche, L., and McComber, P. (1996). "Computer Model of Glaze Accretion on Wires." Journal of Offshore Mechanics & Arctic Engineering, 118(2), 148-157.

Druez, J., McComber, P. (1996). "Field Data on Power Line Icing." Transactions of the Canadian Society of Mechanical Engineering, 20(3), 259-273.

ElFashny, K. (1995). “Reliability Analysis of Telecommunication Towers.” Master of Engineering thesis, Department of Civil Engineering and Applied Mechanics, McGill University, Montreal.

ElFashny, K., Chouinard, L., and McClure, G. (1998). “Reliability Analysis of a Telecommunication Tower.” Canadian Journal of Civil Engineering, CSCE, 26, 1-12.

ElFashny, K., Chouinard L., and Nguyen, V. (1998). "Characteristics of Icing Events in Quebec.” ISOPE’98, Montreal, Quebec.

ElFashny, K., Chouinard L., Nguyen, V., and Laflamme, J. (1998). "Spatial Analysis of Ice Observations in Quebec.” IWAIS'98, Reykjavik, Iceland.

ElFashny, K., Nguyen, V., Chouinard L. and Laflamme, J. (1998). "Statistical Analysis of Ice Observations in Quebec.” IWAIS'98, Reykjavik, Iceland.

ElFashny, K, Chouinard L.E. and Laflamme, J. (1996). "Estimation of Combined Wind and Ice Loads on Telecommunication Towers in Québec.” IWAIS'96, Chicoutimi, Quebec.

Eliasson A.J., and Thorsteins E. (1993). “Data Analysis of Icing Measurements in Iceland.” IWAIS’93, Budapest, 217-222.

Environment Canada (1998). "The Worst Ice Storm in Canadian History?" Green Lane, Environment Canada's World Wide Web, http://www.tor.ec.gc.ca/events/icestorm98/

Environment Canada. (1984). “ Principal Station Data,” A summary of hourly weather observations, climate normals and extremes for Canadian principal climate stations.

Ervik, M., Fikke, S. (1990). “Improved Model to Estimate Ice Loads and Combined Wind and Ice Loadings Based on Climatological Data.” IWAIS’90, Tokyo.

Fahleson, Claes. (1995). “Ice and Wind Loads on Guyed Masts.” Doctoral Thesis, Lulea University of Technology, Sweden.

FEMA (1998). "January 1998 New York Ice Storm.", Federal Emergency Management Agency, New York. (Available at http://www.fema.gov/reg-ii/1998/nyice1.htm).

Fikke, S.M., Schjetne, K. and Evensen B.D. (1982). “Iceload Measurements and Design Practice.” IWAIS'82, Hanover, New Hampshire, 277-289.

Félin, Béatrice (1988). “Freezing Rain in Quebec : Field Observations Compared to Model Estimations.” IWAIS’88, Paris, 119-123.

Félin, Béatrice (1986). "Ten Years of Standardized Field Ice Accretion Measurements in Quebec.” IWAIS’86, Vancouver, 9-16.

Félin, Béatrice (1981). "Commentaires sur les recommandations pour le calcul des charge climatiques de la norme S37." Report no. PLT-EN- 81-063.

Félin, Béatrice (1976). "The Observation of Rime and Glaze in Quebec." Canadian Electrical Association Spring meeting, March 22-24, Toronto.

Félin, Béatrice and Rivest, Julien, (1982). "An Application of Dendrochronology to the Determination of the Recurrence of Severe Ice Storms." IWAIS'82, Hanover, New Hampshire, 217-224.

Golikova, T.N., Golikov, B.F. and Savvaitov, D.S. (1982). "Methods of Calculating Icing Loads on Overhead Lines as Spatial Constructions." IWAIS'82, Hanover, New Hampshire, 341-345.

Govoni, J.W. and McKley, S.F. (1982). "Field Measurement of Combined Icing and Wind Loads on Wires." IWAIS'82, Hanover, New Hampshire, 205-215.

Hall, James W. (1996). "Ice Storm Management on an Electrical Utility System." IWAIS'96, Saguenay-Lac Saint Jean, 225-230.

Hosking, J.R.M. and Wallis J.R. (1997). "Regional Frequency Analysis: An Approach Based on L-Moments." Cambridge University Press, Cambridge, U.K.

Hydro-Québec (1998). "Report on January 1998 Ice Storm." Committee of experts appointed by Hydro-Quebec's board of directors.
(Available at http://www.hydroquebec.com/publication/r980727e/index.html).

Hydro-Québec (1993). "Manual for Observation of Glaze, Ice-Meter Observation Program." Division Équipement de Lignes, Services Études et Normalisation, Eighth printing.

Hydro-Québec (1977). "Chargements de vent et de verglas sur les lignes de transport du Québec." Proposition 01-1977, Report no. PLT-EN-77-005.

IEC (2002). "Design Criteria of Overhead Transmission Lines." Draft of International Standard IEC 60826, International Electrotechnical Commission.

IEC (1991). "Loading and Strength of Overhead Lines." Technical Report IEC-826, 1991-04, Second edition, International Electrotechnical Commission.

Isaaks, E.H. and Srivastava, R.M. (1989) " An Introduction to Applied Geostatistics." Oxford University Press.

ISO (1998). "Atmospheric Icing on Structures." ISO-TC98/SC3/WG6, International Organization for Standards.

IWAIS'82 (1982). "First International Workshop on Atmospheric Icing of Structures." proceedings: June 1-3, 1982, Hanover, New Hampshire, U.S.A.

IWAIS'84 (1984) "Second International Workshop on Atmospheric Icing of Structures." proceedings: June 19-21, 1984, Trondheim, Norway.

IWAIS'86 (1986) "Third International Workshop on Atmospheric Icing of Structures." proceedings: May 6-8, 1986, Vancouver, Canada.

IWAIS'88 (1988) "Fourth International Workshop on Atmospheric Icing of Structures." proceedings: September 5-7, 1988, Paris, France.

IWAIS'90 (1990) "Fifth International Workshop on Atmospheric Icing of Structures." proceedings: Oct. 29- Nov. 1, 1990, Tokyo, Japan.

IWAIS'93 (1993) "Sixth International Workshop on Atmospheric Icing of Structures." proceedings: September 20-23, 1993, Budapest, Hungary.

IWAIS'96 (1996) "Seventh International Workshop on Atmospheric Icing of Structures." proceedings: June 3-7, 1996, Saguenay-Lac Saint Jean, Canada.

IWAIS'98 (1998) "Eighth International Workshop on Atmospheric Icing of Structures." proceedings: June 8-11, 1998, Reykjavik, Iceland.

IWAIS'00 (2000) "Ninth International Workshop on Atmospheric Icing of Structures." proceedings: June 5-8, 2000, Chester, UK.

IWAIS'02 (2002) "Tenth International Workshop on Atmospheric Icing of Structures." proceedings: June 17-20, 2002, Brno, Czech Republic.

Jones, Kathleen F. (1998). "A Simple Model for Freezing Rain Ice Loads." Atmospheric Research, Elsevier Science, 46 (1-2), 87-97.

Jones, Kathleen F. (1996). "Ice accretion in freezing rain." Report 96-2, Cold Regions Research and Engineering Laboratory, Hanover, NH. (Available at http://www.crrel.usace.army.mil/techpub/crrel_reports/html_files/cat_f.html)

Jones, Kathleen F., Mulherin, Nathan D. (1998). "An Evaluation of the Severity of the January 1998 Ice Storm in Northern New England." Report for FEMA Region 1, Cold Regions Research and Engineering Laboratory, Hanover, NH. (Available at http://www.crrel.usace.army.mil/techpub/crrel_reports/reports/icestorm98.pdf)

Johnson, N. L. and Kotz, S. (1970). "Distributions in statistics, Continuous Univariate Distributions." John Wiley & Sons.

Kolomeychuk, R.J., Castonguay, G.C., and Welsh, L.E. (1986). "Ice Accretion Data for Model Evaluation.", IWAIS'86, Vancouver, 59-66.

Krishnasamy, S. G. (1982). "Measurement of Ice Accretion on Overhead Transmission Line Conductors." IWAIS'82, Hanover, New Hampshire, 291-298.

Krishnasamy, S. and Kulendran, S. (1998). "Combined Wind and Ice Loads from Historical Extreme Wind and Ice data." Atmospheric Research, Elsevier Science, 46 (1-2), 123-129.

Krishnasamy, S. G., and Brown, R. G. (1986). " Extreme Value Analysis of Glaze Ice Accretion." IWAIS'86, Vancouver, 97-102.

Kromer, I., Csomor M., and Kovacs, F. (1990). " Statistical Procedures for Combined Wind and Ice Loading Assessment." IWAIS'90, Tokyo.

Laflamme, J. N. (1996). "Icing Rate Measurements: A Key Way of Estimating Ice Loads on Structures." IWAIS'96, Saguenay-Lac Saint Jean, 175-180.

Laflamme, J. (1995a). "Surveillance et Mesure du Verglas au Québec, Saison 1994-1995." Internal Report, Hydro-Québec.

Laflamme, J. (1995b). "Spatial Variation of Extreme Values in the Case of Freezing Rain Icing." Atmospheric Research, Elsevier Science, 36(3-4), 195-206.

Laflamme, J. (1992). " Space and Time Estimates of Ice Loads from Two Interactive Networks of Ice Accretion Measurements Sites." International Seminar on Ice Load Measurements, Kristiansand, Norway.

Laflamme, J. (1990). "Spatial Distribution of Ice Accretion Within Icing Storms and Within Transmission lines Routes." IWAIS'90, Tokyo.

Laflamme, J., and Periard, G. (1998). "The Climate of Freezing Rain over the Province of Quebec in Canada: A Preliminary Analysis." Atmospheric Research, Elsevier Science, 46 (1-2), 99-111.

Laflamme, J., and Periard, G. (1995). "Rapport Glacimétrique, Saison 1994-1995." Internal Report, Hydro-Québec.

Larrabee, R.D., and Cornell, C.A. (1981). "Combination of Various Load Processes." Journal of the Structural Division, ASCE, 107-ST1, 223-239.

Magued, M.H., Bruneau, M. and Dryburgh, R.B. (1989). "Evolution of Design Standards and Recorded Failures of Guyed Towers in Canada." Canadian Journal of Civil Engineering, CSCE, 16, 725-732.

Makkonen, L. (1998). "Modeling Power Line Icing in Freezing Precipitation." Atmospheric Research, Elsevier Science, 46 (1-2), 131-142.

Makkonen, L. (1995). "Combined Wind and Ice Loading on Antenna Towers: Discussion." Canadian Journal of Civil Engineering, 22, 205-206.

Makkonen, L., and Ahti, K. (1995). "Climatic Mapping of Ice Loads Based on Airport Weather Observations." Atmospheric Research, Elsevier Science, 36 (3-4), 185-193.

Makkonen, L., and Ahti, K. (1982). "The Effect of Meteorological Parameters on Rime Formation in Finland." IWAIS'82, Hanover, New Hampshire, 167-173.

Mallory, J.H. and Leavengood, D.C. (1982). "Extreme Glaze and Rime Ice Loads in Southern California, Part II: Galze." IWAIS'82, Hanover, New Hampshire, 309-318.

Martoni, Cyr & Associés inc. (1991). "Données sur l'Ensemble des Pylônes Micro-Onde d'Hydro-Québec." Unpublished report, prepared for Telecommunication Planning of Hydro-Québec.

McComber, P., Latour, A., Druez, J., and Laflamme, J. (1996). "The Icing Rate Meter, an Instrument to Evaluate Transmission Line Icing." IWAIS'96, Saguenay-Lac Saint Jean, 159-168.

McComber, P., Druez, J., and Laflamme, J. (1995). "A Comparison of Selected Models for Estimating Cable Icing." Atmospheric Research, Elsevier Science, 36 (3-4), 207-220.

McComber, P., Martin, R., Morin, G., and Van, L.V. (1982). "Estimation of Combined Ice and Wind Load on Overhead Transmission Lines." IWAIS'82, Hanover, New Hampshire, 143-153.

McKay, G.A., and Thompson, H.A. (1969). "Estimating the Hazard of Ice Accretion in Canada from Climatological Data." Journal of Applied Meteorology, 8(6), 927-935.

Mozer, J.D. (1989). "Transmission Line Structure Loading." Proceedings of the sessions related to steel structures at Structures Congress' 89, sponsored by American Society of Civil Engineers, San Francisco.

Mulherin, N.D. (1996). "Atmospheric Icing and Tower Collapse in the United States." presented at IWAIS'96, Chicoutimi. (Available at http://www.crrel.usace.army.mil/ techpub/crrel_reports/reports/mulherin_atmo_icing.pdf)

NBCC (1995). "National Building Code of Canada-11th Edition." National Research Council of Canada, Ottawa, Ontario.

NBCC (1995). "Structural Commentaries: Part 4." National Research Council of Canada, Ottawa, Ontario.

Nikiforov, Eu. P. (1982). “Icing Related Problems, Effect on Line Design and Ice Load Mapping.” IWAIS'82, Hanover, New Hampshire, 239-245.

Peabody, A. B. (1996). “Measurements of Ice and Snow Loads on the Tyee Lake 138 kV Line.” IWAIS’96, Saguenay-Lac Saint Jean, 95-100.

Pezard, J. (1995). “A Method to Estimate Icing Loads on Overhead Lines.”Atmospheric Research, Elsevier Science, 36 (3-4), 303-310.

Pilon, P.J., Condie R., and Harvey K.D. (1985). "Consolidated Frequency Analysis Package, User Manual.", Water Resources Branch, Environment Canada, Ottawa.

Robbins, C., and Cortinas, J. (1996). “A Climatology of Freezing Rain in the Contiguous United States: Preliminary Results.” 15th AMS Conference on Weather Analysis, Norfolk, Virginia.

Seppa, T. O. (1996). “Transmission Line Ice Measurements with Tension Monitoring System.” IWAIS’96, Saguenay-Lac Saint Jean, 155-158.

Shan, L., Marr, L., and McCafferty, R.M. (1998). "Ice Storm Data Base and Ice Severity Maps.” Atmospheric Research, Elsevier Science, 46 (1-2), 159-168.

Stallabrass J. R., and Hearty, P. F. (1967). “The Icing of Cylinders in Conditions of Simulated Freezing Sea Spray.” National Research Council of Canada, Mechanical Engineering Report MD-50, NRC No. 9782, July 1967.

Stottrup-Andersen, U. (1996). “Reanalysis of Existing Telecommunication Masts and Towers in Norway.” Bulletin of the International Association for Shell & Spatial Structures, 37(121), 117-130.

STRUREL (1991). “A Structural Reliability Analysis Program, Theoretical and Users Manual.” RCP Germany and Denmark.

Sundin, E., and Mulherin, N. (1993). “Icing-Related Tower Failures in the USA and Fenno-Scandinavia.” IWAIS’93, Budapest, 273-278.

Tattelman, P. (1982). “Surface Icing Research at AFGL.” IWAIS'82, Hanover, New Hampshire, 195-204.

TIA/EIA (1996). “Structural Standards for Steel Antenna Towers and Antenna Supporting Structures.” TIA/EIA-222-F, Telecommunications Industry Association.

Turkstra, C.J., and Madsen, H. O. (1980). “Load Combination in Codified Structural Design.” Journal of the Structural Division, ASCE, 106-ST12, 2527-2543.

Wahba, Y.M.F., Madugula, M.K.S., Monforton, G.R. (1994). "Limit States Design of Antenna Towers." Canadian Journal of Civil Engineering, CSCE, 21, 913-923.

Wahba, Y.M.F., Madugula, M.K.S., Monforton, G.R. (1993). "Combined Wind and Ice Loading on Antenna Towers." Canadian Journal of Civil Engineering, CSCE, 20, 1047-1056.

Watson, D.F. (1992). "Contouring: A Guide to the Analysis and Display of Spatial Data." Pergamon.

Wen, Yi-Kwei. (1977). "Statistical Combination of Extreme Loads." Journal of the Structural Divison, ASCE, 103-ST5, 1079-1093.

Wilks, D. S. (1993). "Comparison of Three-Parameter Probability Distributions for Representing Annual Extreme and Partial Duration Precipitation Series." Water Resources Research, 29 (10), 3543-3549

Yip, T.C. (1995). "Estimating Icing Amount Caused by Freezing Precipitation in Canada." Atmospheric Research, Elsevier Science, 36 (3-4), 221-232.

Yip, T.C., and Mitten, Paul. (1991). "Comparisons Between Different Ice Accretion Models." Canadian Engineering Association, Engineering and Operation Transactions, vol. 30, 1990/1991.

Zimmerman, D.L. (1994). "Statistical Analysis of Spatial Data." Statistical Methods for Physical Science, Edited by Stanford J.L. and Vardeman, S.B., Chapter 13, Academic Press.

Appendix A

Information about stations
equipped with
Passive Ice Meters

St. No.	Station name	Latitude	Longitude	Elevation	Type	Affil.	Opened	Closed	Region	State
7011947	COTEAU-DU-LAC	45.19	74.1	49	1	1	Oct-85		11	A
7023075	HEMMINGFORD-FOUR-WINDS	45.04	73.43	61	1	1	Nov-90		11	A
7023240	HUNTINGDON	45.03	74.1	49	1	1	Oct-75		11	A
7025250	MONTREAL-INTERNATIONAL-A	45.28	73.45	36	2	2	Oct-75		11	A
7026073	POINTE-CLAIRE	45.28	73.48	41	1	1	Nov-74	May-85	11	F
7027320	SAINT-HUBERT-A	45.31	73.25	27	2	2	Oct-75		11	A
7027540	SAINTE-MARTINE	45.13	73.51	38	1	1	Oct-78		11	A
7040MLR	BAIE-COMEAU	49.14	68.11	69	1	1	Nov-74	Apr-75	13	F
7040440	BAIE-COMEAU-A	49.08	68.12	22	2	2	Oct-75		13	A
7040MMN	BAIE-JOHAN-BEETZ	50.17	62.48	8	1	1	Sep-77		13	A
7040813	BLANC-SABLON-A	51.25	57.13	19	2	2	Oct-83		13	A
7040812	BLANC-SABLON-A	51.25	57.13	19	2	2	Sep-75	Jun-83	13	F
7042378	FORESTVILLE	48.44	69.05	76	1	1	Nov-74		13	A
7042590	GAGNON-A	51.57	68.08	572	2	2	Sep-77	May-84	13	F
7042724	GETHSEMANI	50.13	60.41	8	1	1	Sep-77		13	A
7042749	GODBOUT	49.19	67.37	30	1	1	Oct-75		13	A
7042840	GRANDES-BERGERONNES	48.15	69.31	61	1	1	Nov-74		13	A
7043000	HARRINGTON-HARBOUR	50.32	59.3	8	2	2	Sep-75	Oct-78	13	F
7043012	HAVRE-SAINT-PIERRE	50.15	63.35	6	1	1	Sep-79	Jun-85	13	F
7043018	HAVRE-SAINT-PIERRE-A	50.17	63.37	33	2	2	Dec-83		13	A
7043017	HAVRE-SAINT-PIERRE-A	50.15	63.35	6	2	2	Sep-75	Jun-76	13	F
7044168	LA-TABATIERE	50.5	58.58	8	1	1	Sep-77	Jun-85	13	F
7044981	MINGAN-A	50.17	64.09	22	2	2	Sep-78	Nov-83	13	F
7045400	NATASHQUAN-A	50.12	61.49	5	2	2	Sep-75		13	A
7045910	PENTECOTE	49.44	67.1	15	1	1	Jan-92		13	A
7056200	PORT-MENIER	49.49	64.21	5	2	3	Oct-75	May-81	13	F
7046212	POSTE-MONTAGNAIS	51.53	65.44	604	1	1	Dec-74	Jun-86	13	F
704FEG0	RIVIERE-AU-TONNERRE	50.17	64.46	15	1	1	Sep-75		13	A
7046663	RIVIERE-SAINT-AUGUSTIN	51.14	58.39	8	1	1	Sep-77		13	A
704FFF5	RIVIERE-SAINT-JEAN	50.18	64.2	15	1	1	Sep-77	Jun-86	13	F
7047910	SEPT-ILES-A	50.13	66.16	55	2	2	Sep-75		13	A
7048421	TETE-A-LA-BALEINE	50.42	59.19	9	1	1	Sep-77		13	A
7020828	BONSECOURS	45.24	72.16	297	1	1	Oct-75		30	A
7020840	BROME	45.11	72.34	206	1	1	Nov-74		30	A
701A9EC	DALHOUSIE-STATION	45.18	74.28	70	1	1	May-85		30	A
7022160	DRUMMONDVILLE	45.53	72.29	76	1	1	Nov-74		30	A
70222DR	DURHAM-SUD	45.38	72.21	191	1	1	Nov-85	May-89	30	F
7022300	EAST-HEREFORD	45.05	71.3	358	1	1	Oct-90		30	A
7022320	FARNHAM	45.18	72.54	68	1	1	Nov-90		30	A
7022375	FLEURY	45.48	73	30	1	1	Feb-75		30	A
7022720	GEORGEVILLE	45.08	72.14	267	1	1	Oct-91		30	A
7023270	IBERVILLE	45.2	73.15	30	1	1	Feb-75		30	A
7026040	PHILIPSBURG	45.02	73.04	46	1	1	Oct-75		30	A
7026043	PIERREVILLE	46.05	72.5	15	1	1	Nov-90		30	A
7026465	RICHMOND	45.38	72.08	123	1	1	Oct-75	Oct-85	30	F
7017032	SAINT-CLET	45.23	74.15	61	1	1	Oct-75	Apr-82	30	F
7027772	SAINT-VALERIEN	45.34	72.4	91	1	1	Oct-87		30	A
7027802	SAWYERVILLE	45.21	71.32	346	1	1	Oct-75		30	A
7028124	SHERBROOKE	45.26	71.41	241	2	3	Oct-76		30	A
7028240	STANHOPE	45.01	71.47	389	1	1	Oct-76	May-84	30	F
7028280	STANSTEAD	45.01	72.06	312	1	1	Oct-85	May-91	30	F
7028700	VERCHERES	45.46	73.22	21	1	1	Nov-90		30	A
7050240	ARMAGH	46.45	70.32	358	1	1	Nov-90		40	A
7020567	BEAUSEJOUR	46.4	71.1	107	1	1	Oct-85		40	A
7012240	DUCHESNAY	46.52	71.39	166	1	1	Oct-75		40	A
7042388	FORET-MONTMORENCY	47.19	71.09	640	1	1	Oct-75	May-83	40	F
7022494	FORTIERVILLE	46.28	72.02	67	1	1	Oct-90		40	A
7042870	GRANDS-FONDS	47.45	70.07	366	1	1	Oct-75	May-82	40	F
7053140	HONFLEUR	46.41	70.51	175	1	1	Nov-74		40	A

For definitation of each column, see tables 3.1 and 3.2

St. No.	Station name	Latitude	Longitude	Elevation	Type	Affil.	Opened	Closed	Region	State
7054095	LA-POCATIERE-CDA	47.21	70.02	30	1	5	Feb-79		40	A
7053980	LAMARTINE	47.05	70.21	67	1	1	Oct-75	May-85	40	F
7024000	LAMBTON	45.5	71.05	366	1	1	Oct-75		40	A
7024320	LINGWICK	45.38	71.22	267	1	1	Oct-76		40	A
7055210	MONTMAGNY	46.58	70.35	15	1	1	Oct-85		40	A
7025670	NOTRE-DAME-DES-BOIS	45.24	71.04	503	1	1	Oct-91		40	A
7046004	PETITE-RIVIERE-SAINT-FRANCOIS	47.19	70.34	15	1	1	Nov-74		40	A
7016294	QUEBEC-A	46.48	71.23	73	2	2	Oct-75		40	A
7026739	SACRE-COEUR-DE-MARIE	46.08	71.1	468	1	1	Oct-80	May-85	40	F
7026754	SAINT-ADRIEN-D'IRLANDE	46.07	71.27	442	1	1	Nov-74	Apr-82	40	F
7016800	SAINT-ALBAN	46.43	72.05	76	1	1	Oct-75		40	A
7056930	SAINT-CAMILLE	46.28	70.13	396	1	1	Oct-76		40	A
7027083	SAINT-COME-DE-LINIERE	46.03	70.31	244	1	1	Oct-87		40	A
7027200	SAINT-EPHREM	46.04	70.58	312	1	1	Oct-90		40	A
7027248	SAINT-FERDINAND	46.06	71.35	297	1	1	Oct-75		40	A
7027259	SAINT-FLAVIEN	46.29	71.34	137	1	1	Oct-81		40	A
7027264	SAINT-FORTUNAT	45.58	71.36	465	1	1	Oct-81		40	A
704GC09	SAINT-HILARION	47.36	70.24	411	1	1	Oct-80		40	A
7027382	SAINT-JACQUES-DE-LEEDS	46.16	71.22	290	1	1	Oct-90		40	A
7027391	SAINT-JEAN-CHRYSOSTOME	46.43	71.13	53	1	1	Oct-76	May-85	40	F
7027392	SAINT-JEAN-DE-BREBEUF	46.11	71.27	264	1	1	Nov-82	May-85	40	F
7047396	SAINT-JEAN-ILE-D'ORLEANS	46.55	70.55	30	1	1	Oct-75		40	A
7027516	SAINT-LUDGER	45.45	70.41	335	1	1	Nov-74		40	A
7057600	SAINT-PAMPHILE	46.59	69.47	366	1	1	Oct-85		40	A
7027656	SAINT-PIERRE-DE-BROUGHTON	46.15	71.13	366	1	1	Oct-81		40	A
7027660	SAINT-PROSPER	46.13	70.3	282	1	1	Oct-75		40	A
7027733	SAINT-SEVERIN	46.2	71.03	442	1	1	Oct-76		40	A
7046837	SAINTE-ANNE-DE-BEAUPRE	47.02	70.55	76	1	1	Oct-75		40	A
7017B65	SAINTE-FOY-MATAPEDIA	46.45	71.17	46	1	1	Oct-75	Dec-84	40	F
7027267	SAINTE-FRANCOISE-ROMAINE	46.29	71.56	91	1	1	Oct-75	May-85	40	F
7057515	SAINTE-LUCIE	46.44	70.01	373	1	1	Oct-75		40	A
7027840	SCOTT	46.3	71.05	145	1	1	Oct-81		40	A
7028441	THETFORD-MINES	46.06	71.21	381	1	1	Oct-81		40	A
7028676	VALLEE-JONCTION	46.23	70.56	152	1	1	Oct-90		40	A
7028946	WOBURN	45.23	70.52	396	1	1	Oct-75	Oct-91	40	F
7030170	ANGERS	45.33	75.33	91	1	1	Oct-79		50	A
7030457	BARRAGE-MERCIER	46.43	75.59	236	1	1	Nov-74	May-80	50	F
7030640	BELL-FALLS	45.46	74.41	122	1	1	Nov-74	Oct-90	50	F
7031375	CHENEVILLE	45.54	75.03	223	1	1	Oct-78		50	A
7033650	LACHUTE	45.39	74.2	91	1	1	Apr-75		50	A
7014260	LAVALTRIE	45.56	73.19	30	3	2	Oct-75	Dec-82	50	F
7084276	LE DOMAINE	47.02	76.32	366	1	1	Nov-78	May-86	50	F
7034365	LUSKVILLE	45.33	76.04	69	1	1	Oct-85		50	A
7034395	LYTTON	46.39	76.02	213	1	1	Oct-81	May-94	50	F
7034480	MANIWAKI	46.22	75.59	170	2	2	Oct-76		50	A
7014629	MASCOUCHE	45.45	73.36	15	1	1	Oct-90		50	A
7035160	MONT-LAURIER	46.33	75.32	229	1	1	Oct-75	May-88	50	F
7035110	MONTEBELLO-SEDBERGH	45.4	74.58	197	1	1	Oct-90		50	A
7035520	NOMININGUE	46.24	75.05	274	1	1	Oct-75		50	A
7086380	RAPIDE-DES-JOACHINS	46.12	77.42	137	1	1	Oct-76	Oct-88	50	F
7017100	SAINT-DONAT	46.19	74.12	389	1	1	Feb-75		50	A
7037230	SAINT-FAUSTIN	46.07	74.29	366	1	1	Oct-92		50	A
7017270	SAINT-GABRIEL-DE-BRANDON	46.18	73.23	198	1	1	Oct-75	May-85	50	F
7037310	SAINT-HIPPOLYTE	45.49	74	366	1	1	Nov-90		50	A
7017380	SAINT-JACQUES	45.57	73.35	69	1	1	Oct-85		50	A
7017386	SAINT-JANVIER	45.44	73.53	61	1	1	Oct-85		50	A
7017480	SAINT-LIN-DES-LAURENTIDES	45.51	73.45	64	1	1	Oct-75	May-81	50	F
7077570	SAINT-MICHEL-DES-SAINTS	46.41	73.55	351	1	1	Oct-79		50	A
7036762	SAINTE-AGATHE-DES-MONTS	46.03	74.17	395	2	2	Apr-75	May-92	50	F

For definitation of each column, see tables 3.1 and 3.2

St. No.	Station name	Latitude	Longitude	Elevatior	Type	Affil.	Opened	Closed	Region	State
7036855	SAINTE-ANNE-DU-LAC	46.51	75.2	262	1	1	Oct-88		50	A
7016902	SAINTE-BEATRIX	46.12	73.36	198	1	1	Feb-75		50	A
7027110	SAINTE-DOROTHEE	45.31	73.49	23	1	1	Nov-74	May-82	50	F
7038040	SHAWVILLE	45.37	76.28	168	1	1	Oct-87		50	A
7038080	SHEENBORO	45.58	77.16	137	1	1	Oct-75		50	A
7016906	ST-BENOIT	45.34	74.03	53	1	1	Oct-90		50	A
7038587	VAL-DES-BOIS	45.54	75.36	198	1	1	Oct-76	Sep-87	50	F
7038975	WRIGHT	46.04	76.03	142	1	1	Oct-78		50	A
7020305	ARTHABASKA	46.01	71.57	140	1	1	Oct-84		60	A
7021954	DANVILLE	45.49	71.59	190	1	1	Oct-90		60	A
702A9ND	DAVELUYVILLE	46.11	72.12	84	1	1	Feb-75		60	A
7072816	GRANDE-ANSE	47.03	72.56	119	1	1	Nov-82		60	A
7074240	LA-TUQUE	47.24	72.47	152	1	1	Nov-74		60	A
7024250	LAURIERVILLE	46.2	71.4	152	1	1	Oct-75		60	A
7014332	LOUISEVILLE	46.16	73.01	45	1	1	Oct-85		60	A
7075800	PARENT	47.55	74.37	439	3	4	Oct-74	May-79	60	F
7016816	SAINT-ALEXIS-DES-MONTS	46.32	73.09	183	1	1	Oct-90		60	A
702FR30	SAINT-CAMILLE-DE-WOLFE	45.4	71.44	268	1	1	Oct-81		60	A
7017422	SAINT-JOSEPH-DE-MEKINAC	46.55	72.41	122	1	1	Oct-75		60	A
7017585	SAINT-NARCISSE	46.32	72.26	46	1	1	Nov-90		60	A
7018000	SHAWINIGAN	46.34	72.46	131	1	1	Nov-74		60	A
7018564	TROIS-RIVIERES	46.22	72.36	53	1	1	Nov-74	Oct-85	60	F
7028720	VICTORIAVILLE	46.03	71.58	137	1	1	Oct-75	May-84	60	F
7090120	AMOS	48.34	78.08	310	1	1	Mar-75		70	A
7080468	BARRAGE-TEMISCAMINGUE	46.43	79.06	245	3	5	Nov-78		70	A
7112400	FORT-CHIMO (KUUJJUAQ)	58.06	68.25	36	2	3	Dec-75	Jun-81	70	F
7103282	INUKJUAK	58.27	78.07	5	2	2	Oct-76		70	A
7113532	KOARTAC (QUAQTAQ)	61.04	69.41	28	2	2	Oct-75	Jun-82	70	F
7113534	KUUJJUAK-A (F.C.)	58.06	68.25	36	2	3	Sep-81		70	A
7103536	KUUJJUARAPIK-A (PDB)	55.17	77.46	18	2	3	Sep-82		70	A
7094026	LA MORANDIERE	48.37	77.37	297	1	1	Oct-87		70	A
7093715	LA-GRANDE-A	53.38	77.42	191	2	3	Nov-77		70	A
7093GJ3	LA-GRANDE-IV	53.5	73.24	33	2	2	Oct-85		70	A
709CEE9	LAC-BERRY	48.48	78.17	305	1	1	Oct-75		70	A
709LAF0	LAFORGE	54.33	71.13	0	3	4	Oct-76	May-77	70	F
7083480	LANIEL	47.03	79.16	280	1	1	Oct-75		70	A
708DBCE	LATULIPE	47.26	79.01	274	1	1	Oct-75		70	A
7094275	LEBEL-SUR-QUEVILLON	49.03	76.58	304	1	1	Nov-91		70	A
7094639	MATAGAMI	49.46	77.48	281	2	3	Oct-76	May-91	70	F
7085102	MONTBEILLARD	48.03	79.16	290	1	1	Oct-76		70	A
7095480	NITCHEQUON	53.12	70.54	536	2	3	Oct-76	Jun-86	70	F
7085795	NORANDA-MOUSKA	48.15	79.02	289	3	5	Nov-91		70	A
7106210	POSTE-DE-LA-BALEINE (KUUJJUA	55.17	77.46	18	2	3	Sep-76	Jun-82	70	F
7096215	POULARIES	48.41	78.59	290	1	1	Mar-75		70	A
7116270	QUAQTAQ (KOARTAC)	61.04	69.41	28	2	2	Sep-82		70	A
7086720	ROUYN-NORANDA	48.14	79.02	318	2	3	Oct-75	May-90	70	F
7117825	SCHEFFERVILLE	54.48	66.49	522	2	3	Oct-75		70	A
7097900	SENNETERRE	48.21	77.17	312	1	1	Feb-75	Sep-87	70	F
7098600	VAL-D'OR-A	48.03	77.47	338	2	2	Nov-75		70	A
70986RN	VAL-SAINT-GILLES	48.59	79.05	320	1	1	Oct-77	Sep-87	70	F
7050195	ANSE-AU-GRIFFON	48.56	64.17	61	1	1	Oct-82	May-85	80	F
7051175	CAP-SEIZE	49.01	66.24	213	1	1	Nov-74	Nov-88	80	F
7051200	CAUSAPSCAL	48.22	67.14	168	1	1	Nov-74		80	A
7052316	FAREWELL-COVE	48.52	64.27	15	1	1	Nov-74	Apr-82	80	F
705KL75	FONTENELLE	48.56	64.39	15	1	1	Oct-82		80	A
7052605	GASPE-A	48.46	64.29	33	2	3	Oct-77		80	A
7052820	GRANDE-RIVIERE	48.23	64.32	8	1	1	Oct-75	Dec-99	80	F
7052865	GRANDE-VALLEE	49.12	65.09	8	1	1	Oct-75		80	A

For definitation of each column, see tables 3.1 and 3.2

St. No.	Station name	Latitude	Longitude	Elevation	Type	Affil.	Opened	Closed	Region	State
7053649	LAC-HUMQUI	48.17	67.34	236	1	1	Oct-80		80	A
7054640	MATANE	48.51	67.28	30	1	1	Nov-90		80	A
7055104	MONT-BLEU	47.35	69.22	657	1	1	Oct-81	May-89	80	F
7055120	MONT-JOLI-A	48.36	68.12	46	2	3	Oct-75		80	A
7055380	MURDOCHVILLE	48.57	65.31	575	1	1	Oct-75		80	A
7055420	NEW-CARLISLE	48.02	65.16	45	1	1	Nov-88		80	A
7055430	NEW-RICHMOND	48.1	65.48	47	1	1	Nov-74		80	A
7055675	NOTRE-DAME-DU-LAC	47.36	68.48	320	1	1	Oct-79		80	A
7055705	NOUVELLE	48.06	66.18	7	1	1	Nov-88		80	A
7055770	OUIMET	48.18	68.13	244	1	1	Oct-75	May-93	80	F
7056120	PORT-DANIEL	48.09	64.59	69	1	1	Oct-77	Nov-88	80	F
7056480	RIMOUSKI	48.27	68.31	36	1	1	Nov-74		80	A
7056600	RIVIERE-BLEUE	47.26	69.02	213	1	1	Oct-75		80	A
7056814	SAINT-ALEXIS-DE-MATAPEDIA	47.59	67.04	274	1	1	Oct-75		80	A
7056970	SAINT-CHARLES-GARNIER	48.2	68.02	323	1	1	Oct-93		80	A
7057145	SAINT-ELEUTHERE	47.29	69.17	289	1	1	Nov-74	Sep-87	80	F
7057395	SAINT-JEAN-DE-CHERBOURG	48.53	67.07	351	1	1	Oct-75		80	A
7056850	SAINTE-ANNE-DES-MONTS	49.08	66.28	15	1	1	Oct-75		80	A
7056922	SAINTE-BRUNO-DE-KAMOURASK	47.27	69.47	198	1	1	Oct-87		80	A
7058220	SQUATECK	47.53	68.42	198	1	1	Oct-75		80	A
7058520	TRINITE-DES-MONTS	48.08	68.29	262	1	1	Oct-76		80	A
7058560	TROIS-PISTOLES	48.09	69.08	46	1	1	Oct-75		80	A
7060070	AIGREMONT	49.18	73.51	404	1	1	Oct-75	Apr-82	90	F
7060080	ALBANEL	48.53	72.27	152	1	1	Oct-77	May-92	90	F
7060400	BAGOTVILLE	48.2	71	159	2	3	Oct-75	May-76	90	F
7060825	BONNARD	50.44	71.02	152	1	1	Oct-75		90	A
7091401	CHIBOUGAMAU-A	46.29	74.25	403	2	2	Oct-75	May-83	90	F
7091404	CHIBOUGAMAU-CHAPAIS-A	49.46	74.32	387	2	2	Oct-83	Apr-92	90	F
7062368	FERLAND	48.12	70.5	198	1	1	Oct-85		90	A
7063090	HEMON	49.04	72.36	183	1	1	Nov-74	May-77	90	F
706CP09	LA DOR	48.46	72.43	183	1	1	Oct-93		90	A
7063560	LAC-BOUCHETTE	48.13	72.1	358	1	1	Oct-75		90	A
7063690	LAC-SAINTE-CROIX	48.25	71.45	152	1	1	Nov-74		90	A
7064998	MISTASSINI	48.51	72.12	122	1	1	Oct-75		90	A
7095000	MISTASSINI-POST	50.25	73.53	380	1	1	Oct-75	Jun-80	90	F
7065100	MONT-APICA	47.58	71.25	549	1	2	Dec-74	May-80	90	F
7046010	PETIT-SAGUENAY	48.11	70.03	122	1	1	Oct-75		90	A
7066080	PORTAGE-DES-ROCHES	48.18	71.13	165	1	1	Jan-80	May-84	90	F
7066685	ROBERVAL-A	48.31	72.16	180	2	3	Nov-82		90	A
7067460	SAINT-LEON-DE-LABRECQUE	48.4	71.31	131	1	1	Oct-75		90	A
7110830	BORDER-A	55.2	63.13	486	2	2	Sep-75	Jun-79	99	F
8504175	WABUSH	52.56	66.52	550	2	3	Oct-75	Nov-84	99	F

For definitation of each column, see tables 3.1 and 3.2

Appendix B

Number of glaze ice events
for
each station and
each winter season

no.	Region		station name	74/75	75/76	76/77	77/78	78/79	79/80	80/81	81/82	82/83	83/84	84/85	85/86	86/87	87/88	88/89	89/90	90/91	91/92	92/93	93/94	94/95
1	Others	1	BORDER-A		2	1	1	4																
2			WABUSH		1	1	0	1	0	2	1	2	2	0										
3	LAURENTIDES	1	ANGERS						3	5	4	6	7	5	5	4	4	1	4	6	1	3	2	2
4		2	CHENEVILLE					2	0	3	2	4	2	3	4	1	0	4	4	9	2	3	0	1
5		3	LACHUTE	0	3	2	1	3	0	4	1	7	6	4	5	3	2	4	5	7	6	4	1	2
6		4	LE DOMAINE					1	4	4	1	1	3	2	5									
7		5	LUSKVILLE												5	4	3	4	5	6	7	4	1	3
8		6	LYTTON	1	3	2	0	0	0		1	4	3	5	3	2	1	0	2	0	6	1	0	
9		7	MANIWAKI			3	3	1	3	2	3	6	4	5	7	4	5	4	3	5	5	0	0	2
10		8	MASCOUCHE																	1	1	1	0	1
11		9	MONTEBELLO-SEDBERGH	3	1	1	0	0	1	1	1	0	1	1	1	0	0	1	1	8	4	5	1	2
12		10	NOMININGUE		1	2	2	4	3	4	2	2		11	10	3	8	8	12	6	6	3	1	3
13		11	RAPIDE-DES-JOACHINS			0	0	0	1	0	0	1	0	0	0	1	1							
14		12	SAINT-DONAT	1	0	0	0	0	3	3	3	5	2	3	6	3	1	1	1	2	1	1	1	1
15		13	SAINT-FAUSTIN	0	7	8	9	8	5	4	7	10	10	16	11	4	4	3	12	11	6	1	0	0
16		14	SAINT-HIPPOLYTE																	7	7	4	2	2
17		15	SAINT-JACQUES		2	2	1	1	0	2					6	2	0	2	5	7	5	3	1	2
18		16	SAINT-JANVIER												6	3	6	5	7	7	5	3	2	3
19		17	SAINT-MICHEL-DES-SAINTS						1	2	3	4	2	0	2	1	5	3	3	3	5	4	0	3
20		18	SAINTE-ANNE-DU-LAC		3	0	3	2	1	1	1	5	4				0	1	6	5	9	3	2	2
21		19	SAINTE-BEATRIX	1	2	0	1	0	0	3	1	3	3	2	6	2	0	1	5	9	7	5	1	3
22		20	SHAWVILLE														2	2	3	9	7	4	2	3
23		21	SHEENBORO										9	4	6	4	6	3	4	7	7	2	2	1
24		22	ST-BENOIT	4	4	2	3	4	0	3	3									6	7	3	1	2
25		23	VAL-DES-BOIS			0	0	2	1	1	4	2	1	3	1	1								
26		24	WRIGHT					3	5	9	3	4	4	6	5	2	2	3	2	3	4	0	0	0
27	La Grande	1	AMOS	2	0	0	1	0	0	1	1	1	2	1	0	0	0	0	3	3	2	0	2	1
28		2	BARRAGE-TEMISCAMINGUE					5	5	2	4	4	5	7	6	2	4	2			5	2	2	1
29		3	INUKJUAK			0	2	1	1	3	7	7	3	0	0	1	6	2	2	1	2	10	2	1
30		4	KUUJJUAK-A (F.C.)		0	2		5	2	4	6	6	4	0	0	0	0	1	2	0	0	0	1	0
31		5	KUUJJUARAPIK-A (PDB)			3	0	0		6	1	7	2	0		5	4	1	1	0	2	5	2	1
32		6	LA MORANDIERE	2	1	0	0	0	3	1	0	3	1	2	2	1	1	0	1	0	0	0	0	0
33		7	LA-GRANDE-A				0		1	9	4	2	2	4	2	4	2	2	0	1	4	2	1	0
34		8	LA-GRANDE-IV												0	0	5	4	4	1	4	0	1	1
35		9	LAC-BERRY		0	0	0	0	0	0	1	0	0	1	0	1	0	0	3	1	2	0	1	2
36		10	LAFORGE			2																		
37		11	LANIEL		0	1	0	6	6	9	5	9	5	8	4	3	6	6	8	1	2	1	1	0
38		12	LATULIPE		1	1	0	2	0	1	0	1	0	0	1	0	0	0	1	2	1	0	0	0
39		13	LEBEL-SUR-QUEVILLON			1	0	1	5	2	1	1	1	4	3	0	3	3	2	1	2	0	0	1
40		14	MONTBEILLARD			3	1	2	4	2	1	1	1	0	1	0	2	0	5	7	2	1	1	5

no.	Region		station name	74/75	75/76	76/77	77/78	78/79	79/80	80/81	81/82	82/83	83/84	84/85	85/86	86/87	87/88	88/89	89/90	90/91	91/92	92/93	93/94	94/95
41		15	NITCHEQUON			3	0	1	0	1	3	4	4	1	2									
42		16	NORANDA-MOUSKA		1	1		6	2	5	1	4	2	6	5	1	3	4	4	0		7	4	4
43		17	POULARIES	0	1	2	1	2	1	2	0	1	1	0	0	2	0	0	0	2	1	1	0	2
44		18	QUAQTAQ (KOARTAC)		0	0	0	1	1	3	0			1	0	0	0	0	0	0	0	0	0	0
45		19	SCHEFFERVILLE		0		1	1		1	1	4	3	3	2	3	3	2	11	4	4	1	0	0
46		20	VAL-D'OR-A		1	4	3	5	6	3	6	7	3	2	4	3	4	5	5	7	7	3	1	2
47		21	VAL-SAINT-GILLES				0	2	4	1	1	1	0	1	2	1								
48	Maisonneuve	1	COTEAU-DU-LAC												1	1	0	2	1	3	2	3	0	1
49	Maisonneuve	2	HEMMINGFORD-FOUR-WINDS																	1	5	1	1	1
50	Maisonneuve	3	HUNTINGDON		5	1	3	4	1	3	2	5	4	1	0	1	1	0	1	1	3	2	0	1
51	Maisonneuve	4	MONTREAL-INTERNATIONAL-A		7	3	4	5	2	4	5	8	6	5	4	3	1	3	9	6	7	1	1	1
52	Maisonneuve	5	POINTE-CLAIRE	5	5	4	5	8	1	3	4	9	6	5										
53	Maisonneuve	6	SAINT-HUBERT-A		3	2	4	4	0	7	6	7	5	3	6	2	2	3	5	5	6	2	1	2
54	Maisonneuve	7	SAINTE-MARTINE					2	0	2	2	4	4	1	1	2	0	1	1	2	2	2	1	1
55	Manicouagan	1	BAIE-COMEAU-A	2	6	1	1	3	5	0	1	4	5	6	3	2	4	1	3	5	5	2	3	0
56	Manicouagan	2	BAIE-JOHAN-BEETZ				0	1	1	1	0	0	0	1	1	0	0	0	1	2	1	0	0	0
57	Manicouagan	3	BLANC-SABLON-A		0	1	1	1	3	2	0	2	2	3	2	1	2	1	3	5	6	2	1	0
58	Manicouagan	4	FORESTVILLE	2	2	0	1	1	0	0	0	3	1	0	2	0	1	0	1	3	2	2	1	0
59	Manicouagan	5	GAGNON-A				1	2	5	2	9	3	3											
60	Manicouagan	6	GETHSEMANI																					
61	Manicouagan	7	GODBOUT		4	0	1	1	2	1	1	1	1	2	1	0	0	0	0	1	2	1	0	0
62	Manicouagan	8	GRANDES-BERGERONNES	1	1	2	0	0	1	1	0	2	1	0	1	0	0	0	0	3	2	1	0	0
63	Manicouagan	9	HARRINGTON-HARBOUR		6	3	3																	
64	Manicouagan	10	HAVRE-SAINT-PIERRE-A		6				1	2	1	2	0	1	2		0	2	2	3	2	1	1	
65	Manicouagan	11	LA-TABATIERE				2	1	2	2	0	1	1	0										
66	Manicouagan	12	MINGAN-A					1	2	4	2	2	0											
67	Manicouagan	13	NATASHQUAN-A		5	1	2	1	2	1	3	0	1	2	2	1	0	0	3	3	2	2	1	0
68	Manicouagan	14	PENTECOTE																		2	0	1	0
69	Manicouagan	15	PORT-MENIER		1	1	2	2	1	1														
70	Manicouagan	16	POSTE-MONTAGNAIS																					
71	Manicouagan	17	RIVIERE-AU-TONNERRE		4	2	0	0	2	3	0	0	0	0	1	0	0	0	2	2	3	1	0	0
72	Manicouagan	18	RIVIERE-SAINT-AUGUSTIN				0	2	3	3	1	5	2	2	3	2	5	1	1	4	1	2	1	0
73	Manicouagan	19	RIVIERE-SAINT-JEAN				1	0	0	2	2	0	1	0	1									
74	Manicouagan	20	SEPT-ILES-A		3	1	0	2	2	4	3	9	5	6	5	0	2	3	6	1	4	3	0	0
75	Manicouagan	21	TETE-A-LA-BALEINE				3	1	1	1	2	3	1	1	2	1	1	0	2	1	2	0	2	0
76		1	ANSE-AU-GRIFFON									1	0	0										
77		2	CAP-SEIZE	0	0	0	0	0	0	1	0	0	0	0	0	0	0	0						
78		3	CAUSAPSCAL	0	1	0	0	0	2	0	1	1	3	0	0	0	1	0	0	2	1	0	0	0
79		4	FONTENELLE	2	4	1	0	0	0	0	0	0	0	0	0	0	0	0	0	0	0	0	0	0
80		5	GASPE-A				2	1	3	1	0	8	2	2	2	1	1	3	2	6	3	3	0	0

no.	Region		station name	74/75	75/76	76/77	77/78	78/79	79/80	80/81	81/82	82/83	83/84	84/85	85/86	86/87	87/88	88/89	89/90	90/91	91/92	92/93	93/94	94/95
81	Matapédia	6	GRANDE-RIVIERE		2	0	0	2												2	1	0	0	0
82		7	GRANDE-VALLEE		1	1	0	3	2	2	2	2	4	1	1	0	1	2	1	0	0	1	0	0
83		8	LAC-HUMQUI							3	0	6	4	0	3	0	0	0	0	4	2	1	0	1
84		9	MATANE																	5	5	4	2	1
85		10	MONT-BLEU								4	4	2	3	1	3	1	1						
86		11	MONT-JOLI-A		4	1	0	5	2	0	1	7	3	4	1	2	1	1	2	4	1	1	0	1
87		12	MURDOCHVILLE		1	2	2	0	3	4	0	2	6	5	6	2	5	2	6	7	3	4	0	0
88		13	NEW-CARLISLE															3	1	5	3	3	0	1
89		14	NEW-RICHMOND	0	1	1	0	1	2	0	1	1	1	0	0	0	0	0	5	6	3	5	1	1
90		15	NOTRE-DAME-DU-LAC						0	1	1	4	4	1	4	1	1	0	3	1	2	1	1	2
91		16	NOUVELLE															0	0	2	1	3	0	0
92		17	RIMOUSKI	3	1	1	1	3	2	0	1	1	4	0	3	1	1	2	0	2	1	3	2	2
93		18	RIVIERE-BLEUE		0	2	1	1	1	1	2	4	4	0	3	3	5	0	3	11	2	3	1	2
94		19	SAINT-ALEXIS-DE-MATAPEDIA		9	10	3	2	7	8		8	7	6	5	2	4	2	7	8	3	6	1	2
95		20	SAINT-CHARLES-GARNIER		2	2	1	4	1	3	2	5	6	4	4	1	2	1	0	3	2	1	0	1
96		21	SAINT-JEAN-DE-CHERBOURG		2	0	0	1	2	2	1	3	0	1	1	1	1	0	0	1	0	1	0	0
97		22	SAINTE-ANNE-DES-MONTS		1	0	1	3	1	0	3	7	2	2	3	0	1	0	2	3	1	1	1	1
98		23	SAINTE-BRUNO-DE-KAMOURASKA	2	2	5	1	0	1	0	1	4	5	0	0	1	1	0	3	4	1	1	0	2
99		24	SQUATECK		1	3	0	0	0	1	0	2	3	3	5	2	3	3	0	4	1	3	1	2
100		25	TRINITE-DES-MONTS			4	4	3	1	0	2	3	3	0	1	1	2	0	1	2	4	3	1	3
101		26	TROIS-PISTOLES		1	3	1	1	0	0	1	3	3	0	1	1	0	0	0	4	4	2	2	1
102	Mauricie	1	ARTHABASKA		4	1	1	2	0	0	1	2	6	2	1	1	0	0	1	1	2	1	1	2
103		2	DANVILLE		1				2	0	1	0	1	0	4	3	2	3		2	3	2	0	1
104		3	DAVELUYVILLE	0		3		2	1	0	0	1	3	2	2	0	0	1	3	1	3	1	0	3
105		4	GRANDE-ANSE									0	3	0	0	0	0	0	0	0	0	0	1	0
106		5	LA-TUQUE														2	3	2	1	0	0	2	1
107		6	LAURIERVILLE		5	3	3	2	0	2	0	2	4	2	0	0	1	1	3	2	2	0	0	3
108		7	LOUISEVILLE												2	2	0	0	6	8	9	5	1	4
109		8	PARENT	0	2	1	2	0																
110		9	SAINT-ALEXIS-DES-MONTS		4	3	3	2	2	5	5	6	6	3						4	2	1	0	2
111		10	SAINT-CAMILLE-DE-WOLFE								4	5	3	3	5	1	0	1	3	2	3	1	1	1
112		11	SAINT-JOSEPH-DE-MEKINAC		4	2	1	2	1	2	1	2	5	0	2	0	2	0	0	0	2	1	0	0
113		12	SAINT-NARCISSE																	7	6	4	1	3
114		13	SHAWINIGAN								0	0	1	0	0	2	0	0	2	4	4	2	1	1
115		14	TROIS-RIVIERES	2	3	1	1	1	0	3	2	5	2	1										
116		1	ARMAGH																	9	6	5	0	1
117		2	BEAUSEJOUR			5	3	2	4	4	2	4	4	6	1	2	3	0	2	3	1	2	2	2
118		3	DUCHESNAY														4	1	5	7	3	1	0	2
119		4	FORET-MONTMORENCY		6	4	6	2	6	5	4	6												
120		5	FORTIERVILLE		3	4	5	1	2	3	1	5	5	2						4	8	3	1	3

no.	Region		station name	74/75	75/76	76/77	77/78	78/79	79/80	80/81	81/82	82/83	83/84	84/85	85/86	86/87	87/88	88/89	89/90	90/91	91/92	92/93	93/94	94/95
121		6	HONFLEUR	2	4	1	4	1	1	2	1	8	4	2	1	2	2	0	4	5	3	4	1	2
122		7	LA-POCATIERE-CDA					0	2	2	0	1	1	0	2	1	0	0	1	0	1	0	0	1
123		8	LAMBTON		1	0	0	0	0	0	0	1	0	0	1	0	0	1	2	3	3	1	0	0
124		9	LINGWICK			1	0	1	0	2	3	4	3	0	4	4	3	2	1	2	8	2	1	2
125		10	MONTMAGNY		1	0	1	2	5	3	3	5	2	1	3	1	1	1	2	6	4	2	1	1
126		11	NOTRE-DAME-DES-BOIS																		5	2	0	1
127		12	PETITE-RIVIERE-SAINT-FRANCOIS	0	0	1	0	0	0	0	0	0	2	0	1	0	1	0	2	2	1	0	0	0
128		13	QUEBEC-A		7	5	4	5	5	6	3	6	3	2	6	2	5	4	4	5	5	3	1	3
129		14	SACRE-COEUR-DE-MARIE							1	1	5	5	3										
130		15	SAINT-ALBAN		3	1	0	0	1	0	1	0	1	1	1	1	1	0	3	6	6	2	0	2
131		16	SAINT-CAMILLE			1	4	2	2	1	0	5	2	1	0	3	5	2	4	4	1	2	0	2
132		17	SAINT-COME-DE-LINIERE														0	2	2	1	0	0	0	1
133		18	SAINT-EPHREM																		2	0	0	2
134		19	SAINT-FERDINAND		2	0	0	0	0	0	0	0	1	1	0	6	11	8	8	10	9	3	0	2
135		20	SAINT-FLAVIEN								0	3	7	4	5	2	3	3	9	7	5	5	0	4
136	Montmorency	21	SAINT-FORTUNAT								1	18	11	8	10	5	5	12	6	6	13	7	1	3
137		22	SAINT-HILARION		0	0	0	0	0	0	1	18	11	8	10	5	2	0	0	0	0	0	0	0
138		23	SAINT-JACQUES-DE-LEEDS																	1	3	0	0	2
139		24	SAINT-JEAN-DE-BREBEUF	1	6	3	2	4	0	4	1	9	6	1										
140		25	SAINT-JEAN-ILE-D'ORLEANS		4	3	3	2	2	1	1	6	2	0	2	2	1	0	1	2	3	2	1	0
141		26	SAINT-LUDGER	1	2	1	1	0	0	2	1	4	2	0	3	1	0	1	1	4	5	2	0	1
142		27	SAINT-PAMPHILE												1	2	0	0	1	0	1	1	0	2
143		28	SAINT-PIERRE-DE-BROUGHTON								2	4	8	3	3	2	3	1	2	2	3	2	0	2
144		29	SAINT-PROSPER		4	0	0	1	1	0	1	3	3	1	1	1	0	1	3	1	5	1	0	1
145		30	SAINT-SEVERIN			4	4	2	1	2	2	5	4	2	3	2	0	0	1	1	3	2	0	3
146		31	SAINTE-ANNE-DE-BEAUPRE		6	2	3	3	0	0	0	1	0	1	2	1	1	0	3	2	1	3	1	0
147		32	SAINTE-FOY-MATAPEDIA		6	2	4	3	2	1	3	7	4	0										
148		33	SAINTE-LUCIE		0	0	0	0	3	0	1	2	3	2	3	4	3	0	5	4	3	2	0	1
149		34	SCOTT								2	6	3	3	4	1	1	2	4	4	6	1	1	3
150		35	THETFORD-MINES								0	0	0	0	0	0	0	0	0	0	2	0	0	0
151		36	VALLEE-JONCTION																	2	3	0	0	1
152		37	WOBURN																					
153		1	BONSECOURS		5	0	0	0	0	1	0	0	1	0	3	0	0	2	1	1	0	0	1	3
154		2	BROME	1	2	0	0	0	1	0	0	0	2	0	1	0	1	2	1	0	1	2	0	0
155		3	DALHOUSIE-STATION												3	4	1	2	5	10	4	2	1	2
156		4	DRUMMONDVILLE	2	0	2	7	6	4	8	6	10	13	4	10	3	8	1	3	2	5	0	1	2
157		5	EAST-HEREFORD																	1	0	0	0	0
158		6	FARNHAM																	0	0	3	1	2
159	helieu	7	FLEURY	0	2	0	1	1	0	0	0	4	3	1	2	1	0	1	4	2	2	2	1	3
160		8	GEORGEVILLE			0	1	4	3	1	2	4	3		3	1	3	3	0	2	7	1	2	2

no.	Region		station name	74/75	75/76	76/77	77/78	78/79	79/80	80/81	81/82	82/83	83/84	84/85	85/86	86/87	87/88	88/89	89/90	90/91	91/92	92/93	93/94	94/95
161	Ric	9	IBERVILLE	2	5	2	2	7	1	4	2	5	5	1	2	4	3	5	8	3	5	2	1	2
162		10	PHILIPSBURG		1	0	1	3	3	4	3	2	1	1	1	0	0	2	2	3	5	3	2	2
163		11	PIERREVILLE																	6	6	3	0	3
164		12	SAINT-VALERIEN														0	0	1	1	1	1	0	1
165		13	SAWYERVILLE		2	0	0	2	1	0	3	3	2	0	2	0	1	2	0	1	4	2	1	1
166		14	SHERBROOKE			2	1			1	3	3	2	2	2	3	0	4	1	4	3	3	2	0
167		15	VERCHERES		5	3	3	5	0	4	1	1								4	1	1	0	2
168	Saguenay	1	AIGREMONT		3	0	1	0	0	0	0													
169		2	BONNARD		2	2	0	3	6	11	1	4	4	5	3	0	3	1	1	2	4	0	2	1
170		3	CHIBOUGAMAU-CHAPAIS-A		9	6	1	5	7	4	5	5	10	9	7	4	4	5	2	6	5			
171		4	FERLAND		4					7	3	6			6	0	1	0	1	2	1	1	1	1
172		5	LA DOR	1	2	0	1	0	0	0	0	2	2	0	3	1	2	0	2	3	1	0	0	0
173		6	LAC-BOUCHETTE		2	1	1	0	0	1	0	1	6	1	2	3	0	0	3	5	3	3	3	3
174		7	LAC-SAINTE-CROIX	1	4	1	0	0	1	0	0	4	3	1	3	2	3	1	2	3	1	0	0	3
175		8	MISTASSINI		1	1	2	0	1	1	0	1		4	5	2	2	1	3	5	5	2	3	2
176		9	MISTASSINI-POST		3	0	1	2	0															
177		10	MONT-APICA	3	2	0	3	5	4															
178		11	PETIT-SAGUENAY		3	1	2	1	2	3	2	5	4	1	4	2	0	1	1	3	1	3	0	0
179		12	ROBERVAL-A									2	4	3	4	2	0	1	3	3	2	1	0	2
180		13	SAINT-LEON-DE-LABRECQUE		1	1	0	2	2	1	0	1	0	0	1	2	1	1	1	1	3	0	0	1
			Average	1.4	2.6	1.6	1.4	1.9	1.7	2.2	1.7	3.7	3.1	2.1	2.8	1.6	1.8	1.5	2.7	3.4	3.2	1.9	0.7	1.3
			Max.	5.0	9.0	10.0	9.0	8.0	7.0	11.0	9.0	18.0	13.0	16.0	11.0	6.0	11.0	12.0	12.0	11.0	13.0	10.0	4.0	5.0

Appendix C

Data set of maximum ice thickness per event for the selected stations

Ice thickness in mm	Frequency of ice thickness																																												
	Station number																																												
	5	14	15	21	37	46	50	51	53	55	57	67	74	86	87	89	92	93	95	98	99	101	102	107	121	125	128	130	134	137	140	141	144	146	148	156	159	161	162	165	169	172	173	174	178
1	9		22	6	1	18		16	9	8			6	4	10	2	3	13		1		2		2	1	3	9	5	1	19	1	6	5	1		2		2	1	3	5	2		1	4
2	10	2	25	6	8	27	6	12	10	5	6	3	2	5	12	4	4	8	3	5	1	3	6	1	6	1	7	4	7	9	1	2	5		4	2		1	5	5	3	2	2	2	2
3	11	3	20	4	13	4	4	7	10	8	10	2	7	6	5	6	2	7	4	1	7	1	5	4	2	2	2	3	7	4	7	6	2	2	4	5	3		2	6	6	2	2	4	6
4	7	4	11	6	4	7	2	10	7	7	5	4	3	4	7	2	2	2	2		2	4		1	2	2	8		9	3		2	1	2	3		3	2	2	3	2	2	5		2
5	9	4	7	6	17	6	6	2	6	4	4		6	4	11	3	6	6	10	12	9	2		5	17	8	11	5	9		4	4	2	5	4	36	4	12	4	2	5	5	3	5	3
6		1	13		3	2		3	4	3	2		2	1		2	2	1	5	1		3	3	1		3	4	3	3	2	3				1	6	1		2	1		1	1		3
7	2		2	4	3	2	4	3	3	5	1	4	3	1	2		1	1	2				2	2		3	3		1		3	1	1	4	3		3	3	2			3		1	1
8	1	1	6	3	1	4	1	1	1		1	3	2	3		1	1	1			1						4				1		2				3	5		1	1				1
9	2		3		1	1	1	1	1		1	1	4				2		2	1		1	2	2	1	1	5		4			1	1				2	4	1	1	1	1	3		1
11	6	2	5	2	3	1	2	8	2	2	1	5	4	1	1	1	1	1	4	4	6	5	4	6	11	7	10	3	1	1	1	2	3	3	2	8	2	3	1	1	4		2	7	3
12	1	1			1			1	3	2		2	3	1				1			1						2	1	1	1	2				1	1		1			1	1	1		
13	2		1				1	1	2	2		1	1	1		2			1								3				1			1	1			3	1					1	
14			2	2			2	4	3			1			1									2		1			1	1	1		1				1	3	1	1		1			
15	1			2	3		3	1		2	1		1	1					1	4	2	1	1	1	2	2	3	1		1	3			1		2		1					1	1	1
16			1			1		1	1					1												1	2		1		2						1								
17		1			1	1		1	2			1												1														4					1		
18									1	1		1		2		1															1														
19		1	1	1																				1			2				1										2				
21					1	2		1		1		1	2		1					1		1			4		2			1	1			1		2		2	1						1
22								1					1																					1							1				1
23											1		1														1										1								
24					1							1																1																	
25			1	1	1	2			1								1				1			1	1		1					2				2		1			2			2	
26								2																			1																		
28																																						1							
29								1																																			1		
31																									1		1					1	2	1		4		1			1		1		1
32																	1																												
33																								1																					1
34									1																						1														
35												1												1	1	1									1										1
36							1																																						
38																																						1							
41																				1						1										1									
42																								1																					
43									1																																				
44													1																														1		
45																									1	1																			
46																											1																		
48				1																																									
51												1								1																									
53					1																																								
55					1															2																1									
58									1																																				
59																																								1					
65																						1																							

Appendix D

Description of the Probability Distribution Functions And their parameter estimates

D.1. Beta-K distribution

Parameters: $\alpha > 0, \beta > 0, \ \theta > 0$

CDF:

$$F(x) = \left[\frac{(x/\beta)^{\theta}}{\left(1 + (x/\beta)^{\theta}\right)}\right]^{\alpha} \qquad ,x \geq 0$$

$$F(x) = 0, \qquad ,x \leq 0$$

PDF:

$$f(x) = \frac{\alpha\theta}{\beta}\left(\frac{x}{\beta}\right)^{\alpha\theta - 1}\left[1 + \left(\frac{x}{\beta}\right)^{\theta}\right]^{-(\alpha+1)} \qquad ,x > 0$$

$$f(x) = 0 \qquad ,x \leq 0$$

QF:

$$x(F) = \beta\left[\frac{F^{1/\alpha}}{\left(1 - F^{1/\alpha}\right)}\right]^{1/\theta}$$

Maximum-likelihood parameter estimates:

$$\tilde{\alpha}_j = n\left[\sum_{i=1}^{n} \log\left(1 + \left(\frac{x_i}{\tilde{\beta}_{j-1}}\right)^{-\tilde{\theta}_{j-1}}\right)\right]^{-1}$$

$$\tilde{\beta}_j = n^{-1}\left(1 + \frac{1}{\tilde{\alpha}_j}\right)\tilde{\beta}_{j-1}\sum_{i=1}^{n}\left(1 + \left(\frac{x_i}{\tilde{\beta}_{j-1}}\right)^{-\tilde{\theta}_{j-1}}\right)^{-1}$$

$$\tilde{\theta}_j = n\left[\sum_{i=1}^{n} \frac{\left[\left(\frac{x_i}{\tilde{\beta}_j}\right)^{\tilde{\theta}_{j-1}} - \alpha_i\right]\log\left(\frac{x_i}{\tilde{\beta}_j}\right)}{1 + \left(\frac{x_i}{\tilde{\beta}_j}\right)^{\tilde{\theta}_{j-1}}}\right]^{-1}$$

where j = iteration number

Ref. (Mielke and Johnson, 1974)

D.2. Beta-P distribution

Parameters: $\alpha > 0, \beta > 0, \theta > 0$

CDF:

$$F(x) = \left[1 - \left[1 + \left(\frac{x}{\beta}\right)^{\theta}\right]^{-\alpha}\right] \quad ,x \geq 0$$

$$F(x) = 0 \quad ,x \leq 0$$

PDF:

$$f(x) = \frac{\alpha\theta}{\beta}\left(\frac{x}{\beta}\right)^{\theta-1}\left[1 + \left(\frac{x}{\beta}\right)^{\theta}\right]^{-(\alpha+1)} \quad ,x > 0$$

$$f(x) = 0 \quad ,x \leq 0$$

QF:

$$x(F) = \beta\left[(1-F)^{-1/\alpha} - 1\right]^{1/\theta}$$

Maximum-likelihood parameter estimates:

$$\tilde{\alpha}_j = n\left[\sum_{i=1}^{n} \log\left(1 + \left(\frac{x_i}{\tilde{\beta}_{j-1}}\right)^{\tilde{\theta}_{j-1}}\right)\right]^{-1}$$

$$\tilde{\beta}_j = n^{-1}(1+\tilde{\alpha}_j)\tilde{\beta}_{j-1}\sum_{i=1}^{n}\left(1 + \left(\frac{x_i}{\tilde{\beta}_{j-1}}\right)^{-\tilde{\theta}_{j-1}}\right)^{-1}$$

$$\tilde{\theta}_j = n\left[\sum_{i=1}^{n}\frac{\left[\tilde{\alpha}_j\left(\frac{x_i}{\tilde{\beta}_j}\right)^{\tilde{\theta}_{j-1}} - 1\right]\log\left(\frac{x_i}{\tilde{\beta}_j}\right)}{1 + \left(\frac{x_i}{\tilde{\beta}_j}\right)^{\tilde{\theta}_{j-1}}}\right]^{-1}$$

where j = iteration number

Ref. (Mielke and Johnson, 1974)

D.3. Generalized extreme-value distribution

Parameters: ξ (location), α (scale), k (shape)

Range: $$\begin{cases} -\infty < x \le \xi + \alpha/k & if\ k > 0 \\ -\infty < x < \infty & if\ k = 0; \\ \xi + \alpha/k \le x < \infty & if\ k < 0 \end{cases}$$

CDF: $$F(x) = \exp(-e^{-y})$$

PDF: $$f(x) = \alpha^{-1} \exp\left[-(1-k)y - e^{-y}\right]$$

QF: $$x(F) = \begin{cases} \xi + \alpha\left[1 - (-\log F)^k\right]/k, & k \ne 0 \\ \xi - \alpha \log(-\log F), & k = 0 \end{cases}$$

Where $$y = \begin{cases} -k^{-1}\log(1 - k(x-\xi)/\alpha) & k \ne 0 \\ (x-\xi)/\alpha & k = 0 \end{cases}$$

L-moment parameter estimates:

$$k \approx 7.8590c + 2.9554c^2, \quad c = \frac{2}{3+\tau_3} - \frac{\log 2}{\log 3}$$

$$\alpha = \frac{\lambda_2 k}{(1-2^{-k})\Gamma(1+k)}$$

$$\xi = \lambda_1 - \alpha\left[1 - \Gamma(1+k)\right]/k$$

where $$\Gamma(x) = \int_0^\infty t^{\alpha-1} e^{-t} dt$$

λ_1, λ_2, τ_3, τ_4 are the sample L-moments

Ref. (Hosking and Wallis, 1997)

D.4. Generalized Pareto distribution

Parameters: ξ (location), α (scale), k (shape)

Range:
$$\begin{cases} \xi \le x \le \xi + \alpha/k & \text{if } k > 0 \\ \xi \le x < \infty & \text{if } k \le 0 \end{cases}$$

CDF:
$$F(x) = 1 - e^{-y}$$

PDF:
$$f(x) = \alpha^{-1} \exp[-(1-k)y]$$

QF:
$$x(F) = \begin{cases} \xi + \alpha[1-(1-F)^k]/k, & k \ne 0 \\ \xi - \alpha \log(1-F), & k = 0 \end{cases}$$

Where
$$y = \begin{cases} -k^{-1} \log(1 - k(x-\xi)/\alpha) & k \ne 0 \\ (x-\xi)/\alpha & k = 0 \end{cases}$$

L-moment parameter estimates:

$$k = \frac{(1-3\tau_3)}{(1+\tau_3)}$$

$$\alpha = (1+k)(2+k)\lambda_2$$

$$\xi = \lambda_1 - (2+k)\lambda_2$$

where

λ_1, λ_2, τ_3, τ_4 are the sample L-moments

Ref. (Hosking and Wallis, 1997)

D.5. Generalized Normal distribution

Parameters: ξ (location), α (scale), k (shape)

Range: $$\begin{cases} -\infty < x \le \xi + \alpha/k & \text{if } k > 0 \\ -\infty < x < \infty & \text{if } k \le 0 \end{cases}$$

CDF: $$F(x) = \Phi(y)$$

PDF: $$f(x) = \frac{e^{ky - y^2/2}}{\alpha\sqrt{2\pi}}$$

QF: not explicitly defined

Where $$y = \begin{cases} -k^{-1}\log(1 - k(x-\xi)/\alpha) & k \ne 0 \\ (x-\xi)/\alpha & k = 0 \end{cases}$$

L-moment parameter estimates:

$$k \approx -\tau_3 \frac{E_0 + E_1\tau_3^2 + E_2\tau_3^4 + E_3\tau_3^6}{1 + F_1\tau_3^2 + F_2\tau_3^4 + F_3\tau_3^6}$$

$$\alpha = \frac{\lambda_2 k e^{-k^2/2}}{1 - 2\Phi(-k/\sqrt{2})}$$

$$\xi = \lambda_1 - \frac{\alpha}{k}(1 - e^{k^2/2})$$

where $E_0 = 2.0466534$, $E_1 = -3.6544371$,
$E_2 = 1.8396733$, $E_3 = -0.20360244$,
$F_1 = -2.0182173$, $F_2 = 1.2420401$,
$F_3 = -0.21741801$

λ_1, λ_2, τ_3, τ_4 are the sample L-moments

Ref. (Hosking and Wallis, 1997)

D.6. Pearson type III distribution

Parameters: μ(location), σ (scale), γ (shape)

Range: $\gamma > 0$

$\alpha = 4/\gamma^2$, $\beta = \frac{1}{2}\sigma|\gamma|$, and $\xi = \mu - 2\sigma/\gamma$

$\xi \le x < \infty$

CDF: $$F(x) = G\left(\alpha, \frac{x-\xi}{\beta}\right)/\Gamma(\alpha)$$

PDF: $$f(x) = \frac{(x-\xi)^{\alpha-1}e^{-(x-\xi)/\beta}}{\beta^{\alpha}\Gamma(\alpha)}$$

QF: no explicit analytical form

L-moment parameter estimates:

$$\begin{cases} \alpha \approx \dfrac{1+0.2906z}{z+0.1882z^2+0.0442z^3} & \text{for } 0<|\tau_3|<1/3, \quad z = 3\Pi\tau_3^2; \\ \alpha \approx \dfrac{0.36067z-0.59567z^2+0.25361z^3}{1-2.78861z+2.56096z^2-0.77045z^3} & \text{for } 1/3 \le |\tau_3| < 1, \quad z = 1-|\tau_3| \end{cases}$$

$$\gamma = 2\alpha^{-1/2}sign(\tau_3),$$

$$\sigma = \frac{\lambda_2\pi^{1/2}\alpha^{1/2}\Gamma(\alpha)}{\Gamma(\alpha+\frac{1}{2})},$$

$$\mu = \lambda_1$$

where $\Gamma(x) = \int_0^{\infty} t^{\alpha-1}e^{-t}dt$ is the gamma function

$G(\alpha, x) = \int_0^{x} t^{\alpha-1}e^{-t}dt,$ is the incomplete gamma function

λ_1, λ_2, τ_3, τ_4 are the sample L-moments

Ref. (Hosking and Wallis, 1997)

D.7. Kappa distribution

Parameters: ξ (location), α (scale), k, h

Range:
$$\begin{cases} x \le \xi + \alpha/k & \text{if } k > 0, \\ x < \infty & \text{if } k \le 0, \\ x \ge \xi + \alpha(1-h^{-k})/k & \text{if } h > 0, \\ x \ge \xi + \alpha/k & \text{if } k < 0, \text{and } h \le 0, \\ x > -\infty & \text{if } k \ge o, \text{and } h \le 0 \end{cases}$$

CDF:
$$F(x) = \left[1 - h\left(1 - k(x-\xi)/\alpha\right)^{1/k}\right]^{1/h}$$

PDF:
$$f(x) = \alpha^{-1}\left[1 - k(x-\xi)/\alpha\right]^{1/k-1}\left[F(x)\right]^{1-h}$$

QF:
$$x(F) = \xi + \frac{\alpha}{k}\left\{1 - \left(\frac{1-F^h}{h}\right)^k\right\}$$

L-moment parameter estimates:

$$\lambda_1 = \xi + \alpha(1-g_1)/k$$
$$\lambda_2 = \alpha(g_1 - g_2)/k$$
$$\tau_3 = (-g_1 + 3g_2 - 2g_3)/(g_1 - g_2)$$
$$\tau_4 = (-g_1 + 6g_2 - 10g_3 + 5g_4)/(g_1 - g_2)$$

where
$$g_r = \begin{cases} \dfrac{r\Gamma(1+k)\Gamma(r/h)}{h^{1+k}\Gamma(1+k+r/h)}, & h > 0 \\ \dfrac{r\Gamma(1+k)\Gamma(-k-r/h)}{(-h)^{1+k}\Gamma(1-r/h)}, & h < 0 \end{cases}$$

$\Gamma(x) = \int_0^\infty t^{\alpha-1}e^{-t}dt$ is the gamma function

$\lambda_1, \lambda_2, \tau_3, \tau_4$ are the sample L-moments

Expressions for τ_3 and τ_4 can be solved by iteration for k and h.

Ref. (Hosking and Wallis, 1997)

D.8. Wakeby distribution

Parameters: ξ (location), α , β, γ, δ

Range: $\begin{cases} \xi \le x < \infty & \text{if } \delta \ge 0 \text{ and } \gamma > 0; \\ \xi \le x \le \xi + \alpha/(\beta - \gamma/\delta) & \text{if } \delta < 0 \text{ or } \gamma = 0 \end{cases}$

CDF: not explicitly defined

PDF: not explicitly defined

QF: $$x(F) = \xi + \frac{\alpha}{\beta}\left[1-(1-F)^{\beta}\right] - \frac{\gamma}{\delta}\left[1-(1-F)^{-\delta}\right]$$

L-moment parameter estimates:

β and $-\delta$ are the roots of the quadratic equation (β is the larger root):

$$(N_2 C_3 - N_3 C_2) Z^2 + (N_1 C_3 - N_3 C_1) Z + (N_1 C_2 - N_2 C_1) = 0$$

then $\alpha = (1 + \beta)(2 + \beta)(3 + \beta)\{(1 + \delta) \lambda_2 - (3 - \delta) \lambda_3\}/\{4(\beta + \delta)\}$,

$\gamma = -(1 - \delta)(2 - \delta)(3 - \delta)\{(1 - \beta) \lambda_2 -(3 + \beta) \lambda_3\}/\{4(\beta + \delta\}$,

$\xi = \lambda_1 - \alpha / (1 + \beta) - \gamma / (1 - \delta)$

where $N_1 = 3\lambda_2 - 25\lambda_3 + 32\lambda_4$, $C_1 = 7\lambda_2 - 85\lambda_3 + 203\lambda_4 -125\lambda_5$,

$N_2 = - 3\lambda_2 + 5\lambda_3 + 8\lambda_4$, $C_2 = - 7\lambda_2 + 25\lambda_3 + 7\lambda_4 -25\lambda_5$,

$N_3 = 3\lambda_2 + 5\lambda_3 + 2\lambda_4$, $C_3 = 7\lambda_2 + 5\lambda_3 - 7\lambda_4 - 5\lambda_5$

λ_1, λ_2, τ_3, τ_4 are the sample L-moments

Ref. (Hosking and Wallis, 1997)

D.9. Log Pearson type III distribution

Same as Pearson type III distribution but using (log x) instead of x.

D.10. Gamma distribution

Special case of Log Pearson type III when $\xi = 0$.

D.11. Lognormal distribution

Lognormal distribution is the general case of the Generalized normal distribution where skewness exists (i.e. $k \neq 0$).

D.12. Gumbel distribution

Special case of Generalized extreme-value distribution when parameter $k = 0$,

L-moment parameter estimates:

$$\alpha = \lambda_2 / \log 2, \qquad \xi = \lambda_1 - \gamma\,\alpha$$

Appendix E

Q-Q plots for observed versus fitted
ice thickness
for the selected stations

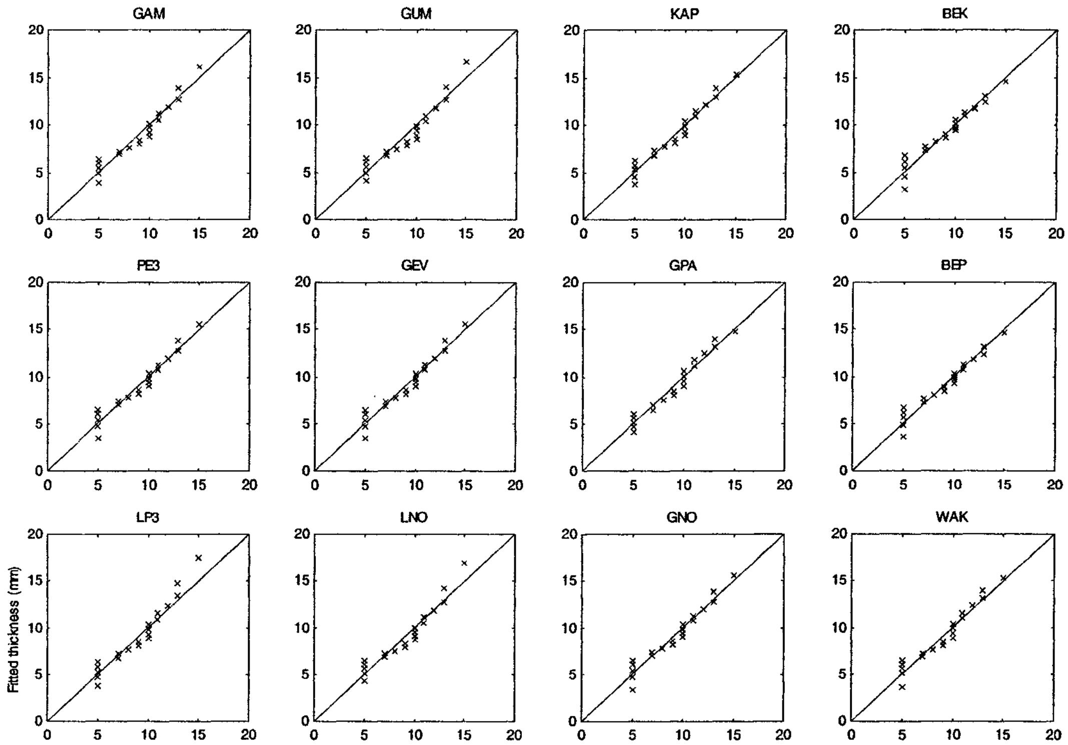

Q-Q plots for fitted distributions, station# 5 N= 20/ 61

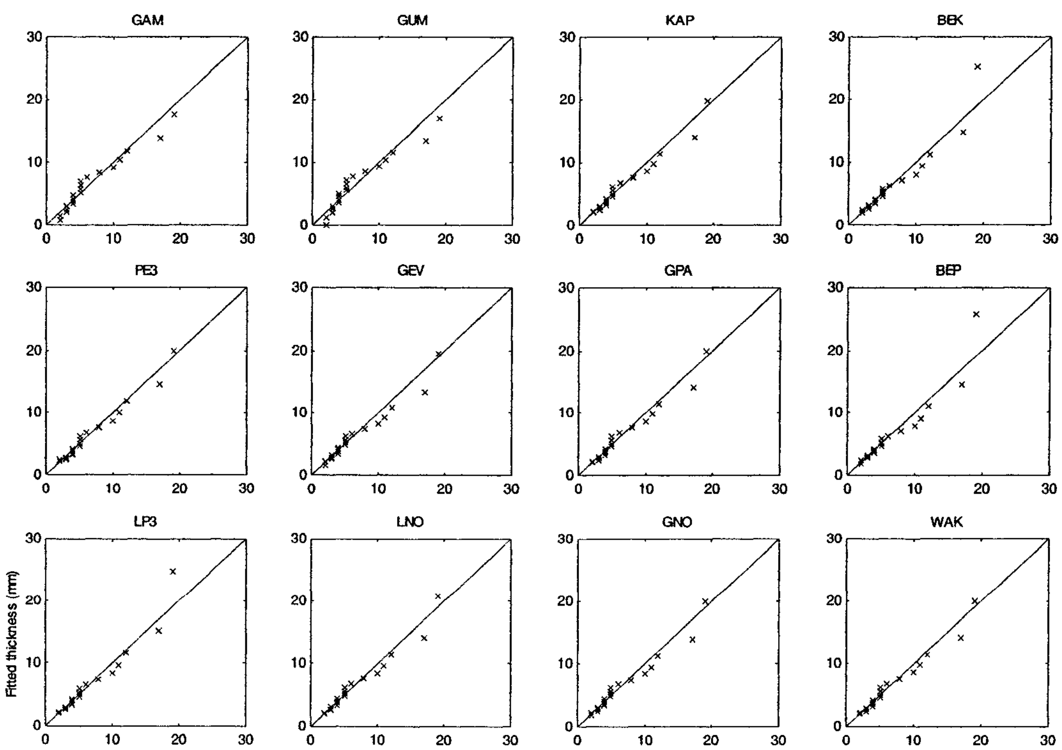

Q-Q plots for fitted distributions, station# 14 N= 20/ 20

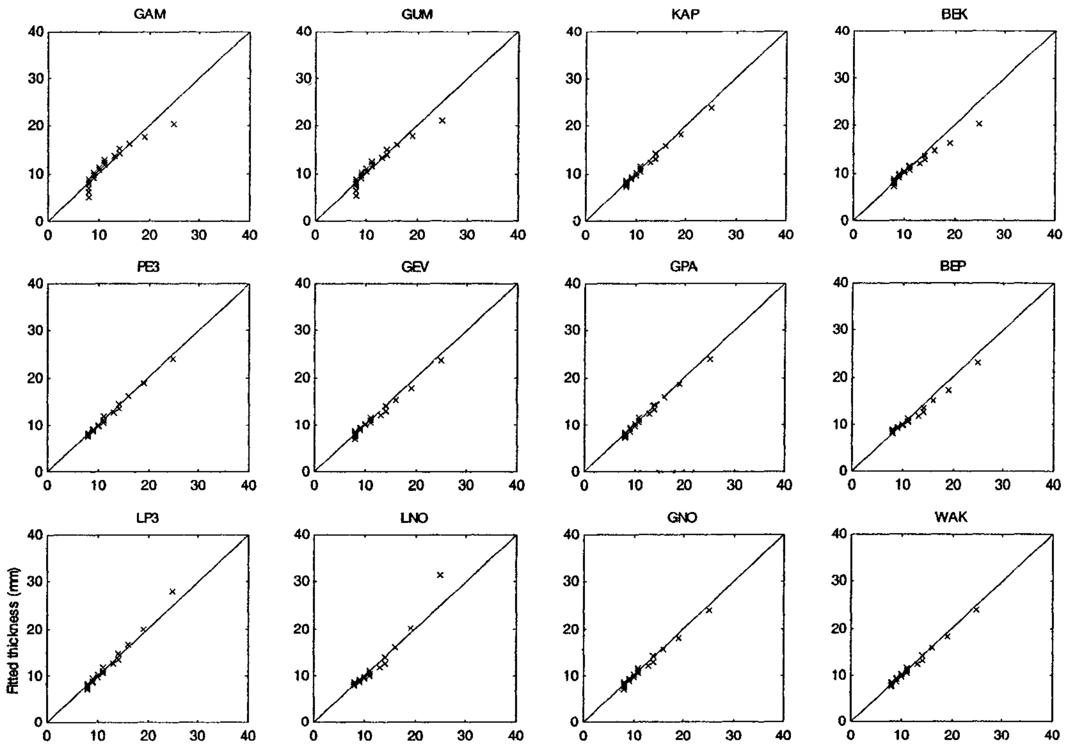

Q-Q plots for fitted distributions, station# 15 N= 20/120

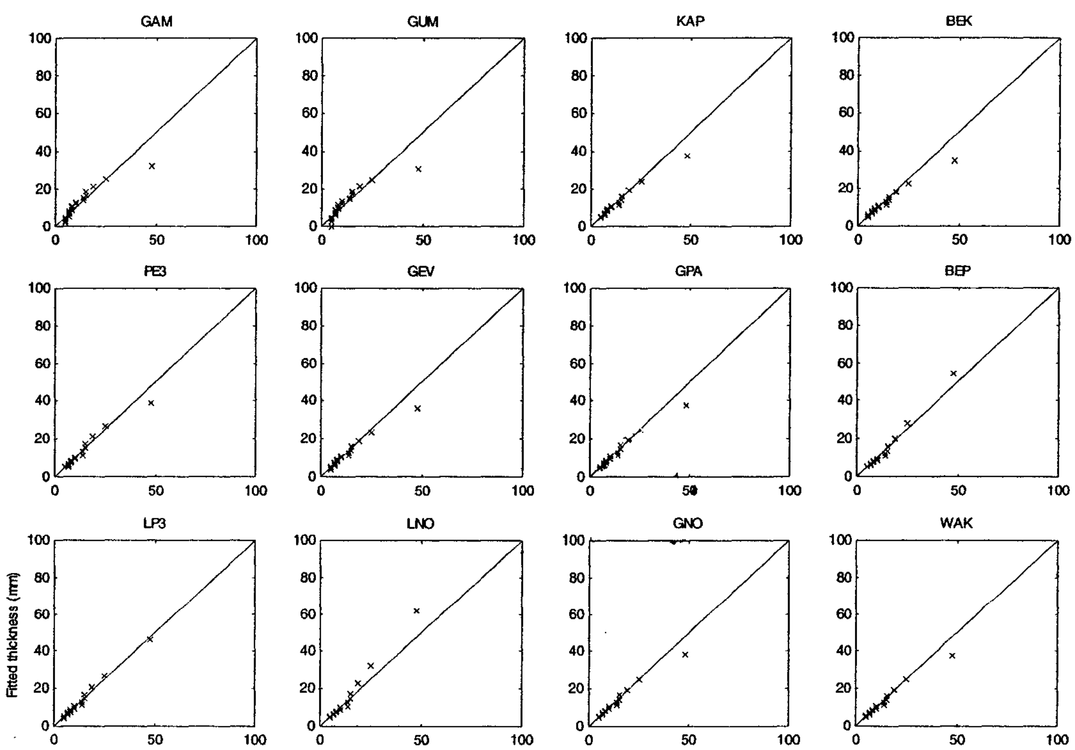

Q-Q plots for fitted distributions, station# 21 N= 20/ 44

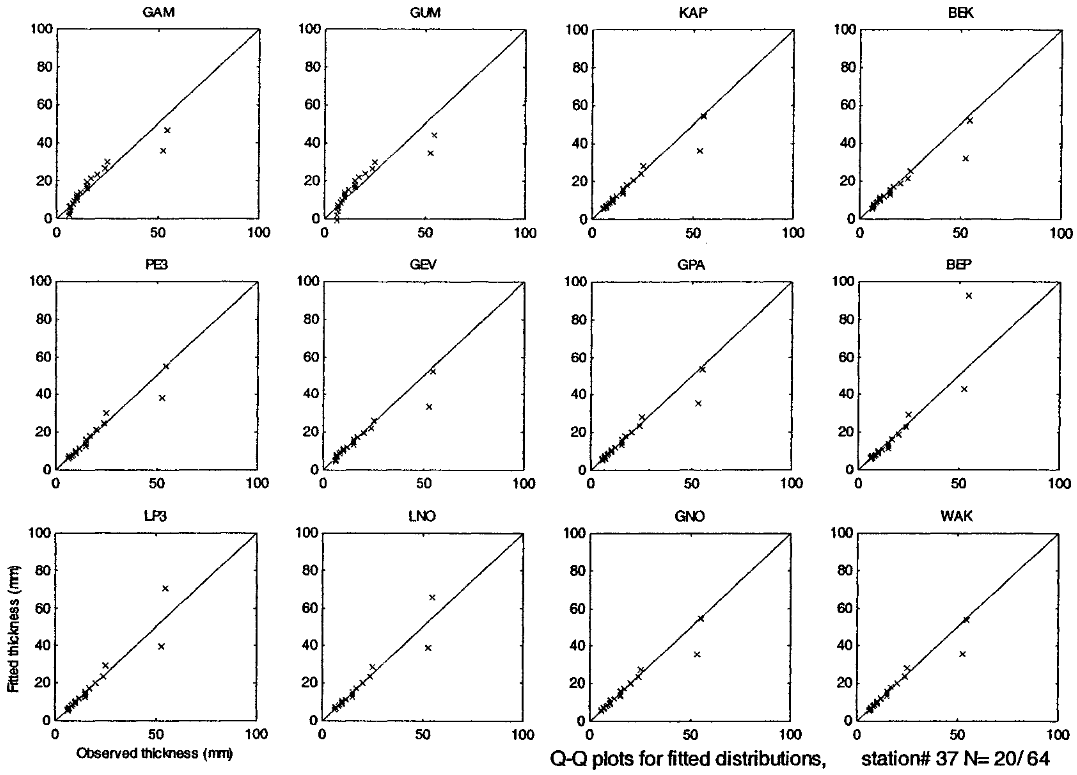

Q-Q plots for fitted distributions, station# 37 N= 20/64

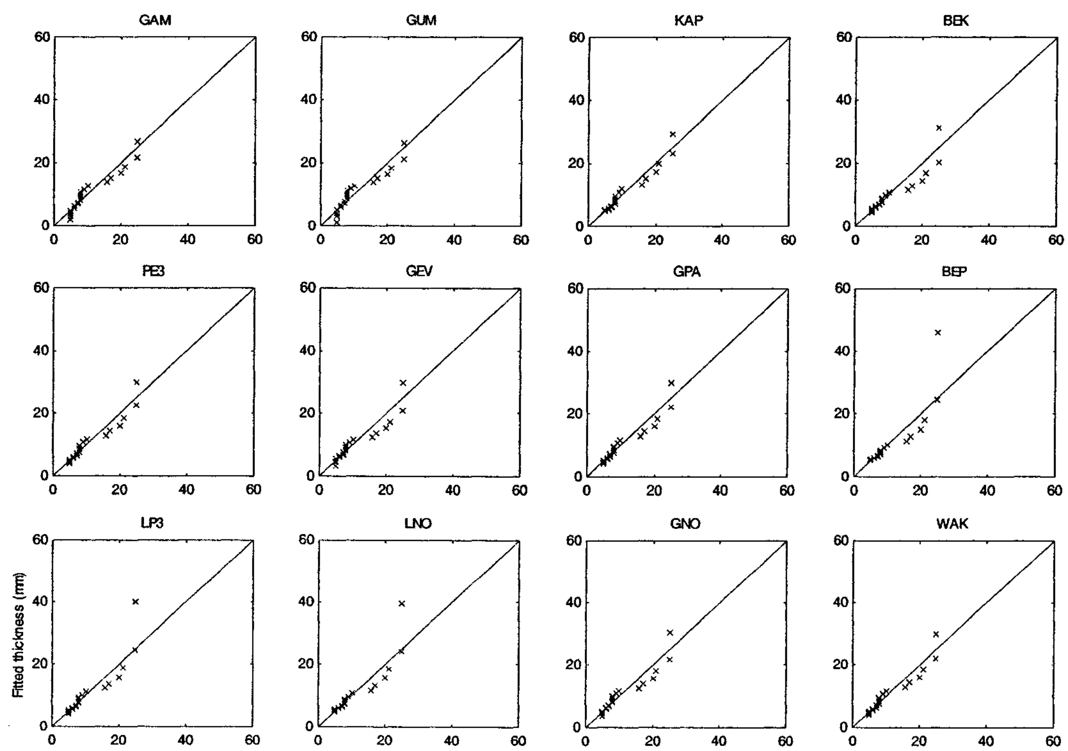

Q-Q plots for fitted distributions, station# 46 N= 20/78

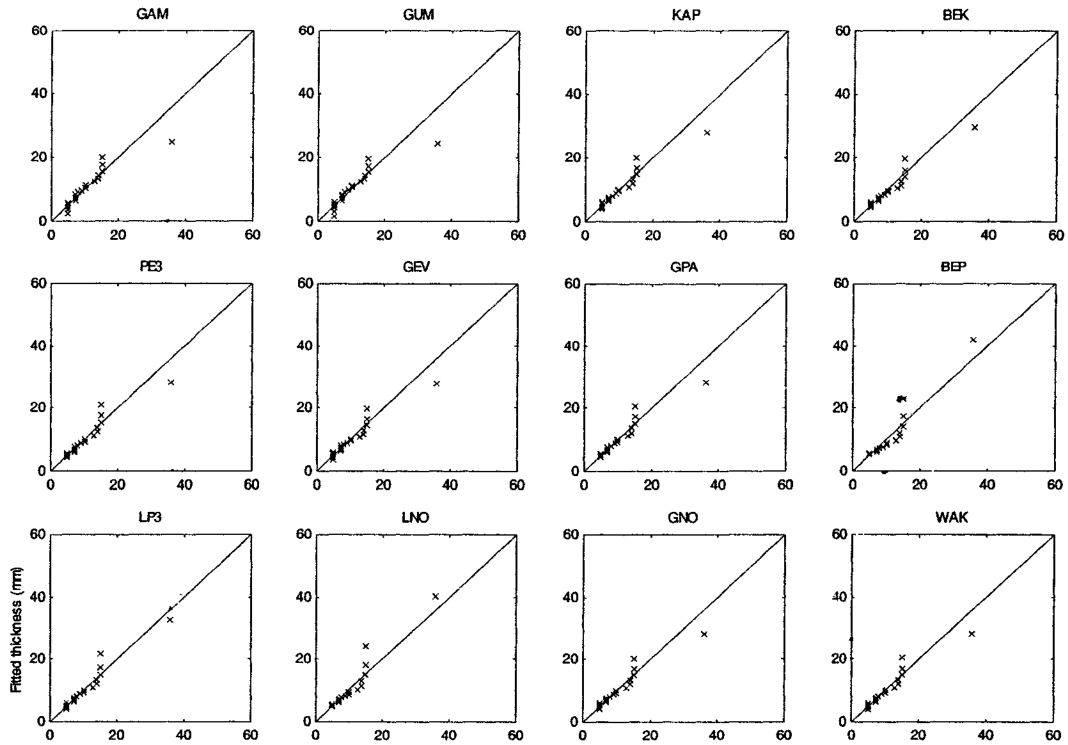

Q-Q plots for fitted distributions, station# 50 N= 20/ 33

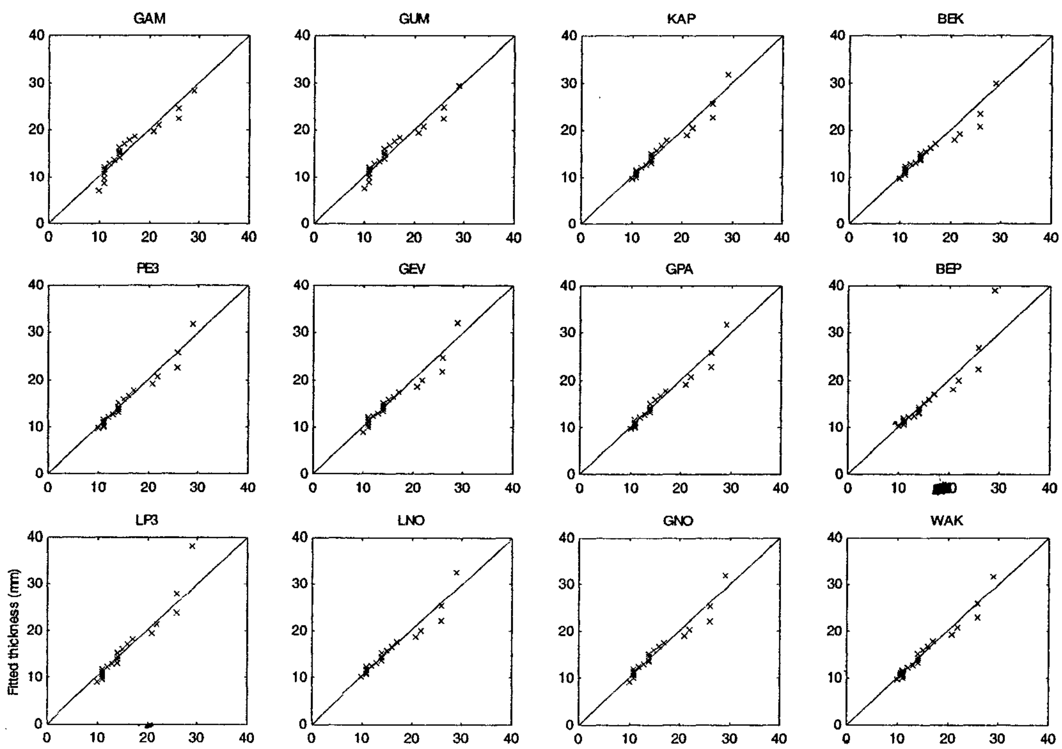

Q-Q plots for fitted distributions, station# 51 N= 20/ 77

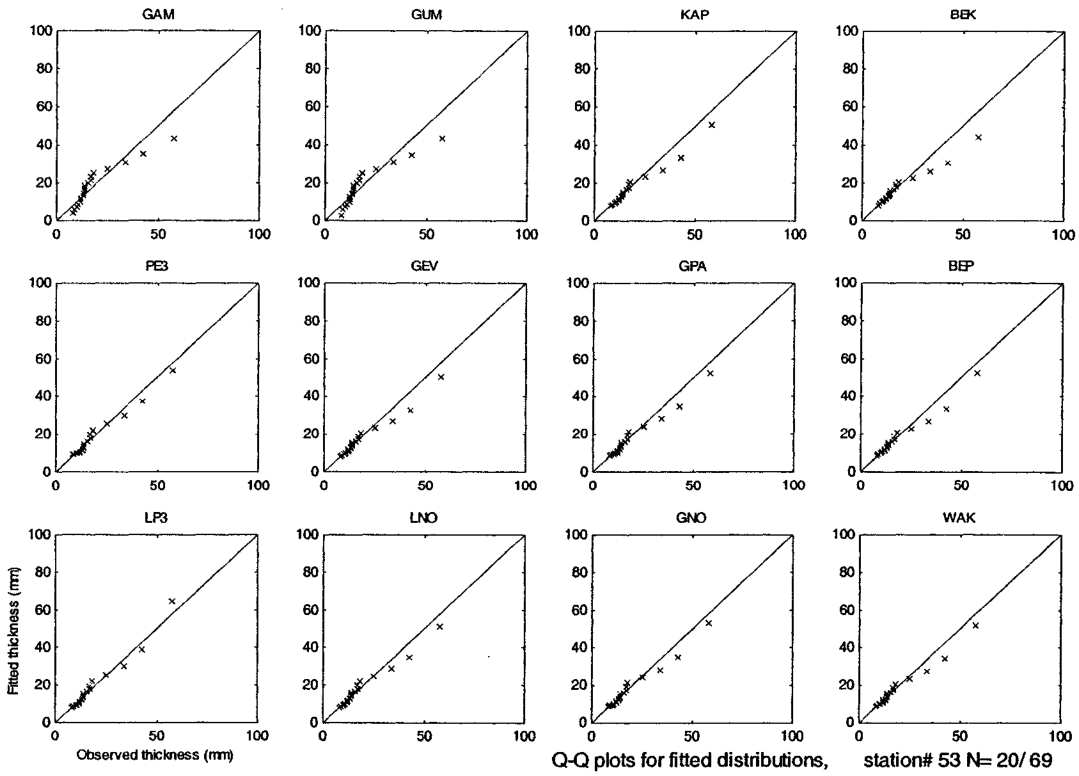

Q-Q plots for fitted distributions, station# 53 N= 20/ 69

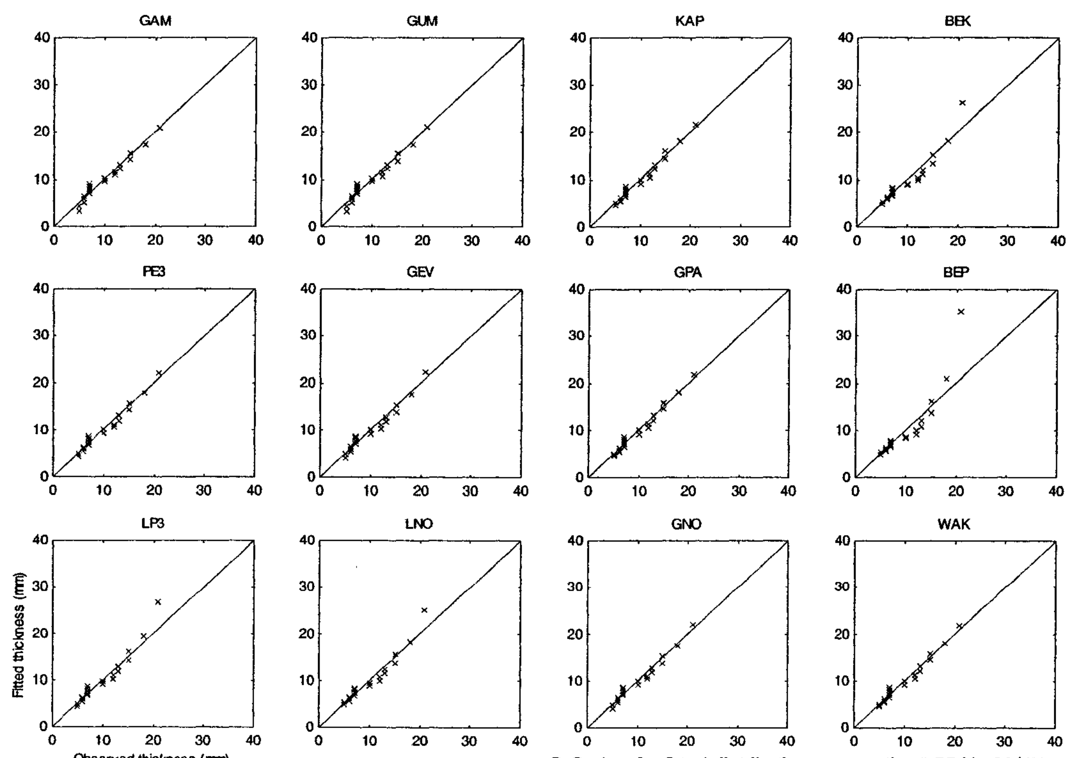

Q-Q plots for fitted distributions, station# 55 N= 20/ 50

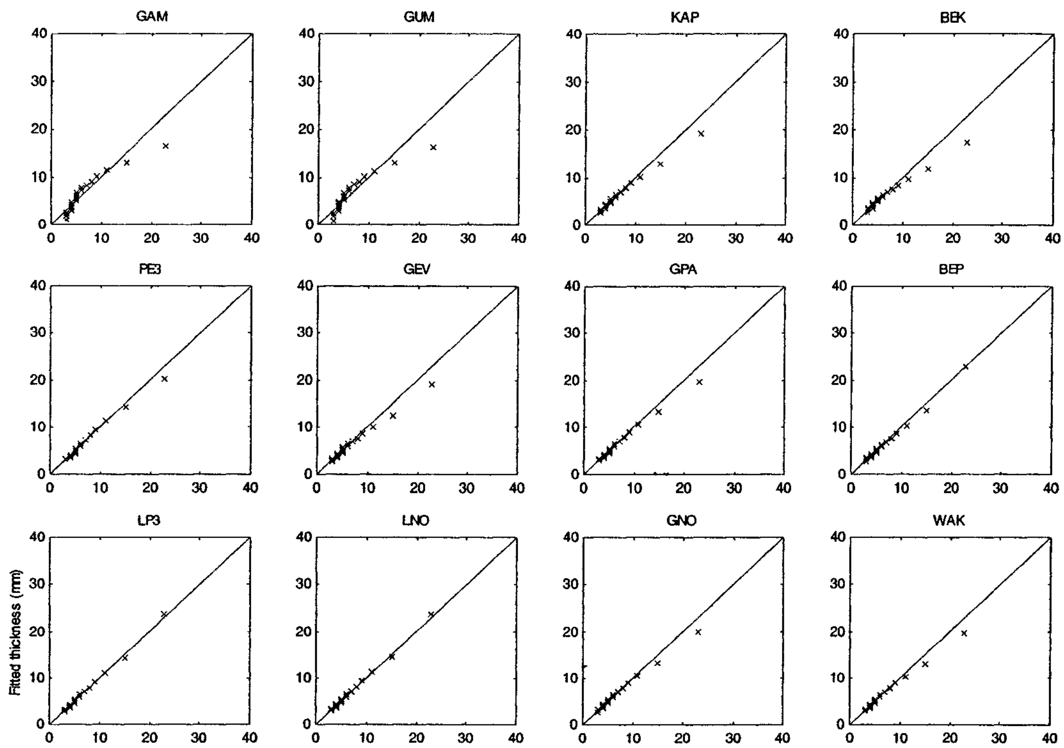

Q-Q plots for fitted distributions, station# 57 N= 20/ 33

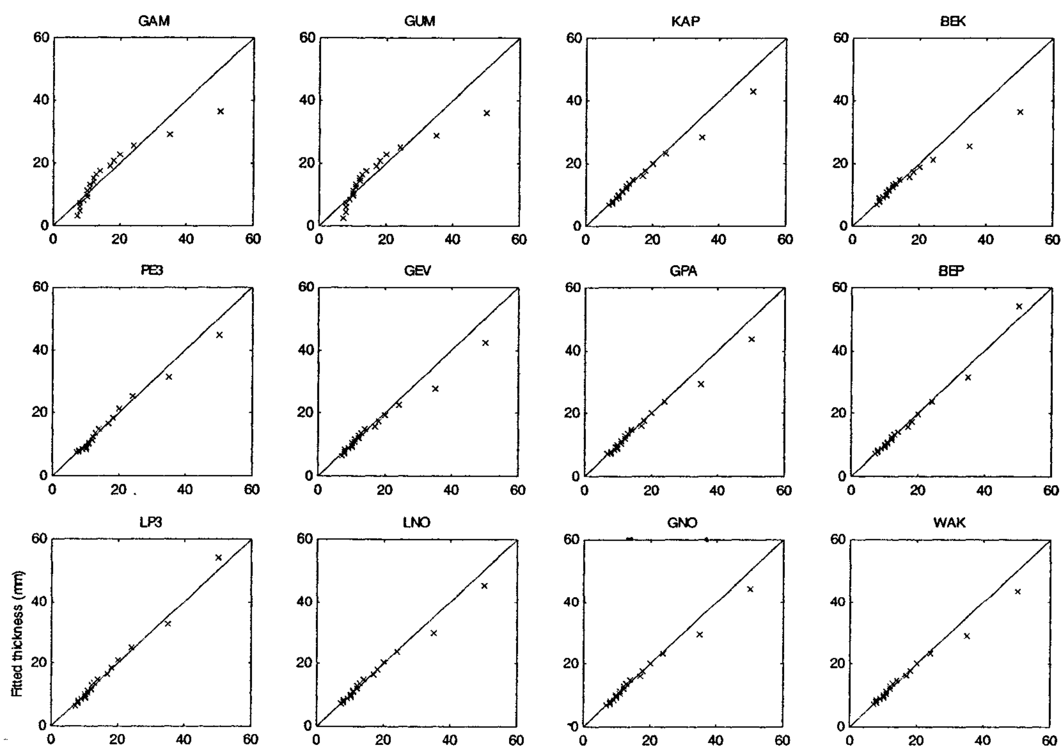

Q-Q plots for fitted distributions, station# 67 N= 20/ 32

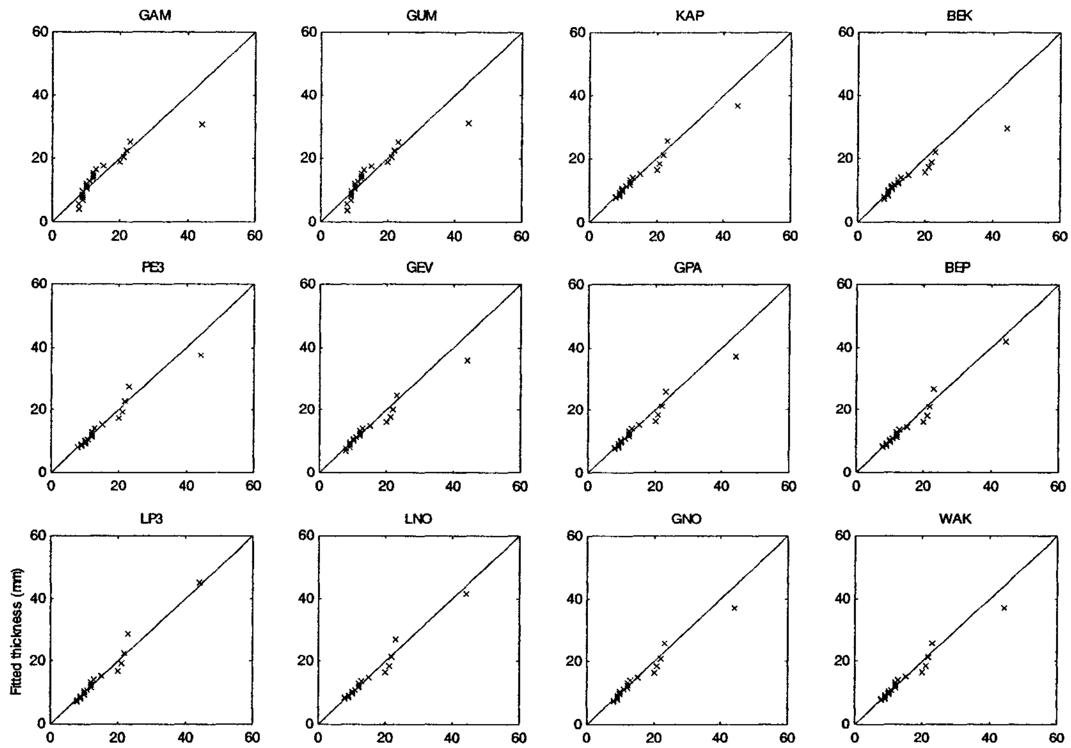

Q-Q plots for fitted distributions, station# 74 N= 20/ 49

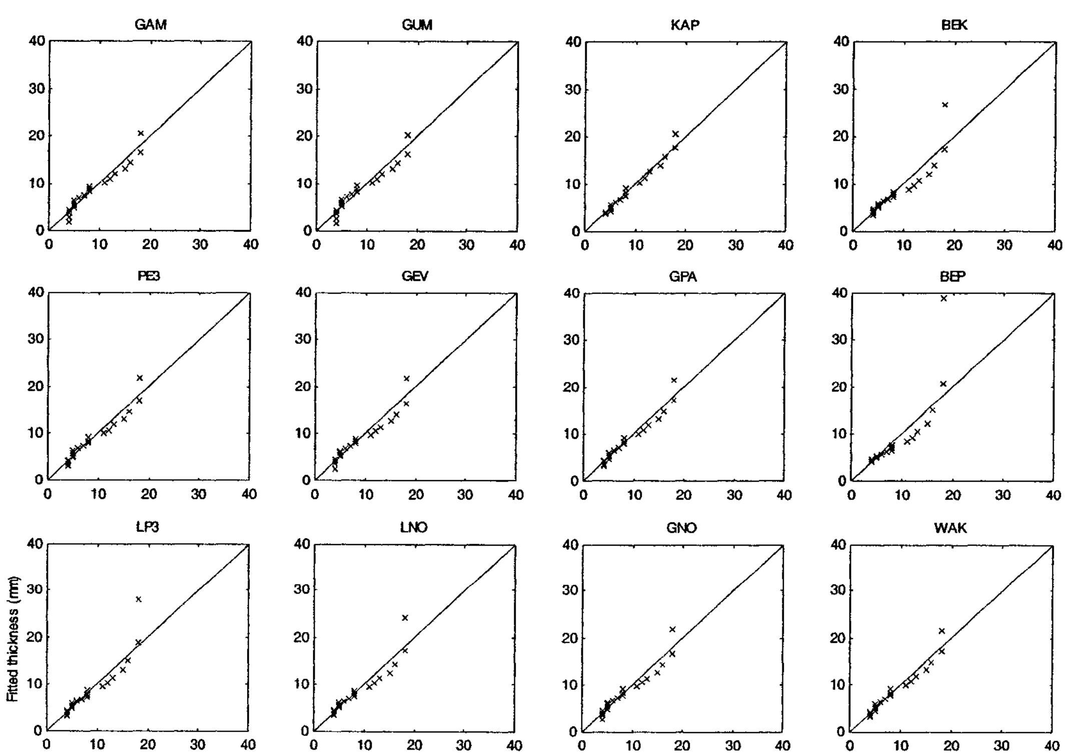

Q-Q plots for fitted distributions, station# 86 N= 20/ 35

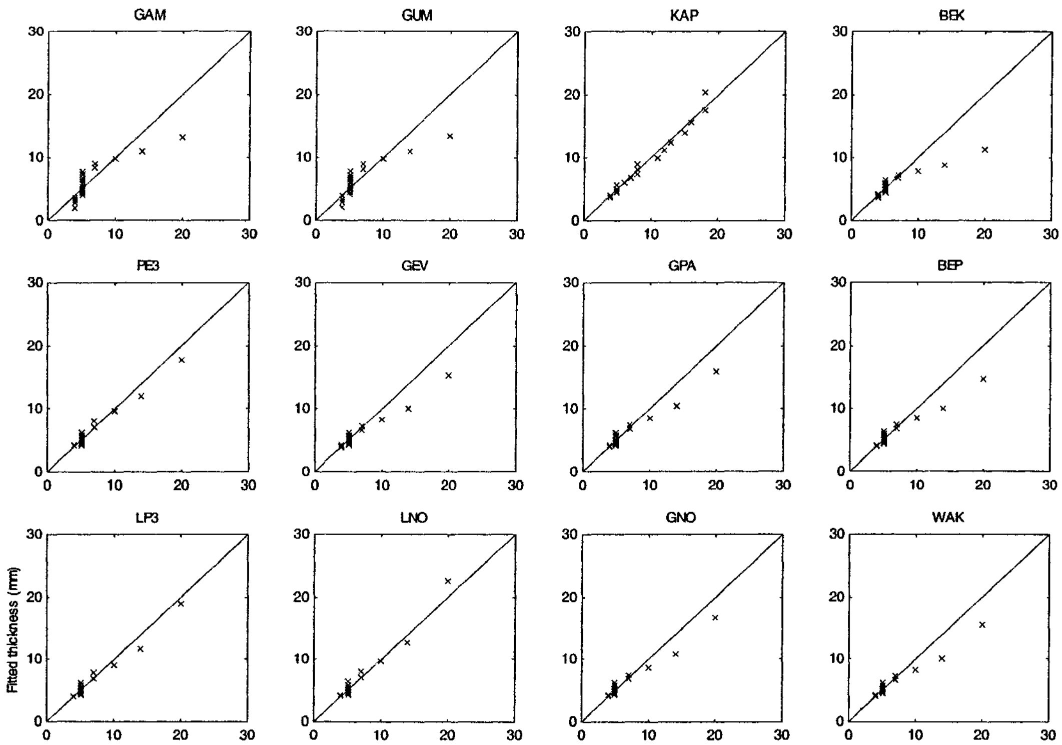

Q-Q plots for fitted distributions, station# 87 N= 20/ 50

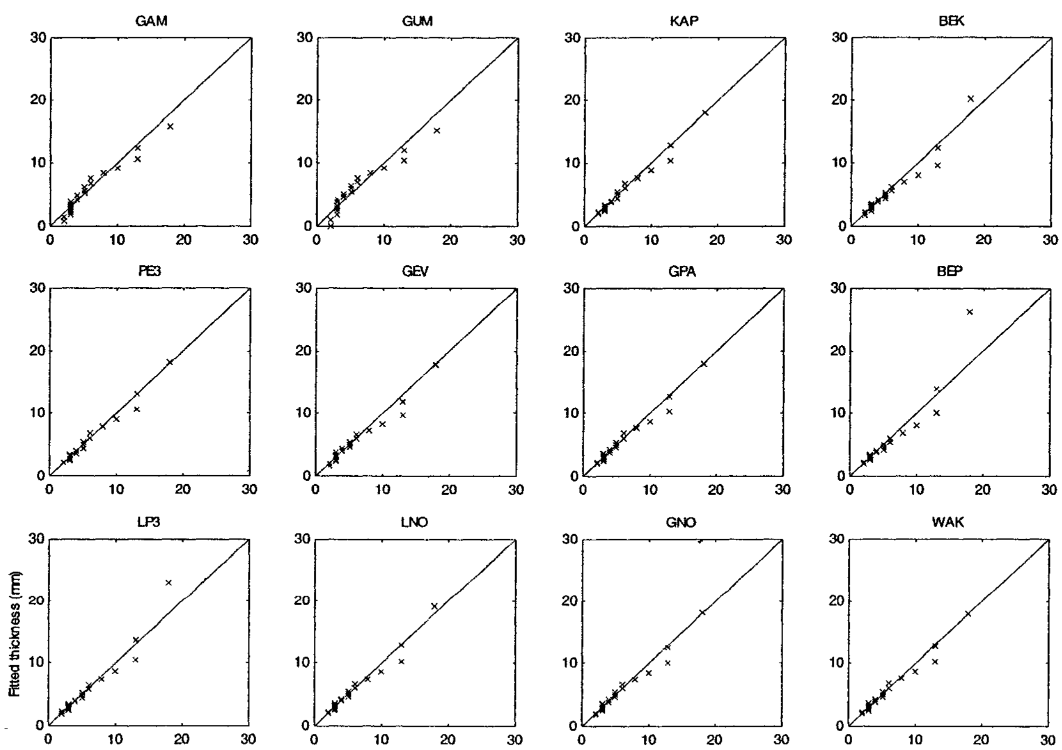

Q-Q plots for fitted distributions, station# 89 N= 20/ 24

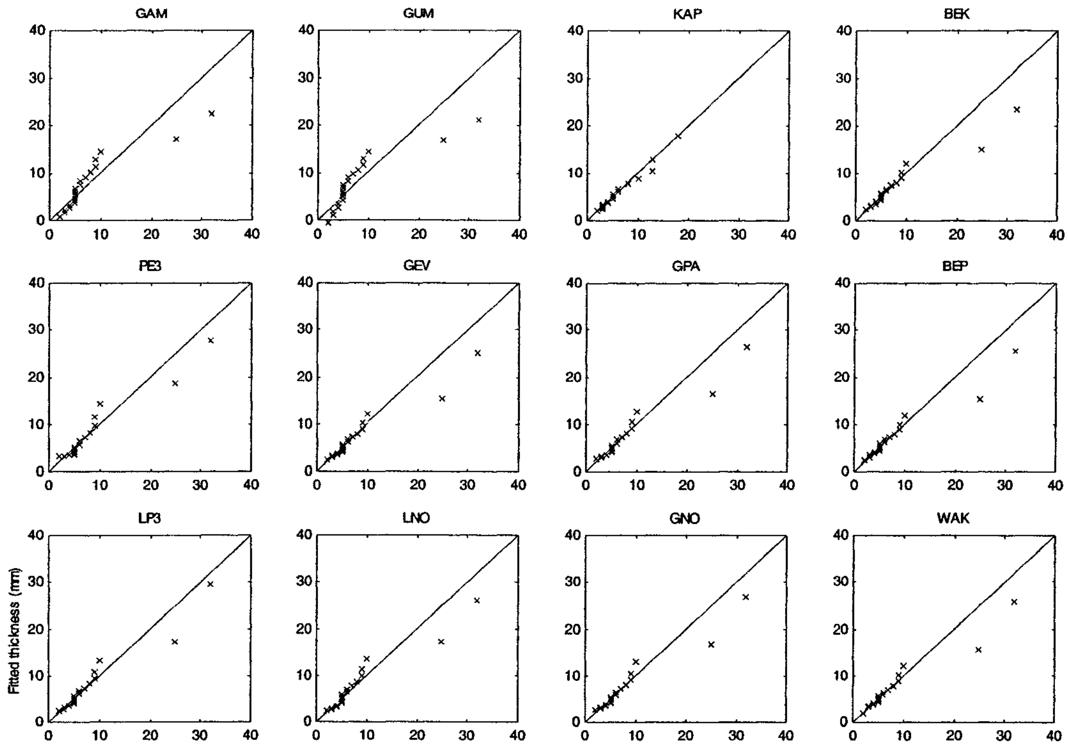

Q-Q plots for fitted distributions, station# 92 N= 20/ 26

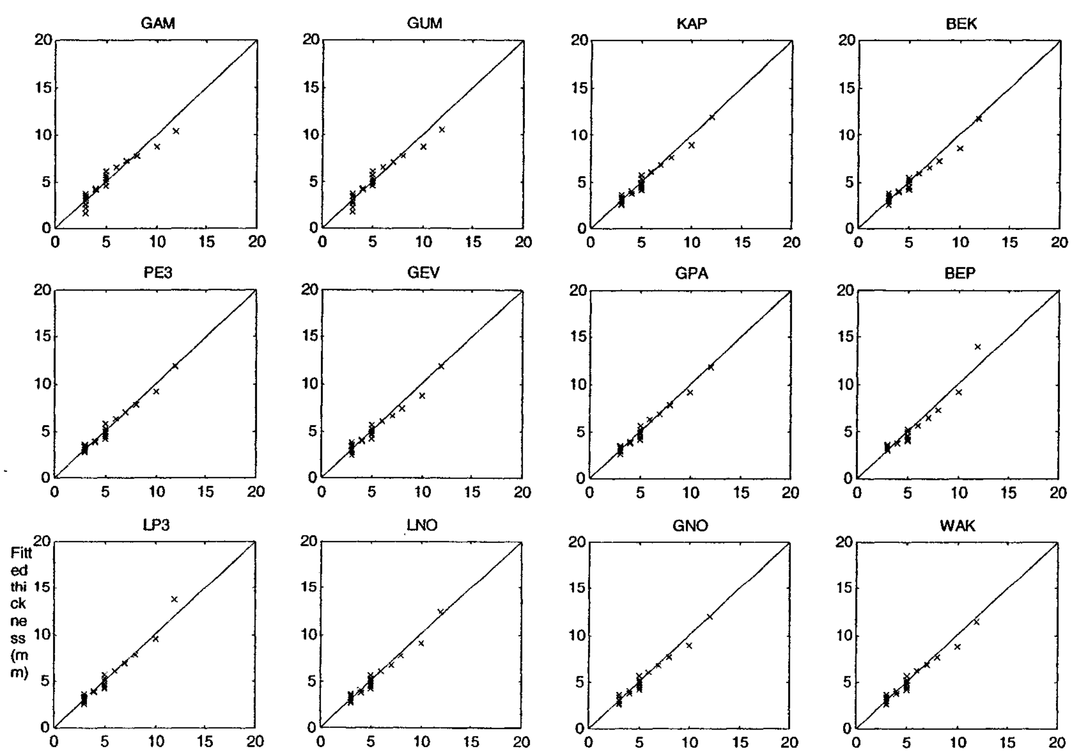

Q-Q plots for fitted distributions, station# 93 N= 20/ 41

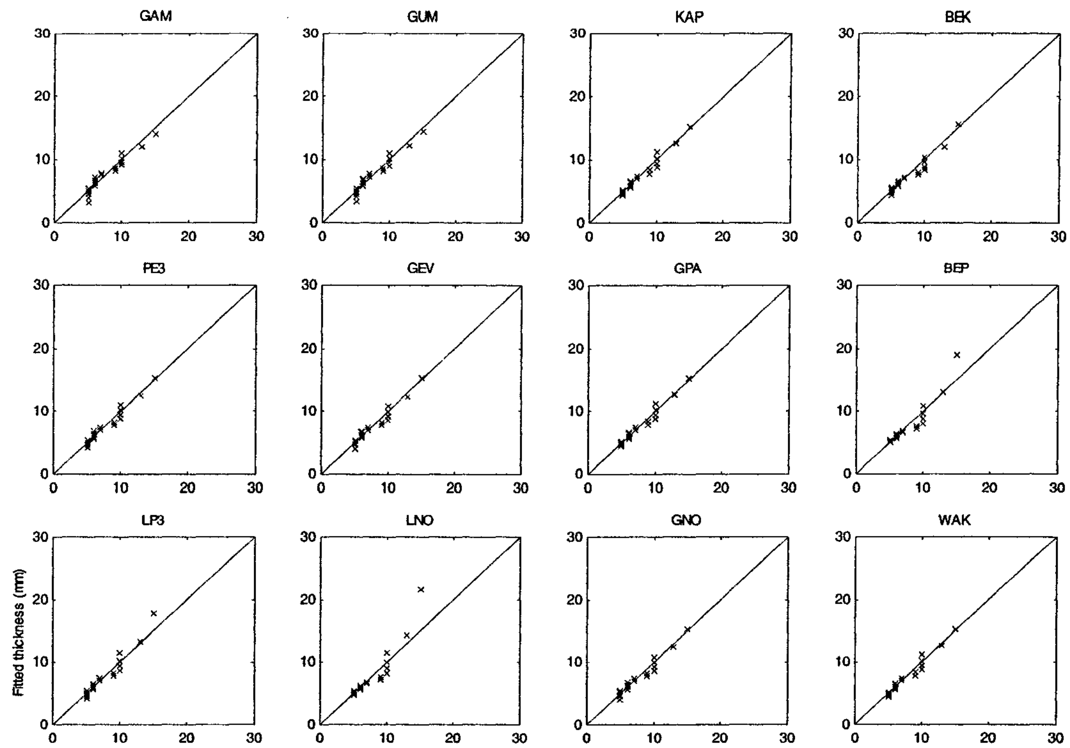

Q-Q plots for fitted distributions, station# 95 N= 20/34

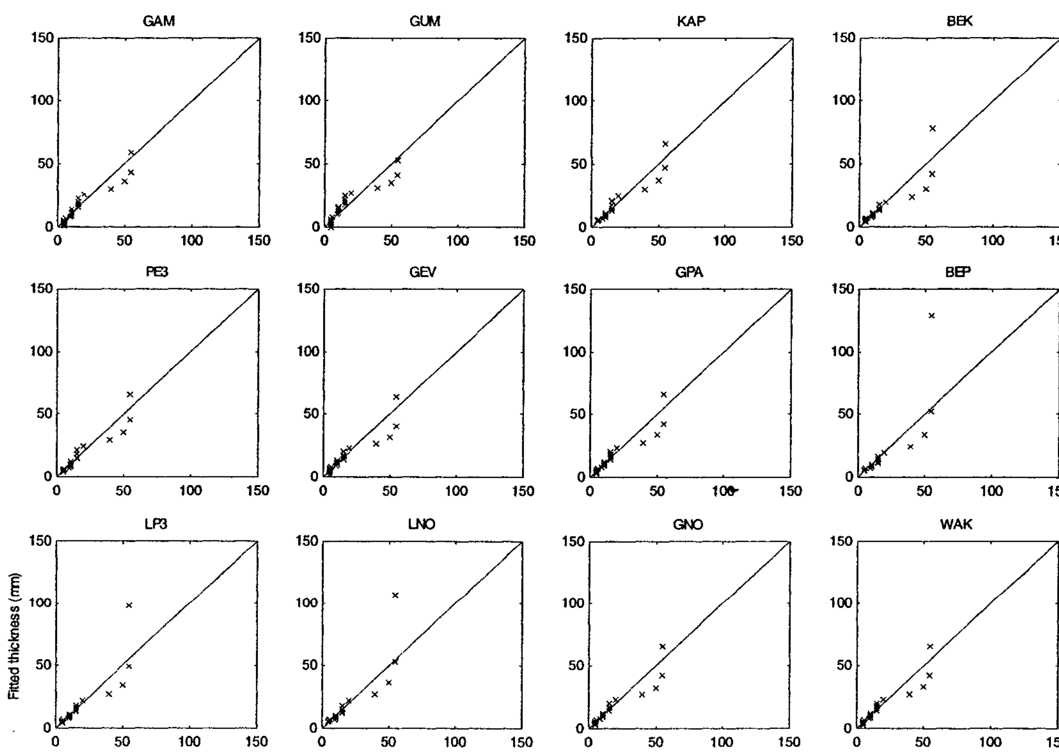

Q-Q plots for fitted distributions, station# 98 N= 20/34

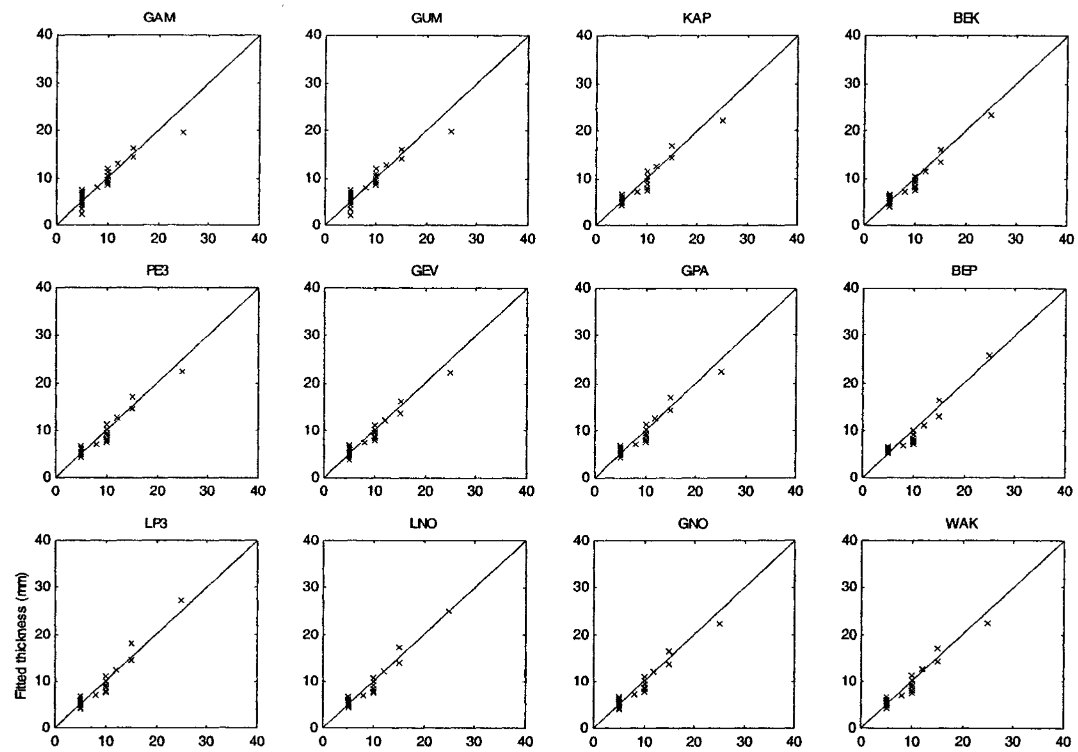

Q-Q plots for fitted distributions, station# 99 N= 20/30

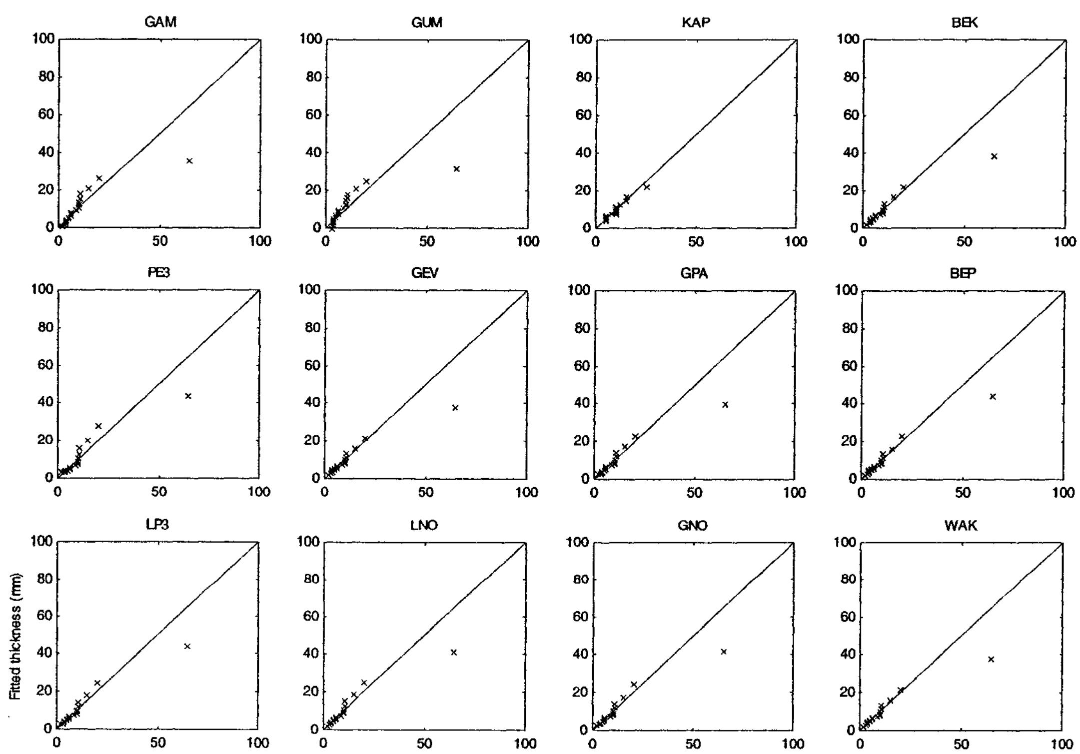

Q-Q plots for fitted distributions, station#101 N= 20/24

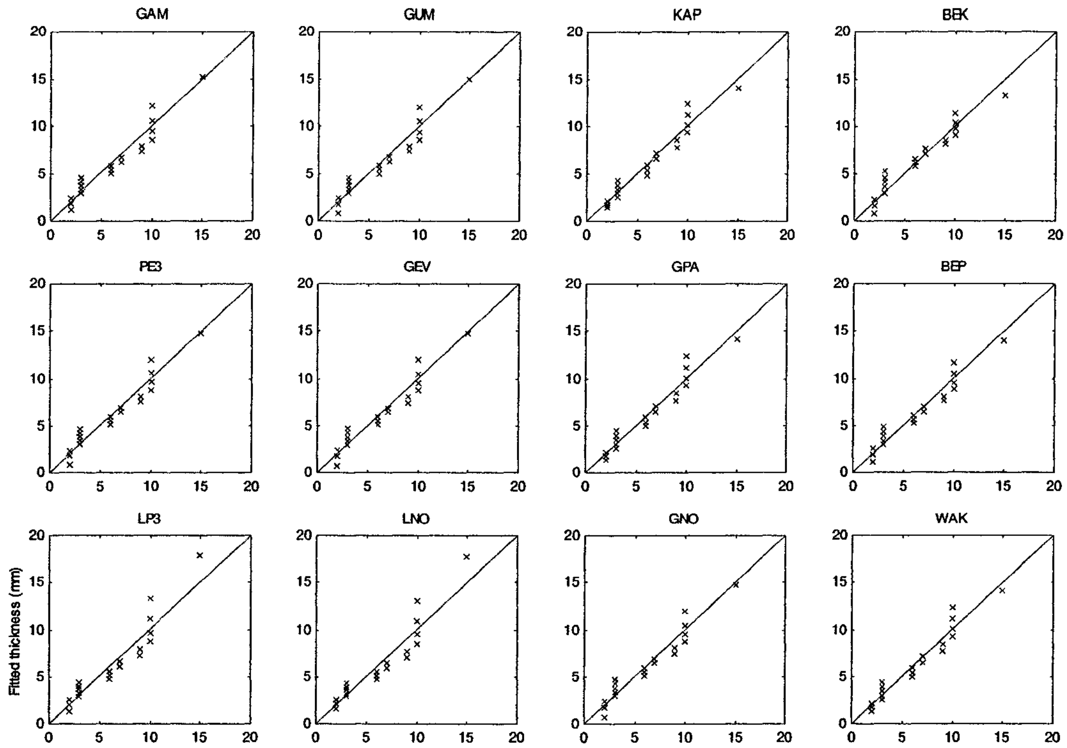

Q-Q plots for fitted distributions, station#102 N= 20/23

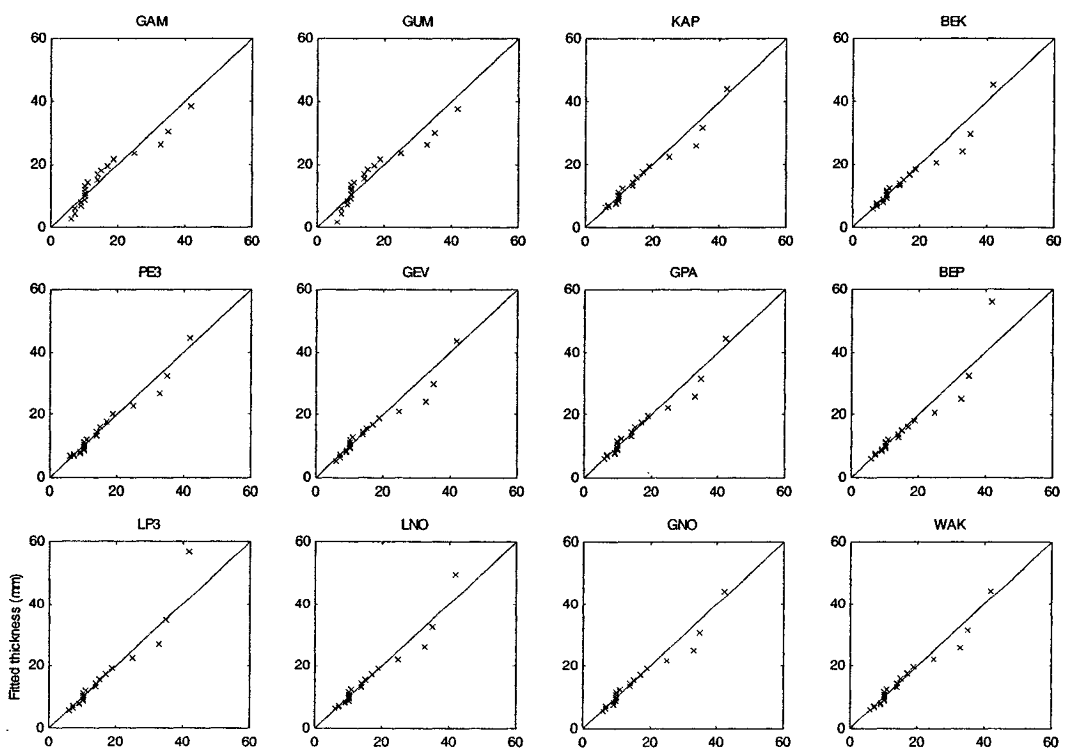

Q-Q plots for fitted distributions, station#107 N= 20/33

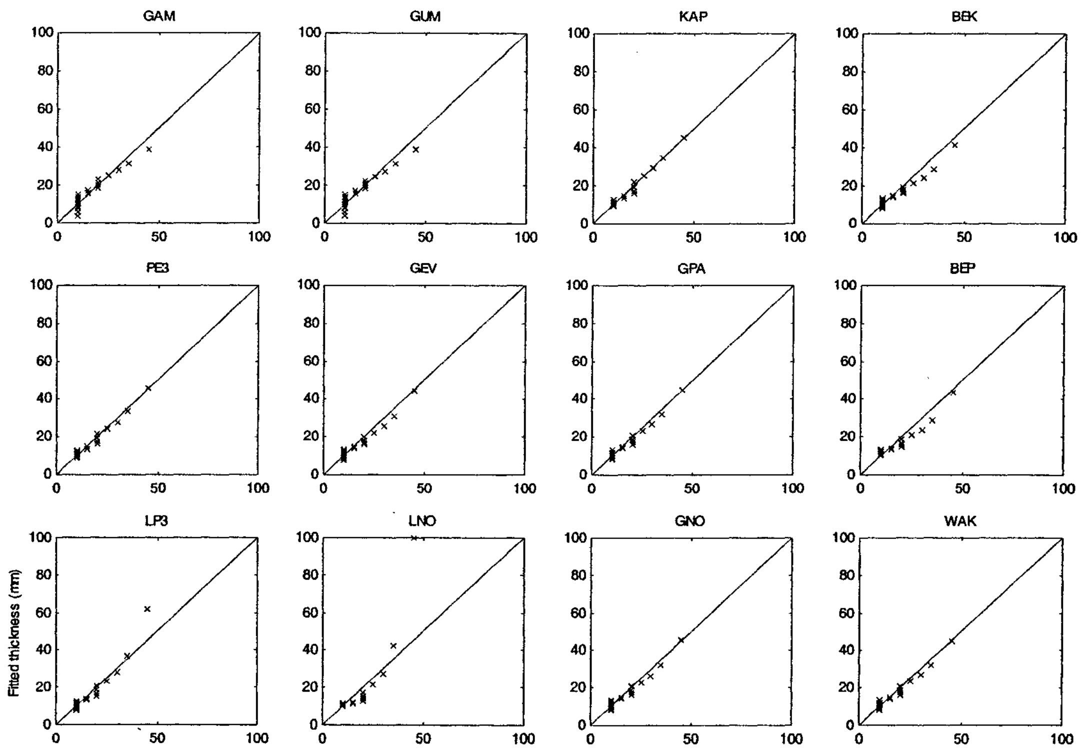

Q-Q plots for fitted distributions, station#121 N= 20/ 50

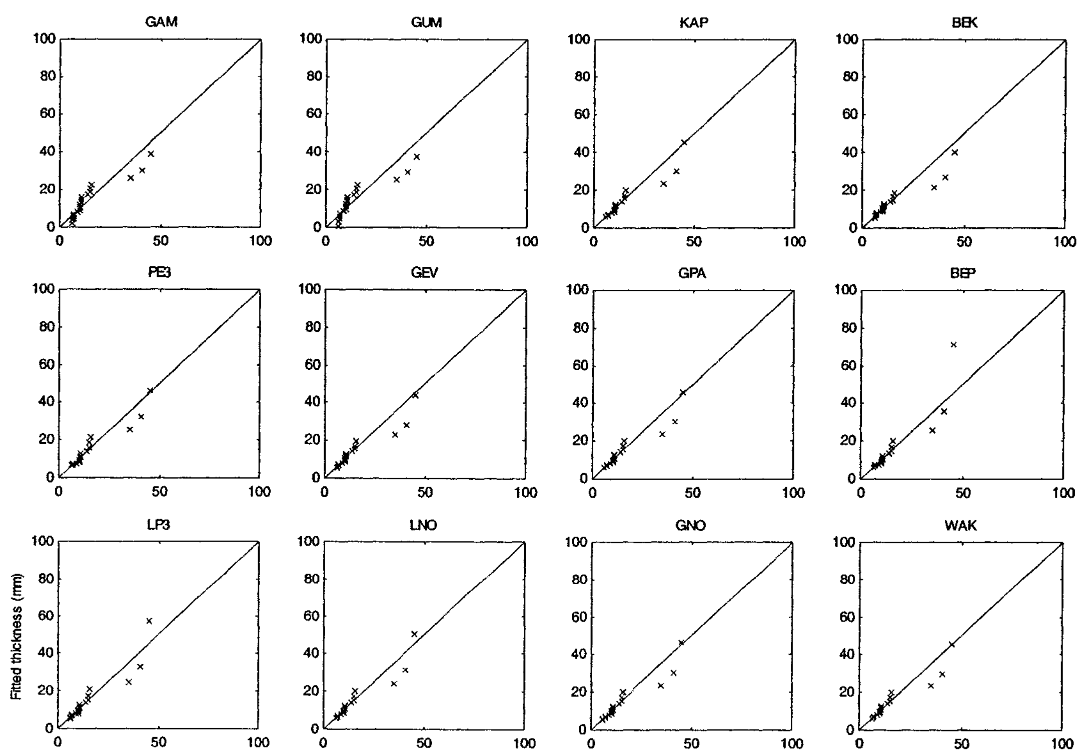

Q-Q plots for fitted distributions, station#125 N= 20/ 37

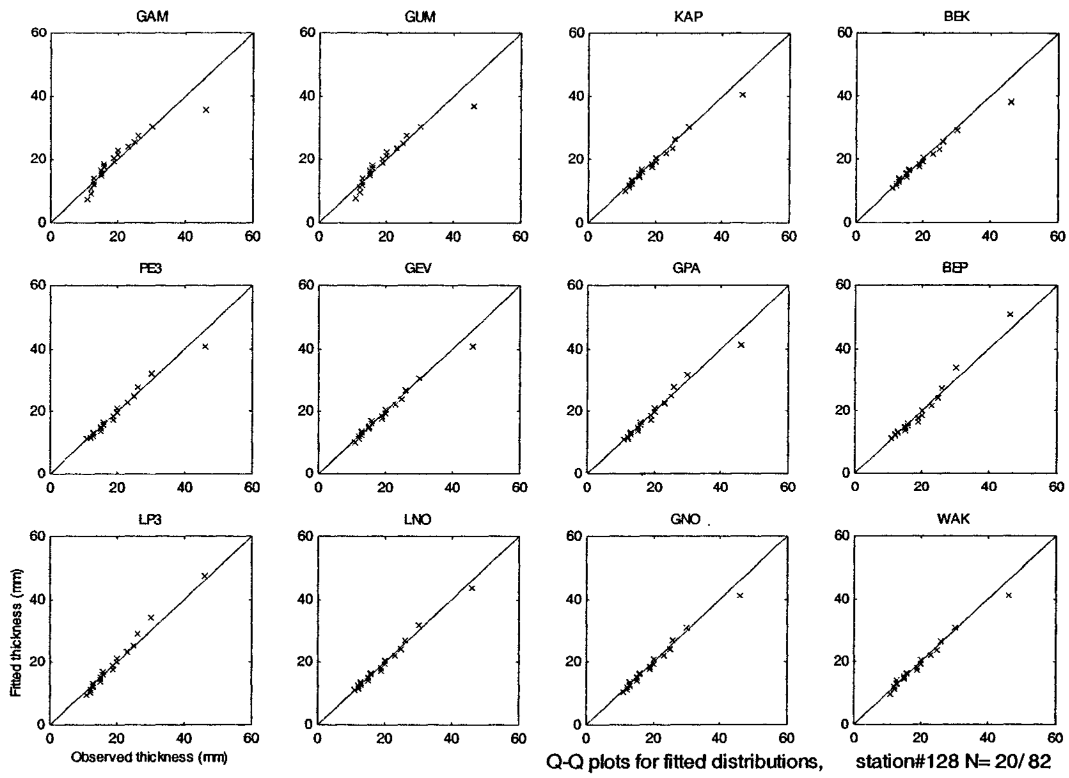

Q-Q plots for fitted distributions, station#128 N= 20/ 82

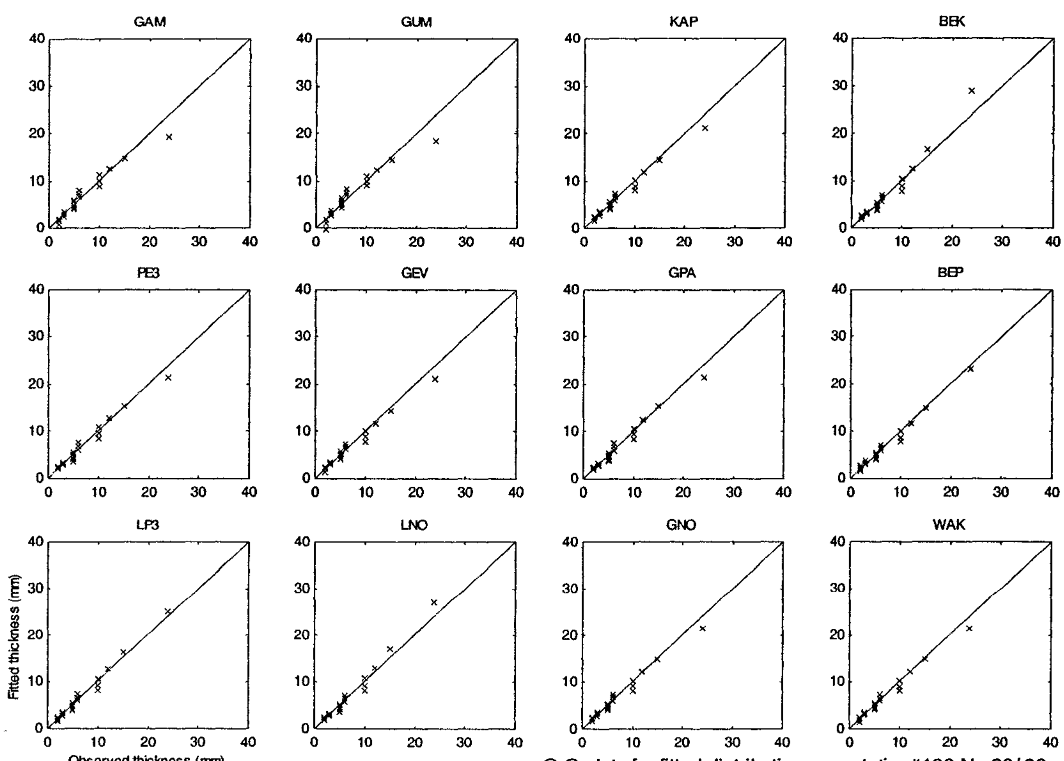

Q-Q plots for fitted distributions, station#130 N= 20/ 26

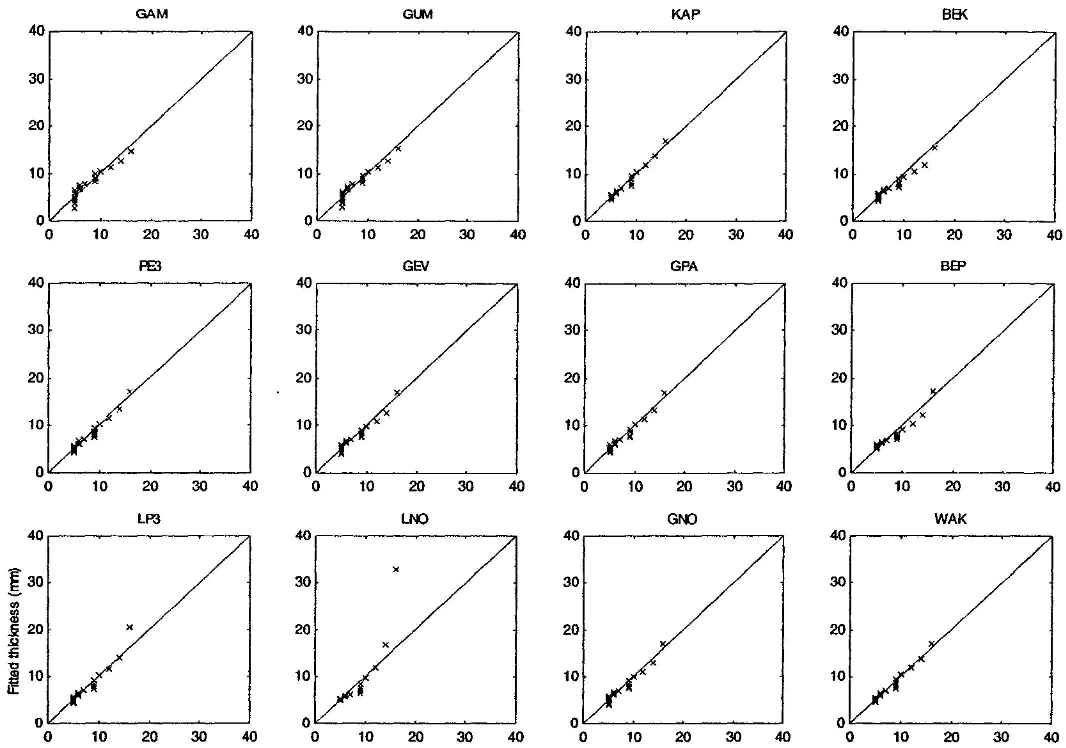

Q-Q plots for fitted distributions, station#134 N= 20/ 45

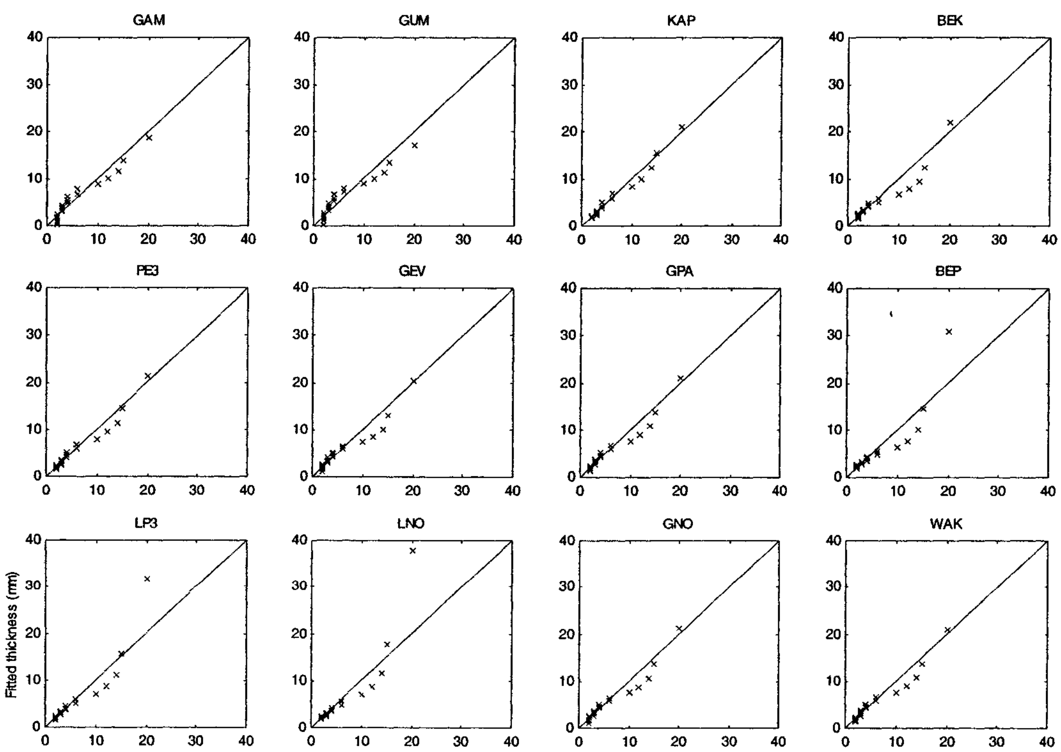

Q-Q plots for fitted distributions, station#137 N= 20/ 42

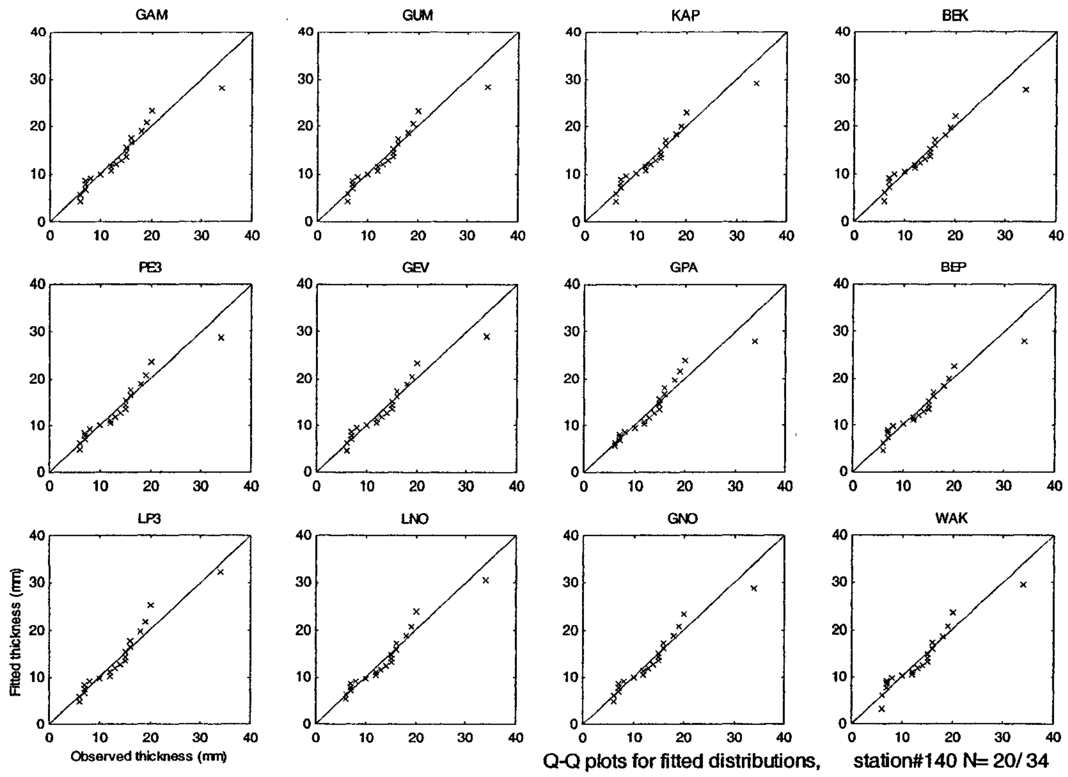

Q-Q plots for fitted distributions, station#140 N= 20/ 34

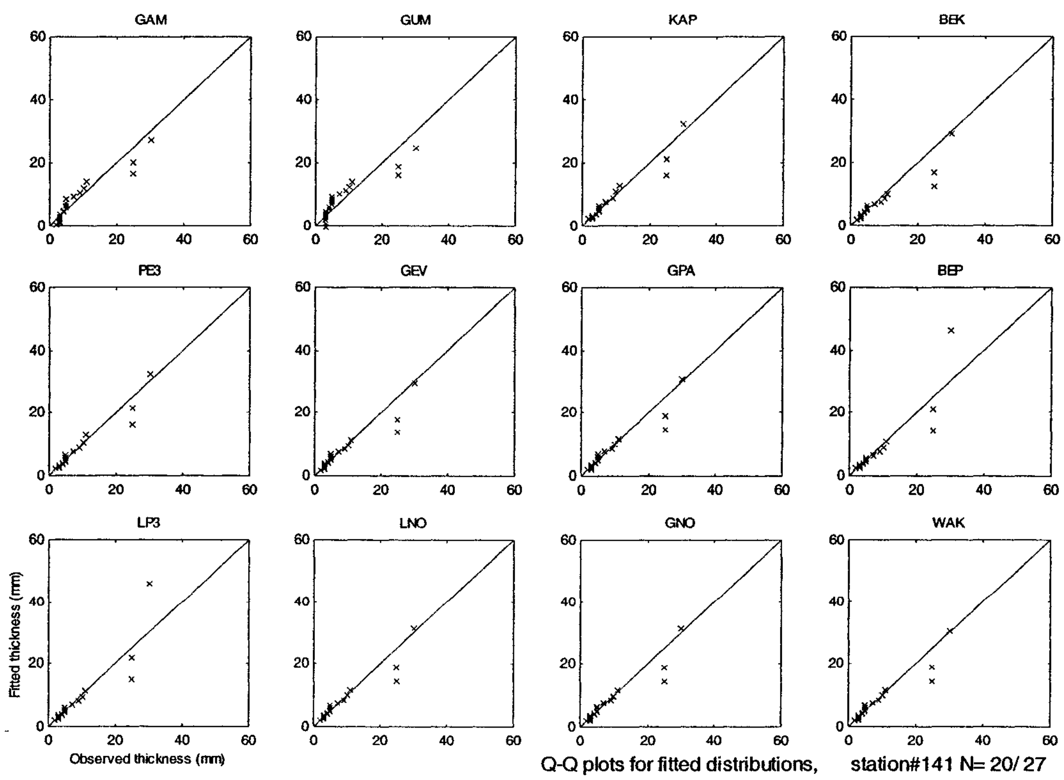

Q-Q plots for fitted distributions, station#141 N= 20/ 27

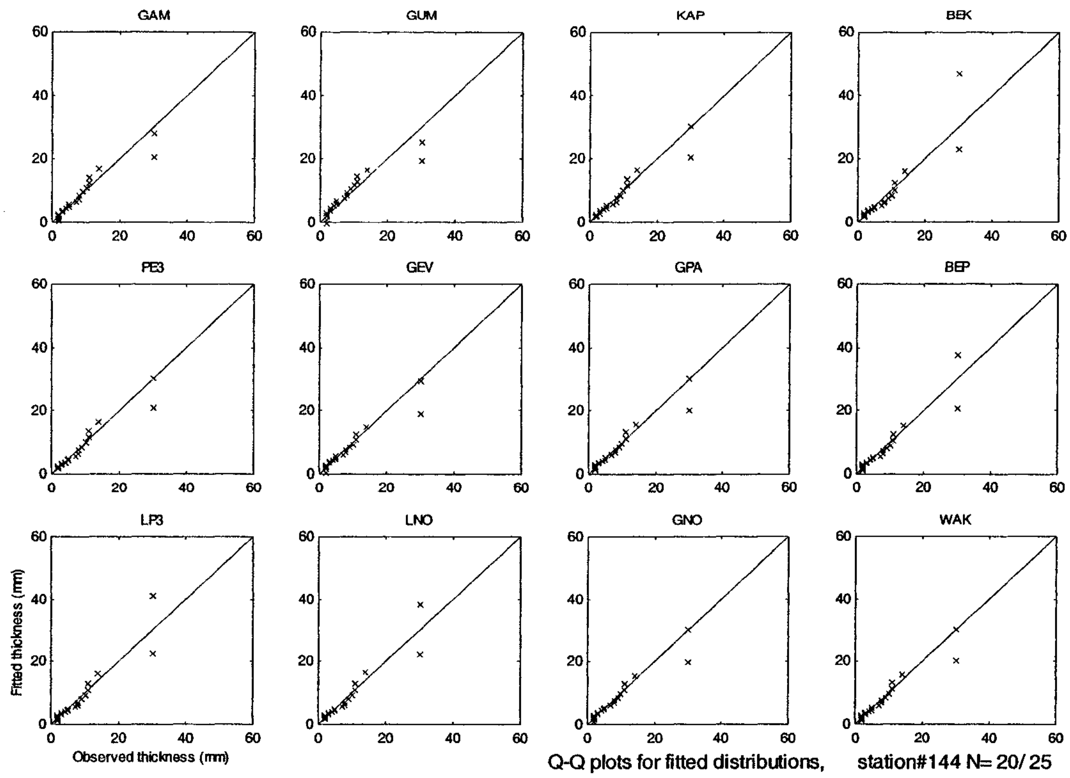

Q-Q plots for fitted distributions, station#144 N= 20/ 25

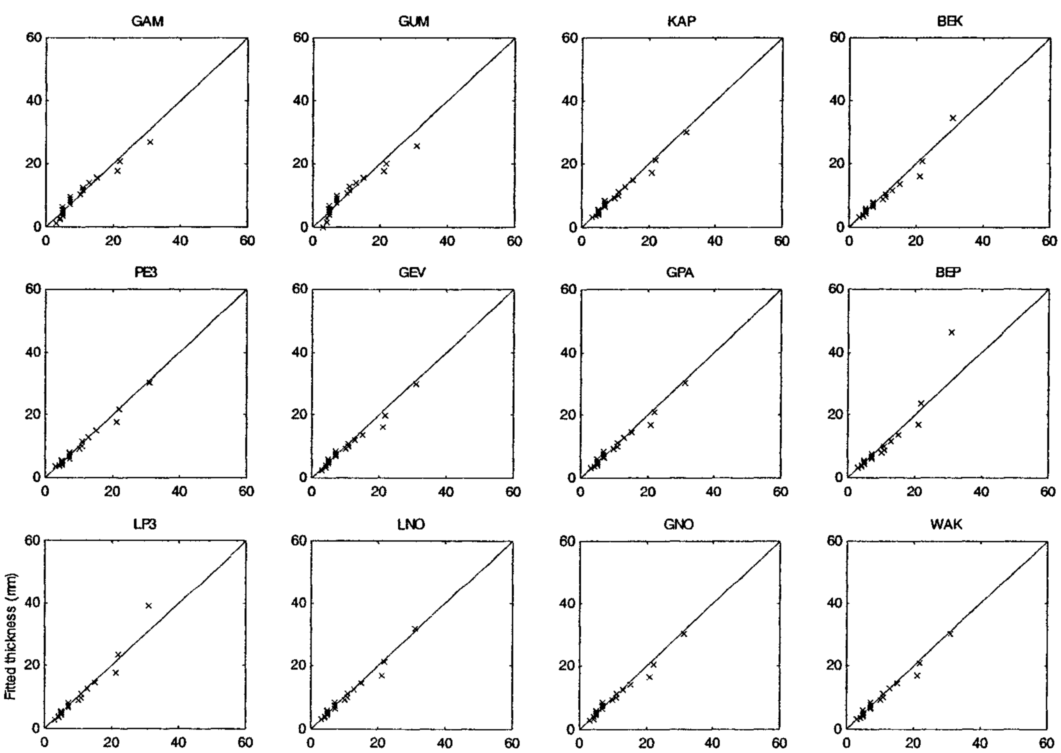

Q-Q plots for fitted distributions, station#146 N= 20/ 22

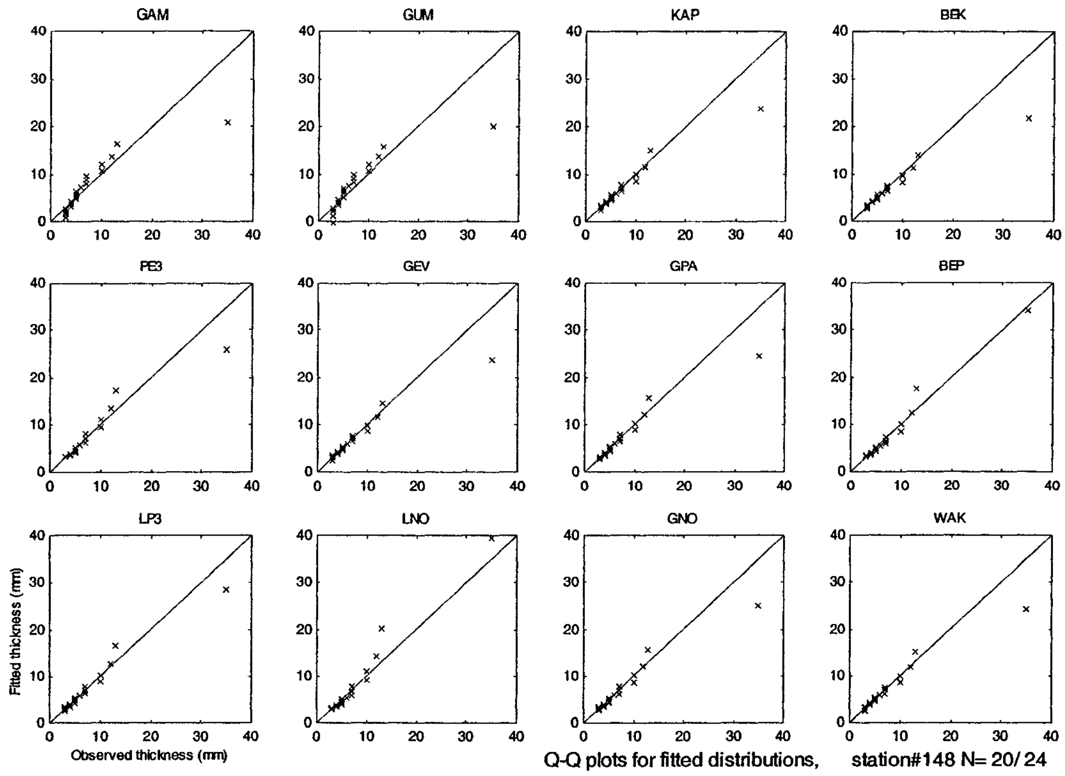

Q-Q plots for fitted distributions, station#148 N= 20/ 24

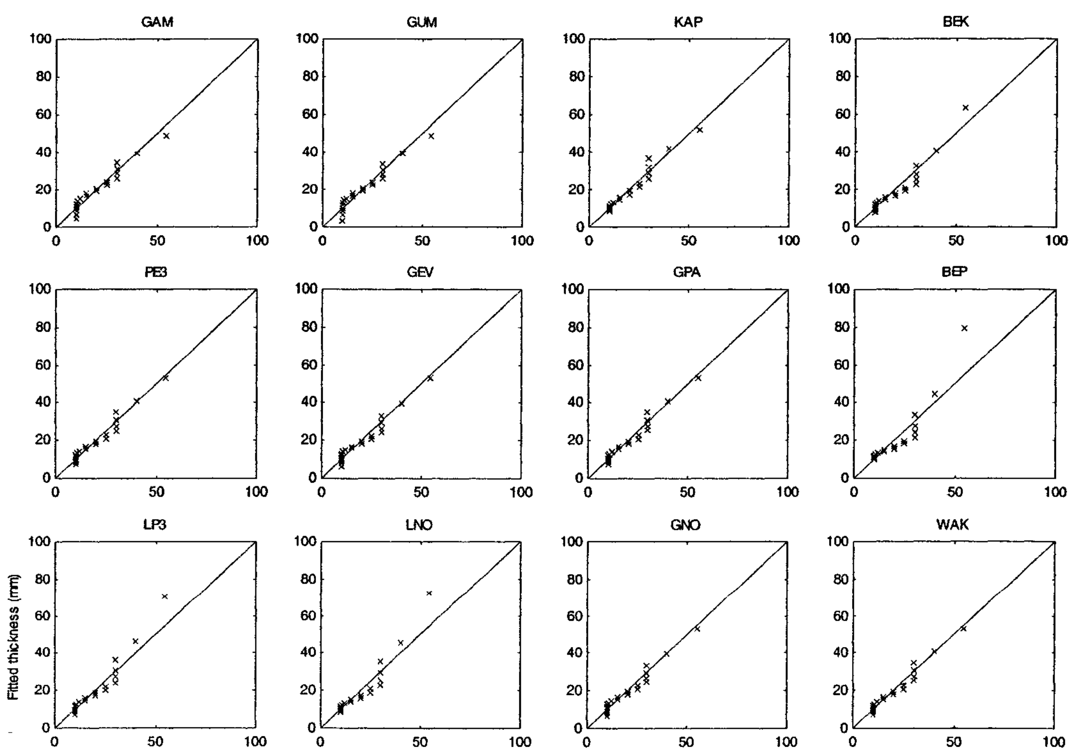

Q-Q plots for fitted distributions, station#156 N= 20/ 72

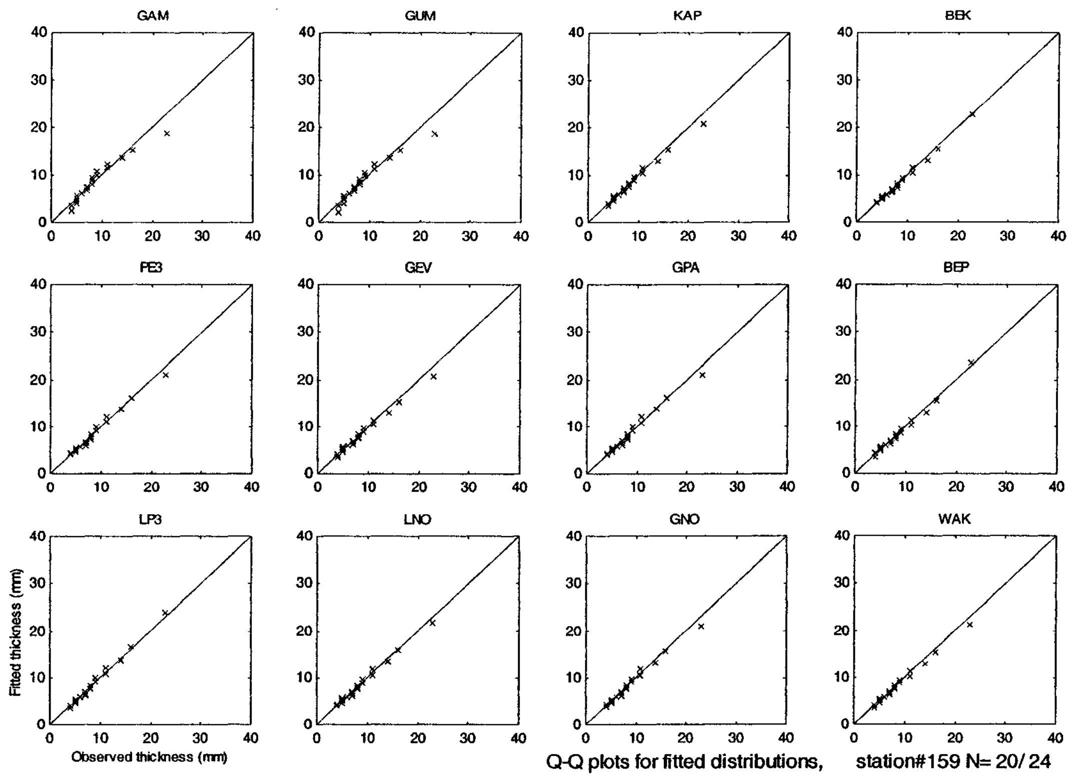

Q-Q plots for fitted distributions, station#159 N= 20/ 24

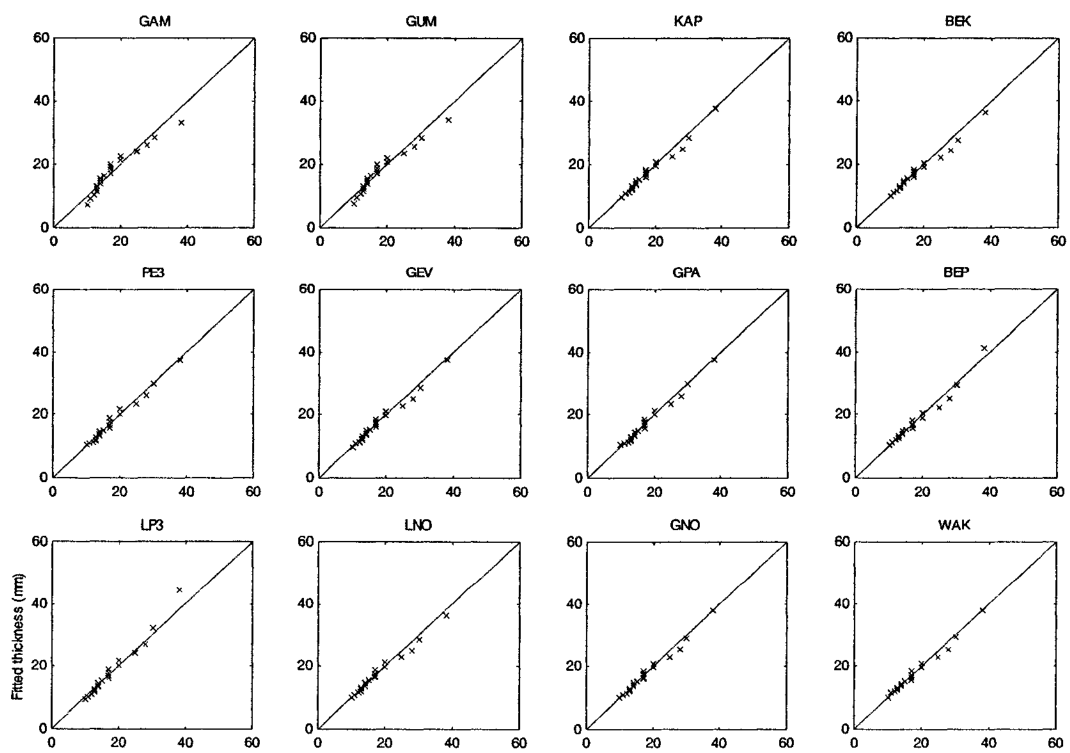

Q-Q plots for fitted distributions, station#161 N= 20/ 50

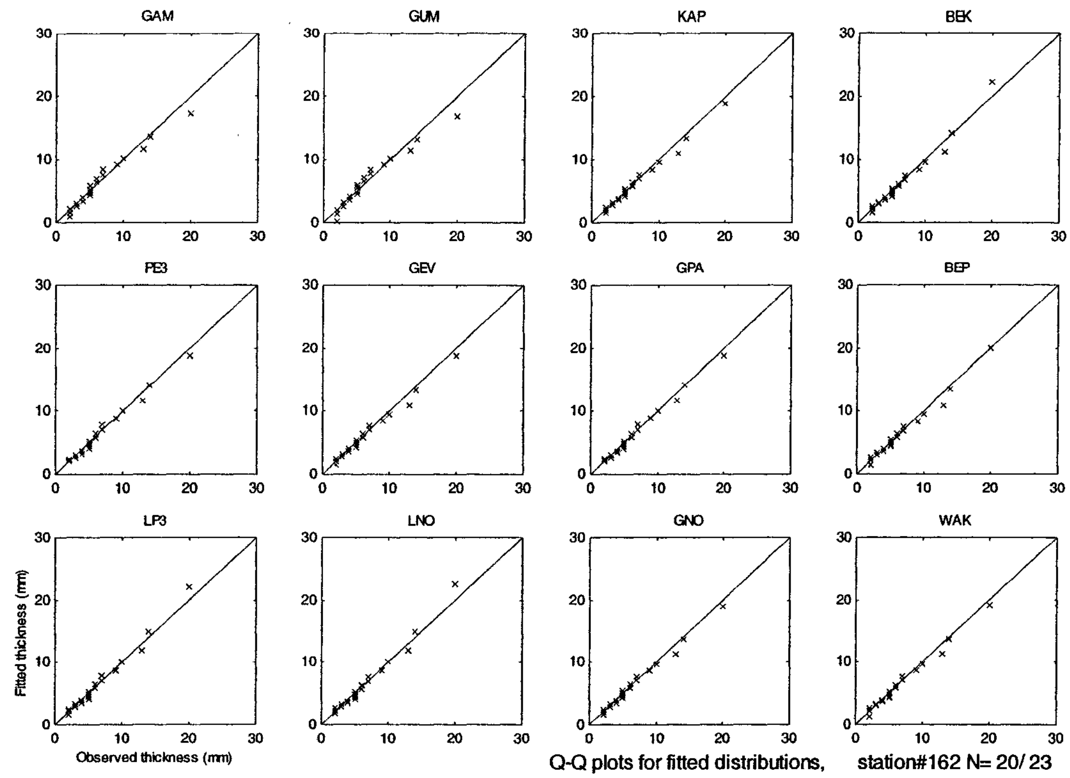

Q-Q plots for fitted distributions, station#162 N= 20/ 23

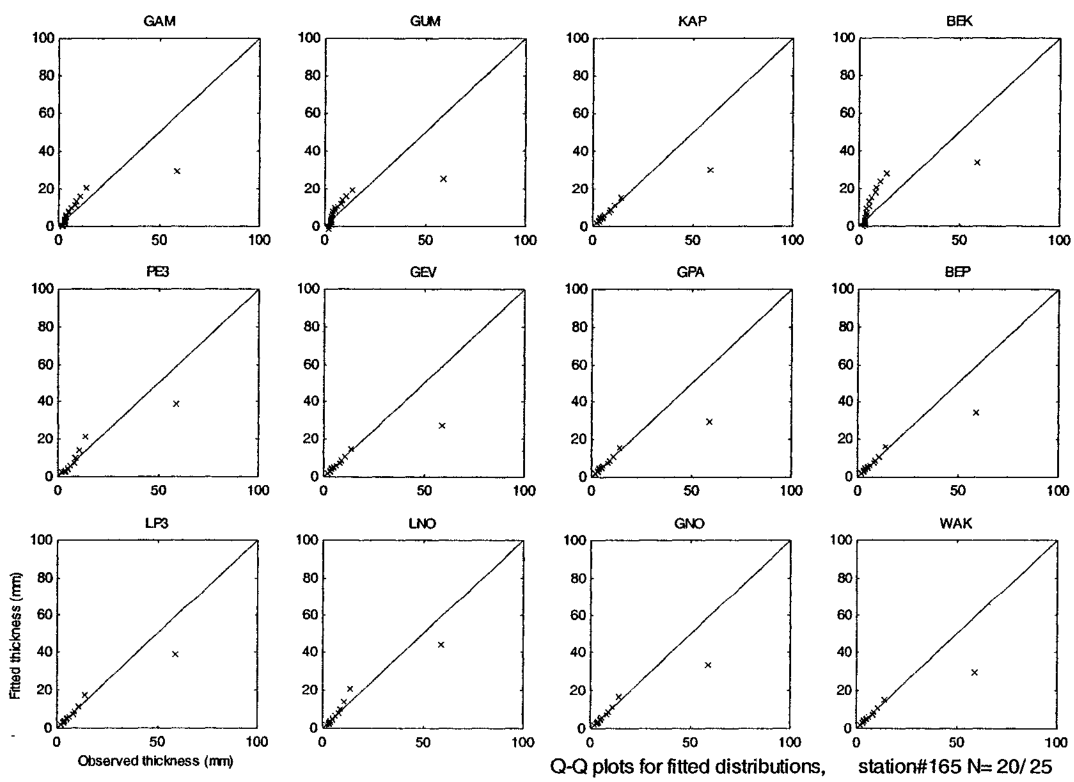

Q-Q plots for fitted distributions, station#165 N= 20/ 25

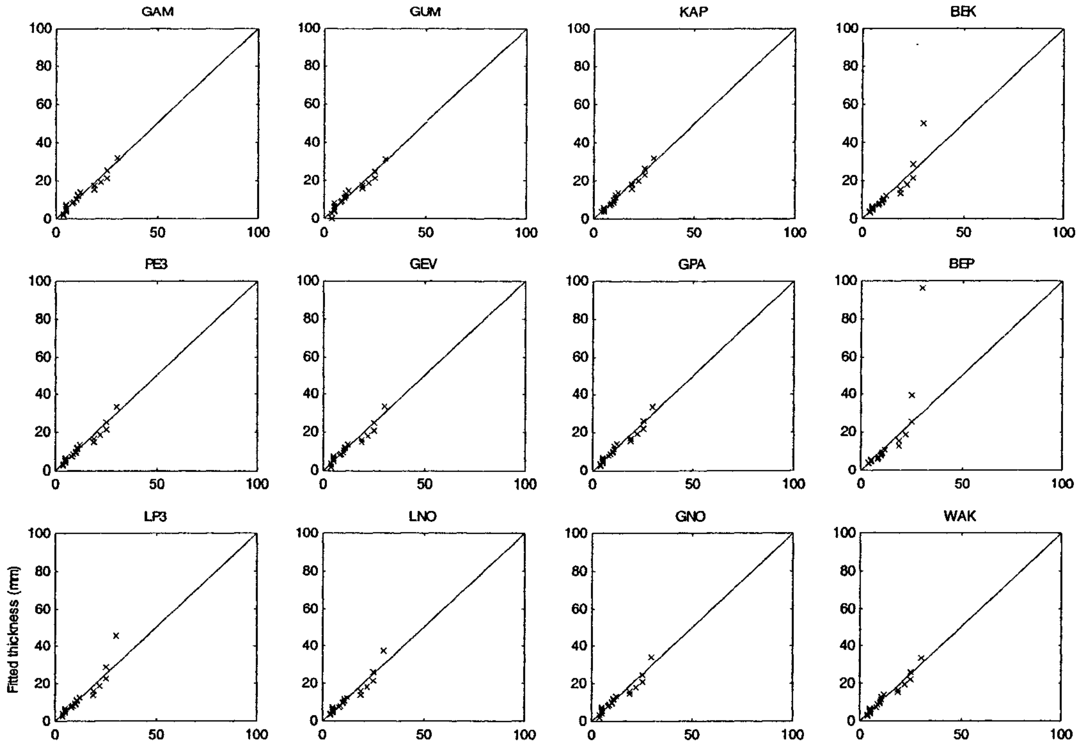

Q-Q plots for fitted distributions, station#169 N= 20/ 34

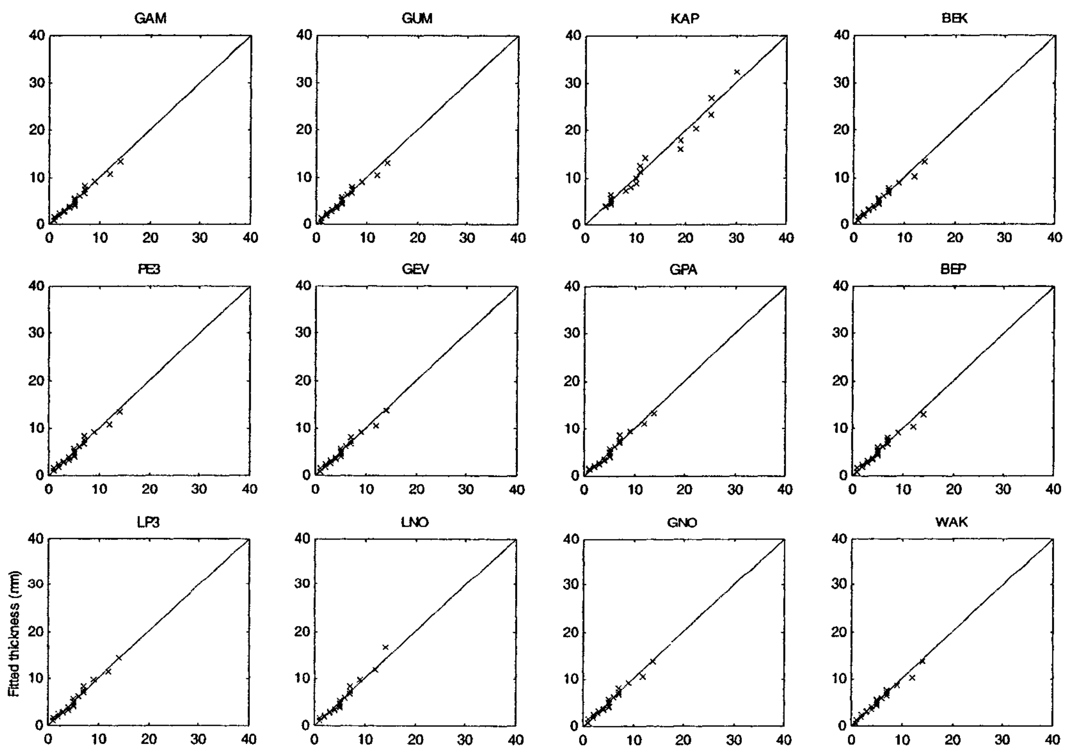

Q-Q plots for fitted distributions, station#172 N= 20/ 20

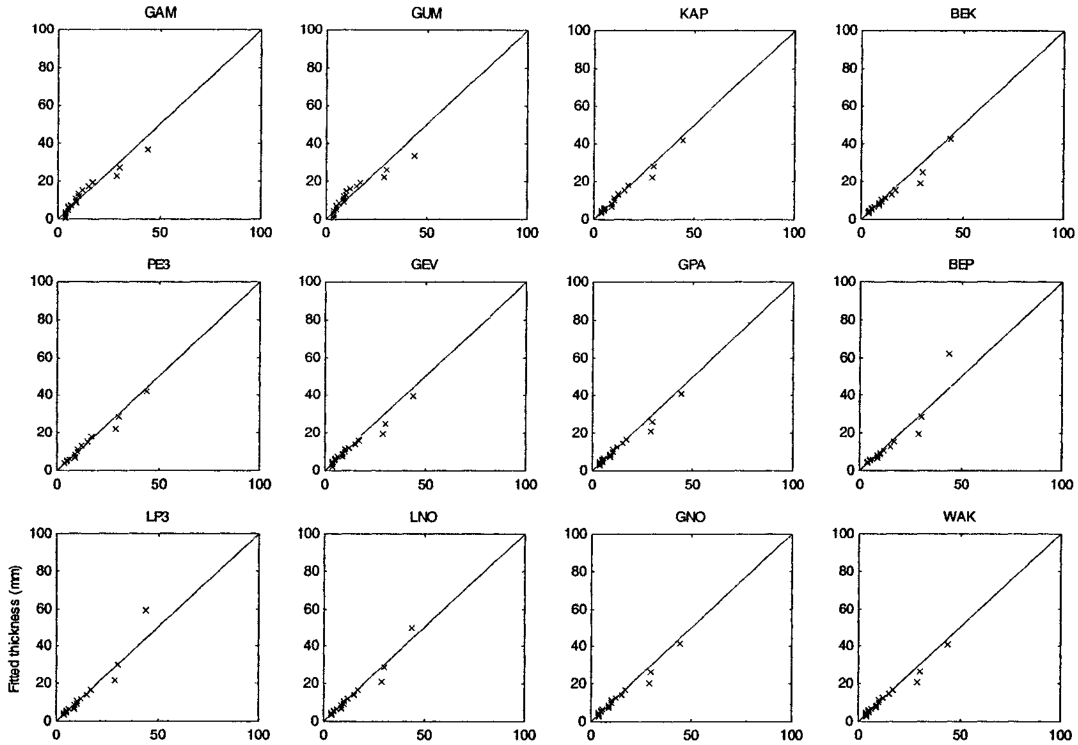

Q-Q plots for fitted distributions, station#173 N= 20/ 24

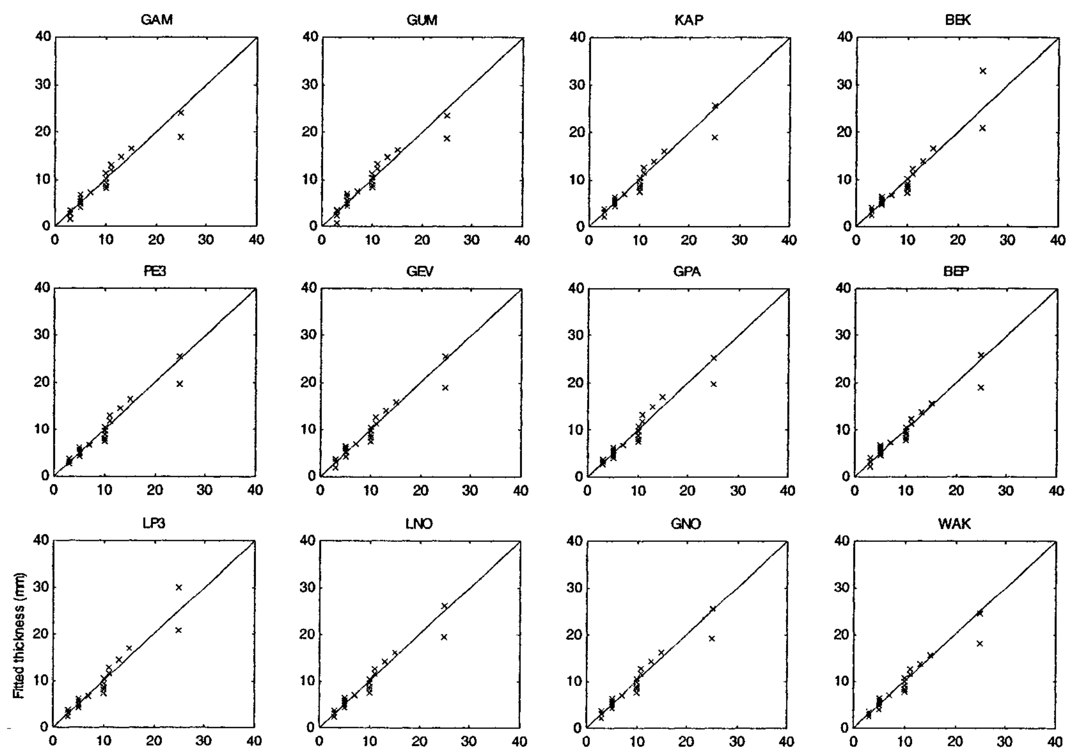

Q-Q plots for fitted distributions, station#174 N= 20/ 24

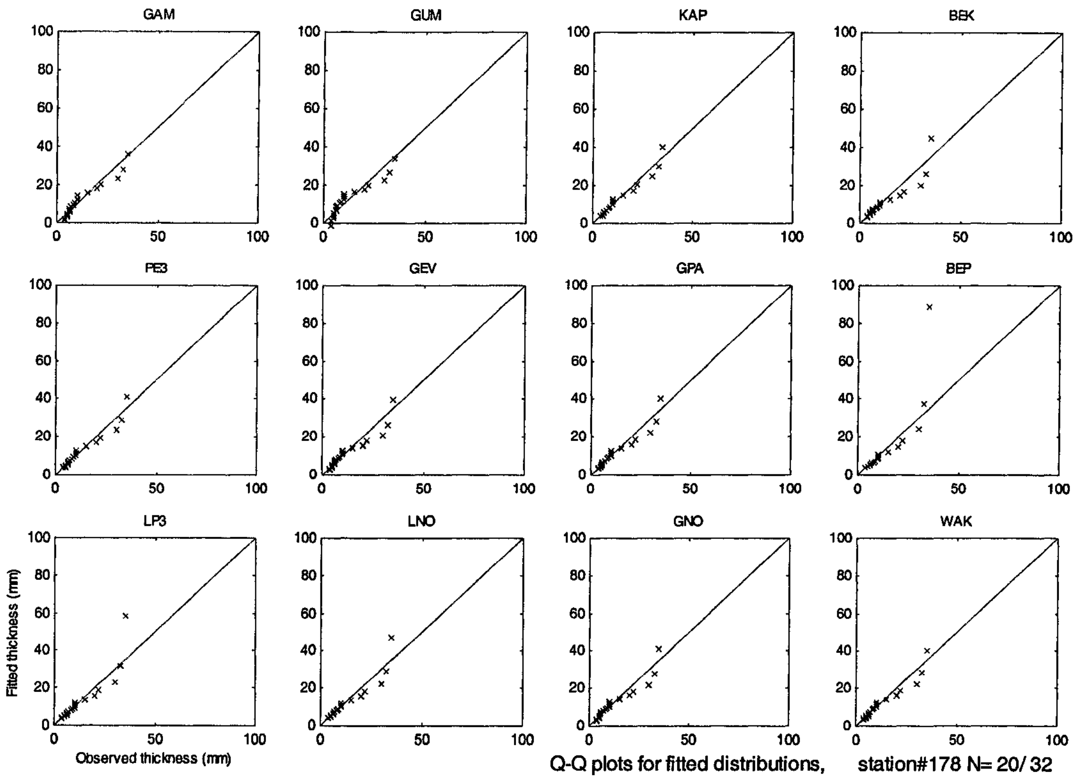
GAM
GUM
KAP
BEK
PE3
GEV
GPA
BEP
LP3
LNO
GNO
WAK
Fitted thickness (mm)
Observed thickness (mm)
Q-Q plots for fitted distributions, station#178 N= 20/ 32

Appendix F

Box plots for bootstrap data
for the selected stations

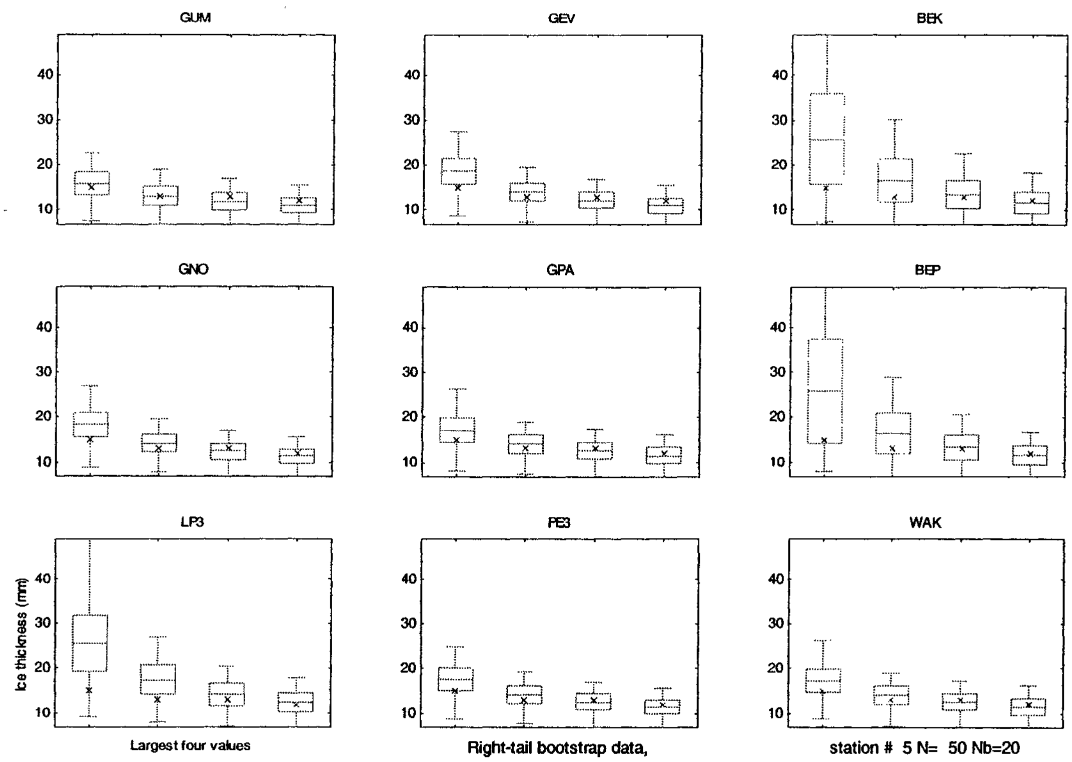

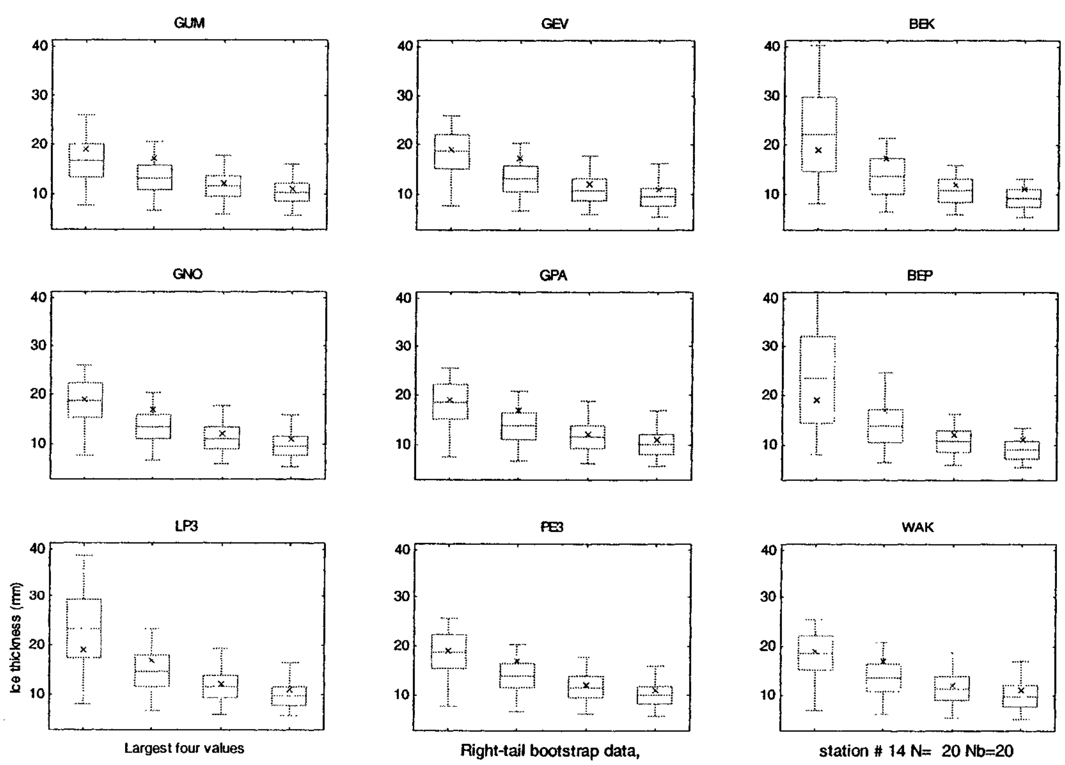

Box plots for bootstrap data for the selected stations

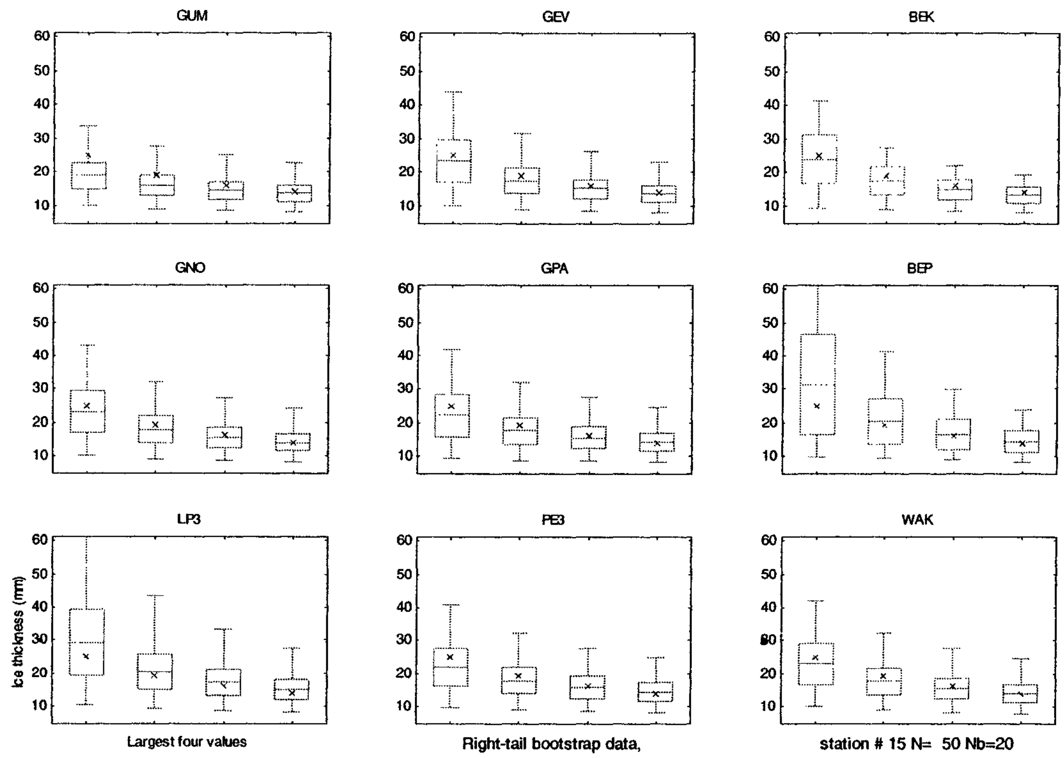

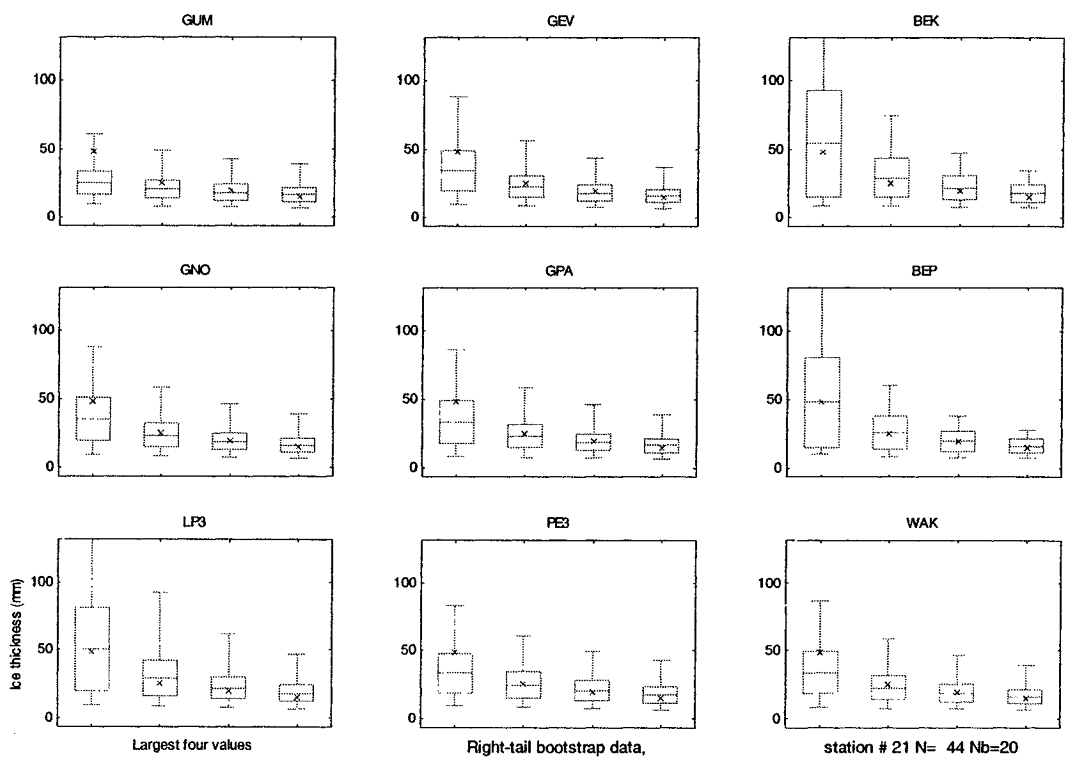

Box plots for bootstrap data for the selected stations

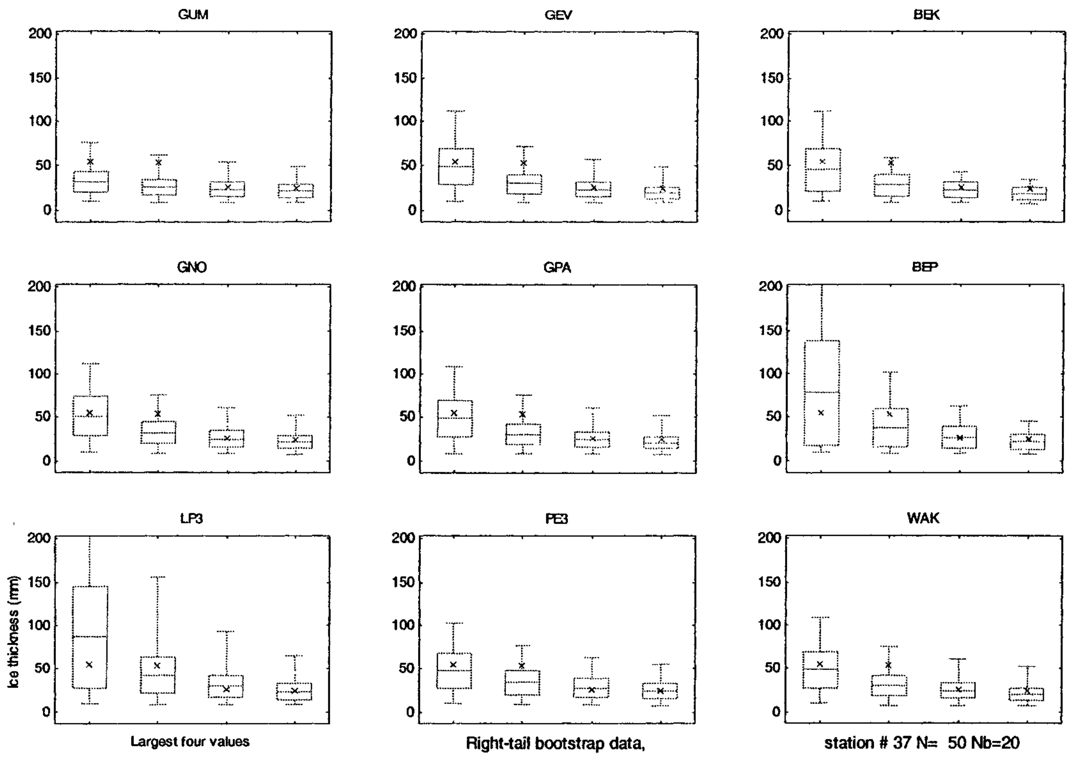

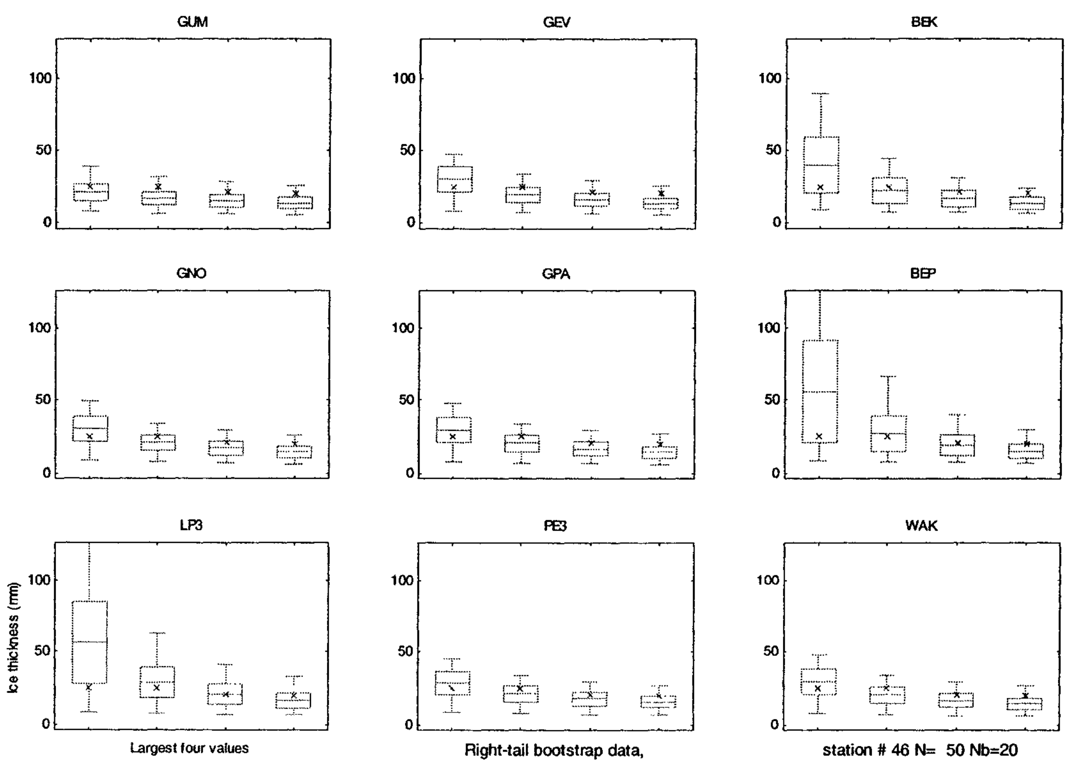

Box plots for bootstrap data for the selected stations

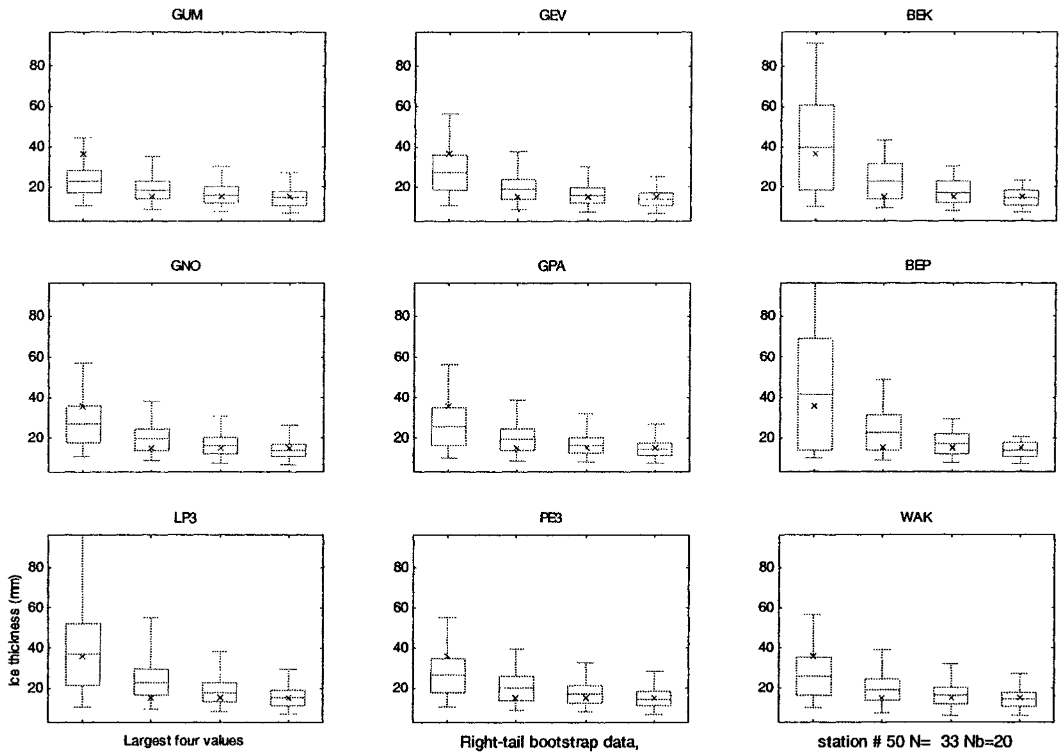

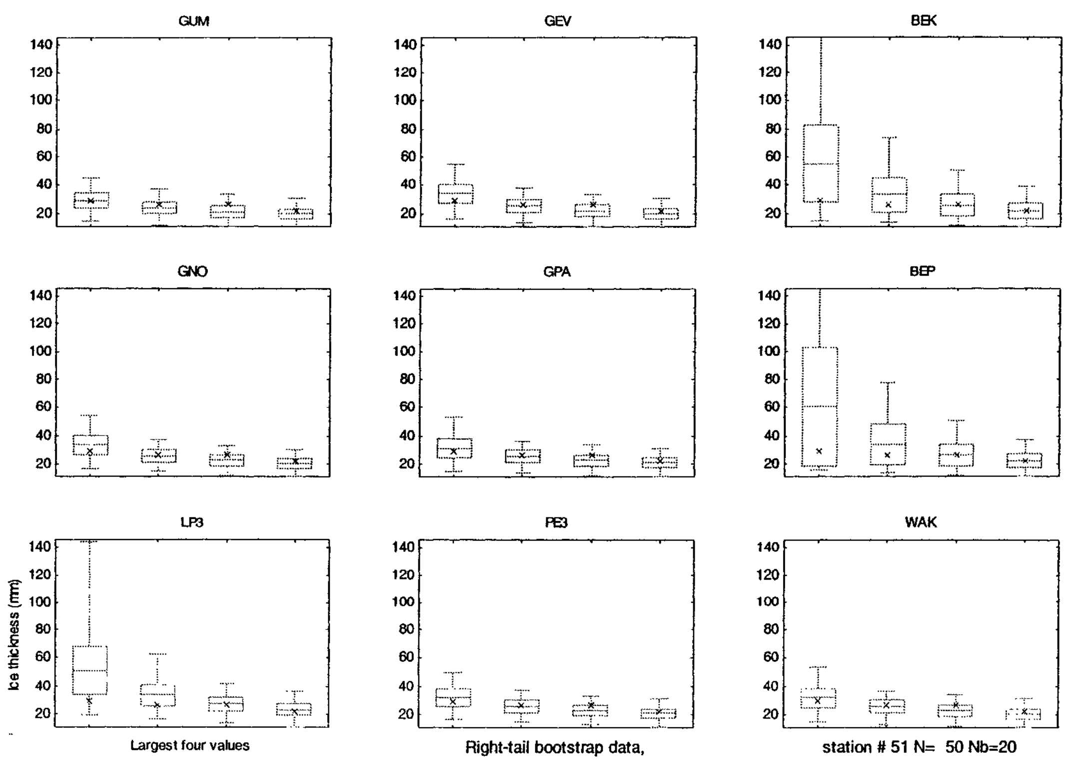

Box plots for bootstrap data for the selected stations

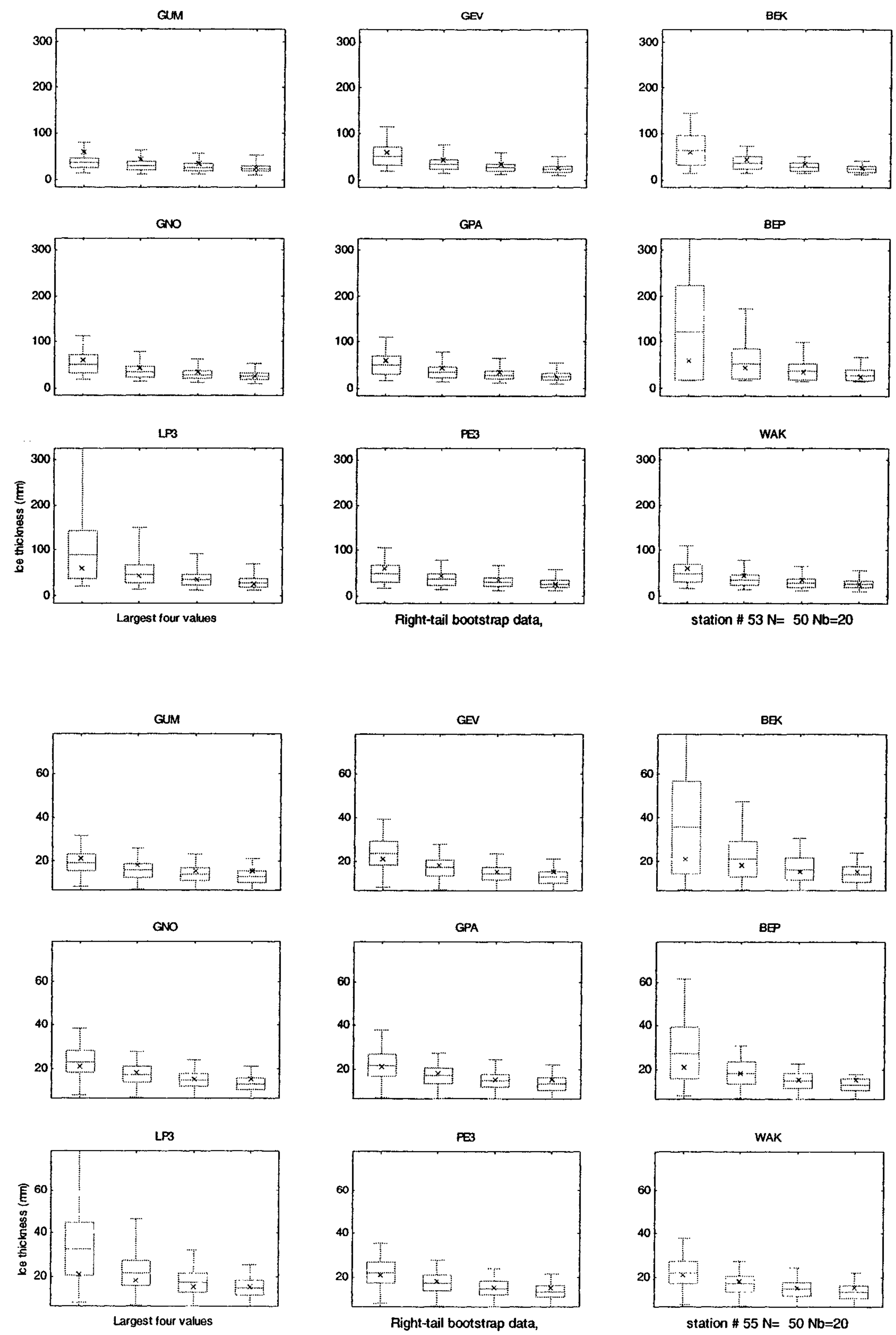

Box plots for bootstrap data for the selected stations

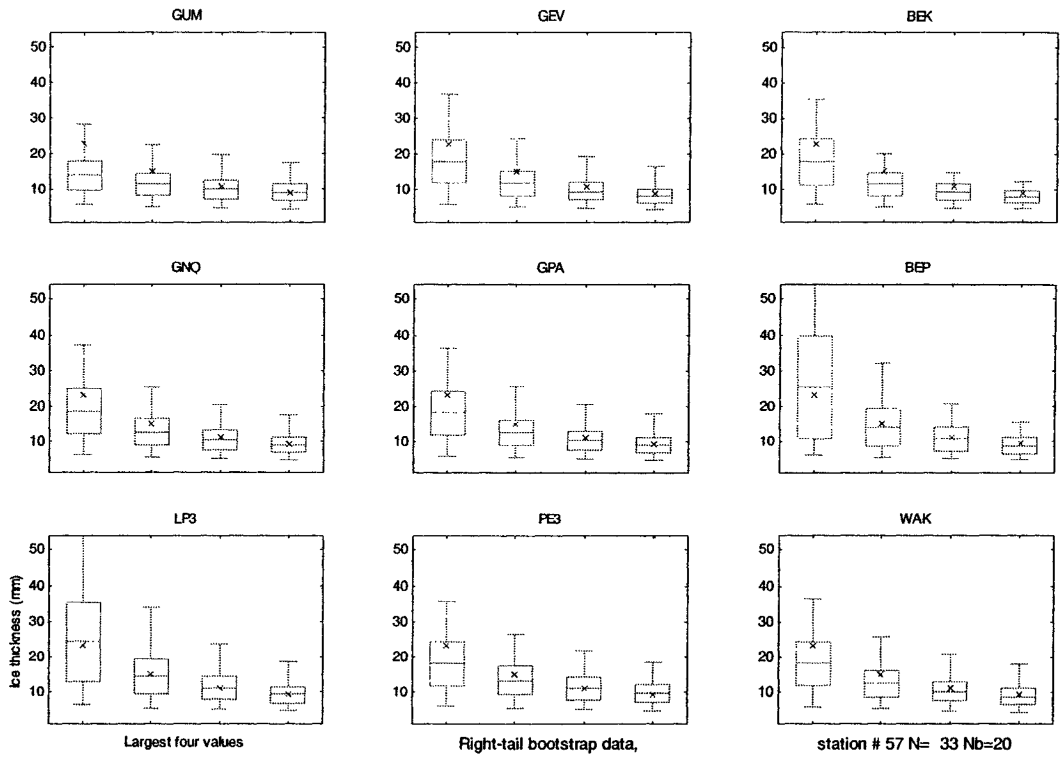

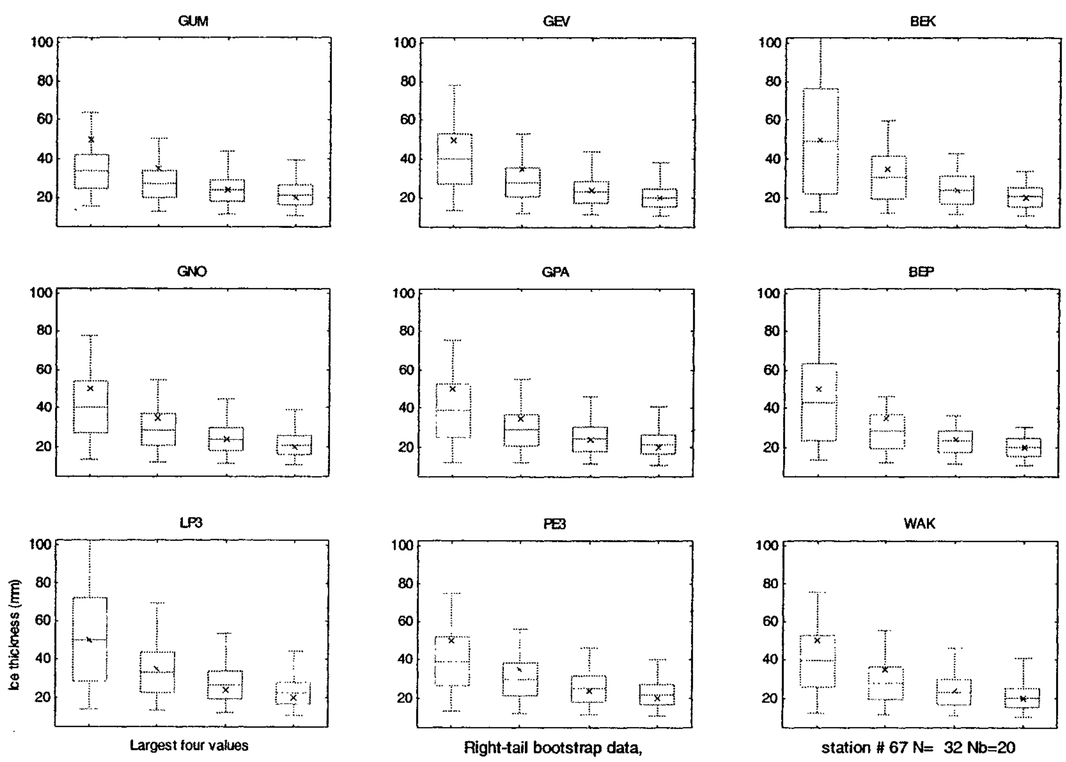

Box plots for bootstrap data for the selected stations

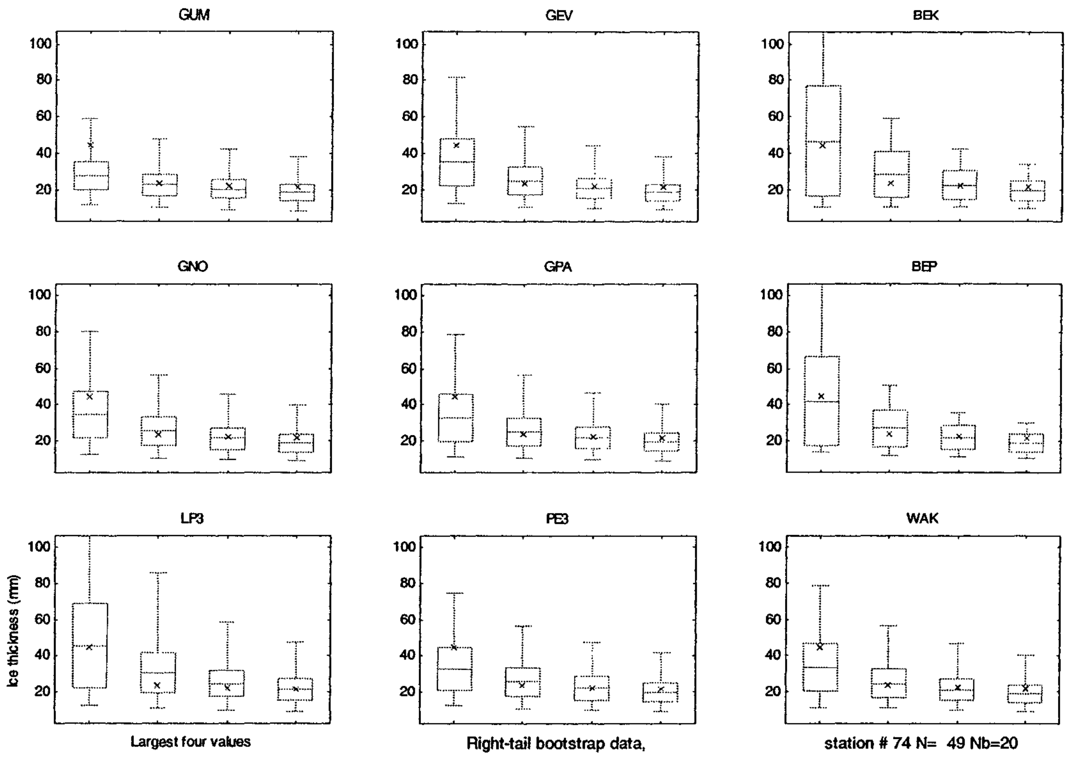

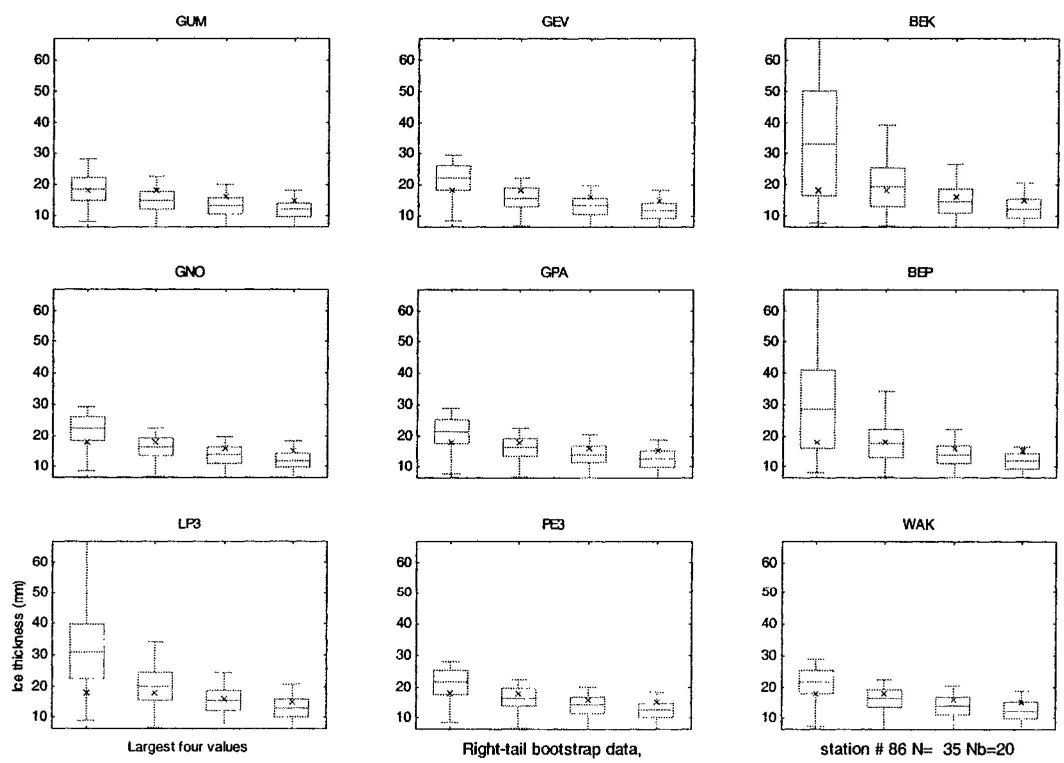

Box plots for bootstrap data for the selected stations

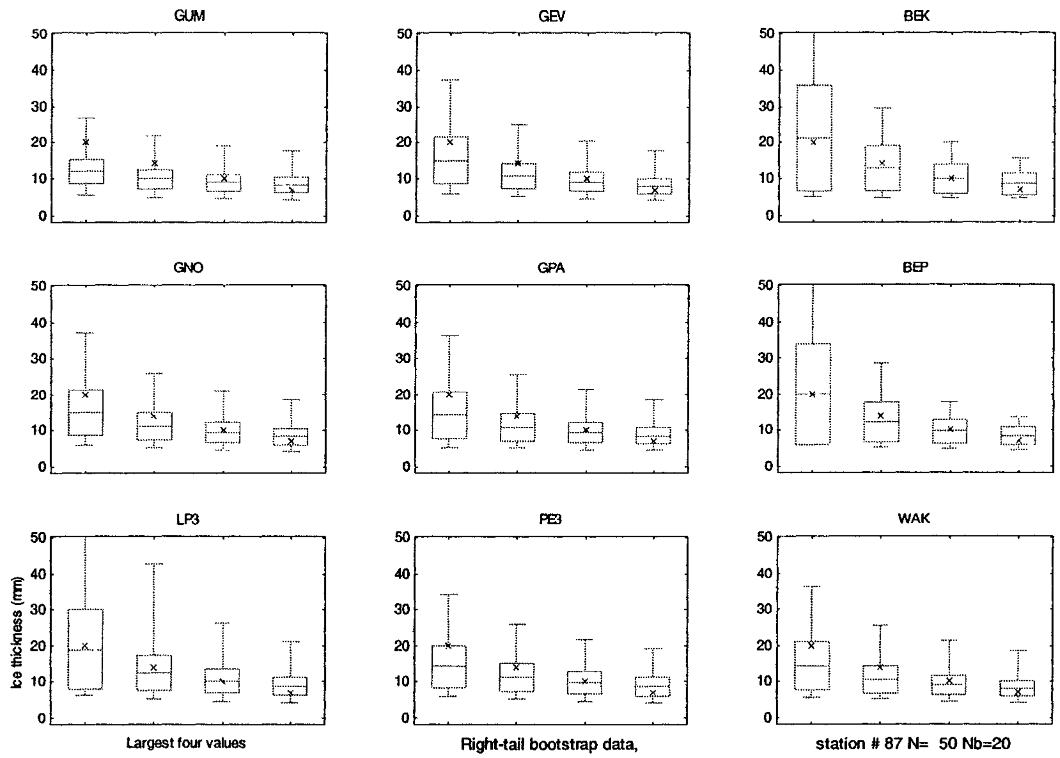

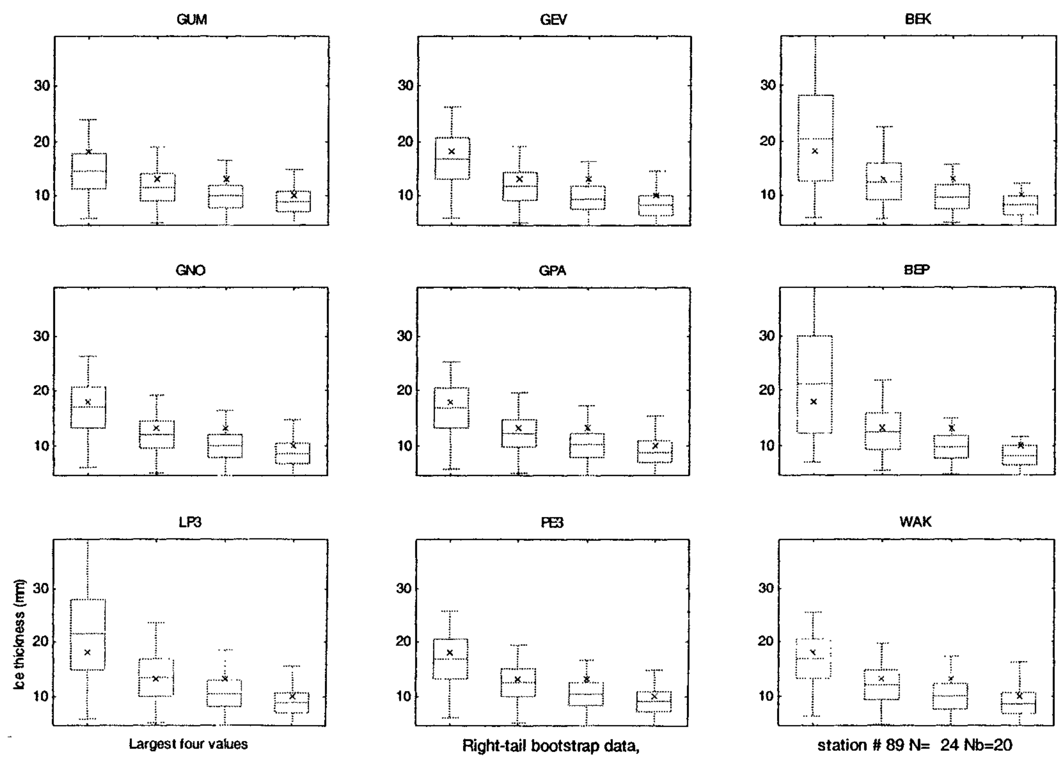

Box plots for bootstrap data for the selected stations

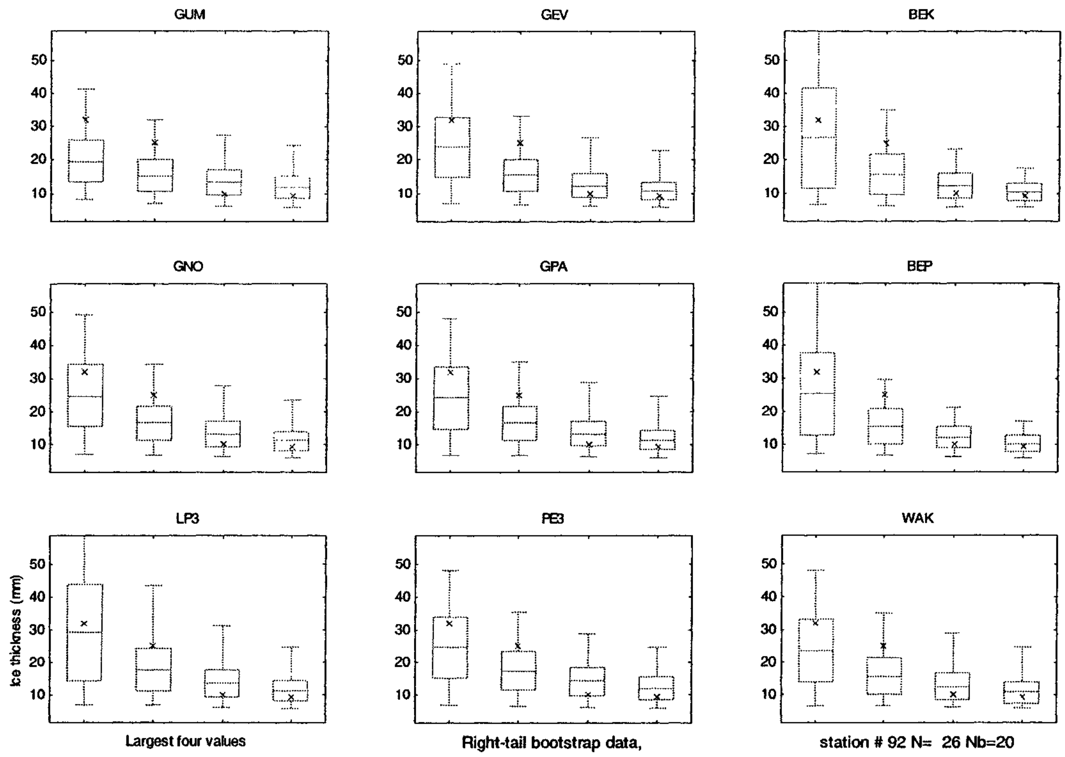

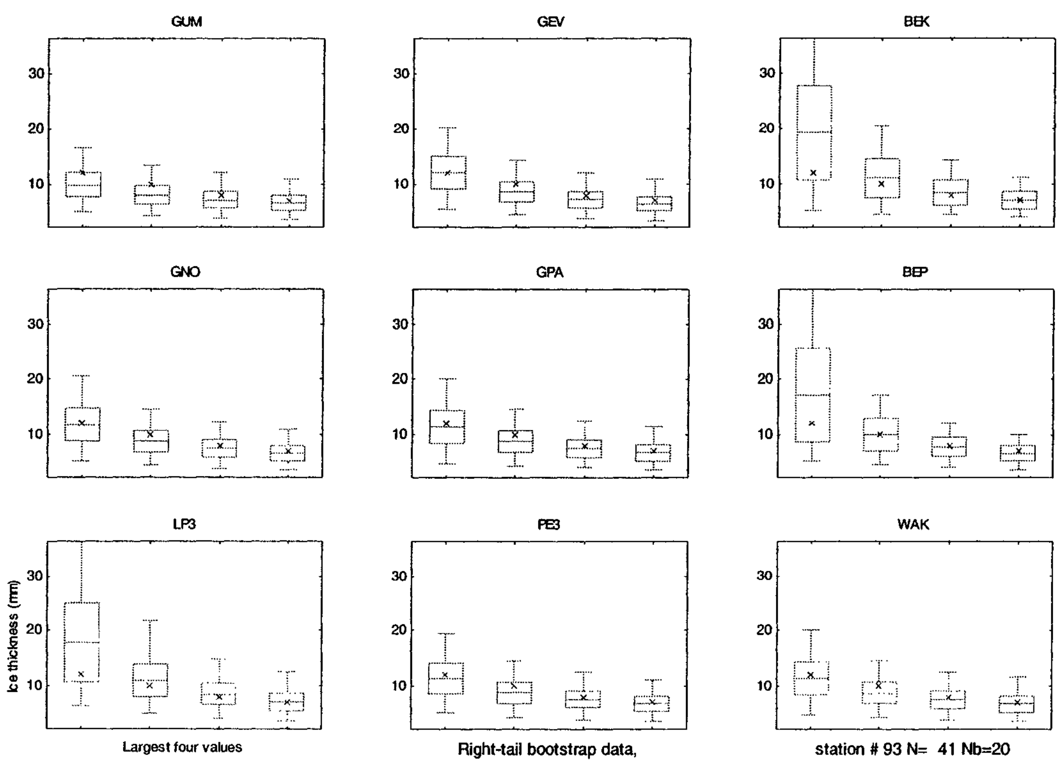

Box plots for bootstrap data for the selected stations

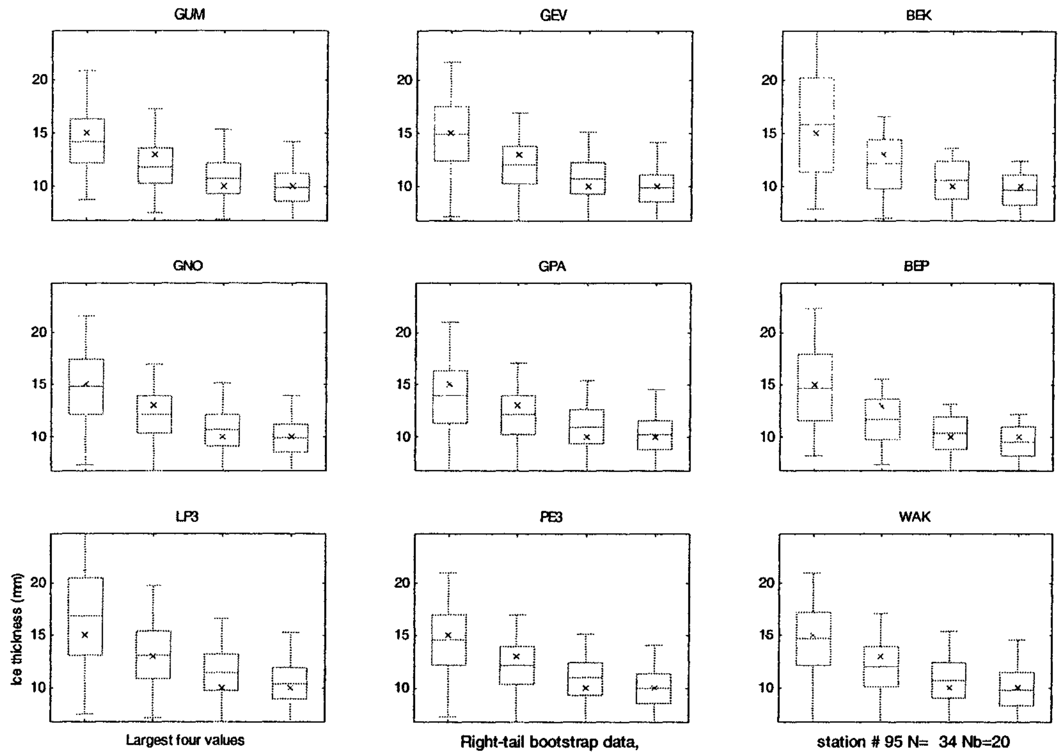

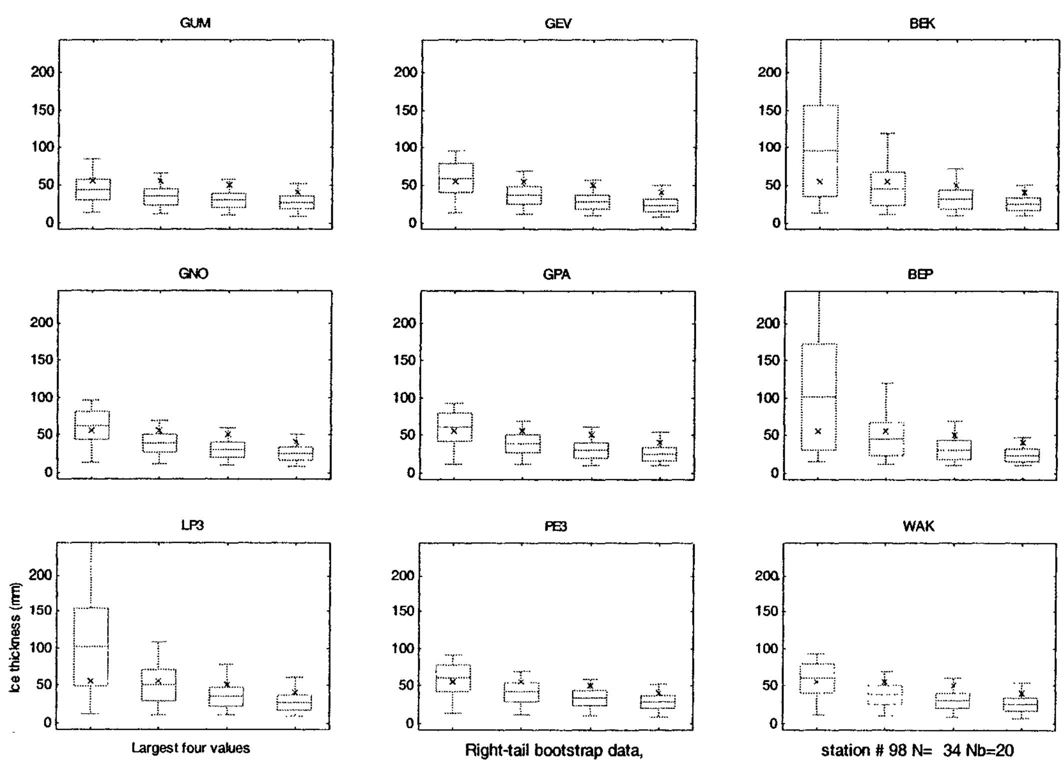

Box plots for bootstrap data for the selected stations

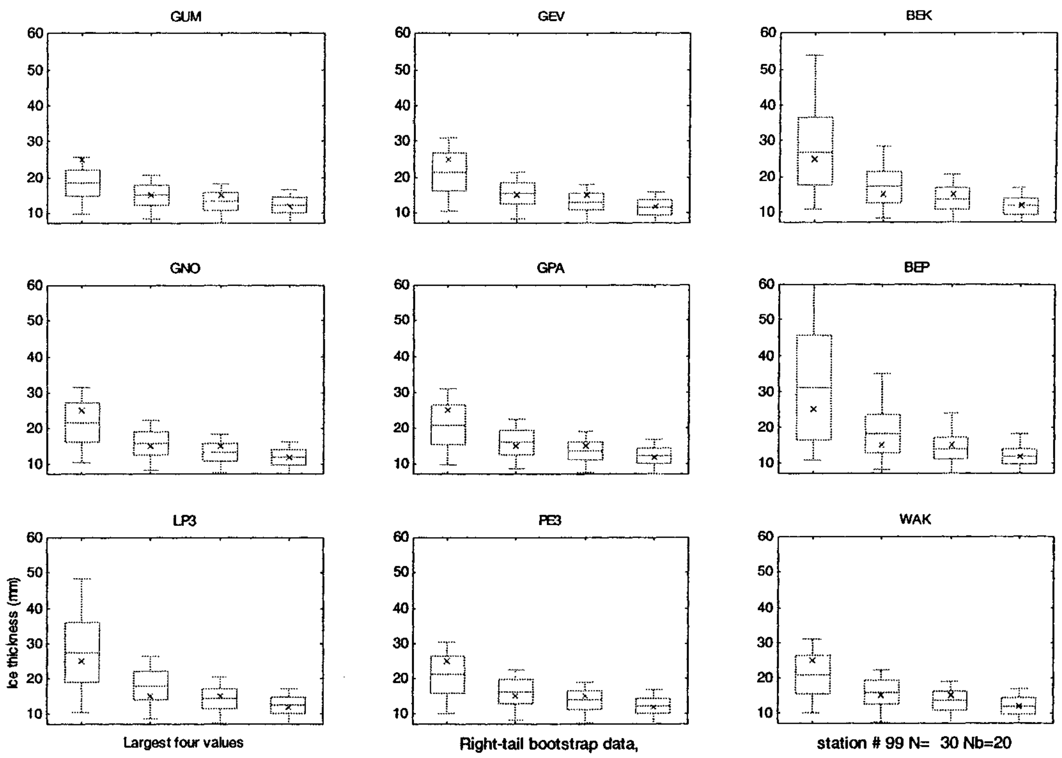

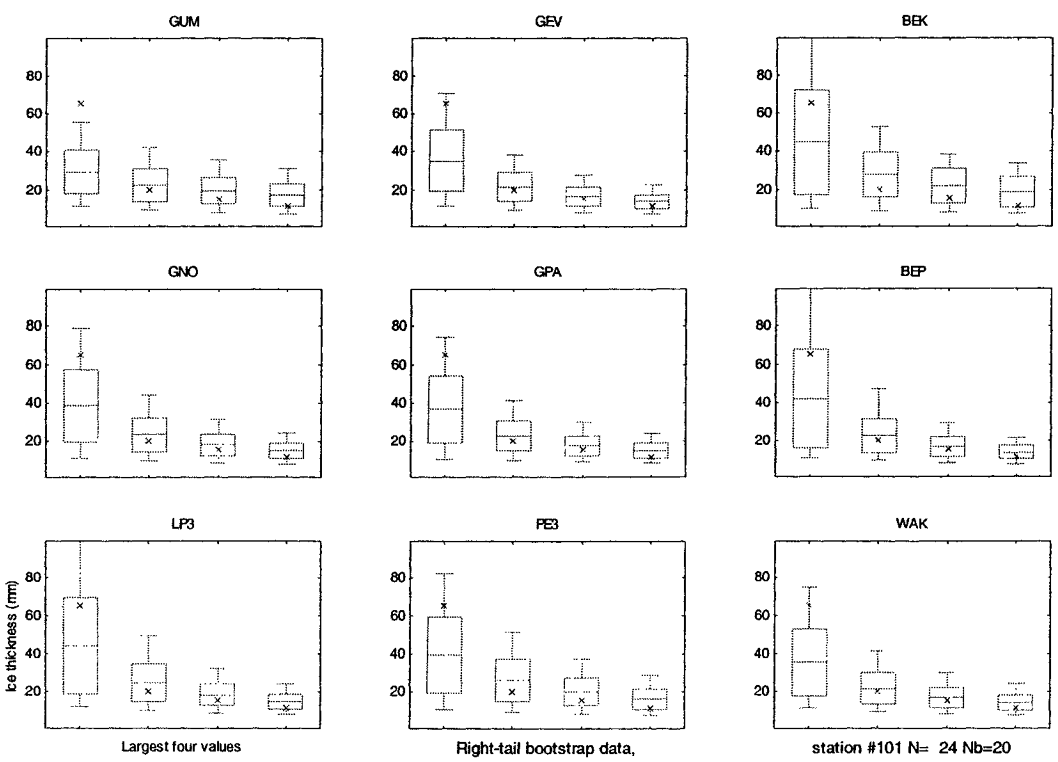

Box plots for bootstrap data for the selected stations

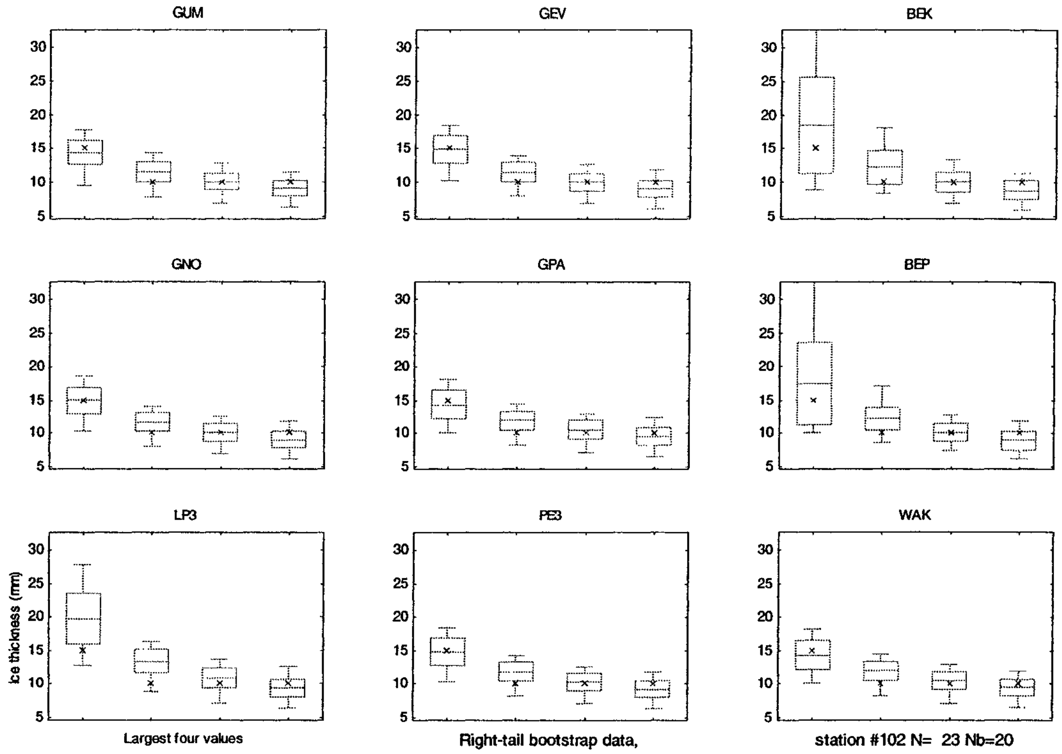

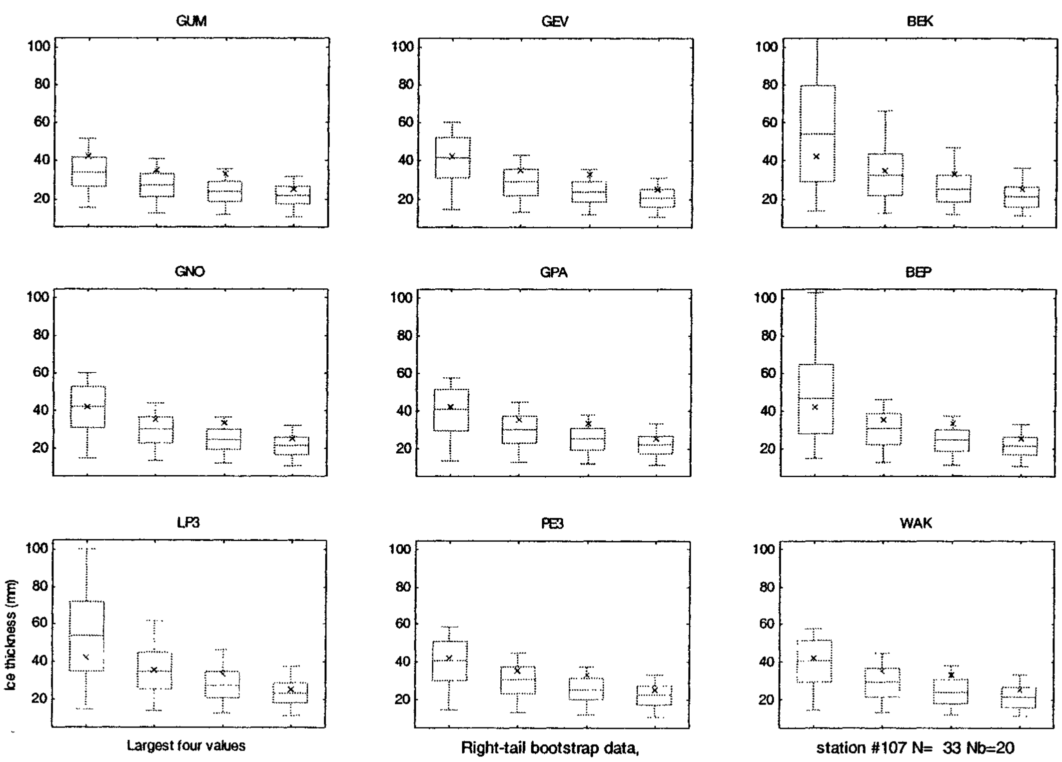

Box plots for bootstrap data for the selected stations

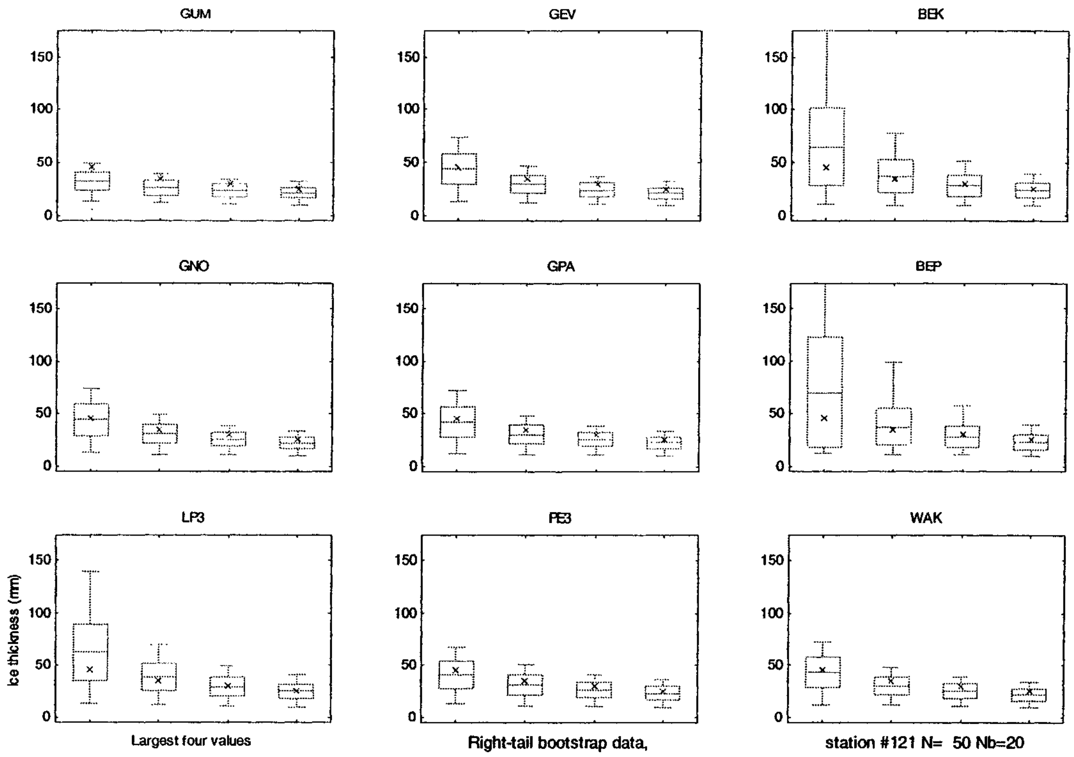

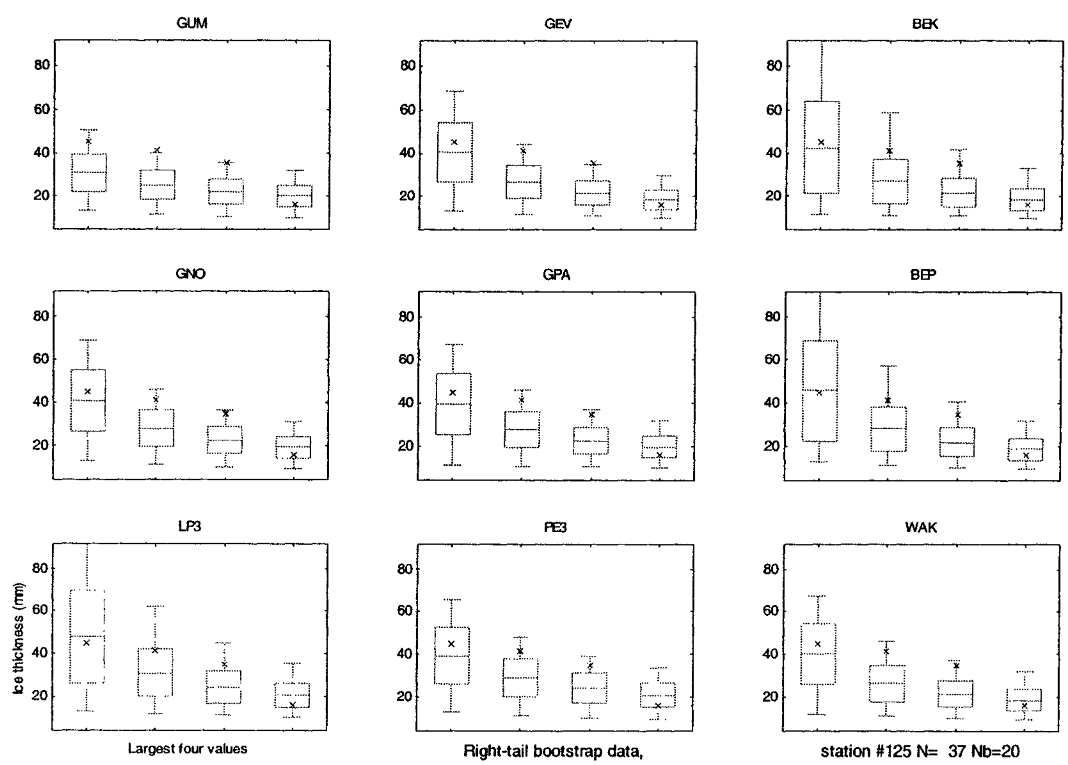

Box plots for bootstrap data for the selected stations

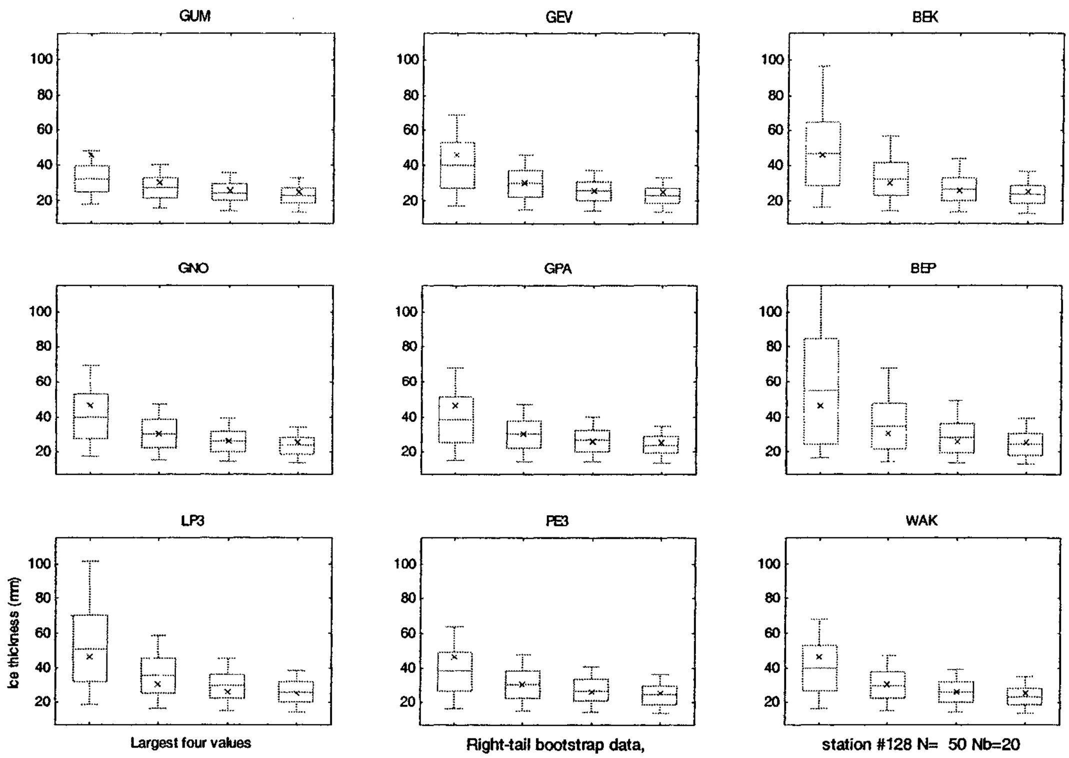

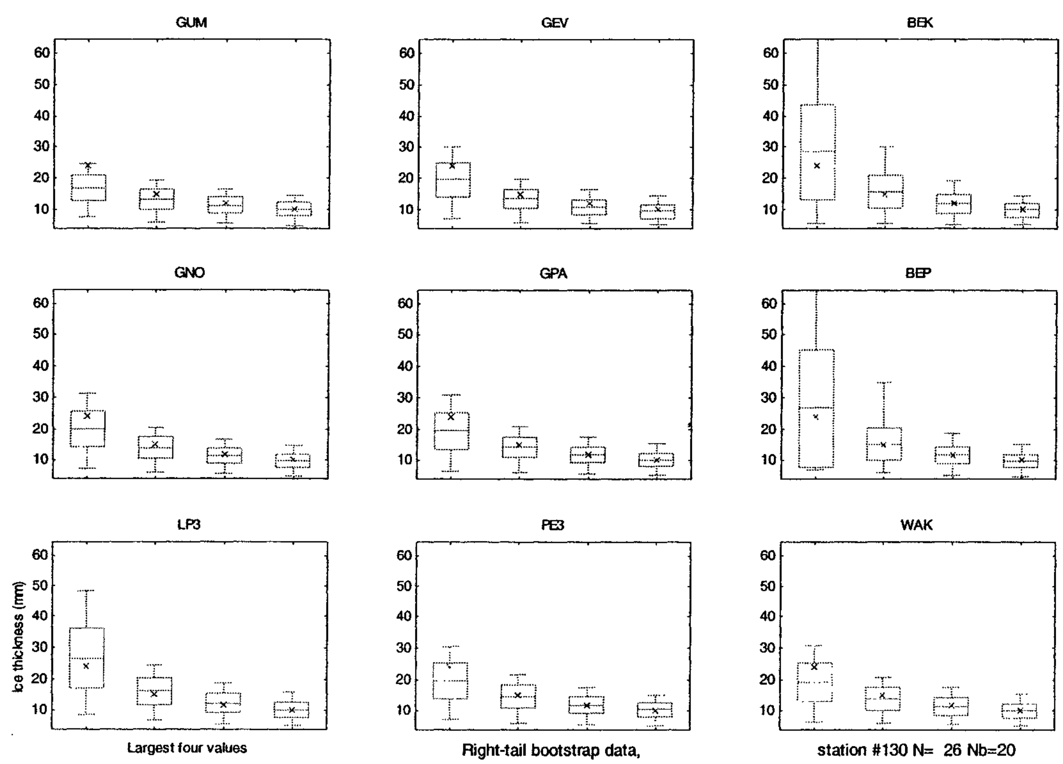

Box plots for bootstrap data for the selected stations

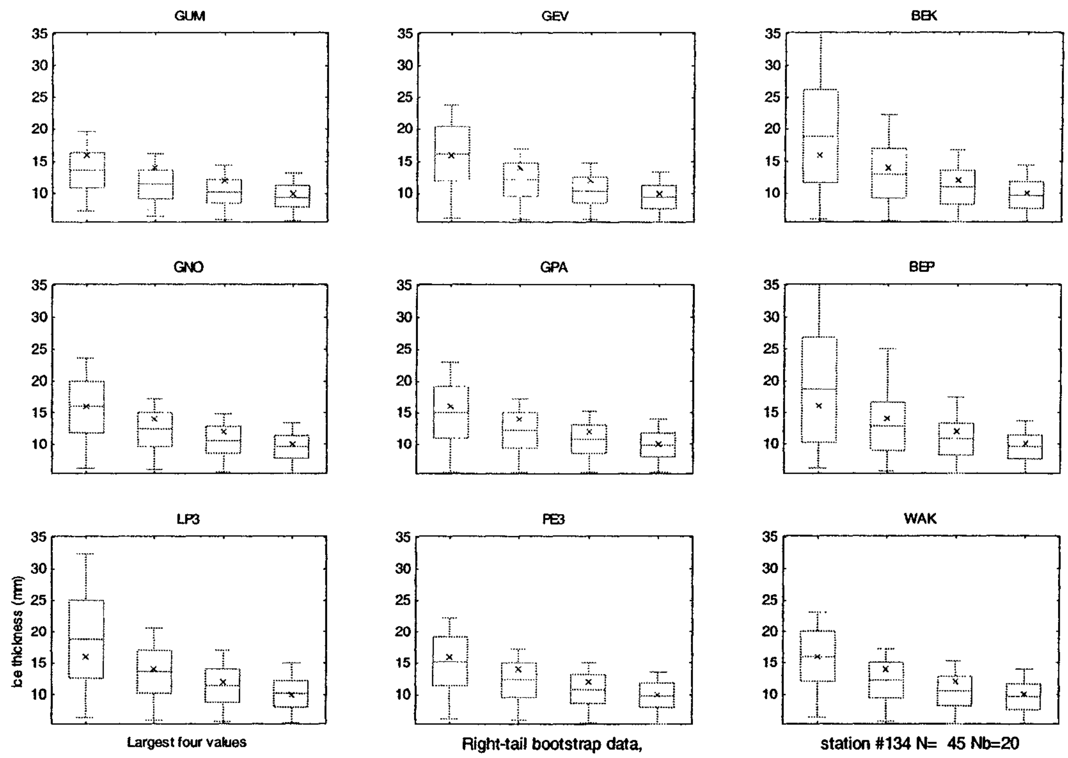

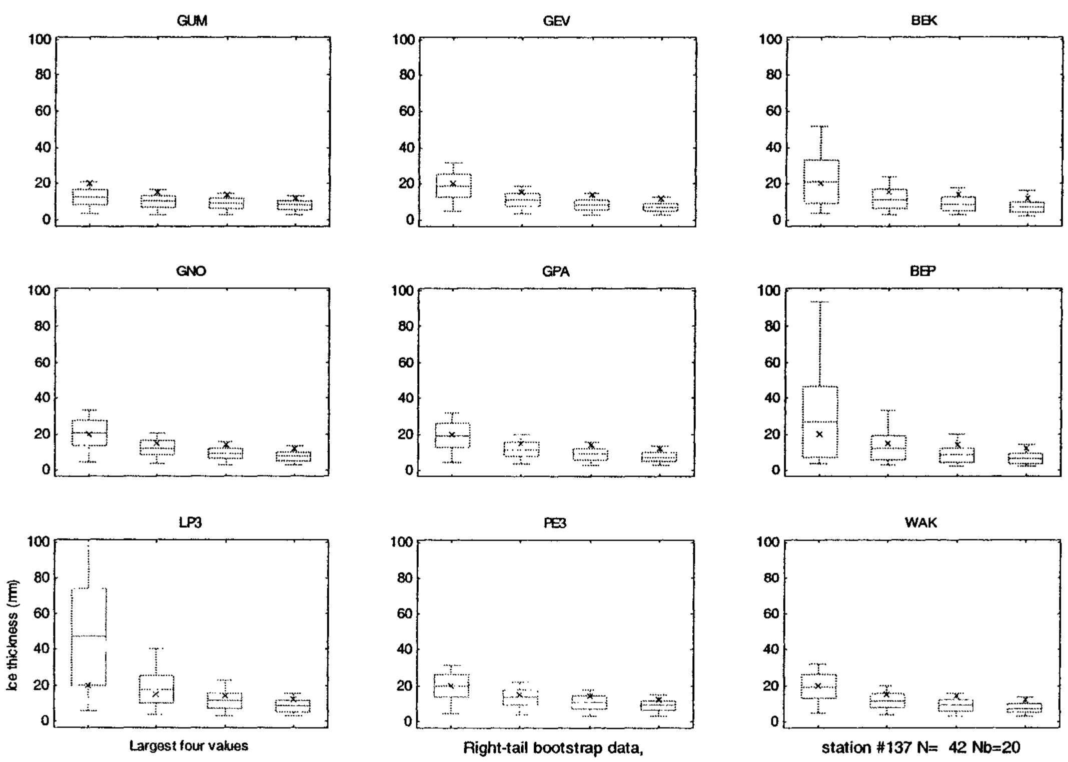

Box plots for bootstrap data for the selected stations

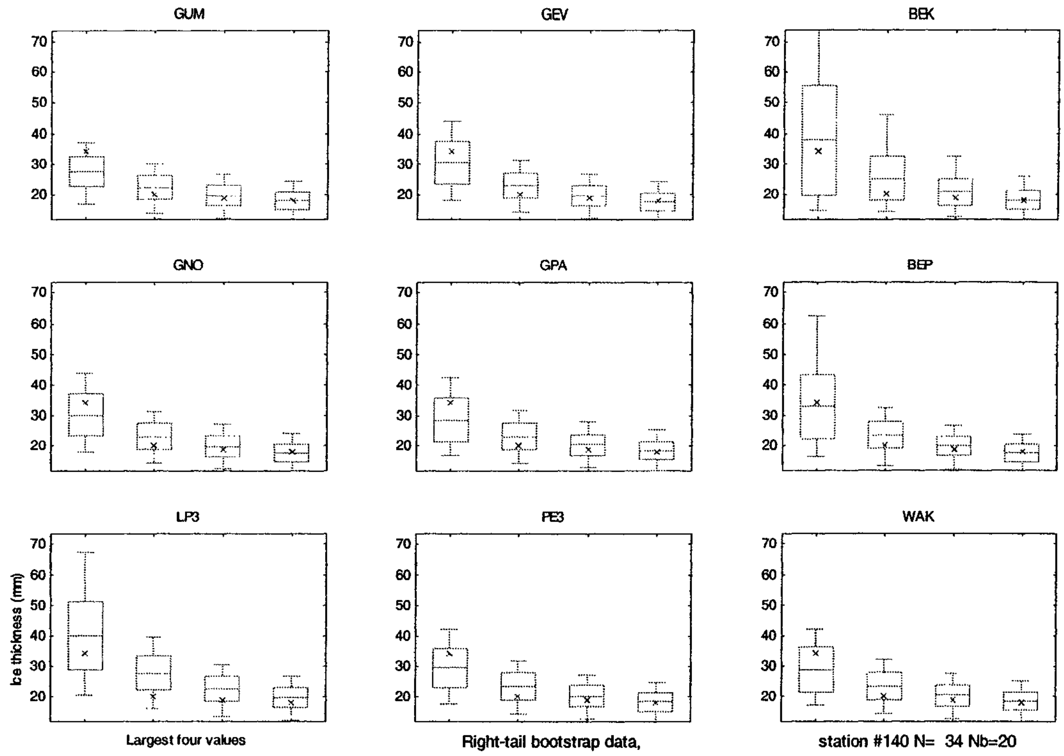

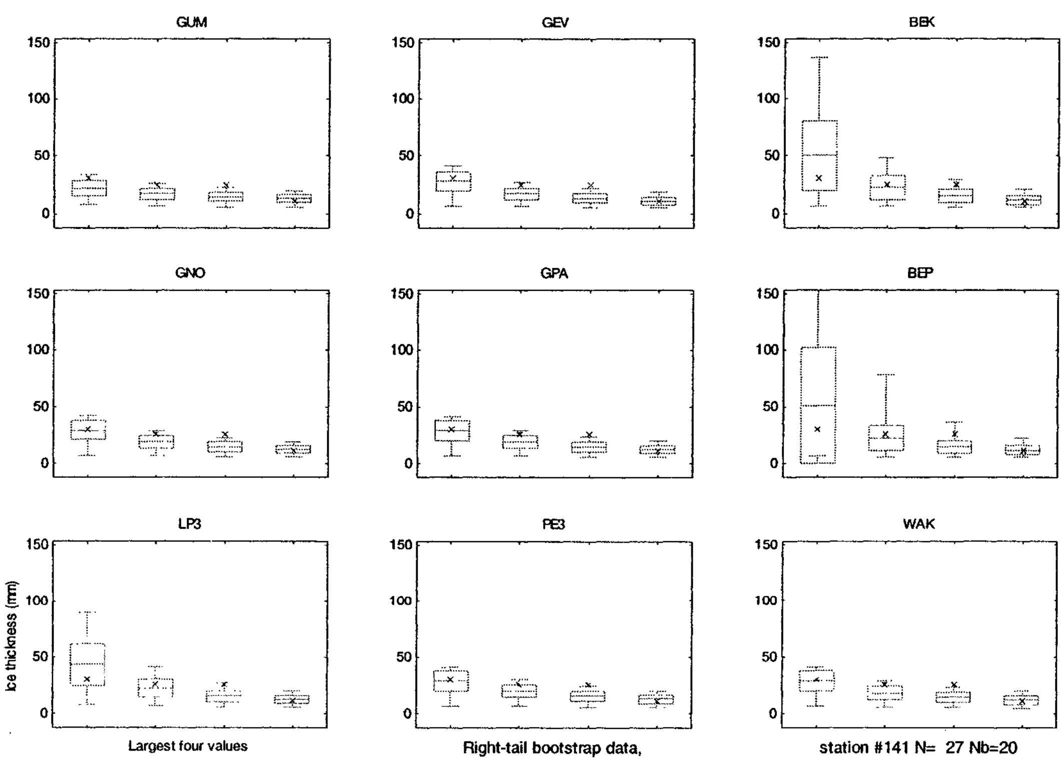

Box plots for bootstrap data for the selected stations

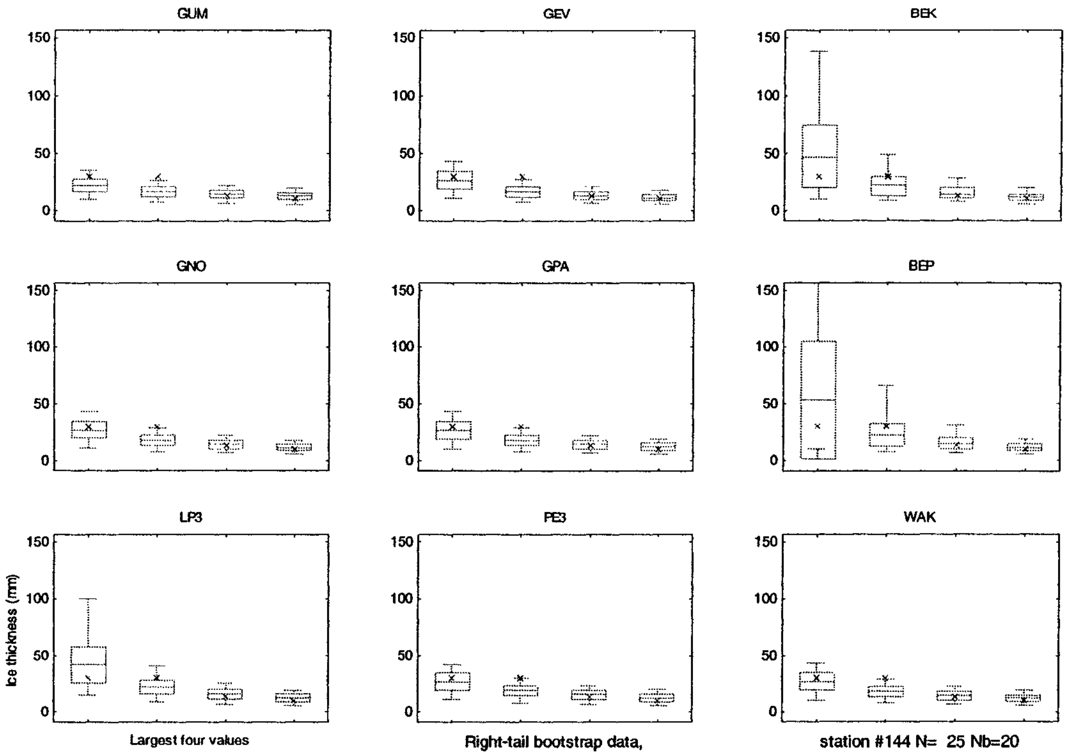

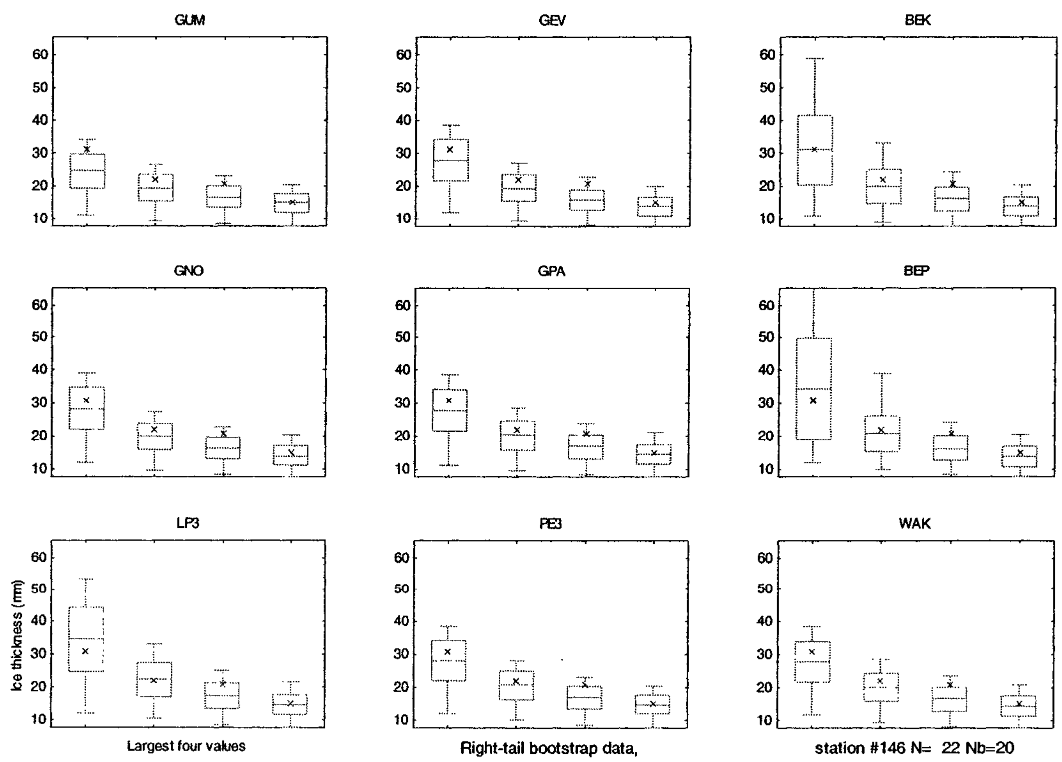

Box plots for bootstrap data for the selected stations

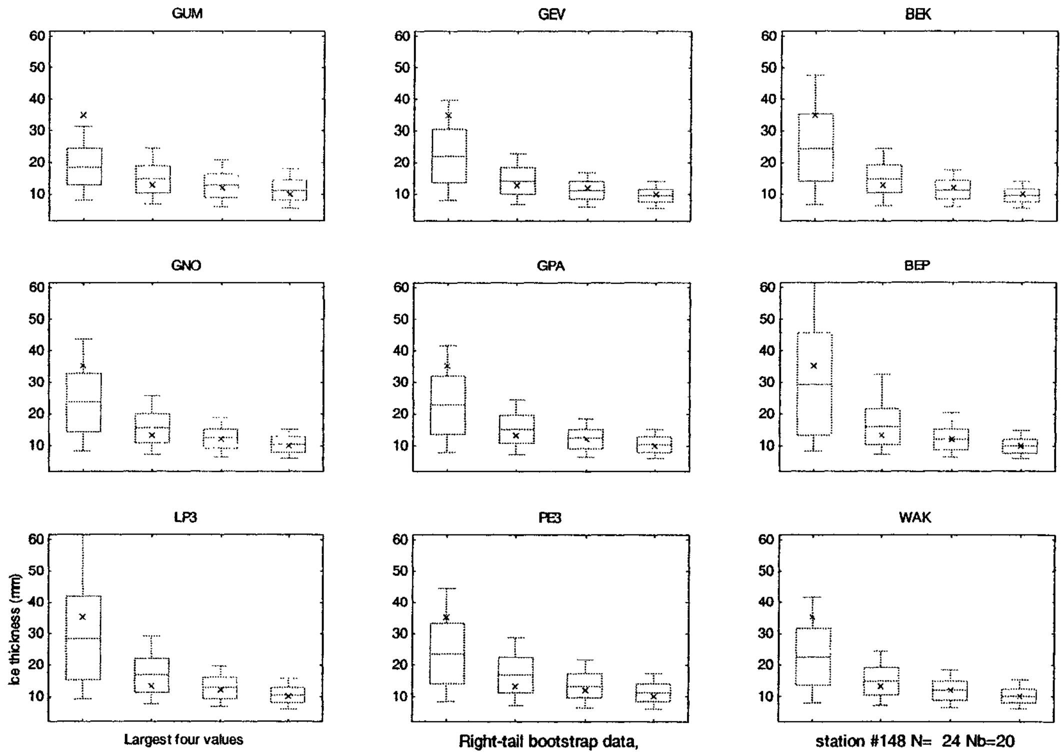

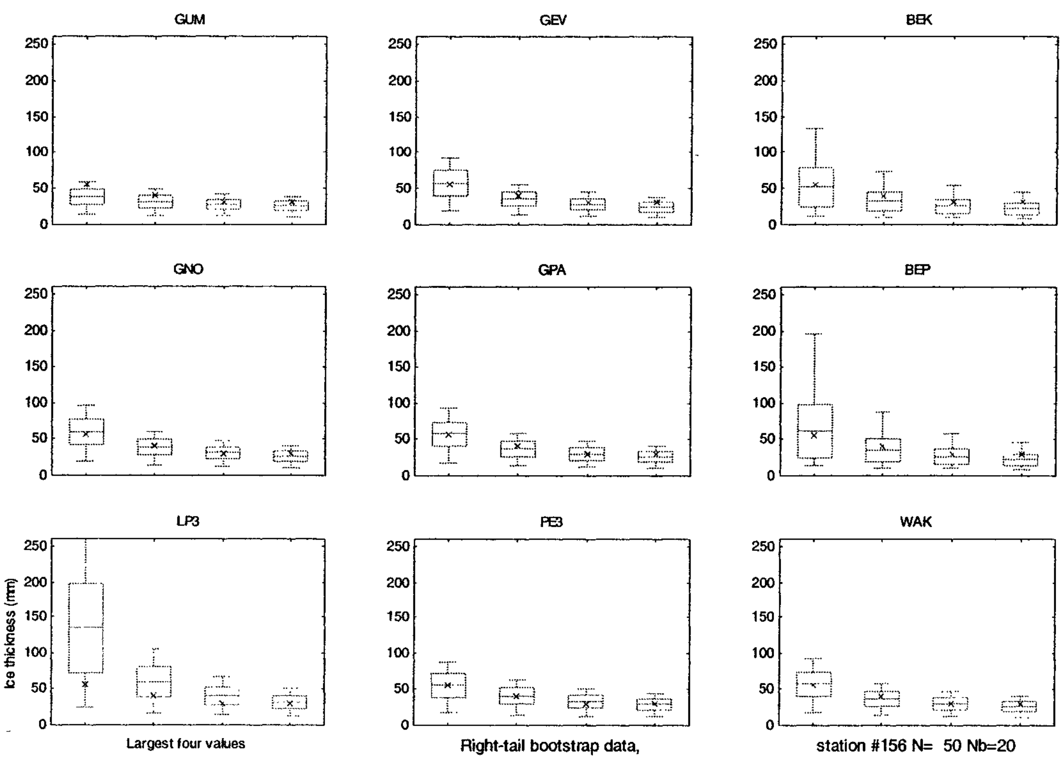

Box plots for bootstrap data for the selected stations

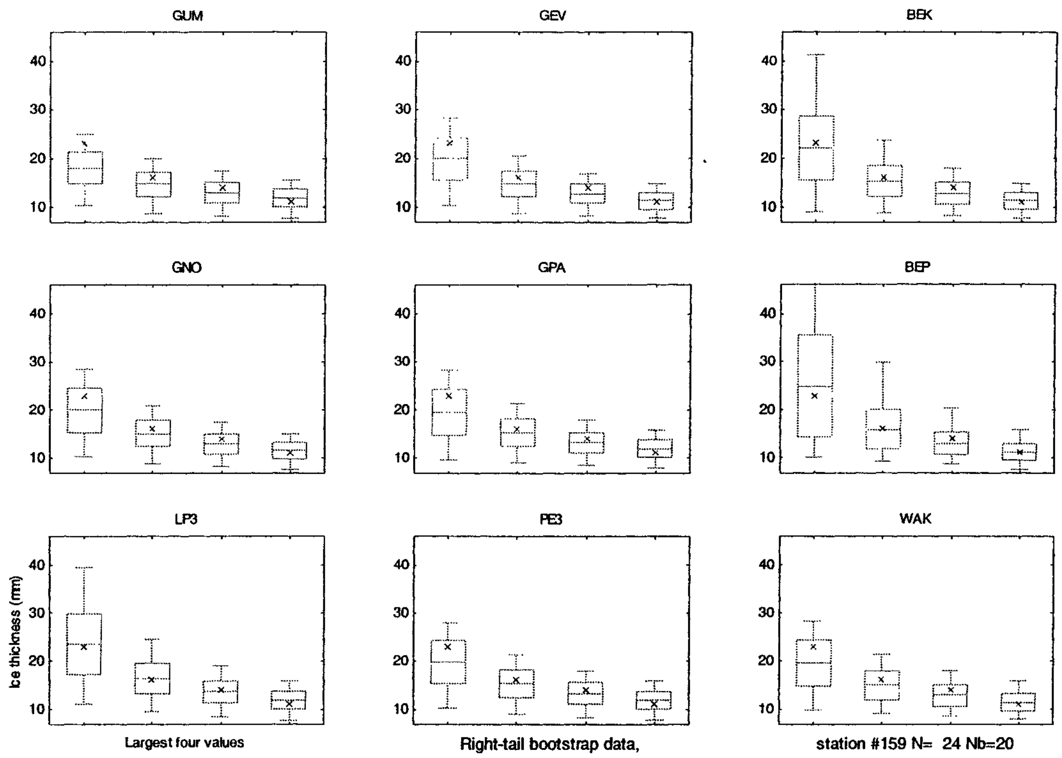

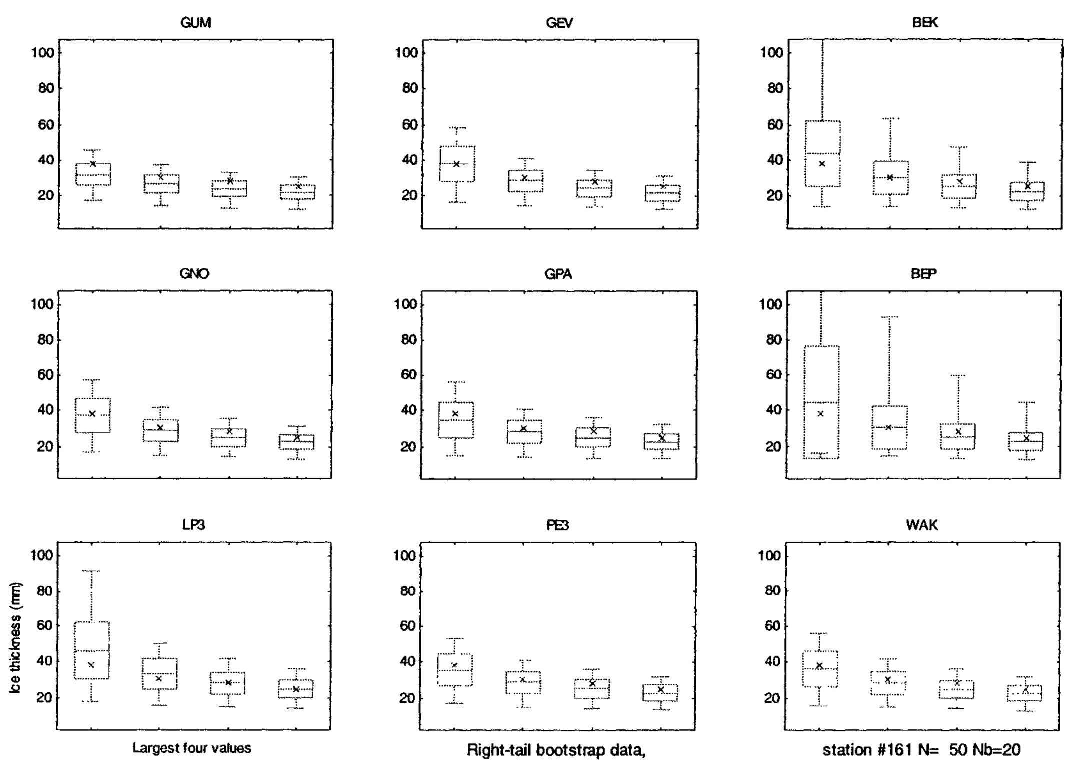

Box plots for bootstrap data for the selected stations

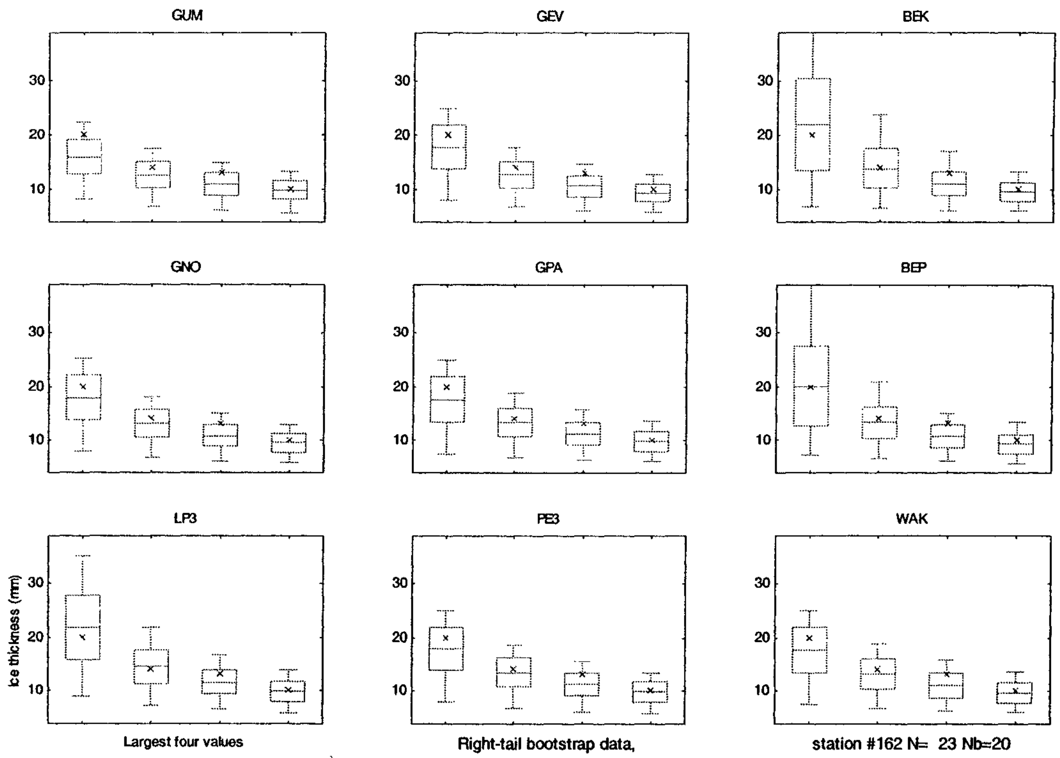

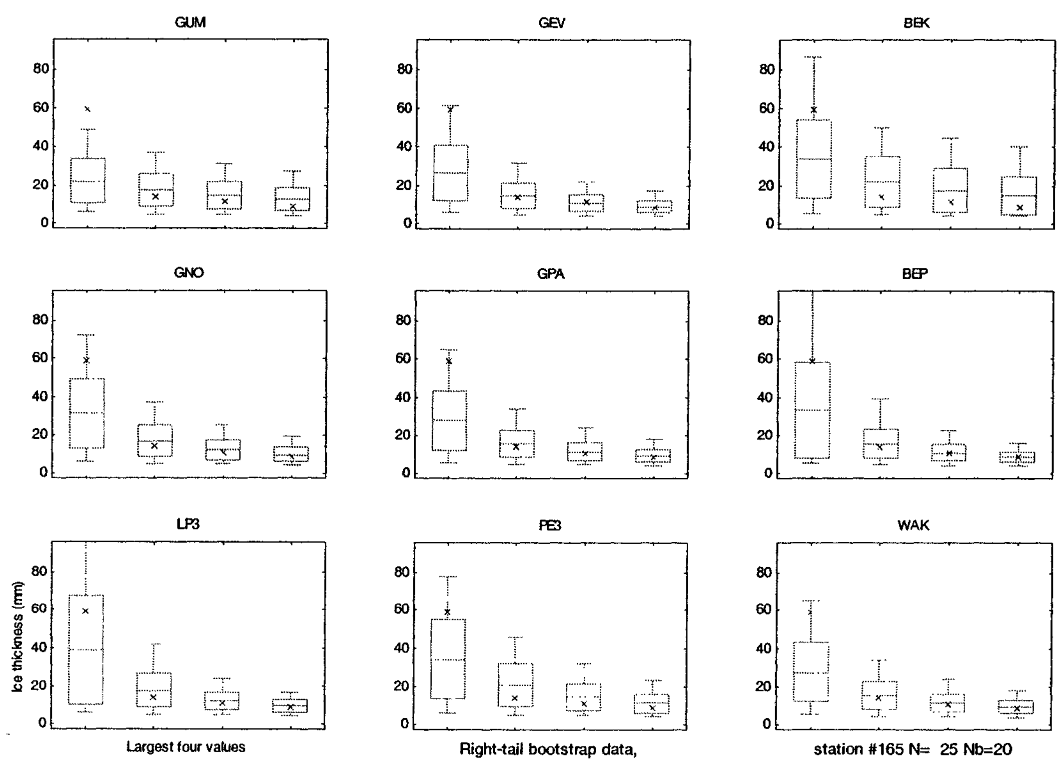

Box plots for bootstrap data for the selected stations

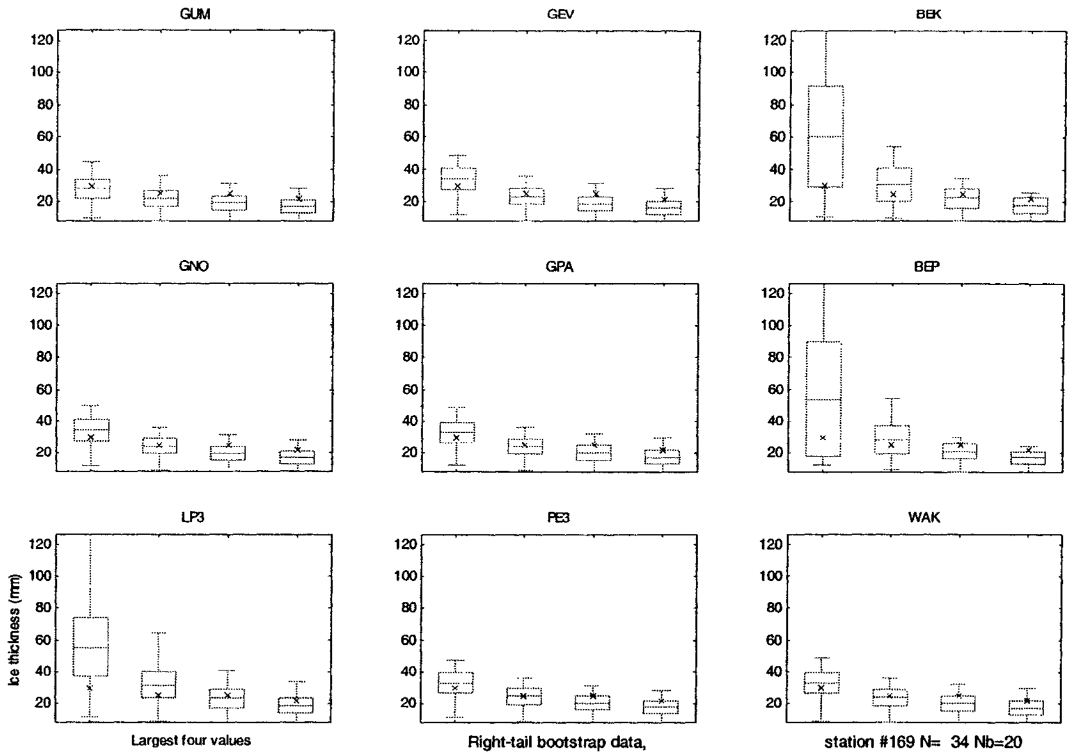

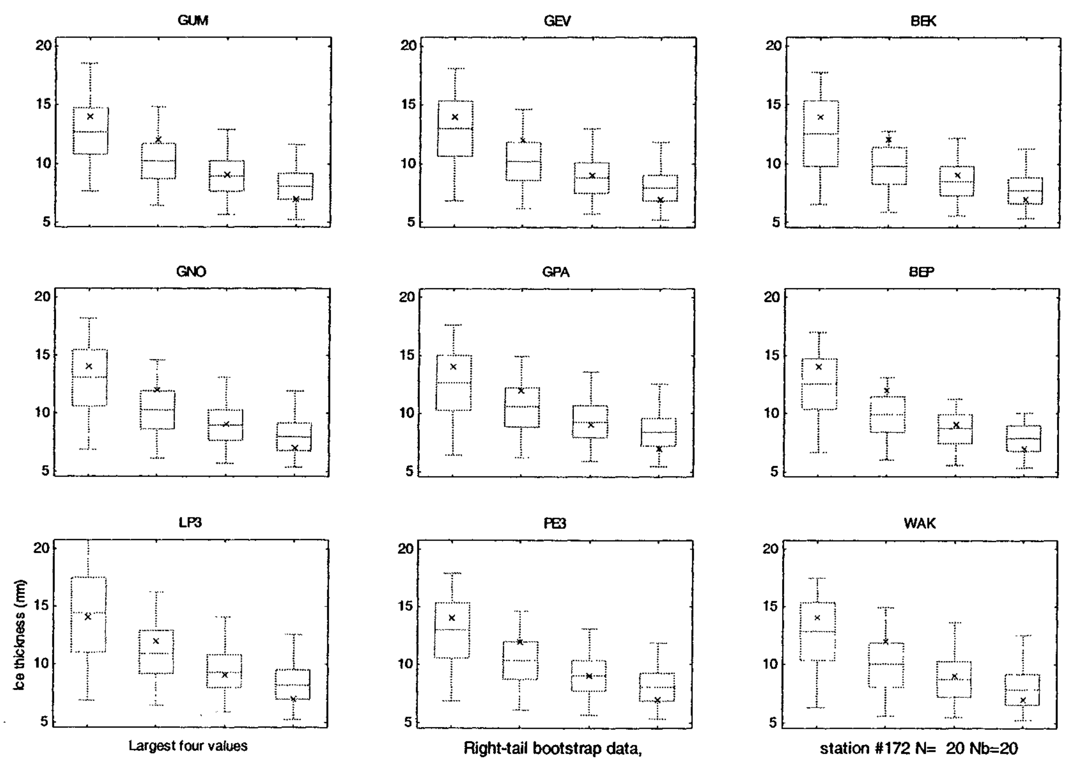

Box plots for bootstrap data for the selected stations

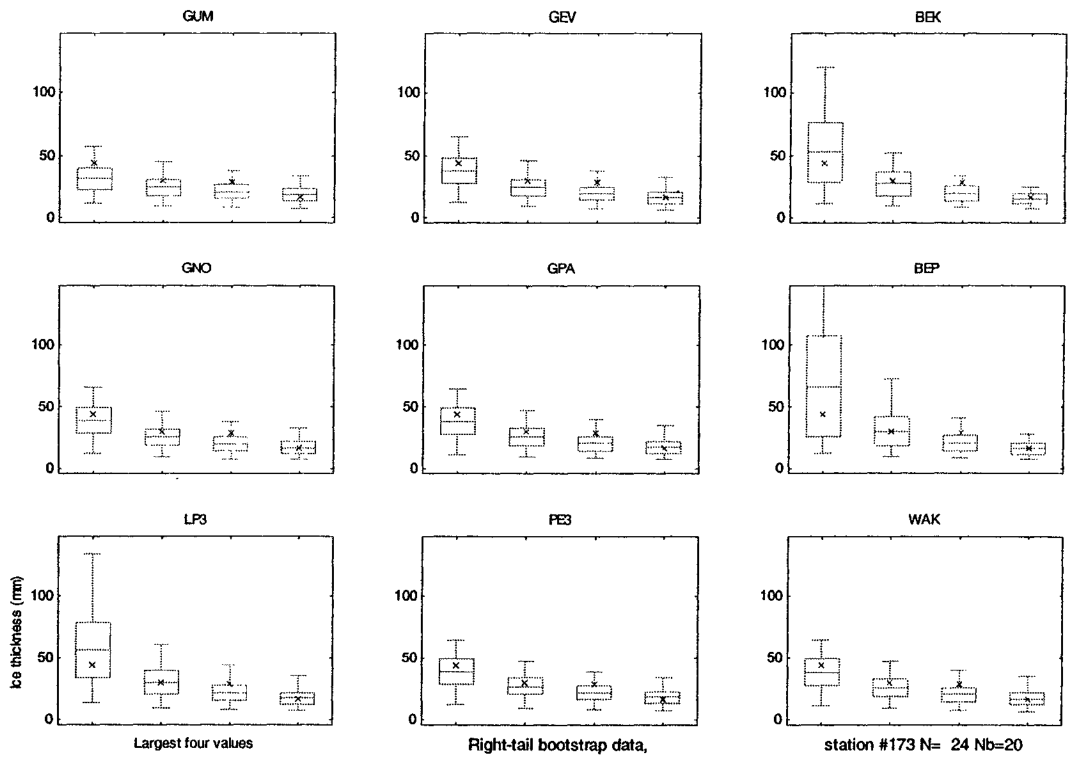

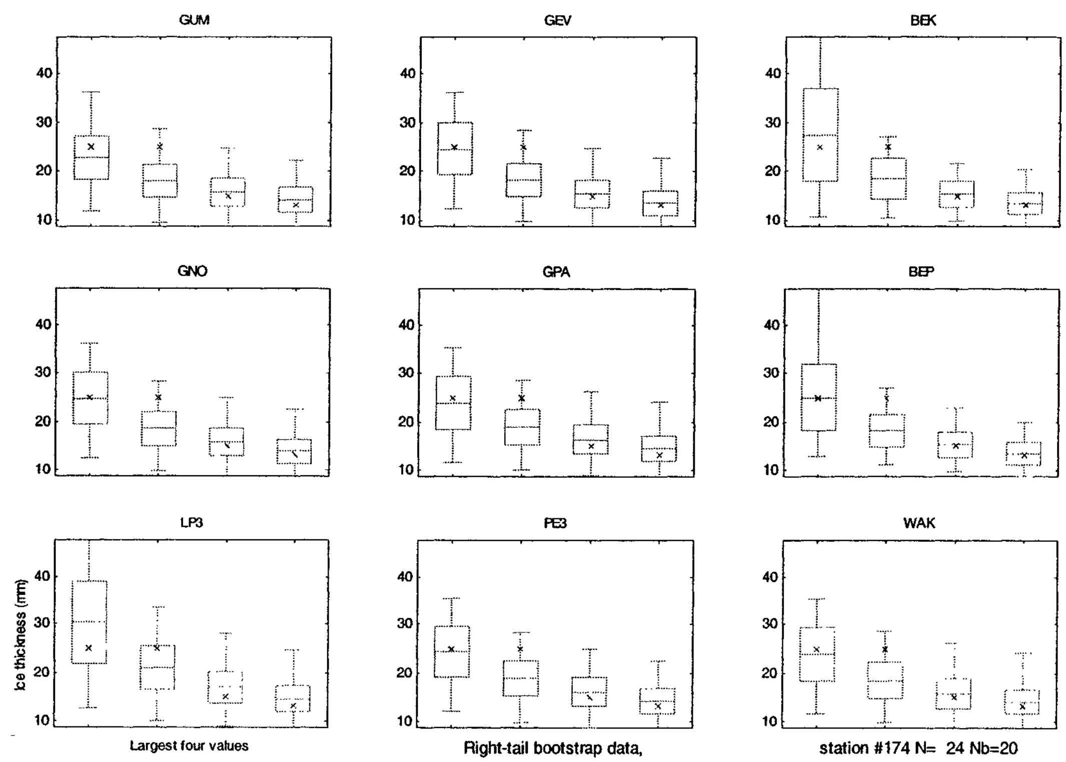

Box plots for bootstrap data for the selected stations

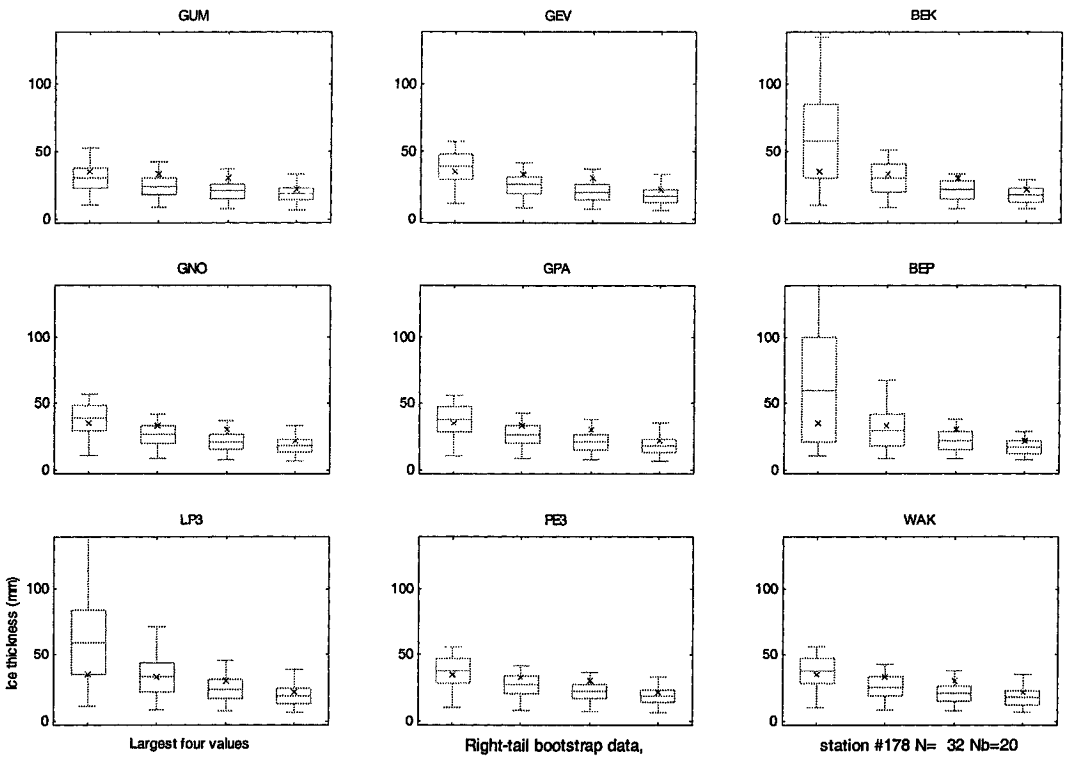

Box plots for bootstrap data for the selected stations